Project HYD-III-CEH-5

Determination of Relevant Parameters for the Alternative Assessment of Intact Stability Weather Criterion On Experimental Basis

Project Report

Gabriele Bulian (gbulian@units.it), Alberto Francescutto (francesc@units.it), Fabio Fucile (ffucile@units.it)
Department of Naval Architecture, Ocean and environmental Engineering (DINMA) - University of Trieste - Via A. Valerio, 10 - 34127 - Trieste - Italy

Document History:

Revision	Type	Date	Corresponding author	Notes
0.0	Draft	2009/03/27	Gabriele Bulian (gbulian@units.it)	Draft
1.0	Final	2009/11/22	Gabriele Bulian (gbulian@units.it)	Final version

Availability of experimental data:

All experimental data from this campaign are available to the public upon request to the authors.

Abstract

This paper reports the outcomes from an extensive series of experimental tests on three GEOSIM models (scales 1:65, 1:50 and 1:33) in the framework of the alternative experimental assessment of the Weather criterion as allowed by the recent MSC.1/Circ.1200. Roll decay tests, test in regular beam waves and drift tests have been carried out. Obtained results have been discussed in view of their relevance to the determination of parameters for the application of Weather Criterion. In case of beam waves tests, the performances of two simplified nonlinear dynamical models for roll motion prediction have been assessed.

Summary

Introduction

In the framework of the revision of the IMO Intact Stability Code [1], recently culminated with the issuing of the "International Code on Intact Stability, 2008 (2008 IS Code)" [2][3] as a mandatory instrument under SOLAS and International Load Lines Convention, IMO has also issued the MSC.1/Circ.1200 - "Interim Guidelines for the Alternative Assessment of the Weather Criterion" [4]. The MSC.1/Circ.1200 [4] contains guidelines for conducting experiments aimed at determining the relevant parameters for the assessment of the "Severe wind and rolling criterion (weather criterion)" on an experimental basis. In particular, the alternative experimental method allows to determine the following quantities by means of experiments:

- The wind heeling moments through wind tunnel tests;
- The moment due to the hydrodynamic reaction during steady lateral drift;
- The angle of roll due to the action of waves.

The availability of an experimental alternative to the statutory rules represents a potential for the optimization of the design of a ship on the base of her real(istic) performances at sea and thus from a safety point of view. Although MSC.1/Circ.1200 [4] can be considered as an important step forward concerning international rules for intact stability assessment of standard ships, it must be emphasized that a limited experience is presently available concerning the application of the methodologies in MSC.1/Circ.1200 [4]: the MSC.1/Circ.1227 - "Explanatory notes to the interim guidelines for alternative assessment of the weather criterion" [5] reports the unique example (at the moment of writing of this report) of a partial application of MSC.1/Circ.1200 [4].

The present research is aimed at investigating a series of still open matters regarding some aspects of the experimental approach proposed in MSC.1/Circ.1200 [4] and in particular:

- Possible scale effects on ship roll damping as estimated from free roll decay tests;
- Possible scale effects associated to the roll response in beam waves;
- Magnitude of the roll moment induced by a steady lateral drift under the hypothetical action of beam steady wind.

The possible presence of significant scale effects has been investigated in this research through a series of experiments using three GEOSIM models. Experiments have been carried out at "Canal de Experiencias Hidrodinámicas de El Pardo (CEHIPAR)" and comprised:

- Free roll decays;
- Roll tests in regular beam waves;
- Drift tests.

The analysis of free roll decays represents the easiest means (though not necessarily an easy one) to obtain suitable mathematical models representing energy dissipation for the roll degree of freedom. Results from roll decay analysis are used in MSC.1/Circ.1200 [4] to predict the ship rolling amplitude when tests in regular waves at the required wave steepness cannot be carried out due to limitations in the maximum generable wave height in the towing tank.

Roll tests in regular beam waves should be the preferred method to assess the rolling qualities of a ship when subjected to regular beam waves. However, it is not always possible to carry them out for large models. Indeed the natural roll period for standard ships in standard loading conditions is usually quite long. In order to carry out synchronous rolling tests in a towing tank, waves have to be generated in a region of

frequencies close to the ship natural period and this, especially in case of large models, requires the generation of long waves. For a given wave steepness, i.e. the ratio between the wave height and the wave length, long waves correspond to large heights that are often outside the generation range of the wavemaker. Direct measurement of rolling amplitude in beam waves, hence, could be a difficult task especially if large steepnesses are required, as it is the case of MSC.1/Circ.1200 [4].
Drift tests deal with the problem of estimating the moment due to the hydrodynamic reaction when the ship moves transversally in calm water. This condition is a (rough) simplification of part of the scenario assumed by the Weather Criterion, where a ship drifts due to the action of beam wind while rolling due to the action of waves. In practice, the Weather Criterion assumes a sort of superposition approximation and, as a consequence, the experimental procedure [4] separates the contributions from wind, hydrodynamic reaction and waves. Although this superposition is questionable, it serves as a practical means to address the complex interaction between the actors involved in the assumed scenario. The standard Weather Criterion considers a moment due to drift calculated by assuming an hydrodynamic reaction acting at half draught, equal in magnitude and opposite in sign to the lateral wind force. On the other hand, according to [5], this assumption could be far from reality. Hence this aspect, needing further attention, has been considered in this research. Unfortunately, although the maximum care has been given to obtain reliable data of a high quality standard from all the experiments, it is important to note, at the very beginning of this report, that data obtained from the towing tank concerning drift tests contained a series of inconsistencies preventing a robust interpretation of the results of the analysis. Since it was not possible to clarify the source of such inconsistencies after the execution of the tests, the results from drift tests have been reported, for sake of completeness, in a separate appendix and they should be considered with caution.
This report is structured as follows.
Firstly a description of the hull form is given, in order to provide all the data necessary for a complete understanding of the subsequent discussions.
Roll decay tests are then described and results from the analysis of data is reported, with reference also to Appendix 1 where the theoretical background of the analysis technique is described. Results are linked with the IMO procedure for the alternative assessment of the Weather Criterion by discussing the effect of application of the IMO frictional correction in [4].
Afterwards a description of roll tests in beam waves is given. A description of the analysis technique is provided, with reference to the method for obtaining ship motions in a tank fixed reference system from measured data (reference is made to Appendix 2). An analysis of generated waves is carried out in order to determine tests with possible errors in wave generation. The effect of the depth of the tank is discussed. Two mathematical models used for the prediction of the rolling motion are then described. Hence experimental roll response curves are reported and compared with numerical predictions using roll damping data obtained from the analysis of roll decays. Motions other than roll are also critically addressed, with reference to Appendix 2.
Drift tests are described in the subsequent section. The experimental setup and the technique of analysis are described. The section deals with the measured lateral force at steady drift. Due to a series of doubts concerning data for the roll moment induced by the steady drift, such topic is described in the separate Appendix 4.
Some final remarks are provided at the end of the paper.

Hull form - The CEHIPAR2792

The hull form used in this study has been provided by CEHIPAR. According to the information given by the towing tank the hull CEHIPAR2792 does not correspond to any real ship and it was built for the purpose of this research. A series of 3D views of the hull are shown in Figure 1, while the body plan of the ship is shown in Figure 2. Concerning the body plan, it must be said that the aft perpendicular (section 0) is conventionally intended in this report as the extreme aft end of the ship at a "design draught" of 6.8m (even keel) as given by the towing tank, while the forward end of the waterline at the same draught is conventionally referred to as the forward perpendicular (section 20). What is referred in this report as "ship length" is actually the waterline length of the ship at a draught of 6.8m. It is important to note, however, that experimental tests have been carried out for a draught of 6.6m.

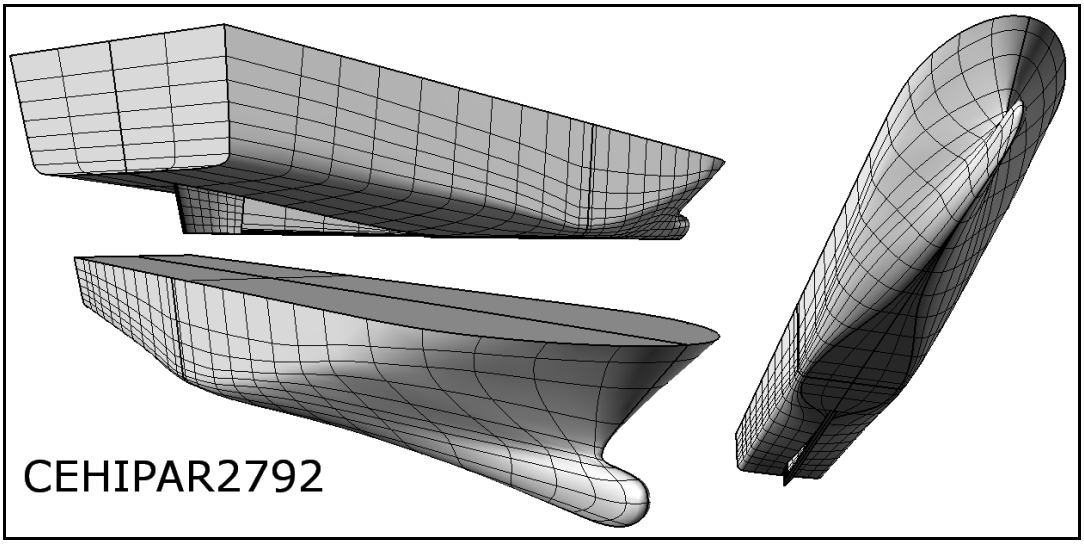

Figure 1: CEHIPAR2792. 3D view.

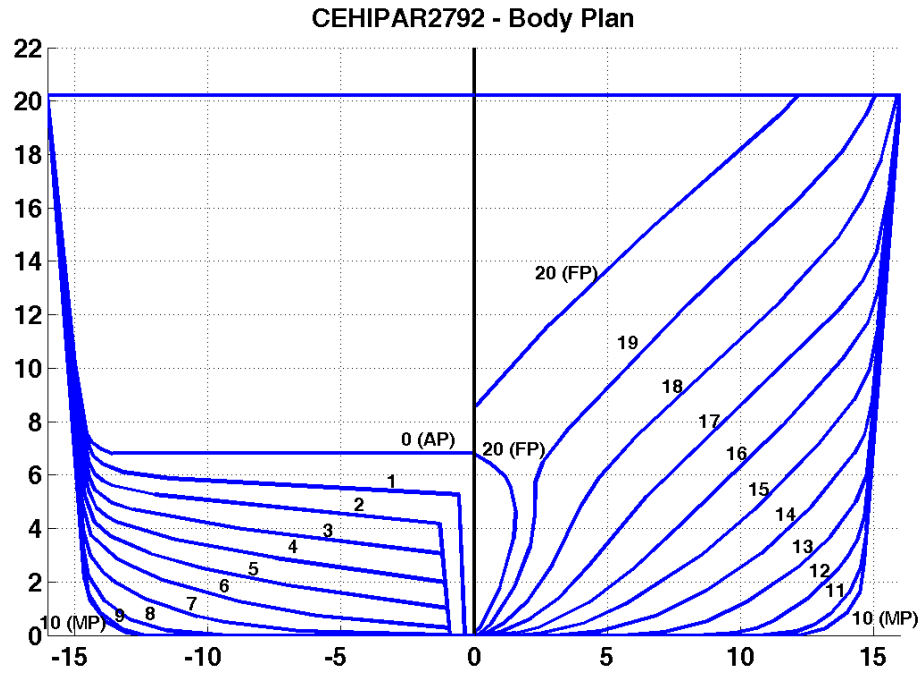

Figure 2: CEHIPAR2792. Body plan (full scale).

The main particulars of the ship are reported in Table 1. Due to the presence of the flare of the sides, the tested ship cannot be considered as a conventional hull form, because conventional cargo and passenger ships are usually designed with vertical sides. However, looking at the body plan in Figure 2 and at the main particulars in Table 1 it could be said that the tested ship has characteristics that are not far from those typical of relatively fast ferries. Moreover the B/T ratio at a draught of 6.6m is approximately 4.5 that is not far from the B/T ratio typical of post-panamax large passenger ships.

Table 1: Main particulars (full scale).

Ship:		CEHIPAR2792
Reference Length	[m]	205.7
Length overall	[m]	220.1
Depth	[m]	20.2
Breadth overall	[m]	32.00
L_{WL} @T=6.6m	[m]	207.0
Breadth @T=6.6m	[m]	29.90
Volume @T=6.6m	[m^3]	23986
C_B @T=6.6m	[nd]	0.587
KB @T=6.6m	[m]	3.794
BM_T @T=6.6m	[m]	14.064
A_X @T=6.6m	[m^2]	192.1
C_P @T=6.6m	[nd]	0.603
A_W @T=6.6m	[m^2]	5157
C_{WP} @T=6.6m	[nd]	0.833

Experimental tests have been conducted with the model in bare hull condition and fitting the model with bilge keels. The bilge keels on each side are split in two parts, and the main particulars of the bilge keels are reported in Table 2. Table 3 reports some main data concerning the skeg.

Table 2: Main particulars of bilge keels (full scale). Positions are given with respect to the reference mid perpendicular.

		Aft bilge keels	Fwd bilge keels
Start position	[m]	-46.850	2.151
End position	[m]	-11.851	25.250
Length	[m]	35.173	23.209
Maximum span	[m]	0.800	0.800
Projected area	[m^2]	24.6	16.5
Total wetted surface = 164.4m^2 Total projected area / (L*B) = 1.3%			

Table 3: Main data of skeg. Positions are given with respect to the reference mid perpendicular.

Skeg	Extreme aft position from MP [m]	Extreme forward position from MP [m]	Max height from the baseline [m]	Projected area [m^2]	Total wetted surface [m^2]
	-95.5	-25.6	5.588	146.5	414.0
Projected area / (L*B) = 2.4% - Projected area / (L*T) =10.7%					

Three models have been built with three different scales, namely:

- Scale 1:33, corresponding to an overall length of 6.67m (CEHIPAR2792-33)
- Scale 1:50, corresponding to an overall length of 4.40m (CEHIPAR2792-50)
- Scale 1:65, corresponding to an overall length of 3.38m (CEHIPAR2792-65)

It is anticipated here that in case of roll decay tests and tests in beam waves all three different models have been tested, while in case of drift tests only two model scales (1:50 and 1:65) have been used. A more thorough discussion on the loading conditions for each type of test is left to the relevant sections of this report.

Roll decay tests

Introduction

When safety is of concern, roll is probably the most important among the ship's degrees of freedom (DOFs). Indeed, in case of a capsize, either in intact or damaged condition, the transition from the upright to the capsized position is, basically always, associated to the occurrence of large amplitude roll. In case of a damaged ship it could be roughly said that the capability of the ship to withstand heeling causes possibly leading to a capsize lies in the ship's static restoring moment and that a quasi-static (at least mental) approach to the problem is not extremely far from the reality, apart, probably, from the initial phase of flooding and the final phase just before capsize (although dynamics effects cannot be, of course, completely neglected). In case of rolling motion in intact condition dynamics effects usually plays a dominant role, apart from some peculiar cases (e.g. the pure loss of stability on the wave crest in following waves). When strong roll dynamics is to be avoided (as it is usually the case) an efficient energy dissipation through damping is necessary (although not always sufficient). Unfortunately the wave radiation associated to the roll motion of standard monohull ships is usually quite limited, whereas other motions, in particular pitch and heave, benefit from a relatively large amount of energy that can be transferred to the water through wave radiation. Since the so-called "potential part" of the roll damping, namely the wave damping, is a very limited fraction of the overall roll damping, other dissipation mechanisms become important. It is customary to separate the roll damping into different components (see [6][7][8][9]), with each component associated to a particular distinct dissipation mechanism. At zero speed we can consider:

- Damping due to skin friction;
- Damping due to the generation of vortices;
- Damping due to wave radiation.

In addition to the three components above, also surface tension effects should be considered [10][11]. However, according to [6] the effect of surface tension is difficult to be considered from a practical point of view because it depends strongly on the condition of the painted surface of the model as well as on that of the water surface. According to [10] the surface tension could have a significant effect in case of small models and small rolling amplitudes, however in [6] it is stated that surface tensions effects can usually be neglected in the case of roll amplitude with moderate magnitude for ship models of ordinary size (although the quantification of "ordinary size" is missing). If the ship is fitted with bilge keels, vortex shedding at the edges of the bilge keels represents an additional efficient dissipation means. If the ship moves with a certain non-zero forward speed, roll is damped, in addition, by a damping moment associated to lift effects arising on the hull which, in presence of an advance

speed, behaves like a low aspect ratio wing. In this discussion we do not deal with additional damping systems like stabilizing fins, anti-rolling tanks, etc. . Moreover, in the framework of the alternative assessment of the Weather Criterion [4][5] our interest is focussed on the case of beam waves with the ship at zero forward speed, or, more precisely, on the case of "dead ship condition" [3][12]. For this reason forward speed effects are not of importance in the context of this research, and it could be said that our interest is mainly devoted to frictional, eddy making and wave-making effects (with a question mark to be placed close to possible surface tension effects). As already said, the energy dissipation associated to wave radiation represents a minor part of the overall damping especially at large rolling amplitude. Therefore, friction and eddy making are the two most important components to be considered in case of roll at zero speed. Both frictional effects and eddy making dissipation are associated to the water's viscosity (wave making damping, on the other hand, can be captured by the potential flow modelling). Experiments are carried out under "Froude similarity law" and, as a consequence, "Reynolds similarity law" is not fulfilled: this means that possible scale effects could be present if the model is too small, i.e. if the Reynolds number at model scale is too small compared to the full scale Reynolds number. According to [6][7] (and see also [9]) the eddy making component of damping is expected not to be affected by (significant) scale effects. On the other hand, again referring to ([6][7][9]), the frictional component of roll damping could be significantly affected by scale effects. Unfortunately (from the safety point of view) the model scale frictional damping, when transformed to full scale under Froude similarity, is expected to be larger than the actual frictional damping at full scale (this is almost exactly the same phenomenon occurring in standard calm water resistance tests concerning the frictional component of the ship's resistance). On the other hand the fortunate aspect of the problem is that usually the frictional damping contribution to the overall damping moment is significant only for small rolling angles, whereas the almost-scale-effects-free eddy making damping becomes dominant at large rolling angles [6][9].

In the context of the alternative assessment of the Weather Criterion it is therefore worth to better understand whether scale effects on roll damping could have a significant influence on the estimated "safety level" of the ship. Indeed the resonant rolling amplitude of a ship in beam waves having frequency close to the natural roll frequency, i.e. part of the scenario addressed by the Weather Criterion [3], is approximately inversely proportional to the equivalent linear damping calculated at the stationary rolling amplitude. An overestimation of the roll damping from model experiments could cause an underestimation of the actual rolling amplitude of the full scale ship, with obvious consequences regarding the actual level of safety of the ship.

In the field of Naval Architecture the majority of the interest associated to scale effects has been historically devoted to the problem of the estimation of the full scale ship resistance and propulsion characteristics from model scale experiments. Notwithstanding the strong economical interests involved in this aspect, only a limited number of families of GEOSIM models have been created and tested in order to better understand scale effects involved in the frictional / viscous component of the ship resistance ([13] p.97) due to the large involved costs. Concerning scale effects on roll damping the situation is even worse and, in the best authors' knowledge, a sufficiently large family of GEOSIM models has never been tested, or at least, has never been made public. Some experimentation on this aspect is nevertheless available (see, e.g., [14][15]) but considerations on the existence and possible magnitude of scale effects

on roll damping has mostly been based on theoretical / semi-empirical calculations (e.g. [4][11]).
According to these premises and taking into account that roll damping is one of the relevant parameters in the experimental assessment of the Weather Criterion [4][5], part of this research addresses the analysis of experimentally obtained roll decays. The present section of this final report is structured as follows:

- First a description of the tested loading conditions and model scales is reported, together with a description of the experimental apparatus and technique used in roll decay experiments. Practical difficulties in the execution of experiments are reported and discussed.
- Then the methodology of analysis is described, together with the associated theoretical background.
- Results from the analysis of the experiments are reported and discussed.
- And finally some concluding comments are made.

Loading conditions, testing setup and technique

Roll decay tests have been performed for the three available model scales (1:33, 1:50 and 1:65), in the following conditions (full scale data):

- Model Scale: 1:33
  - $\overline{GM} = 2m$, Draught=6.6m, with and without bilge keels
  - $\overline{GM} = 4m$, Draught=6.6m, with and without bilge keels
- Model Scale: 1:50
  - $\overline{GM} = 2m$, Draught=6.6m, with and without bilge keels
  - $\overline{GM} = 4m$, Draught=6.6m, with and without bilge keels
- Model Scale: 1:65
  - $\overline{GM} = 2m$, Draught=6.6m, with and without bilge keels
  - $\overline{GM} = 4m$, Draught=6.6m, with and without bilge keels

The full scale natural rolling period has been specified for the two values of metacentric height in bare hull condition as follows:

- $\overline{GM} = 2m$, ship natural period 18.4s, corresponding to a wet radius of inertia of $0.405B_{OA}$
- $\overline{GM} = 4m$, ship natural period 13.0s, corresponding to a wet radius of inertia of $0.405B_{OA}$

The value of the metacentric height has been checked by means of inclining tests. The natural rolling period has been obtained, as usual, by symmetric transversal shifting of masses using a trial-and-error procedure. The original intention was to specify the roll dry radius of inertia and obtain the natural roll period as a consequence. However, the uncertainty in the measurement of the roll dry radius of inertia was considered too large for the purpose of these tests. Hence, assuming that scale effects on the added mass are negligible, it has been decided to specify the natural rolling period, for which a much lower measuring uncertainty was achievable. The selection of the metacentric height and of the ship roll natural period was mainly driven by the necessity of performing a sufficient number of beam waves tests (see the relevant section of this report) inside the working range of the basin's wavemaker. The selection of the ship natural period was also significantly constrained by the practical limitations in the modification of mass distribution for the models.
For each case, a series of five roll decays have been performed, with three decays starting from approximately 30deg of heel and two decays starting from

approximately 10deg of heel. At a first glance one could think that performing roll decay tests is an easy task: unfortunately this way of thinking could be rather optimistic when using large models. Indeed, while heeling a small model to relatively large heeling angles is usually not difficult (at least for monohull ships with reasonable $\overline{GM}$ values), the same cannot be said in the case of large models, especially if the metacentric height is quite large. In Figure 3 the righting arm curves for the two tested loading conditions are reported (full scale data). If we concentrate on the condition $\overline{GM} = 4m$, it can be seen that the corresponding $\overline{GZ}$ is slightly more than 1.4m at a heeling angle of 30deg. The corresponding full scale restoring moment is about $3.3 \cdot 10^8$ N*m. In the case of the largest tested model the scaled restoring moment is about 278N*m. This is a significant heeling moment to be applied in order to heel the ship at 30deg. To have a more practical idea, in order to obtain the static heel of 30deg for the model CEHIPAR2792-33 it would be necessary to shift a mass of approximately 67kg from the centreline to the side of the model. Using an external vertical force (typically applied, in roll decay tests, by a single person by means of a rod) of approximately the same magnitude would create a significant disturbance concerning the heave motion (the mass of the model at scale 1:33 is approximately 667kg) and it would in any case be difficult to apply such a force by a single person.

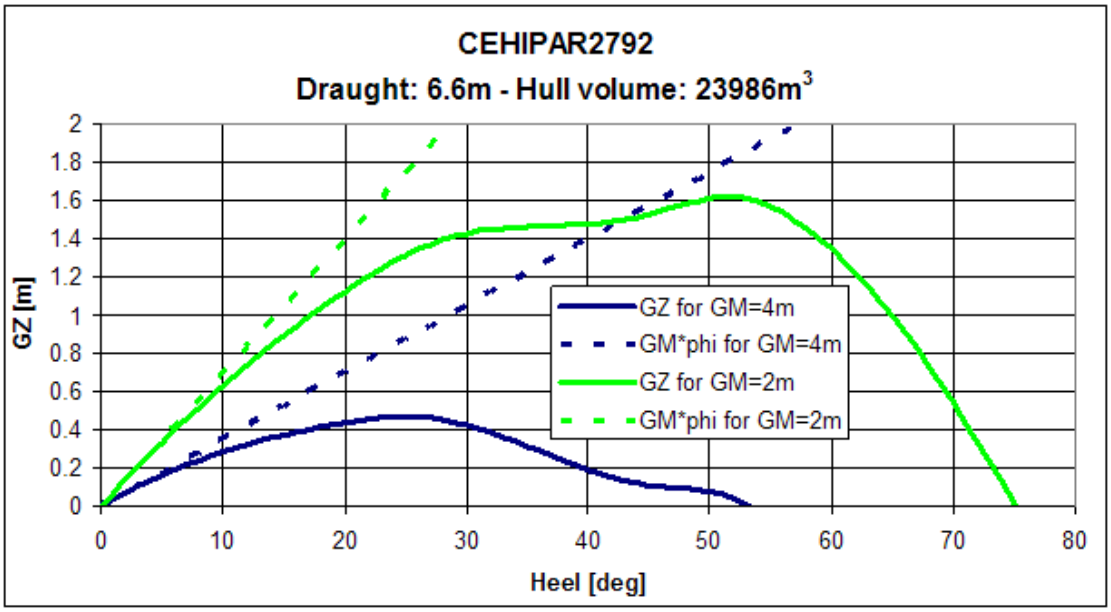

Figure 3: GZ curves for the two tested metacentric heights.

In order to try to overcome such difficulties the initial heel was imposed for all models in the decay tests by means of an experimental apparatus schematically reported in Figure 4, while a picture of the actual realization is reported in Figure 5. By means of the pulling force F applied to the system of ropes the model is heeled up to the required angle thanks to the moment induced by the ropes on the model. The force F is obtained by hanging the ropes to a lifting hook connected to the turret by means of a plastic clip. Although the tension of the ropes is significant, the actual parasitic vertical force on the model is limited (unfortunately it cannot be said it is actually "small") because the inclination angle of the ropes connected to the model is relatively small in the actual arrangement (see Figure 5). The used experimental arrangement allows applying to the model a system of forces that is close to a pure heeling moment, although, as already said, a residual additional vertical force

(generally directed downwards) on the model is present. The sudden removal of the pulling force F, with the consequent start of the roll decay, is obtained by cutting the plastic clip by means of scissors. The roll angle (actually, all the 6-DOFs) is measured by means of a non intrusive RODYM system [16] (the motion measuring cameras are pointed out in Figure 5).

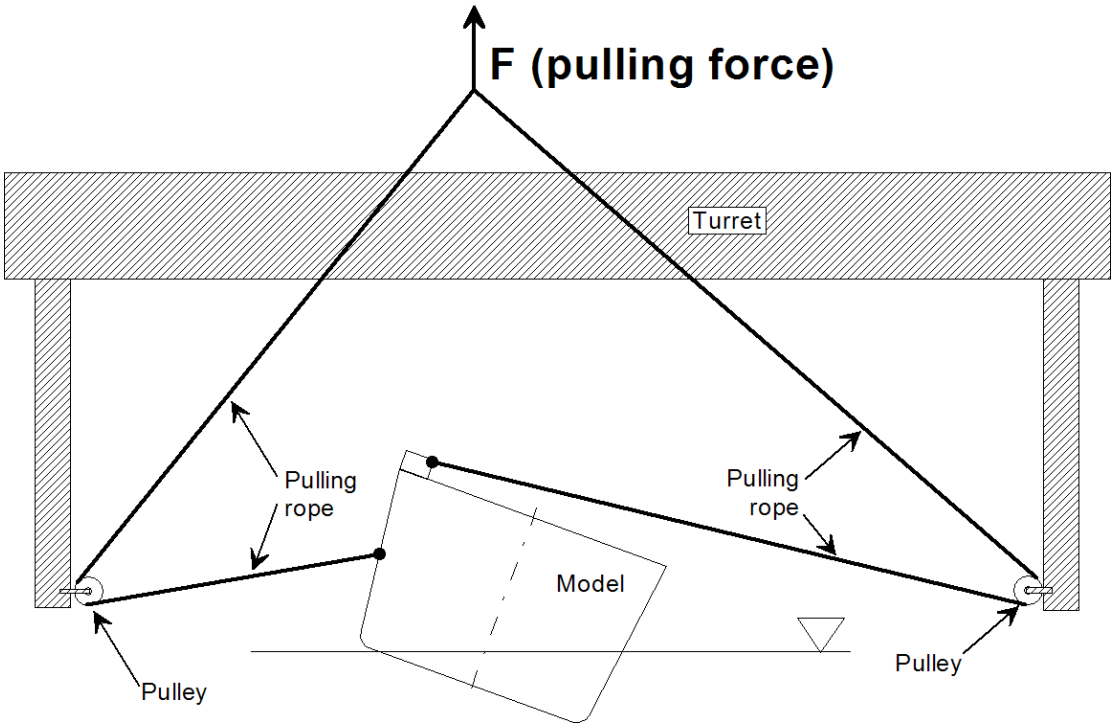

Figure 4: Schematic diagram of the experimental arrangement used for roll decay tests.

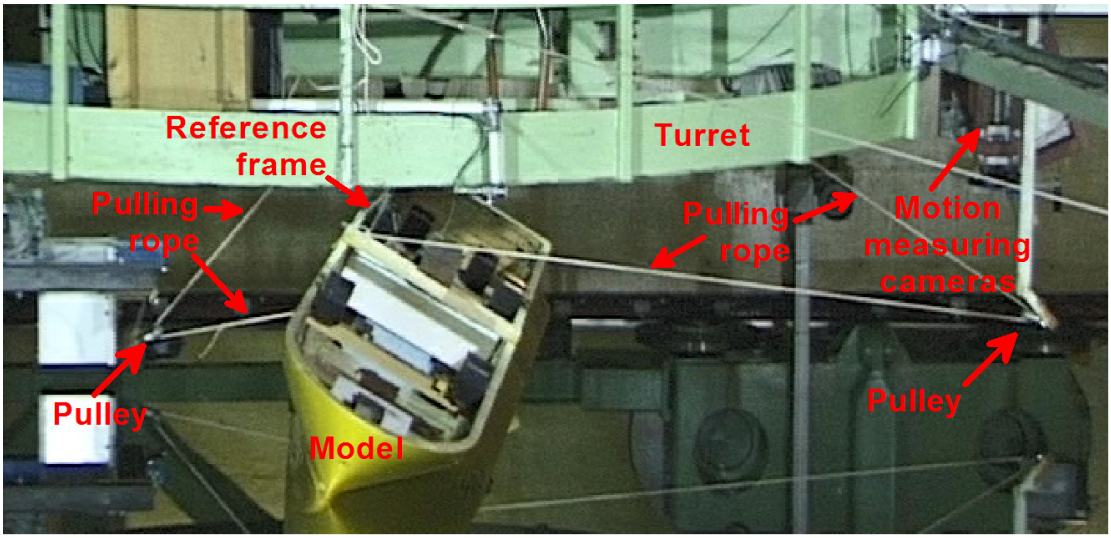

Figure 5: Actual realization of the experimental arrangement used for roll decay tests.

Methodology of analysis

In order to aggregate as many data as possible for the five roll decays performed for each model / condition, it has been decided to use an analysis technique based on the determination of the roll amplitude dependence of the roll damping and oscillation frequency by means of the so-called roll-decrement curve (or logarithmic roll-

decrement curve, or roll extinction curve). This method of analysis is well known in a series of variants (see, e.g., [6][11][17]). It is important to underline that the analysis of roll decays by means of the roll extinction curve is the methodology reported in [4]. The approach used in the present work is slightly different from what can usually be found in literature due to the fact that in the present analysis the variation of the frequency with the roll amplitude is explicitly taken into account, while usually the parametric fitting of the amplitude dependent equivalent linear damping is performed assuming that the oscillation frequency is, with good accuracy, almost independent from the rolling amplitude. Analytical details of the methodology of analysis are reported in Appendix 1.
The scope of the roll decrement analysis is to obtain:

- The roll amplitude dependence of the oscillations frequency, that is mainly associated with nonlinearities of roll restoring.
- The roll amplitude dependence of the equivalent linear damping coefficient, that is mainly associated with nonlinearities of damping.

The scatter plots of the oscillation frequency as a function of the oscillation amplitude are useful to check the correctness of the imposed roll natural period and, to some extent, the setup metacentric height. The scatter plots of the equivalent linear damping as a function of the oscillation amplitude are useful to have:

- A (mostly qualitative at the beginning) picture concerning the functional representation of nonlinearities in the roll damping analytical model
- Indications concerning the presence of potential differences, imputable to scale effects, among models having different scales.

After this first part of the analysis, that mostly involves subjective / qualitative judgements, it is possible to make a step forward by post-processing the scatter plots from the decrement analysis by means of suitable parametric models in order to obtain numerical estimates of the coefficients of the model especially for the damping function. Finally, a systematic comparison of linear / nonlinear damping coefficients, as well as a systematic comparison of the equivalent linear damping at different amplitudes can be used to disclose possible trends associated to scale effects.
It is anticipated here that, according to the obtained results, there seems not to be any significant scale effect affecting the roll damping, or, it would be better to say that the necessarily present scale effects have an influence on the roll damping that is much smaller than the overall uncertainty involved in the analysis of the experimental roll decay time series.

Results from the experiments

Roll decays have been analysed according to the technique reported in Appendix 1. The original aim of the experiments and of the associated analysis was to:

- Assess the presence and magnitude of possible systematic scale effects.
- Assess the influence of bilge keels on roll damping, both in terms of magnitude of the difference of equivalent linear damping with and without bilge keels for different rolling amplitude, and also in terms of variation of the functional dependence of roll damping on roll amplitude.
- Provide a base for subsequent analysis of tests carried out in beam waves (see the relevant section of this report).

Five roll decays have been performed for each condition, with three decays starting from approximately 30deg of heel and two decays starting from approximately 10deg of heel, for a total of 60 decay tests. In the analysis of the obtained roll decays the first half roll cycle has been neglected for a series of reasons. First of all it was not easy to

associate a precise time instant to the starting of the roll decay (and thus to the first "extreme"), since the initial part of each experimental record shows a steady heel equal to the initial roll angle. On the other hand the remaining extremes can clearly be associated to the relevant magnitudes and time instants of occurrence. Then, in the process of analysis, it was noticed a not negligible distortion of the first half roll cycle, which could have been induced by some parasitic effect of the experimental arrangement at the beginning of the decay, just after the release of the restraining ropes. In particular it was noticed a not negligibly faster roll oscillation in comparison with the remaining part of the record. Finally, the first half roll peak has been neglected also because it was considered as a transient in the developing of the fluid field from the rest condition, hence a situation not fully comparable with the remaining part of the decay where vortex shedding has already been initiated. Due to the neglecting of the first half roll cycle the first available peak is roughly around 20deg with an actual value that is lower in tests carried out with bilge keels, and larger in tests carried out in bare hull condition.
From a preliminary visual observation of the experimentally obtained curves of the amplitude dependent equivalent linear damping $\mu_{eq}(A)$ and of the amplitude dependent equivalent linear natural frequency $\omega_{0,eq}(A)$ the following analytical models have been employed (see Appendix 1 for details):

- Restoring: $\omega_0^2 \cdot r(\phi) = \omega_0^2 \cdot \left(1 + \gamma_3 \cdot \phi^3 + \gamma_5 \cdot \phi^5\right)$
- Damping:
  - Bare hull condition: $d(\dot{\phi}) = 2 \cdot \mu \cdot \dot{\phi} + \beta \cdot \dot{\phi}\left|\dot{\phi}\right| + \delta \cdot \dot{\phi}^3$
  - Bilge keels condition: $d(\dot{\phi}) = 2 \cdot \mu \cdot \dot{\phi} + \beta \cdot \dot{\phi}\left|\dot{\phi}\right|$

First of all we report, in Figure 6 to Figure 9, the results of the analysis and fitting of the decrement curves by considering data from different scales, with models in the same condition, on the same graph. Experimental data are all transformed to full scale for sake of comparison. Each figure reports also the values of the root mean squared error (RMSE) in order to give an order of magnitude of the residual dispersion of data with respect to the selected fitting model. The RMSE as reported in the figures has been calculated as:

$$RMSE = \sqrt{\frac{\sum_{j=1}^{N_{data}} \left(y_{\exp,j} - y_{fit,j}\right)^2}{N_{data} - n_{par}}} \tag{1}$$

where N_{data} is the total number of data, n_{par} is the number of free parameters (degrees of freedom), $y_{\exp,j}$ is the j-th experimental value and $y_{fit,j}$ is the value as obtained from the fitting. In the case of fitting of the frequency the number of degrees of freedom is 3 (ω_0, γ_3 and γ_5), and the same holds in the case of fitting of the damping model in bare hull condition where the free parameters are μ, β and δ. In case of models fitted with bilge keels n_{par} reduces to two in case of fitting of the damping model because it is assumed $\delta = 0$. It is however important to note that, due to the large number of experimental points (of the order of 100-200 depending on the case) obtained by the aggregation of different decays for each condition we have that

$$\frac{N_{data}-n_{par}}{N_{data}} \approx 1 \Rightarrow RMSE \approx \sqrt{\frac{\sum_{j=1}^{N_{data}} \left(y_{\exp,j} - y_{fit,j} \right)^2}{N_{data}}} \tag{2}$$

An approximate 95% confidence bound can be considered as the region of $\pm 1.96 RMSE$ around the fitting, while a region of $\pm 2 RMSE$ around the fitting can be considered as an approximation of a 95.5% confidence bound for a new observation. This is actually true under the assumption of Gaussian residuals with a distribution of residuals that is independent on the independent variable. Although these conditions are not strictly fulfilled in the present analysis (e.g. the dispersion of ω_0 and μ_{eq} is usually larger in the region of smaller rolling amplitudes), the reported RMSE is considered as a practical means to have a rough idea of the residual level of dispersion associated to the fittings.

Since Figure 6 to Figure 9 do not allow an easy direct assessment of the effect of bilge keels, Figure 10 to Figure 15 report a comparison of the amplitude dependent equivalent linear frequency and damping as obtained from the experiments, with the associate fitting, for each different model scale and GM value. A series of summarising plots concerning the additional damping created by the bilge keels are reported in Figure 16 to Figure 19. In particular Figure 16 shows the ratio between the equivalent linear damping with bilge keels and the equivalent linear damping without bilge keels as given by the fitted models for all the conditions. However damping due to bilge keels shall be assumed to be an additional damping term with respect to the bare hull condition, and not a multiplicative factor. Hence, although data in Figure 16 could serve as an interesting reference (that will be discussed later) concerning the overall influence of fitting of bilge keels for this particular ship, it is not suitable for being used as a prediction means in case of other ships. In order to see the effect of bilge keels as an addition of roll damping, Figure 17 and Figure 18 have been prepared, where the difference between the amplitude dependent linear equivalent roll damping is reported in case of $\overline{GM} = 2m$ and $\overline{GM} = 4m$, respectively. In each figure some additional data are reported, and, in particular:

- The average full scale roll frequency ω_0 for all conditions (with and without bilge keels) together with the sample standard deviation. Although the experimentally estimated frequency ω_0 is different for each condition for a given metacentric height, the dispersion (quantified by the reported standard deviation) is sufficiently small to be neglected in comparison with the magnitude of the discrepancies obtained for the additional linear equivalent damping at different scales given by the fitting of bilge keels.
- The average value of the root mean squared error (RMSE) for the fitted model (with and without bilge keels) together with the sample standard deviation. The RMSE represents, basically, the residual standard deviation of the experimental data with respect to the fitted model. Hence a band of +/- 1.96RMSE around the fitted model roughly contains about 95% of the data. As already said, this is actually true under the assumption of Gaussian residuals with a distribution of residuals that is independent on the independent variable. Although these assumptions are not strictly fulfilled in the present analysis, the average RMSE is reported as a means to have a rough idea of the residual level of dispersion for the fittings of the damping data.

Moreover, it should also be pointed out that, since the plots in Figure 17 and Figure 18 report a difference between models associated with a certain level of uncertainty, an approximation of the RMSE associated to such difference should be considered as roughly $\sqrt{2}$ times the RMSEs reported in the figures.

Finally, Figure 19 tries to summarise Figure 17 and Figure 18 in a single plot by making the differences of linear equivalent damping dimensionless by dividing them by the average natural frequency ω_0.

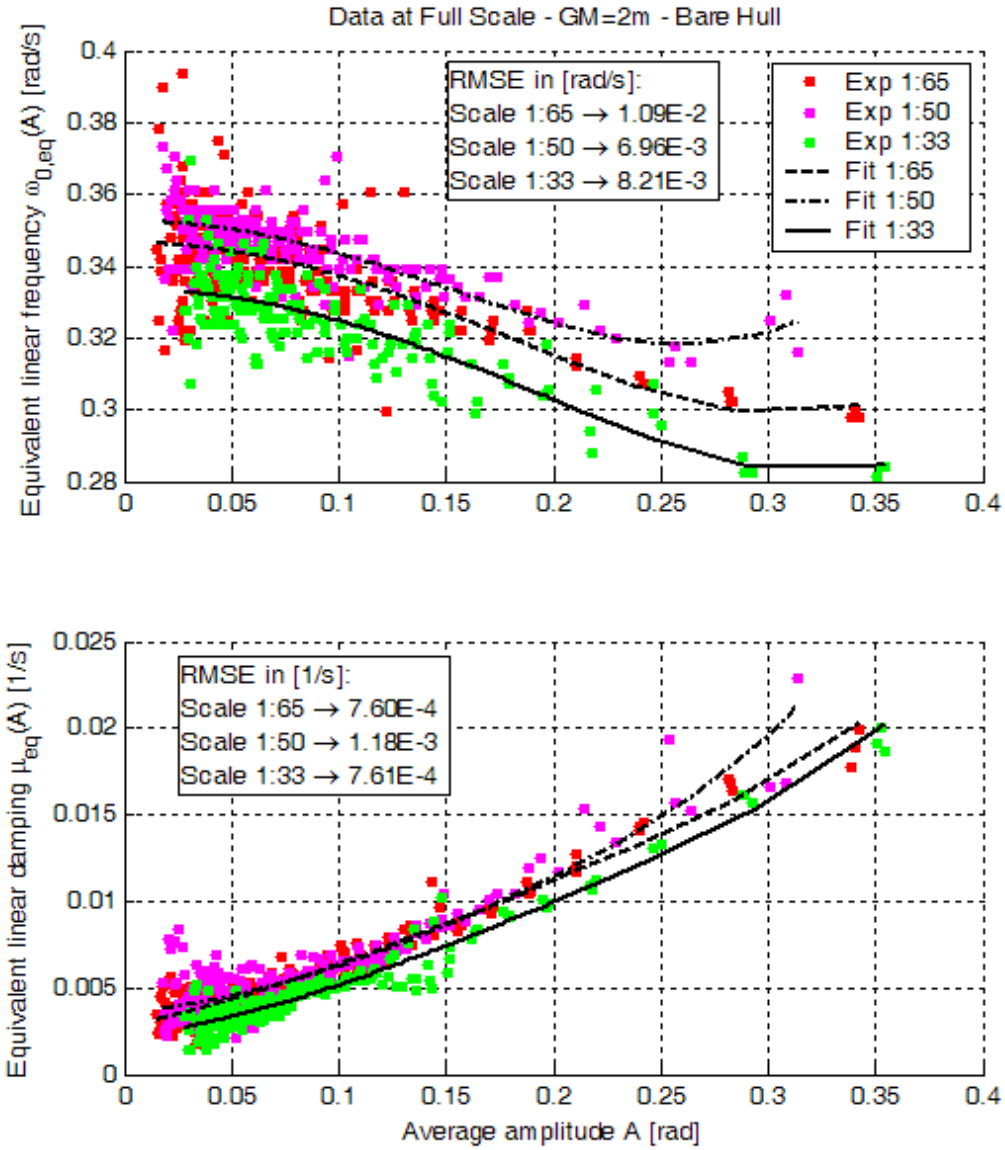

Figure 6: Analysis of decays. GM=2m, bare hull condition. All scales.

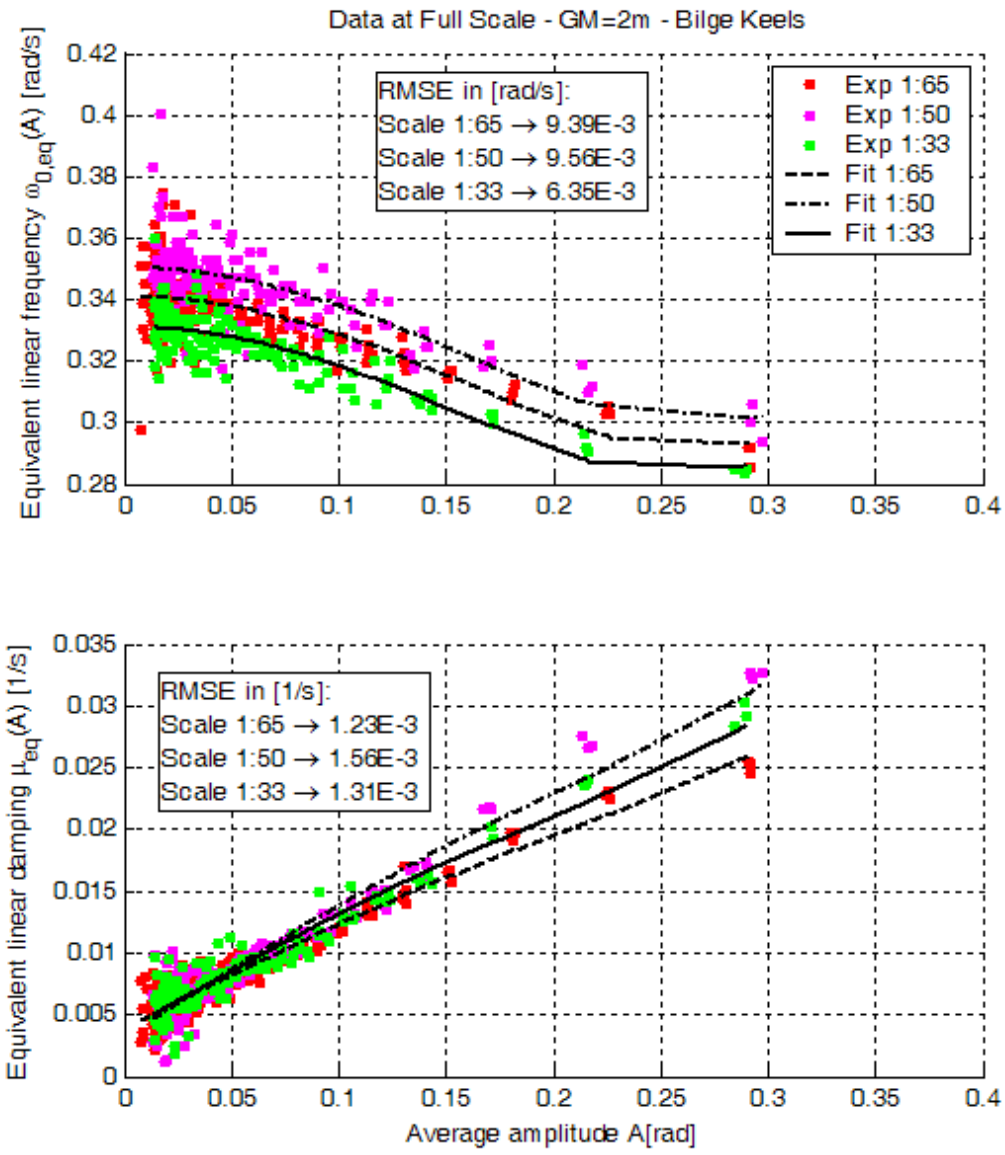

Figure 7: Analysis of decays. GM=2m, bilge keels condition. All scales.

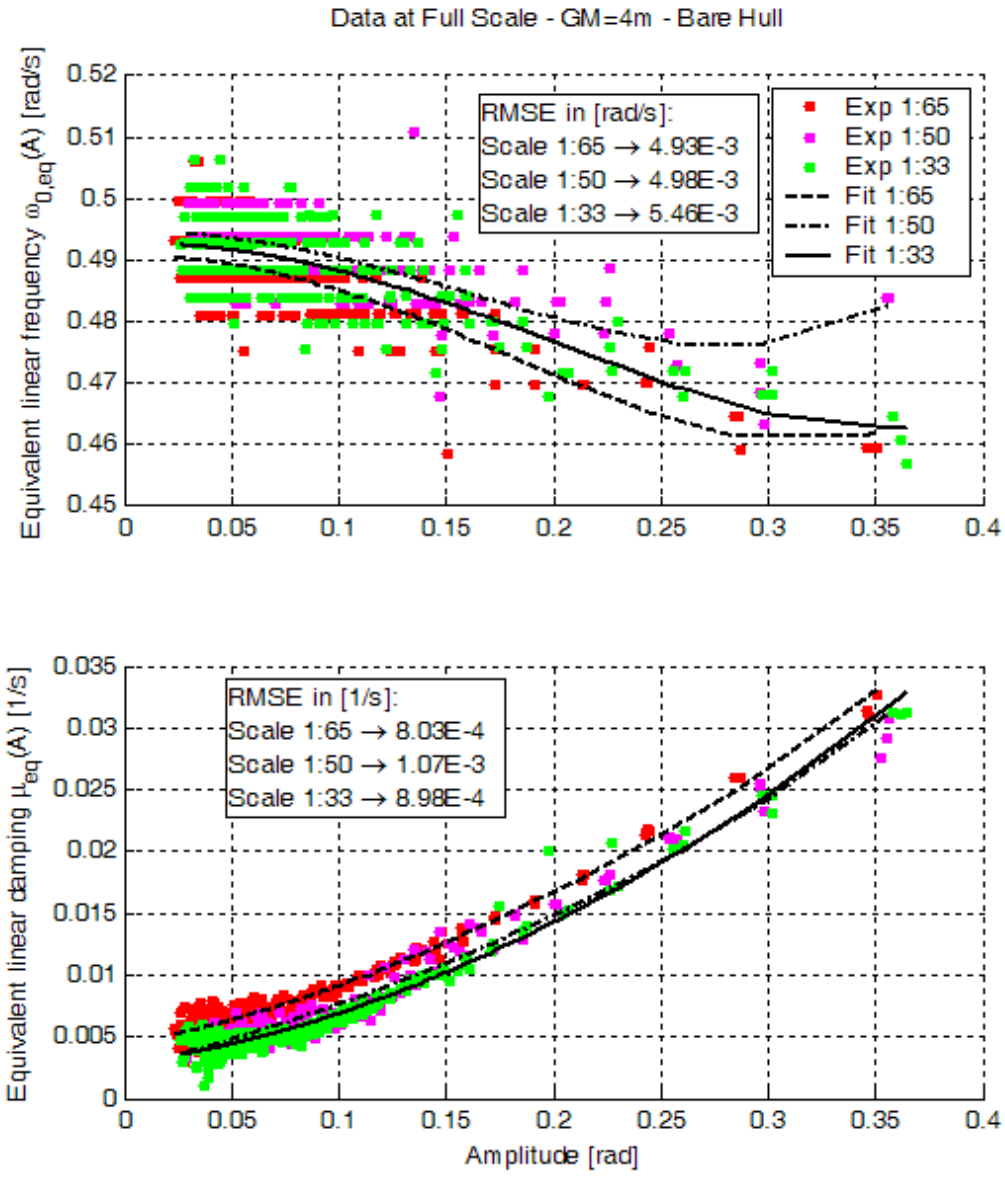

Figure 8: Analysis of decays. GM=4m, bare hull condition. All scales.

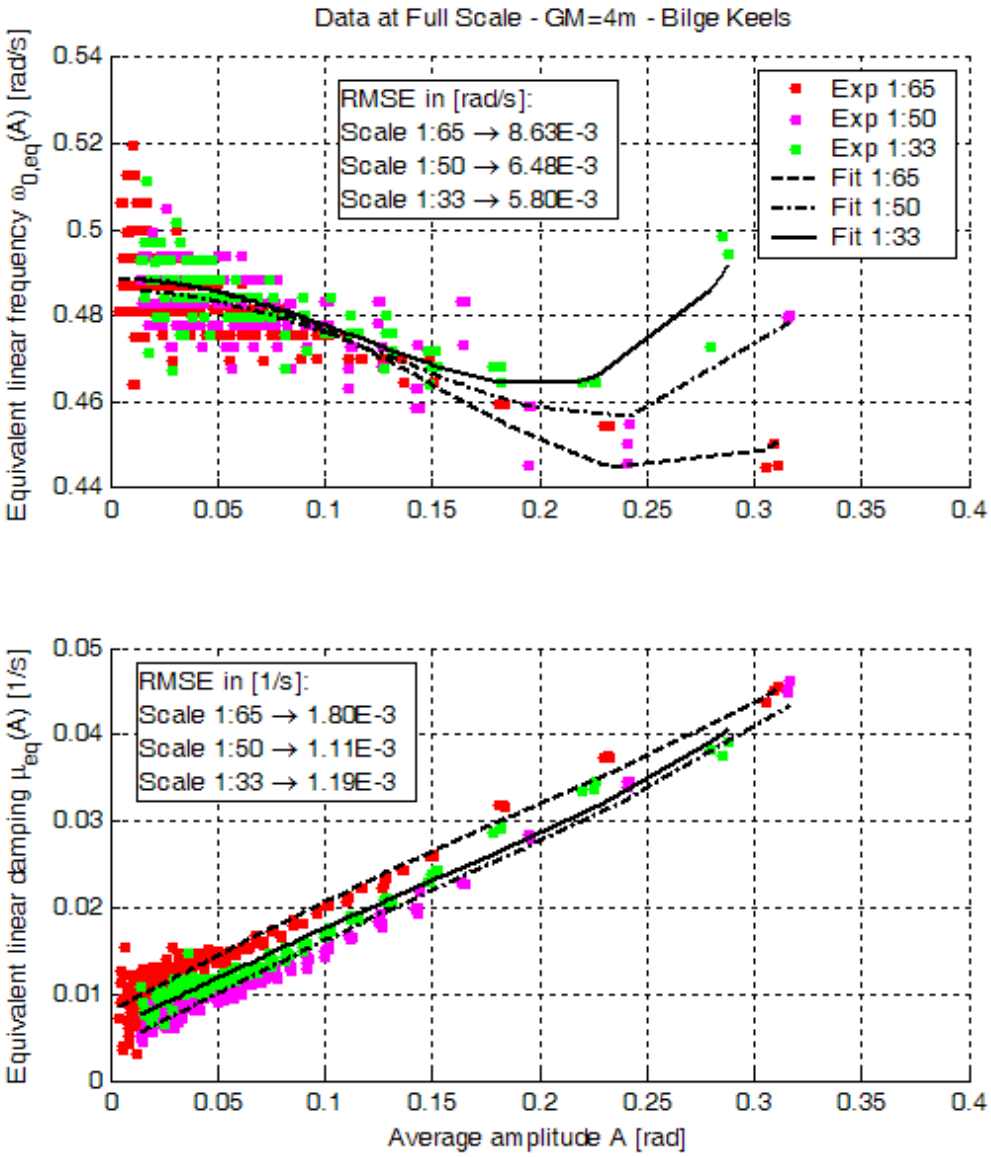

Figure 9: Analysis of decays. GM=4m, bilge keels condition. All scales.

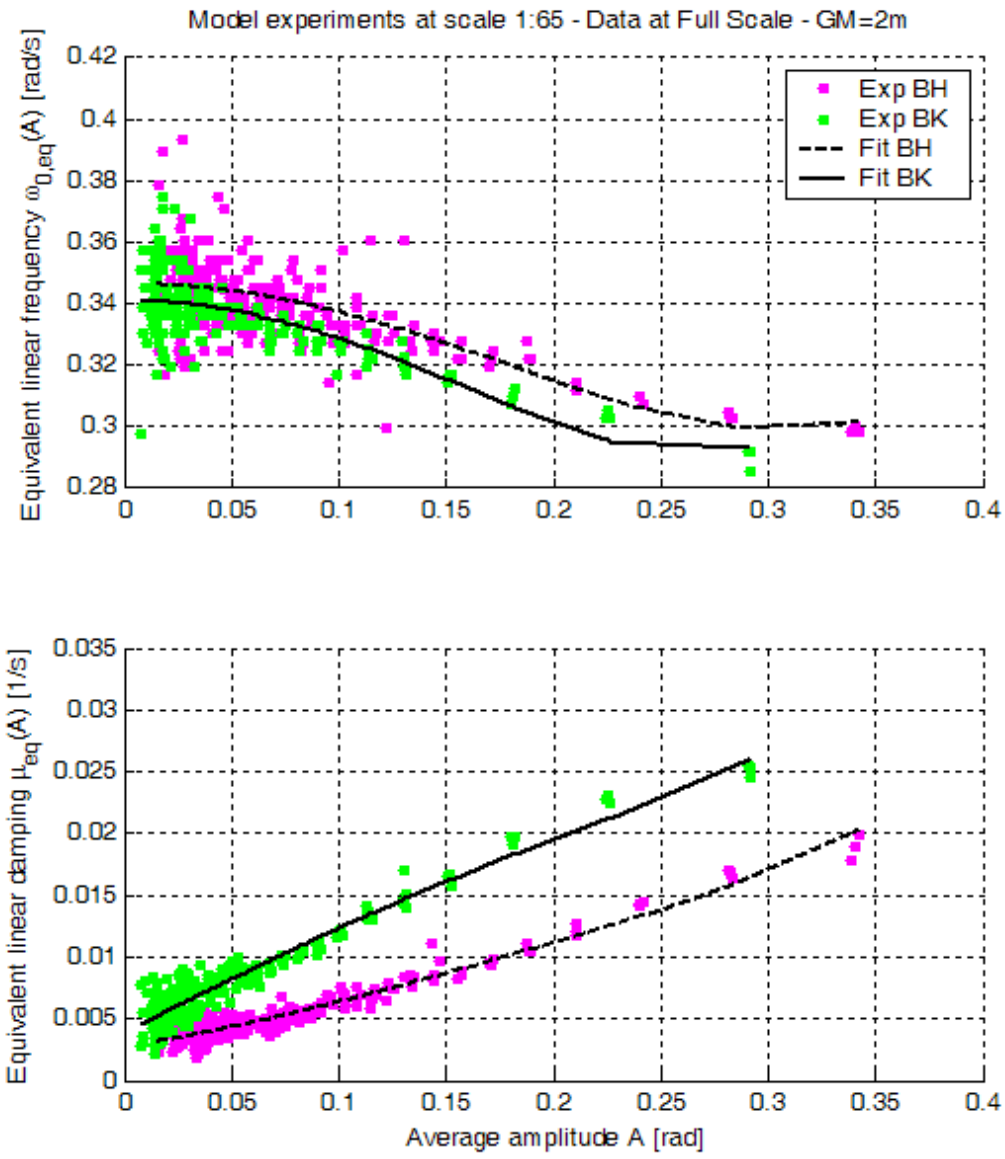

Figure 10: Analysis of decays. Effect of bilge keels. GM=2m, model scale 1:65.

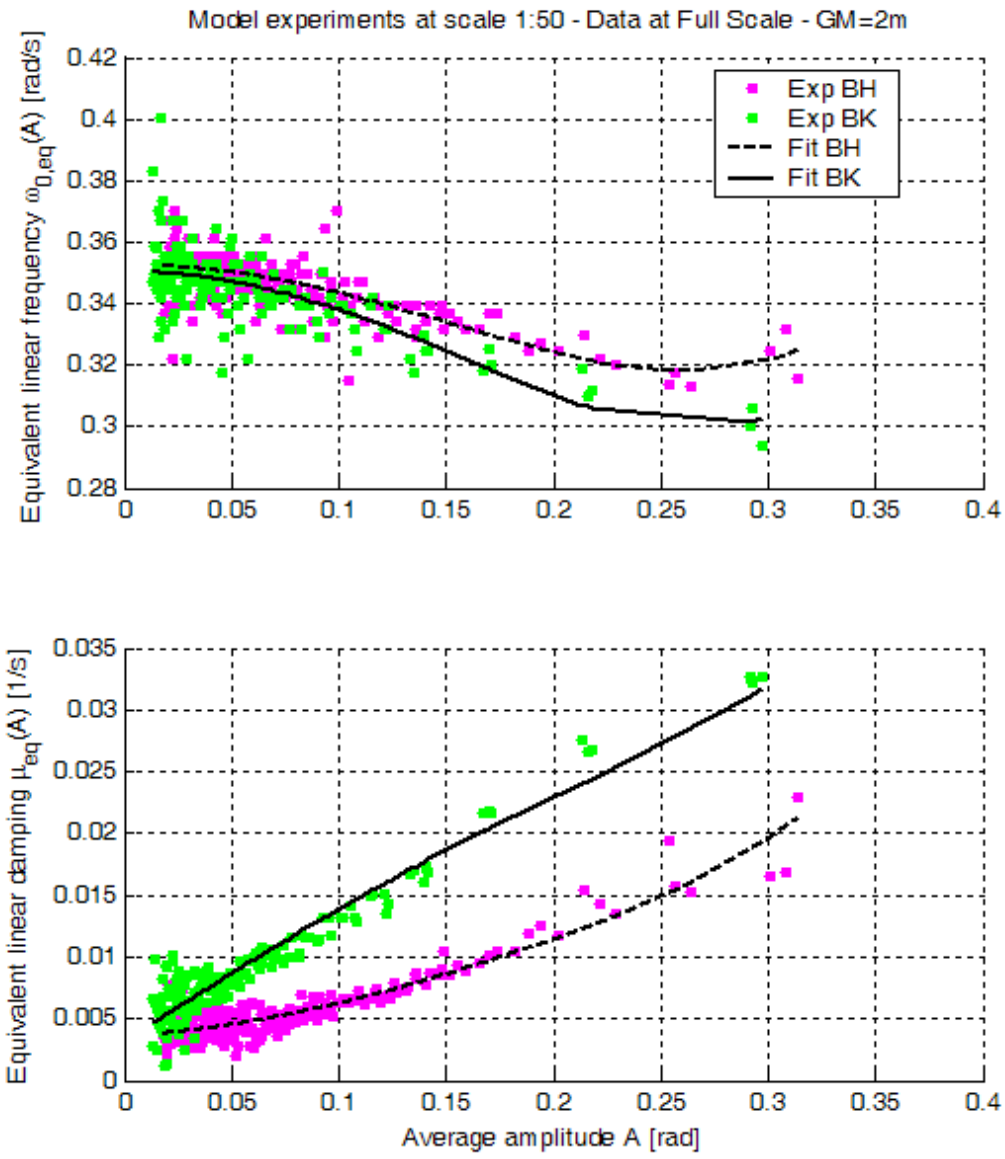

Figure 11: Analysis of decays. Effect of bilge keels. GM=2m, model scale 1:50.

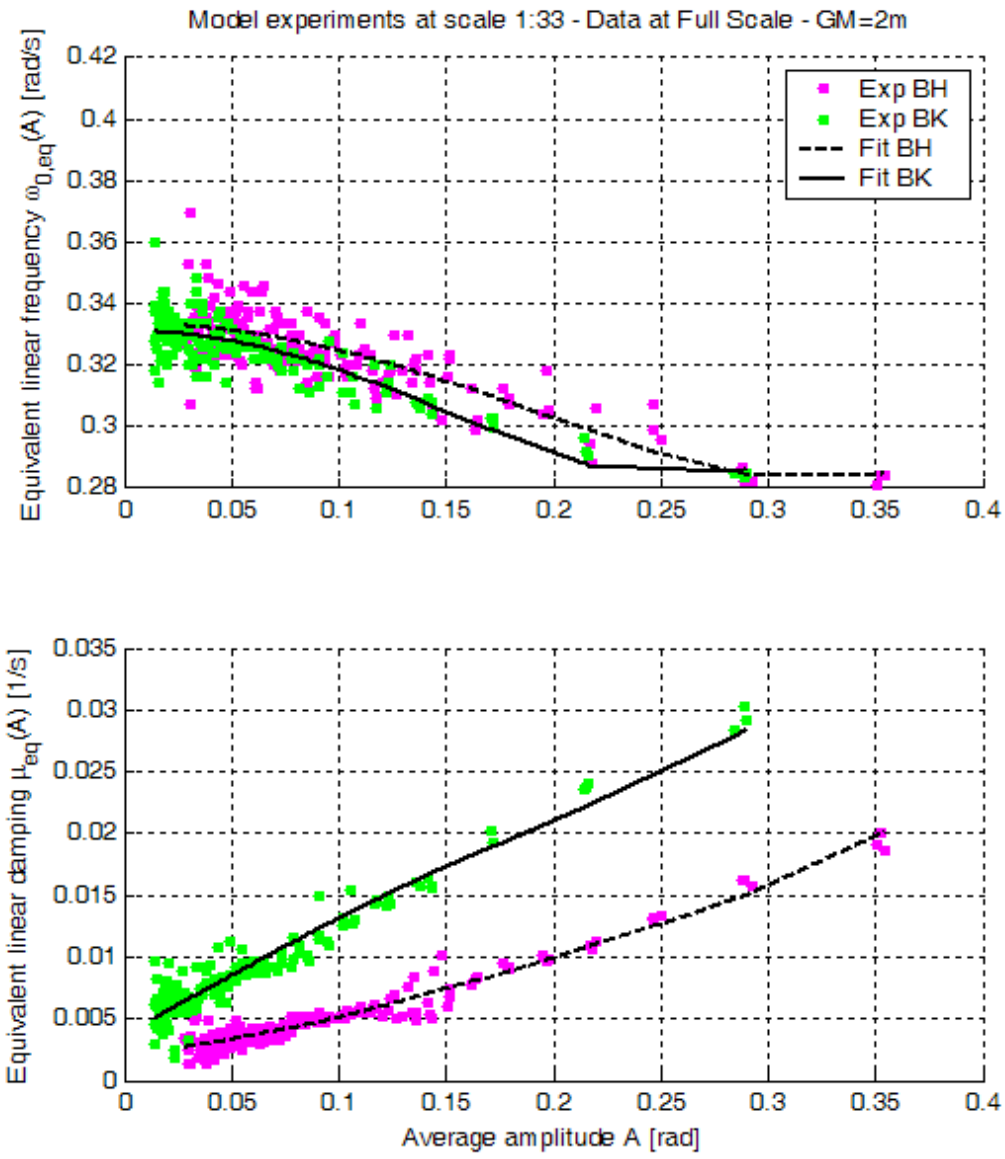

Figure 12: Analysis of decays. Effect of bilge keels. GM=2m, model scale 1:33.

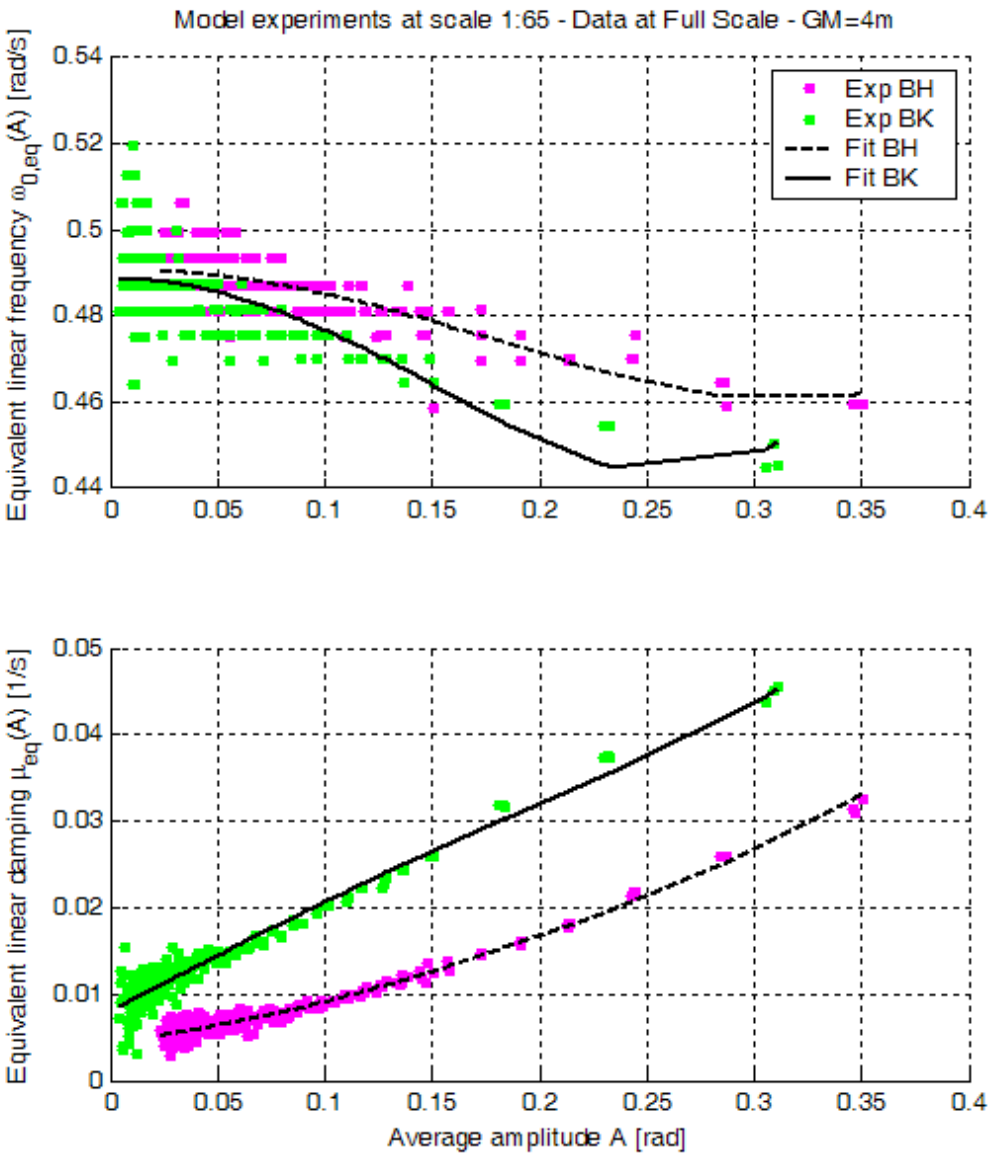

Figure 13: Analysis of decays. Effect of bilge keels. GM=4m, model scale 1:65.

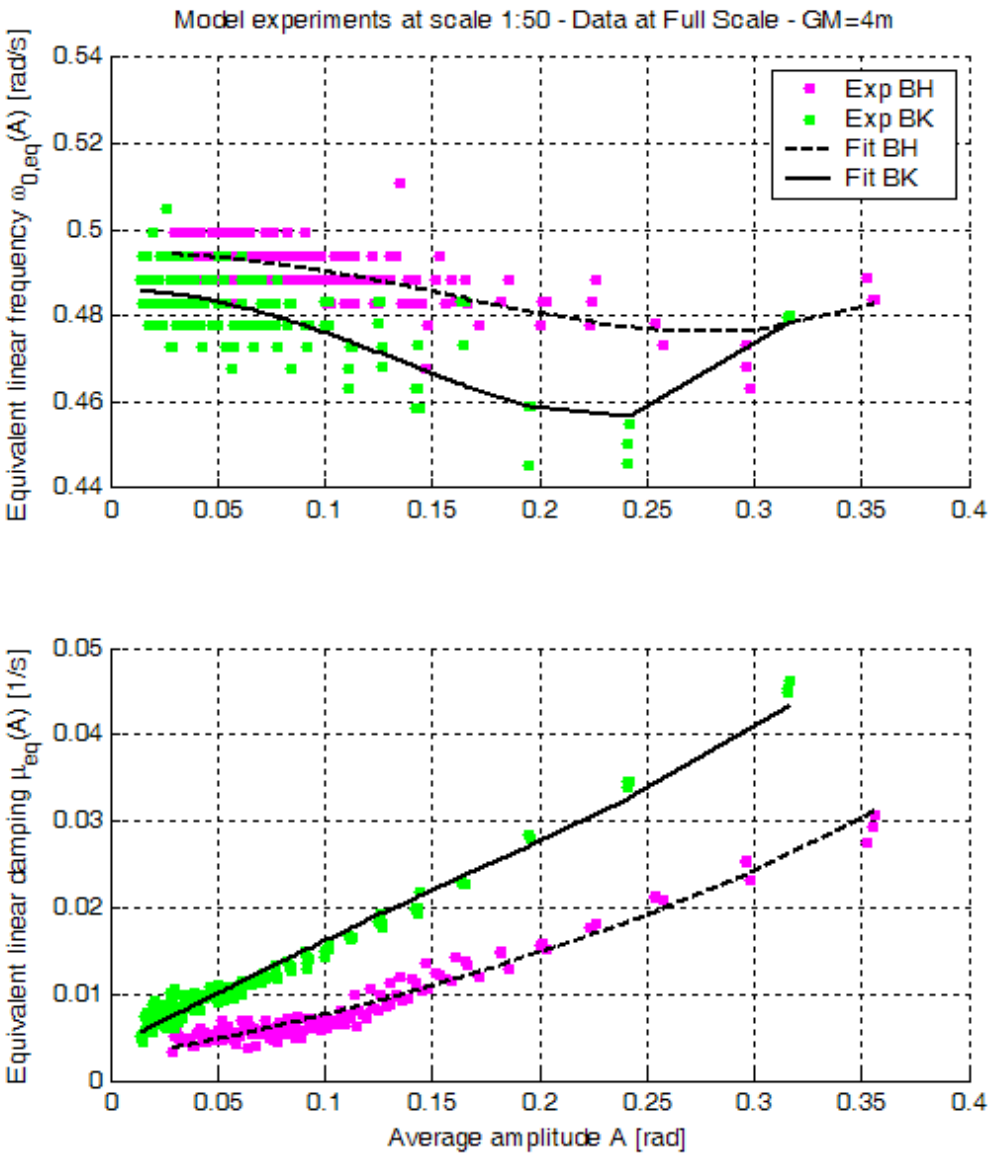

Figure 14: Analysis of decays. Effect of bilge keels. GM=4m, model scale 1:50.

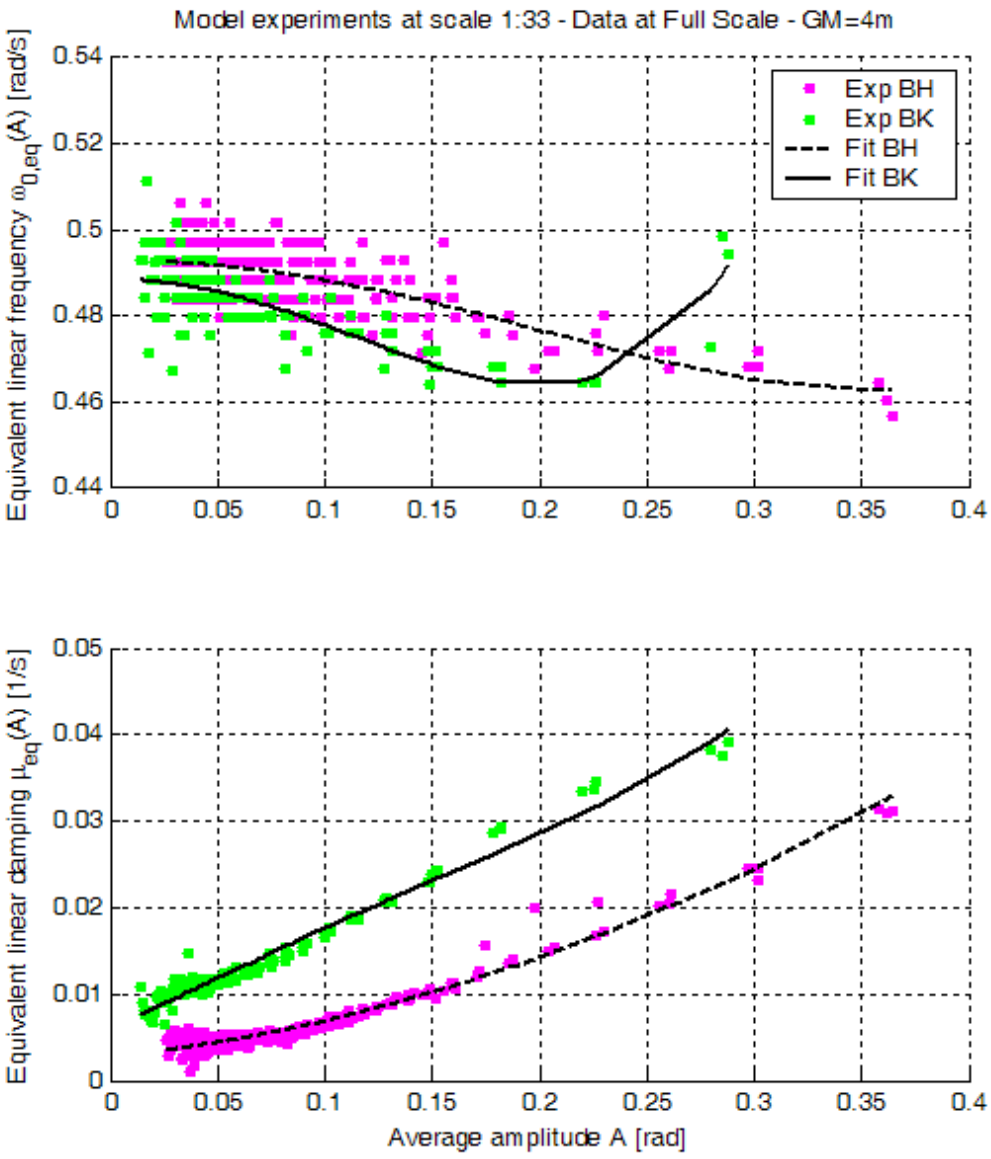

Figure 15: Analysis of decays. Effect of bilge keels. GM=4m, model scale 1:33.

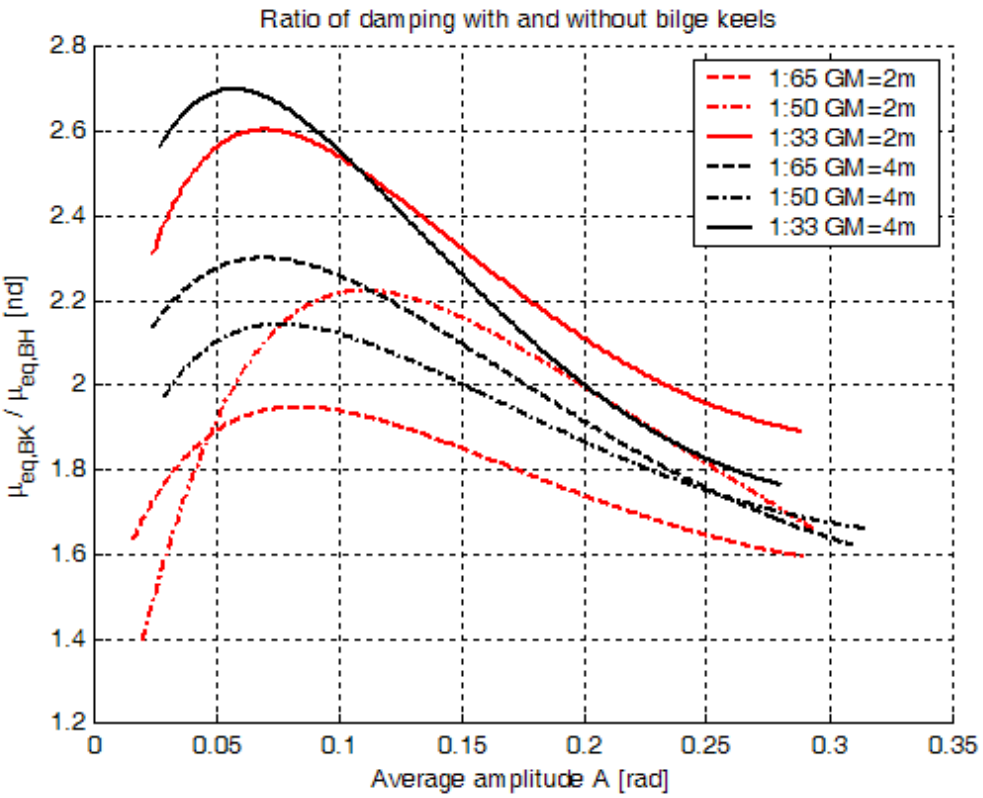

Figure 16: Analysis of decays. Effect of bilge keels. Ratio between equivalent linear damping with bilge keels and damping without bilge keels.

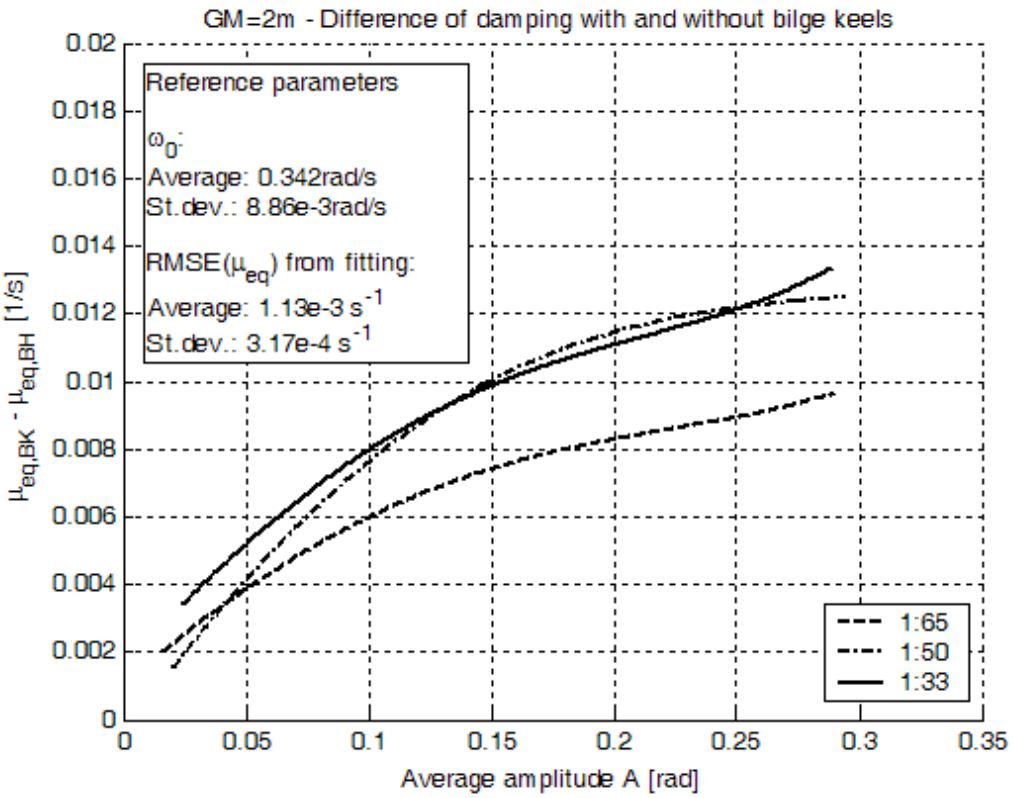

Figure 17: Analysis of decays. Effect of bilge keels. GM=2m. Additional equivalent linear damping due to the fitting of bilge keels.

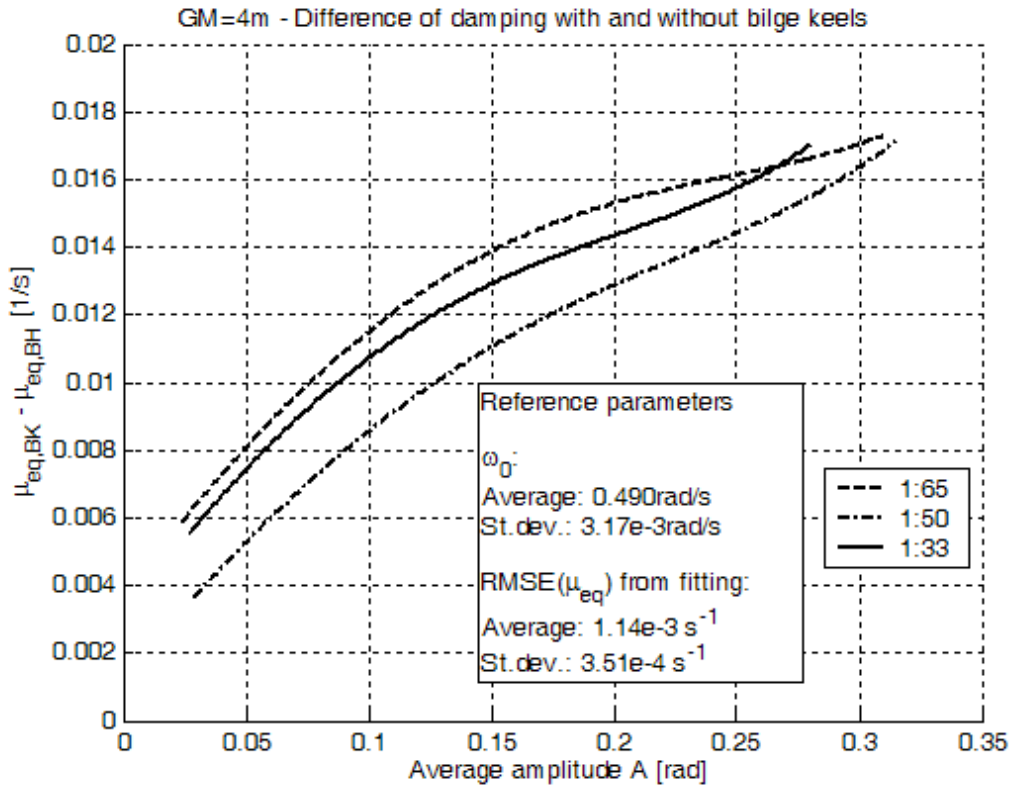

Figure 18: Analysis of decays. Effect of bilge keels. GM=4m. Additional equivalent damping due to the fitting of bilge keels.

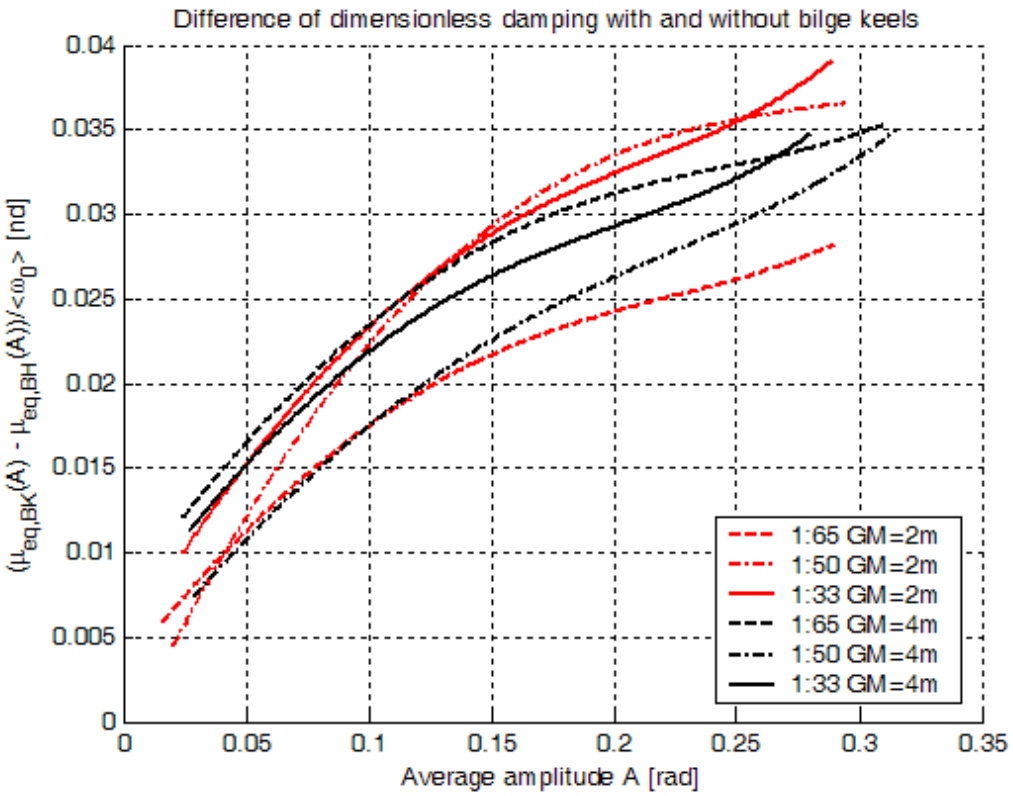

Figure 19: Analysis of decays. Effect of bilge keels. All conditions. Additional nondimensional equivalent linear damping due to the fitting of bilge keels.

It is possible to provide a first series of comments looking at Figure 6 to Figure 19:

- The experimentally imposed roll natural frequency ω_0 is quite well reproduced among different scales. The natural frequency in bare hull condition is always slightly larger than ω_0 after fitting of bilge keels, but the differences are usually very limited, with an average reduction of ω_0 of about 1%. The full scale average roll natural frequency ω_0 is 0.342rad/s with a coefficient of variation of 2.6% in case of $\overline{GM} = 2m$ (see, in particular, Figure 6, Figure 7 and Figure 17), while the full scale average roll natural frequency ω_0 is 0.490rad/s with a coefficient of variation of 0.6% in case of $\overline{GM} = 4m$ (see, in particular, Figure 8, Figure 9 and Figure 18).
- By looking at the scatter plots of the amplitude dependent natural oscillation frequency in Figure 10 to Figure 15 it is possible to disclose a systematic effect of the bilge keels. Apart from the already discussed small increase in the value of $\omega_0 = \omega_{0,eq}(A=0)$, bilge keels modified also the functional behaviour of $\omega_{0,eq}(A)$, or, it would be better to say, of $\omega_{0,eq}^2(A)/\omega_0^2$. This is likely to be associated to the fact that the model of $\omega_{0,eq}(A)$ based on the hydrostatic quantity $\overline{GZ}(\phi)/\overline{GM}$ is too simplified, since it neglects any (transient) hydrodynamic effect. However the differences of $\omega_{0,eq}(A)$ with and without bilge keels are sufficiently small to be of minor importance in practical applications.
- The dispersion of experimental data is significant, especially at small amplitude.
- The difference in the behaviour of $\mu_{eq}(A)$ when bilge keels are fitted with respect to the bare hull condition is evident (Figure 10 to Figure 15). While a linear+quadratic model seems to be sufficient to describe the dissipation mechanism in the case with bilge keels ($\mu_{eq,BK}(A)$), an additional cubic term is necessary to reproduce $\mu_{eq}(A)$ in bare hull condition ($\mu_{eq,BH}(A)$). The reason is mainly to be sought in the fact that $\mu_{eq,BH}(A)$ requires larger rolling amplitudes to show a significant derivative with respect to the amplitude A, while $\mu_{eq,BK}(A)$ shows a significant derivative already at small rolling amplitudes. It could be guessed that this behaviour is associated to a retardation in the vortex shedding in bare hull condition, while significant vortices generate even at small rolling amplitudes when bilge keels are fitted thanks to the strong separation points at the edges of the bilge keels. As a consequence, larger rolling amplitudes are necessary, in bare hull condition, to initiate a significant vortex shedding from the hull alone (at least far from the region of the skeg) and this could be associated to the quite large bilge radius (around 2.5m amidships). This ship, because of the large bilge radius, cannot be considered as a ship having "sharp bilges" according to the definition given in [4]. According to [4], a ship is indeed considered to have "sharp bilges" when the bilge radius is smaller than 1% of the ship's breadth (this meaning about 0.3m for the CEHIPAR2792 compared to the actual radius of about 2.5m) and the angle between the piece-wise lines representing the bilge is

smaller than 120deg (this angle is actually about 94deg for the CEHIPAR2792). Although the requirement concerning the angle is fulfilled, the bilge radius is too large, hence the tested hull form in bare hull condition should be considered as having "round bilges". It is also interesting to see that, at large rolling amplitudes, the curves of $\mu_{eq,BH}(A)$ and $\mu_{eq,BK}(A)$ tend to become almost parallel. Unfortunately the range of available rolling amplitudes from decays does not allow to draw a definite conclusion on this point, however it is extremely important to underline that the assumed linear+quadratic and linear+quadratic+cubic models cannot show such parallelism of $\mu_{eq,BH}(A)$ and $\mu_{eq,BK}(A)$. It is indeed unavoidable that, if $\delta > 0$, above a certain amplitude $\mu_{eq,BH}(A)$ becomes larger than $\mu_{eq,BK}(A)$. This is of course, in general, unreasonable and poses the well known problem of the extrapolation of damping models out of the tested range from decays.

- There is a tendency, as expectable, for the smaller model (scale 1:65), to have a larger equivalent linear equivalent damping than the largest model (scale 1:33) (see Figure 6 to Figure 9) especially in the range of small rolling amplitudes, where the effects of friction (and possibly surface tension) are more important. However this tendency is not always clear, also in view of the less systematic behaviour of the average size model (scale 1:50). In general the situation is quite fuzzy, and a systematic tendency cannot be seen also considering the relatively large dispersion of data at small rolling amplitudes.
- The effect of bilge keels is twofold. As already said, the fitting of bilge keels changes the functional dependence of $\mu_{eq}(A)$ and in addition, as expectable, increases the roll damping. However, looking at Figure 10 to Figure 15, and in particular to the summarising plots in Figure 16 to Figure 19, there is a significant dispersion of data among different scales. Analysing data in Figure 16 it can be seen that the percentage of increase of the linear damping coefficient due to the fitting of bilge keels shows a maximum around 3-5deg, with the case $\overline{GM} = 2m$, scale 1:50 showing an odd behaviour in comparison with the other cases. The relative increase of damping due to the fitting of bilge keels reduces at small rolling amplitude. This can be understood when thinking to the fact that the additional wave-making and skin friction, which usually dominates at small rolling amplitudes, as given by the bilge keels are relatively small in comparison to the contribution from the hull. On the other side, the additional damping effect of bilge keels reduces, in percentage, also at larger rolling amplitudes. This is due to the increase of the bare hull damping at large rolling amplitudes, likely thanks to the increase in vortex shedding, as already discussed when commenting the differences in the functional behaviour of $\mu_{eq,BH}(A)$ and $\mu_{eq,BK}(A)$. The reason for the reduction in the ratio $\mu_{eq,BK}(A)/\mu_{eq,BH}(A)$ for large rolling amplitudes can be understood looking at Figure 17 and Figure 18. First of all it is important to note the significant dispersion, in Figure 17 and Figure 18, among different scales, without a clear systematic behaviour. On the other hand, what is visible in all cases, is a tendency towards a saturation effect of the additional contribution of the bilge keels, with a less than linear behaviour at large rolling angles (tails of the curves at large rolling amplitudes should be considered with caution because they are to some extent governed by the a-priori

selection of the damping model, and the reader should concentrate on the inner part of the tested range). Figure 19 aggregates data of Figure 17 and Figure 18 by using a nondimensionalization based on the average natural frequency ω_0. Although curves in Figure 19 show a significant dispersion, data for $\overline{GM} = 2m$ and $\overline{GM} = 4m$ tend to converge when reported in nondimensional form. It is interesting to underline the already noticed saturation effect and also the likely (since we discuss of an extrapolation) non-zero additional damping at $A = 0$, that could be associated to additional wave-making and friction due to the fitting of bilge keels. Using data reported in Figure 17 and Figure 18, and assuming that the dispersion of ω_0 for a given metacentric height is negligible, it is possible to associate an average RMSE to the curves in Figure 19 of about $\sqrt{2} \cdot \frac{1}{2} \cdot \left(\frac{1.13}{0.342} + \frac{1.14}{0.490} \right) \cdot 10^{-3} = 4 \cdot 10^{-3}$, where the factor $\sqrt{2}$ is considered in order to take into account the difference operation between assumed independent approximately Gaussian random variables. According to this (though quite rough) estimate it can be seen that the differences in the curves in Figure 19 are, in general, at the limit of the significance considering the 95% uncertainty band associated to each curve (i.e. $\approx \pm 7.8 \cdot 10^{-3}$).

- It is also to be underlined that a possible reason for the not systematic differences in the obtained results could be sought in a not perfect reproduction and/or positioning of bilge keels at different scales. On this aspect unfortunately there are no information at the moment of writing.

The analysis of the decrement curves allowed having a first impression of the behaviour of the experimental results, however, in order to provide a more quantitative assessment of the fitted models it is necessary to analyse the obtained fitted coefficients from each condition. Since we are interested in possible scale effects it will be convenient to plot the obtained data as functions of the model scale. All the numerical values of the coefficients obtained from the fitting of the experimental data are reported in

Table 4.

Table 4: Fitted coefficients for all the tested conditions. Red cells correspond to coefficients not used in the a-priori selected models.

	GM [m]	Append.		ω_0 [rad/s]	μ [1/s]	β [1/rad]	δ [s/rad^2]	γ_3 [1/rad^2]	γ_5 [1/rad^4]
Scale 1:65	2	BH	**Fitted coefficient**	**0.3464**	**0.002738**	**0.1820**	**2.415**	**-7.274**	**46.42**
			Lower bound 95%-CI	0.3446	0.002468	0.1430	1.923	-8.868	26.24
			Upper bound 95%-CI	0.3483	0.003007	0.2210	2.907	-5.681	66.59
	4	BH	**Fitted coefficient**	**0.4907**	**0.004313**	**0.1554**	**1.849**	**-3.206**	**19.22**
			Lower bound 95%-CI	0.4898	0.003992	0.1266	1.621	-3.715	13.17
			Upper bound 95%-CI	0.4916	0.004633	0.1844	2.076	-2.696	25.28
	2	BK	**Fitted coefficient**	**0.341**	**0.003808**	**0.6133**	**0**	**-10.14**	**85.47**
			Lower bound 95%-CI	0.3394	0.003556	0.5877	0	-12.34	48.98
			Upper bound 95%-CI	0.3426	0.004059	0.6389	0	-7.949	121.9
	4	BK	**Fitted coefficient**	**0.4887**	**0.007975**	**0.6269**	**0**	**-6.930**	**60.55**
			Lower bound 95%-CI	0.4872	0.007627	0.6030	0	-8.250	41.36
			Upper bound 95%-CI	0.4901	0.008324	0.6508	0	-5.610	79.74
Scale 1:50	2	BH	**Fitted coefficient**	**0.3525**	**0.003544**	**0.07376**	**3.738**	**-7.229**	**63.31**
			Lower bound 95%-CI	0.3512	0.003078	0.007513	2.889	-8.396	45.29
			Upper bound 95%-CI	0.3537	0.004011	0.1400	4.587	-6.061	81.33
	4	BH	**Fitted coefficient**	**0.4946**	**0.002516**	**0.1874**	**1.353**	**-2.479**	**18.80**
			Lower bound 95%-CI	0.4935	0.001936	0.1443	1.055	-2.998	13.03
			Upper bound 95%-CI	0.4958	0.003097	0.2305	1.652	-1.961	24.58
	2	BK	**Fitted coefficient**	**0.3504**	**0.003135**	**0.7509**	**0**	**-9.949**	**83.03**
			Lower bound 95%-CI	0.3485	0.002756	0.7159	0	-12.26	46.31
			Upper bound 95%-CI	0.3523	0.003513	0.7859	0	-7.639	119.8
	4	BK	**Fitted coefficient**	**0.4859**	**0.003749**	**0.6163**	**0**	**-5.832**	**64.94**
			Lower bound 95%-CI	0.4847	0.003475	0.6007	0	-6.749	52.25
			Upper bound 95%-CI	0.4872	0.004023	0.6318	0	-4.914	77.63
Scale 1:33	2	BH	**Fitted coefficient**	**0.3334**	**0.002075**	**0.1301**	**3.304**	**-7.206**	**41.51**
			Lower bound 95%-CI	0.3317	0.001681	0.07887	2.688	-8.422	27.40
			Upper bound 95%-CI	0.3351	0.00247	0.1813	3.921	-5.990	55.62
	4	BH	**Fitted coefficient**	**0.4928**	**0.002826**	**0.1040**	**2.132**	**-2.539**	**12.27**
			Lower bound 95%-CI	0.4918	0.002474	0.0736	1.903	-3.037	6.718
			Upper bound 95%-CI	0.4937	0.003178	0.1343	2.361	-2.041	17.83
	2	BK	**Fitted coefficient**	**0.3311**	**0.003629**	**0.7048**	**0**	**-10.79**	**97.21**
			Lower bound 95%-CI	0.3299	0.003312	0.6734	0	-12.42	70.04
			Upper bound 95%-CI	0.3323	0.003946	0.7361	0	-9.160	124.4
	4	BK	**Fitted coefficient**	**0.4884**	**0.005879**	**0.5781**	**0**	**-6.502**	**97.32**
			Lower bound 95%-CI	0.487	0.005537	0.5597	0	-7.542	79.72
			Upper bound 95%-CI	0.4898	0.006221	0.5965	0	-5.463	114.9

First of all we analyse the fitted roll natural frequency ω_0 for the various conditions, as reported in Figure 20 and Figure 21.

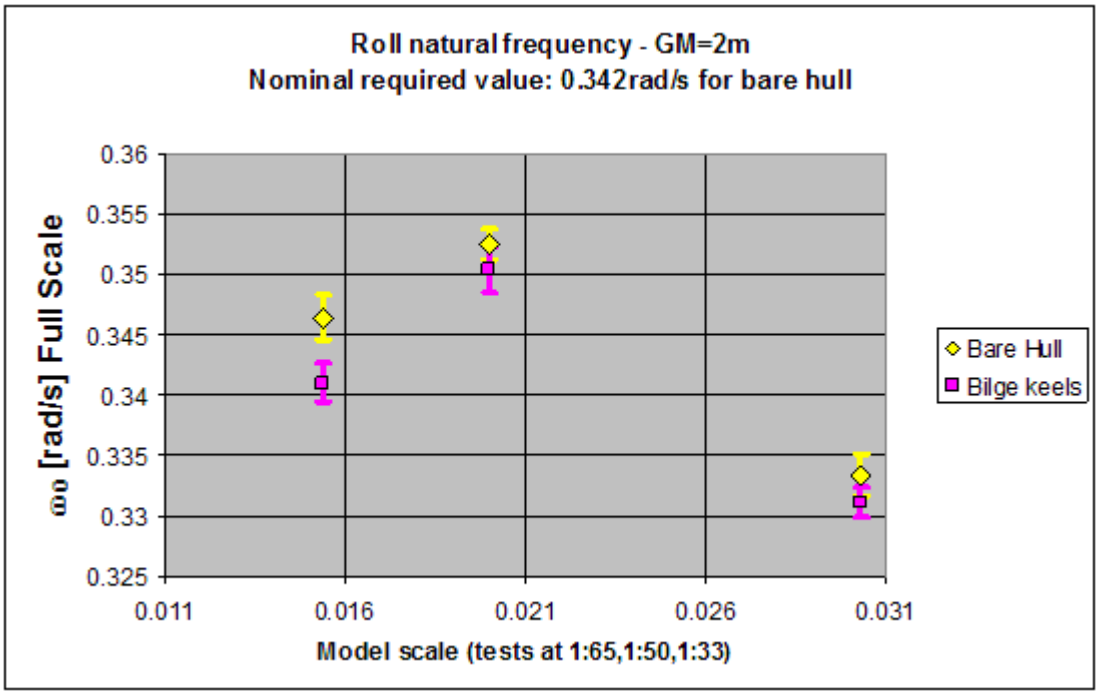

Figure 20: Fitted roll natural frequency ω_0 in case of $\overline{GM} = 2m$.

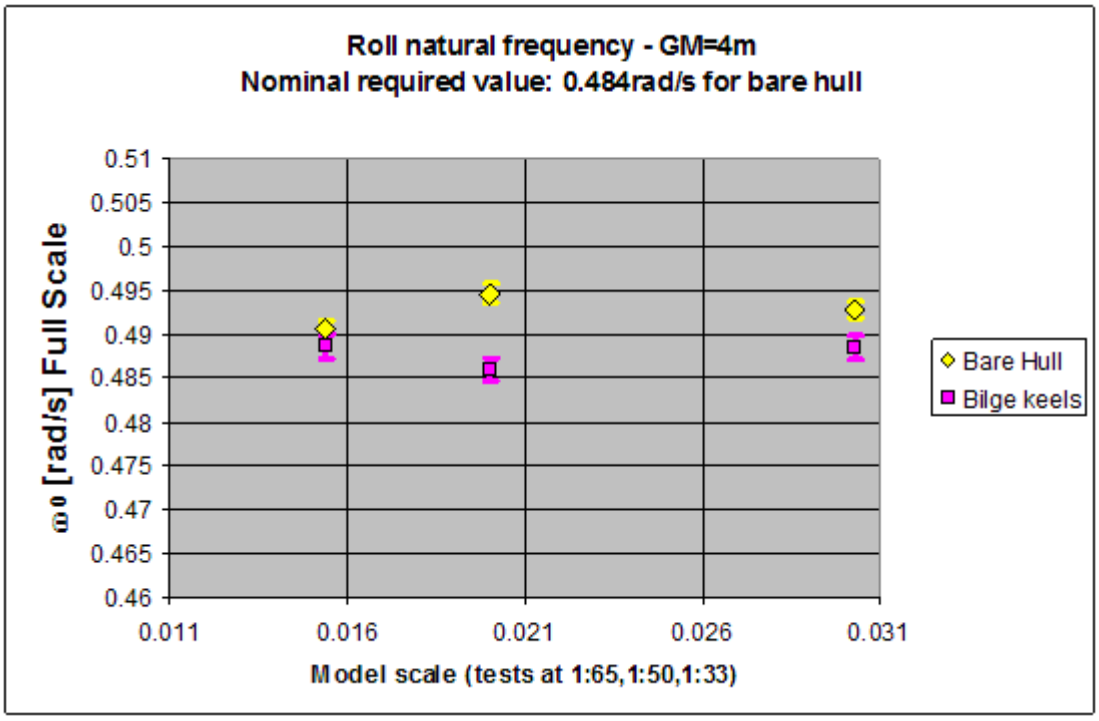

Figure 21: Fitted roll natural frequency ω_0 in case of $\overline{GM} = 4m$.

The natural frequency ω_0 is a parameter ideally expected to be the same for all the scales for a given metacentric height in bare hull condition, because it was experimentally imposed by a trial and error procedure according to the nominal values of 0.342rad/s ($\overline{GM} = 2m$) and 0.484rad/s ($\overline{GM} = 4m$). The actual natural frequency ω_0 as obtained from the analysis of roll decays is always slightly higher than the required nominal value, with the exception of the case $\overline{GM} = 2m$ and scale 1:33 where it was impossible to increase the natural frequency due to limitations in the arrangements of masses onboard the model. The reason for the small systematic difference is immediately clear when looking at the dependence of the oscillation frequency on the amplitude in Figure 6 and Figure 8. The estimated natural frequency of the model was set by a trial and error procedure letting the model oscillate at "sufficiently small" rolling amplitudes, until the required nominal frequency was obtained with sufficient accuracy. However, according to Figure 6 and Figure 8, the oscillation frequency is always smaller than ω_0, i.e. $\forall \text{tested } A : \omega_{0,eq}(A) \le \omega_0 = \omega_{0,eq}(A=0)$. This means that, setting the natural frequency according to the measured oscillation period at "sufficiently small" rolling amplitude, but not at an infinitesimally small oscillation amplitude, leads to an experimental underestimation of the actual natural frequency ω_0 for ships, as it is the CEHIPAR2792, having softening (less-than-linear) restoring. In addition, part of the underestimation of ω_0 could come from the, though small, difference between damped oscillation frequency and undamped oscillation frequency. Fortunately, however, when the oscillation amplitude is small enough the error is limited, and in

this case the error between the actual fitted value of ω_0 and the corresponding nominal value is below 3% in all cases.
Figure 20 and Figure 21 also report the 95% confidence intervals for the fitted coefficient ω_0. It is very important not to confuse these confidence intervals with those associated to the residual dispersion of data around the assumed fitted model, these latter being represented by the RMSE. As can be seen, the confidence interval for the fitted coefficient ω_0 are extremely small, thus the natural frequency ω_0, as fitted parameter, can well be approximated as a parameter known with zero uncertainty. This approximation will be used later when constructing nondimensional linear and nonlinear damping coefficients, together with associated confidence intervals, starting from the corresponding dimensional values obtained from the direct fitting of $\mu_{eq}(A)$.
Before moving to the analysis of damping coefficients, it is worth briefly discussing the remaining parameters associated to the restoring, namely γ_3 and γ_5, as shown in Figure 22 to Figure 25. It is important to give a correct interpretation of the "confidence interval" indicated in each figure for the coefficients obtained from the fitting of hydrostatically computed restoring. Of course this type of fitting is not associated to any random error, because $\overline{GZ}$ is a deterministic quantity. On the other hand the selection a quintic polynomial to reflect the actual behaviour of $\overline{GZ}$ is just an approximation and it does not completely "explain" the shape of $\overline{GZ}$. In the least-square fitting the final disagreement between the fitted selected model and the actual deterministic quantity to be fitted is seen as a residual "unexplained" dispersion of data. The lack of capability of the selected model to reproduce exactly the shape of $\overline{GZ}$ finally leads the least-square procedure to produce "confidence intervals" for the fitted coefficients as if there were some randomness in the data, which is also assumed to be Gaussian. However, the observed residual dispersion in the fitting of $\overline{GZ}$ reflects nothing but the so called "model uncertainty". The "model uncertainty" is a portion of the so called "epistemic uncertainty". The "epistemic uncertainty" contains the "model uncertainty" and, in addition, the "statistical uncertainty". While the "statistical uncertainty" is missing in the fitting of hydrostatically calculated $\overline{GZ}$, it is instead present in the determination of γ_3 and γ_5 from the analysis of roll decays. Of course the residuals associated to the "model uncertainty" are neither random, nor normally distributed, hence the application of standard Gaussian confidence intervals is theoretically inappropriate. Nevertheless we have decided, for sake of consistency, to report the "confidence intervals" also when fitting $\overline{GZ}$ because the "model uncertainty" is necessarily embedded also in the confidence intervals determined by the least-square procedure for γ_3 and γ_5 when analysing roll decays. Accordingly, part of the uncertainty in the fitting of γ_3 and γ_5 from roll decays is inherent to the limitations of the selected quintic model. It must however be borne in mind that in case of the fitting of hydrostatically calculated $\overline{GZ}$ the indication "95% confidence intervals" must not be misunderstood. Indeed, being the residuals neither random not normally distributed, the requirements needed for a proper calculation of confidence intervals are not fulfilled. For this reason the reported confidence intervals must be understood simply as a measure of dispersion of the original $\overline{GZ}$ with respect to the fitted model. They are indicated as "CI@95%" only to recall that, in the least square

procedure, they have been *algorithmically* calculated with standard Gaussian techniques at a confidence level of 95%.

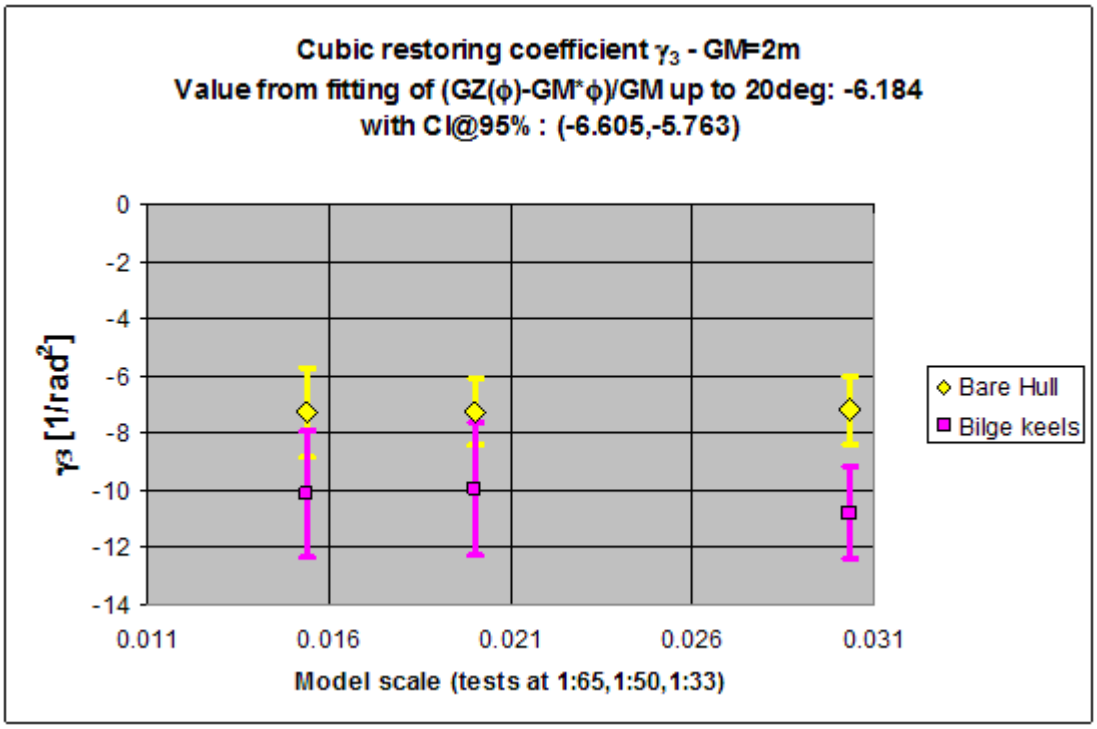

Figure 22: Fitted cubic restoring coefficient γ_3 in case of $\overline{GM} = 2m$.

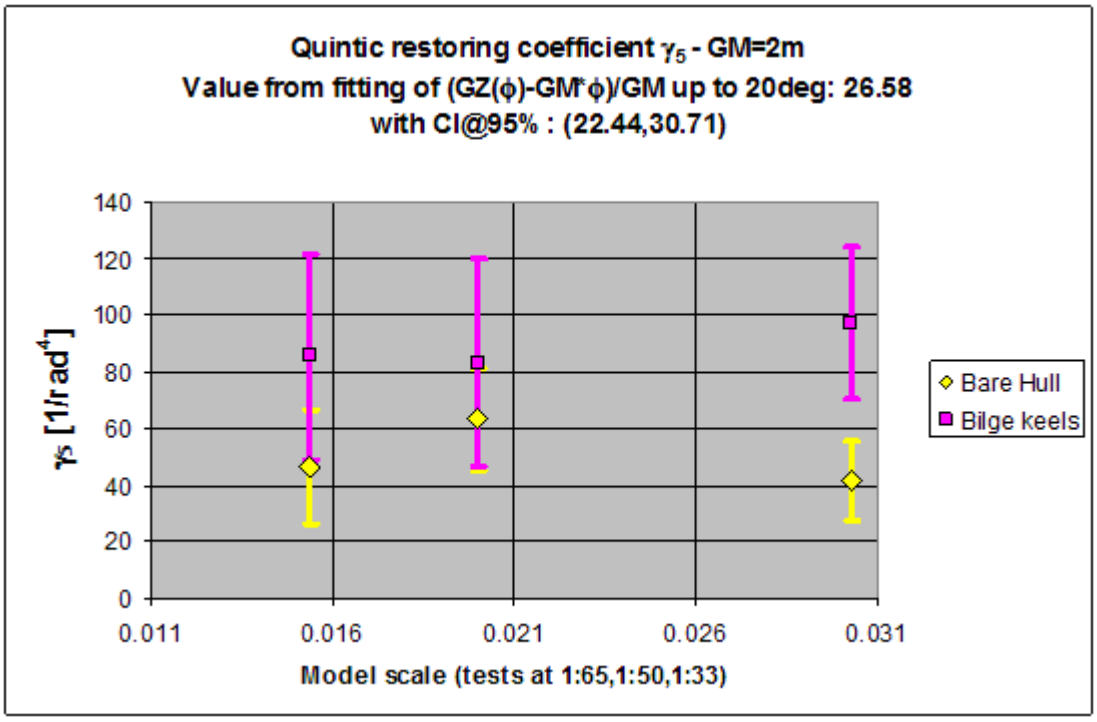

Figure 23: Fitted quintic restoring coefficient γ_5 in case of $\overline{GM} = 2m$.

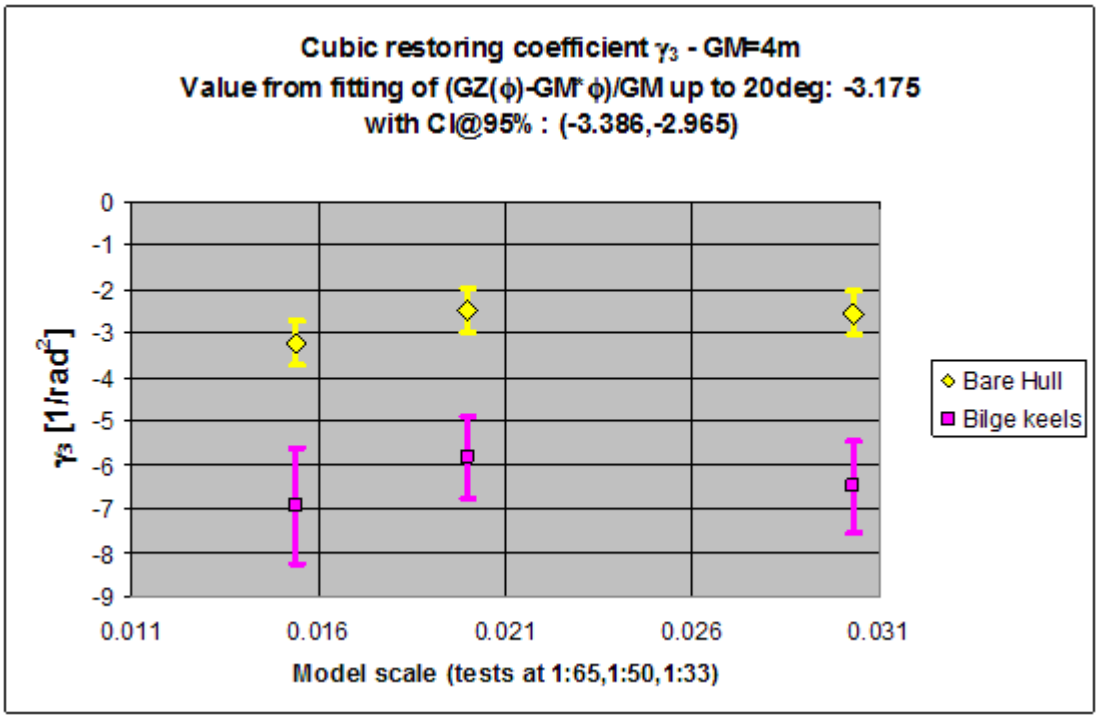

Figure 24: Fitted cubic restoring coefficient γ_3 in case of $\overline{GM} = 4m$.

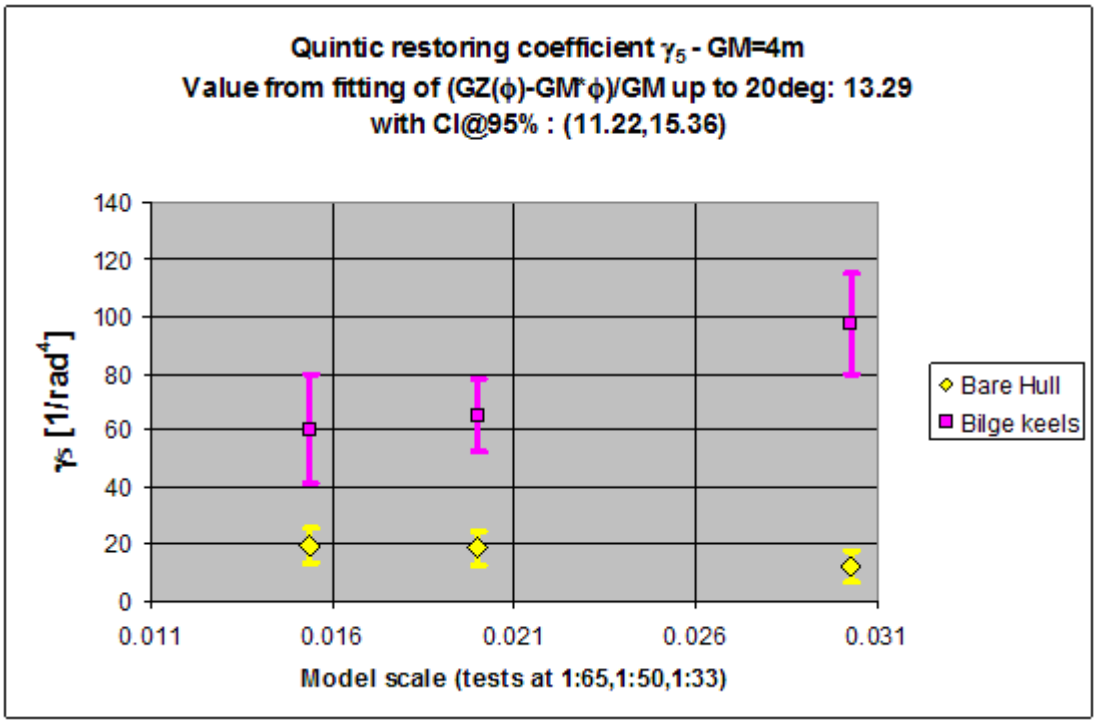

Figure 25: Fitted quintic restoring coefficient γ_5 in case of $\overline{GM} = 4m$.

It can be seen that there is an overall consistency among data for different scales, and there is a systematic modification of the parameters when changing the model condition from bilge keels to bare hull. However, the fitting of bilge keels should have very little to do with the restoring itself, hence the systematic differences observed for γ_3 and γ_5 are likely to be associated to a general oversimplification introduced by the

1-DOF modelling with constant coefficients, possibly concerning transient (nonstationary) hydrodynamic effects. When comparing the fitted coefficients in Figure 22 to Figure 25 with the corresponding values obtained from the hydrostatically computed $\overline{GZ}$ curve, it can be seen that the differences are, in general not negligible. However, it is important to notice that there is a compensation between the error in γ_3 and the error in γ_5, and this compensation is typical when there are difficulties in separating different nonlinear contributions. Interestingly this sort of compensation is also evident in the modification of coefficients γ_3 and γ_5 when changing the condition from bare hull to bilge keels: a reduction of γ_3 is always associated to an increase in γ_5. In Figure 26 and Figure 27, the hydrostatically computed nondimensional restoring $r(\phi) = \overline{GZ}(\phi) / \overline{GM}$ is compared with the reconstructed one, $r(\phi) = \phi + \gamma_3 \cdot \phi^3 + \gamma_5 \cdot \phi^5$, using fitted coefficients as in

Table 4. As anticipated the differences in γ_3 and γ_5 globally compensate to give, finally, a reconstructed restoring that closely reproduce the hydrostatically computed one for the two tested values of metacentric height. This is true up to an angle of about 10-15deg. For larger angles the quintic term with positive γ_5 dominates, and the reconstructed restoring curves all tend to a strong increase. This behaviour is associated on one side to the selection of a model limited to a fifth degree, and on the other side the increase of reconstructed $r(\phi)$ is associated to the fact that the measured oscillation frequency for the first few cycles tends to be larger than the one in the immediately following cycles and this is particularly evident when the model is fitted with bilge keels (see, e.g., Figure 9). However, in the inner portion of the tested range or rolling amplitudes, the agreement between the hydrostatically computed $r(\phi)$ and the reconstructed curves is good.

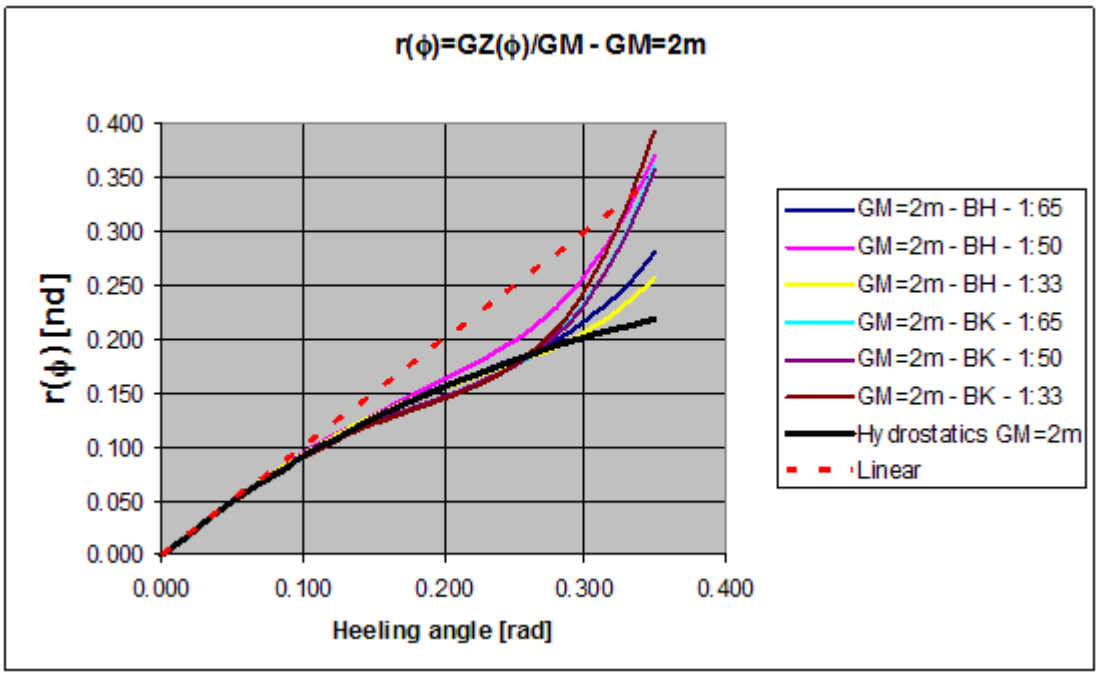

Figure 26: Reconstructed restoring and comparison with hydrostatic calculations. $\overline{GM} = 2m$.

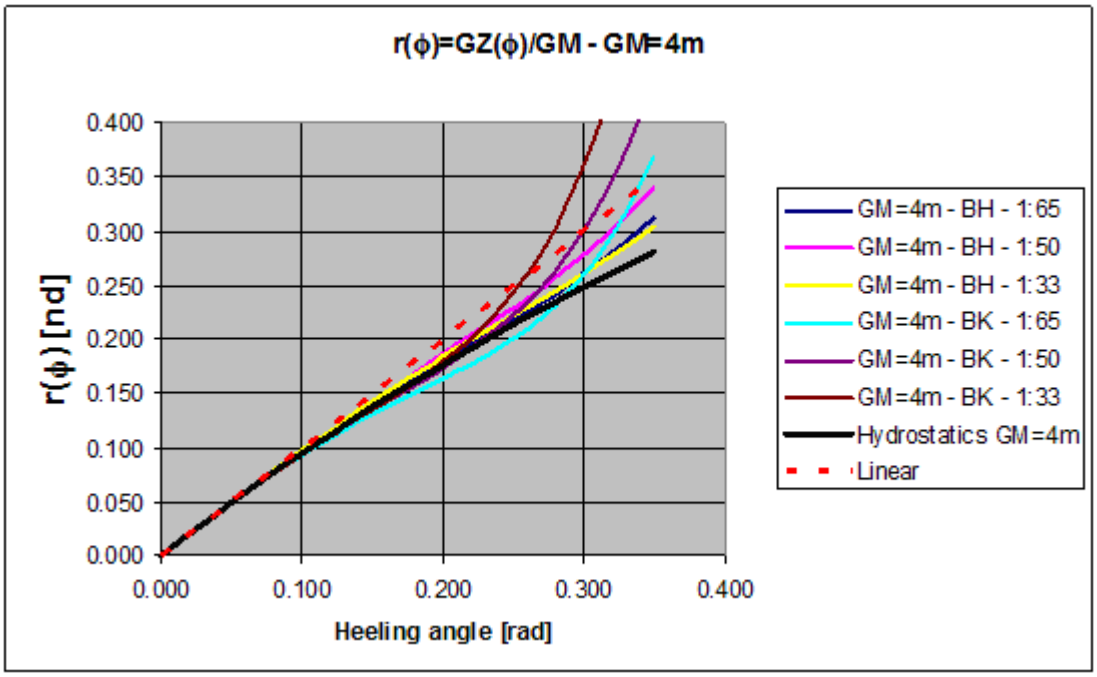

Figure 27: Reconstructed restoring and comparison with hydrostatic calculations. $\overline{GM} = 4m$.

These observations lead to a series of comments:

- The restoring coefficients determined from the fitting of $\overline{GZ}$ are not in good agreement with the experimental determined values when taken alone, but due to the interrelation of the parameters for the model of restoring, the dependence of the oscillation frequency on the amplitude can be predicted with reasonable accuracy using $\overline{GZ}$, at least after the first few roll cycles .
- The linear+quadratic+quintic model for the restoring, with constant coefficients, is likely to be an oversimplification, but it seems to be suitable for practical applications.
- There is not a good separation capability between cubic and quintic restoring terms.

After discussing the model for restoring, let us going on with the discussion of the parameters of the damping model(s). We start with the fitted parameters in the case of bare hull condition, as reported in Figure 28 to Figure 30. As anticipated, the 95% confidence intervals for the nondimensional coefficients μ / ω_0 and $\delta \cdot \omega_0$ have been calculated from the dimensional confidence intervals obtained in the fitting procedure for μ and δ simply by dividing / multiplying by the fitted value of ω_0, considering that the uncertainty in the fitted parameter ω_0 is sufficiently small to be neglected.

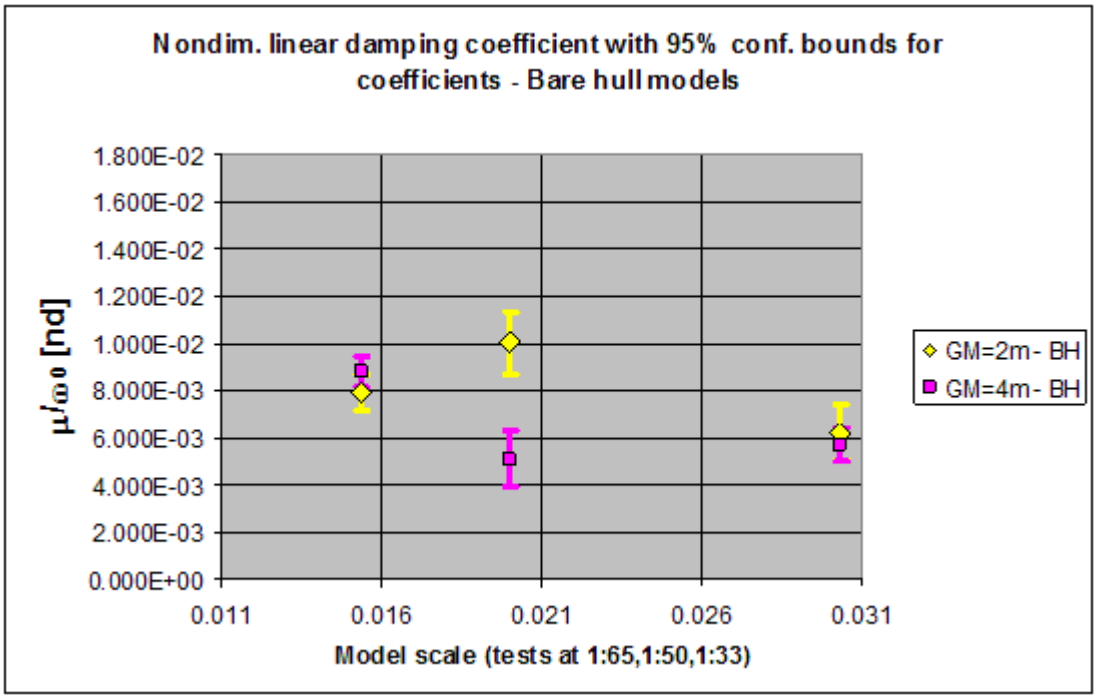

Figure 28: Nondimensional linear damping coefficient μ / ω_0. Bare hull condition.

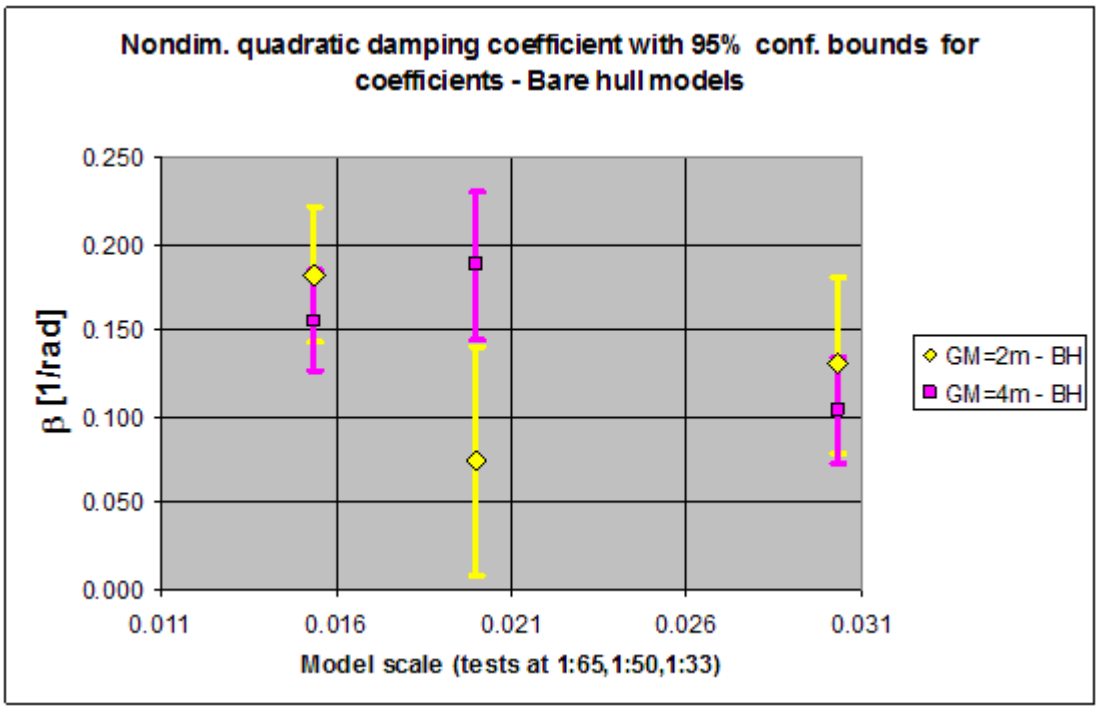

Figure 29: Nondimensional quadratic damping coefficient β. Bare hull condition.

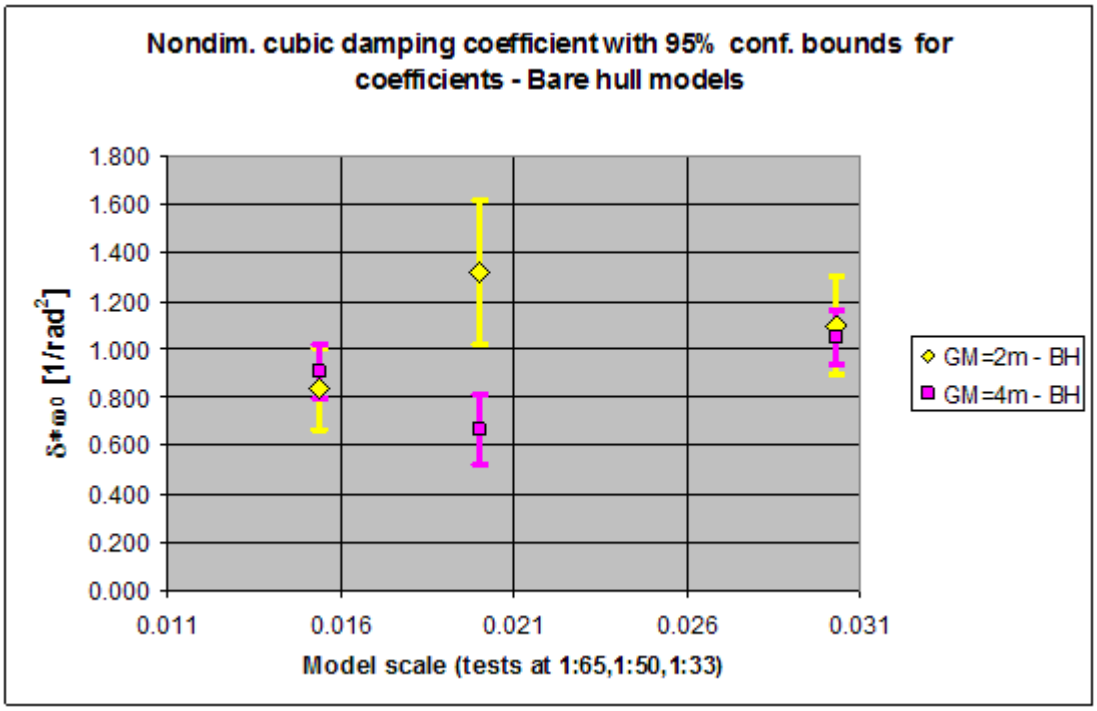

Figure 30: Nondimensional cubic damping coefficient $\delta \cdot \omega_0$. Bare hull condition.

According to the results in Figure 28 to Figure 30, it is possible to make a series of comments:

- There seems to be a trend for μ / ω_0 (Figure 28) towards a decreasing as the model size increases, with a relative difference between the value for the largest and the smallest model of the order of 30% with respect to the average value.
- When looking at β and $\delta \cdot \omega_0$ (Figure 29 and Figure 30 respectively) it is possible to notice that the confidence intervals for the fitted coefficients are quite large in comparison with the confidence intervals for μ / ω_0 (Figure 28). Moreover, it can be seen that the largest uncertainty is associated to the medium size model (scale 1:50), in bare hull condition with $\overline{GM} = 2m$, and it is interesting to link this characteristic with the odd behaviour observed for this model in Figure 16. Moreover, although there seems to be a decrease in the coefficient β as the size of the model increases, there is an opposite tendency for the coefficient $\delta \cdot \omega_0$ that prevents any definite conclusion at this stage. This competing behaviour of the quadratic and cubic damping coefficients as obtained from the fitting of the decays is likely a consequence of the well known difficulty in separating different nonlinear contributions to the damping (see, e.g., [18][24]).

After the bare hull condition, Figure 31 and Figure 32 show the obtained coefficients for the linear+quadratic damping model for models fitted with bilge keels.

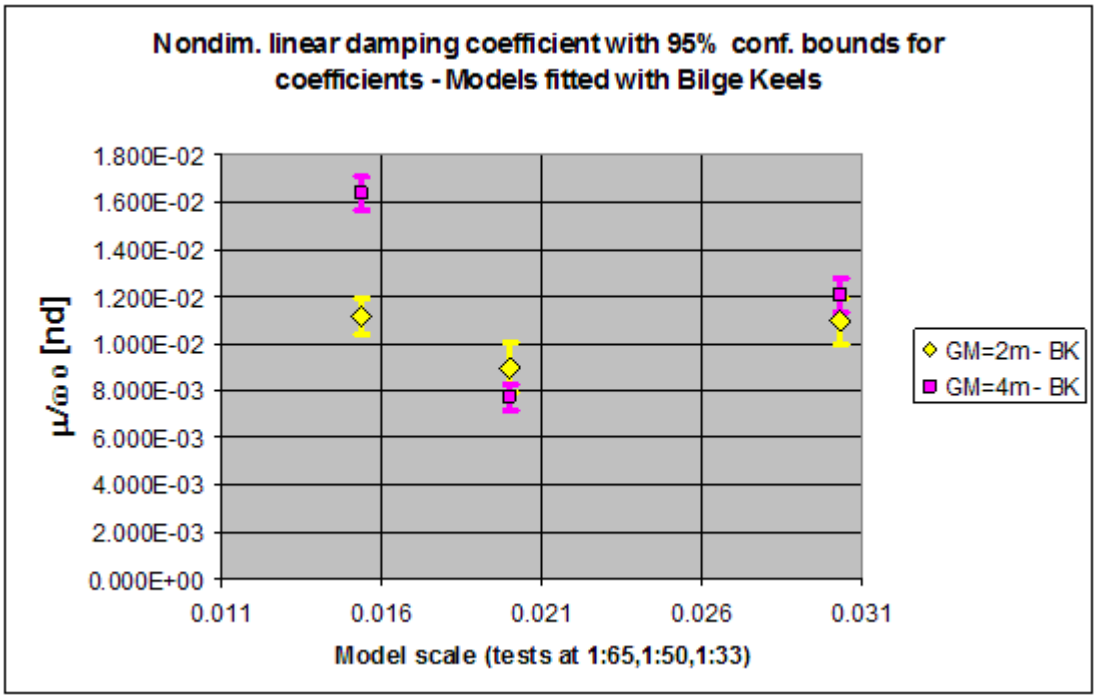

Figure 31: Nondimensional linear damping coefficient μ/ω_0. Models with bilge keels.

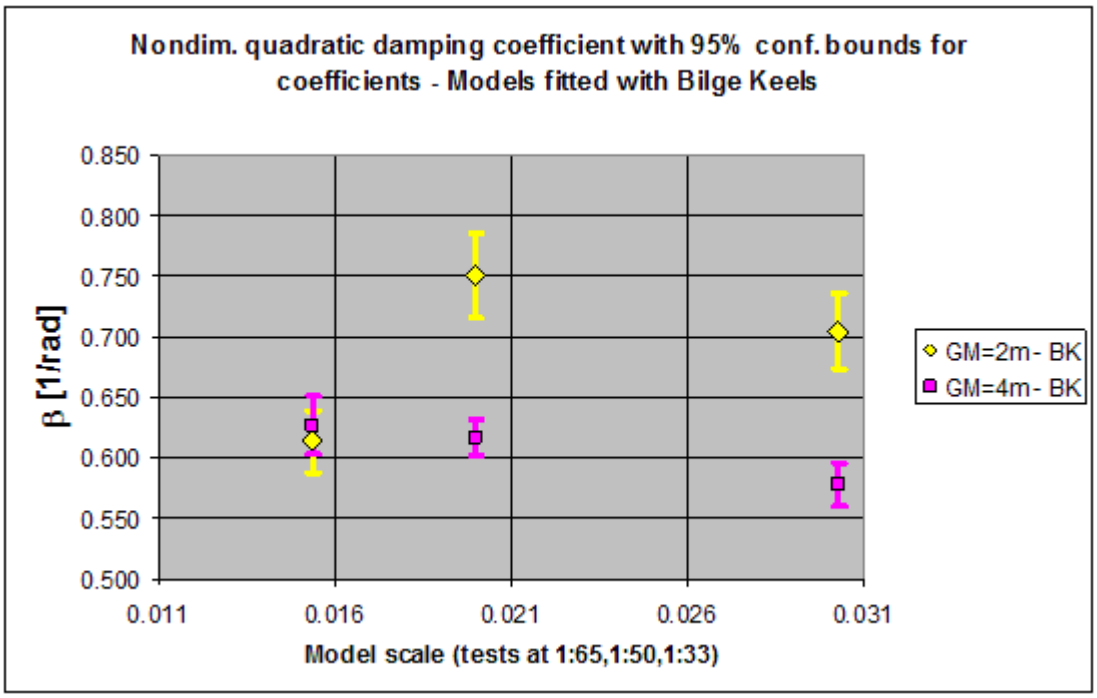

Figure 32: Nondimensional quadratic damping coefficient β. Models with bilge keels.

According to the results in Figure 31 and Figure 32:

- It is not possible to see a clear trend for μ/ω_0, although there seems to be a tendency towards a decreasing as the model size increases.
- Also in case of β it is not possible to see a clear trend.
- However, it must be stressed that the increase of the average μ/ω_0 for the smallest model (scale 1:65) is accompanied by a decrease of the average

quadratic damping coefficient β with respect to the other models (especially for the case $\overline{GM} = 2m$). This behaviour could indicate a problem in the separation of the linear and nonlinear component of damping model, or some problem in the actual reproduction of the geometry of bilge keels at different scales, or some effect of the relative thickness of the boundary layer.

- In case of scales 1:50 and 1:33, bilge keels seem to be more effective for $\overline{GM} = 2m$ leading to a larger β in comparison with the cases with $\overline{GM} = 4m$.

According to the obtained results it is difficult to see any clear trend on single damping coefficients. In addition, when discussing the behaviour of nonlinear damping coefficients, an opposite trend of the coefficients β and $\delta \cdot \omega_0$ as the scale of the model was changed, was noticed. In order to aggregate the effect of the changes of all the damping coefficients we have therefore calculated the linear equivalent damping coefficient $\mu_{eq}(A)$ for three different rolling amplitudes, namely 0deg, 5 deg and 15deg (for $A = 0$ it is actually $\mu_{eq}(A = 0) = \mu$), and we have compared the results. The amplitude dependent equivalent damping coefficient $\mu_{eq}(A)$ comprises the effects of all the damping coefficients used in the modelling (see (43)), and it is therefore a global quantity that is expected to partially cope with separation problems on different damping components. Some simplifying assumptions have been used in the process of calculation of $\mu_{eq}(A)$ and it is hence worth to explicitly report the complete procedure. For each tested condition, given the fitting of the amplitude dependent equivalent roll natural frequency and of the amplitude dependent linear damping coefficient, the following coefficients were available: $\omega_0, \gamma_3, \gamma_5, \mu, \beta, \delta$ with $\delta = 0$ in the bare hull condition. The linear equivalent damping coefficient $\mu_{eq}(A)$ was calculated under the approximation that the undamped ($\omega_{0,eq}(A)$) and the damped ($\widetilde{\omega}(A)$) amplitude dependent roll frequency were not significantly different, i.e.:

$$\omega_{0,eq}^2(A) = \omega_0^2 \cdot \left(1 + \frac{3}{4} \cdot \gamma_3 \cdot A^2 + \frac{5}{8} \cdot \gamma_5 \cdot A^4\right)$$

$$\widetilde{\omega}(A) = \sqrt{\omega_{0,eq}^2(A) - \mu_{eq}^2(A)} \approx \omega_{0,eq}(A)$$

$$\mu_{eq} = \mu + \frac{4}{3\pi} \cdot \beta \cdot \left(\widetilde{\omega}(A) \cdot A\right) + \frac{3}{8} \cdot \delta \cdot \left(\widetilde{\omega}(A) \cdot A\right)^2 \approx \tag{3}$$

$$\approx \mu + \frac{4}{3\pi} \cdot \beta \cdot \left(\omega_{0,eq}(A) \cdot A\right) + \frac{3}{8} \cdot \delta \cdot \left(\omega_{0,eq}(A) \cdot A\right)^2$$

The approximation $\widetilde{\omega}(A) \approx \omega_{0,eq}(A)$ in (3) was used in order to avoid solving a polynomial equation for $\mu_{eq}(A)$. In the presentation of the results $\mu_{eq}(A)$ has been made dimensionless by dividing it by the fitted natural frequency ω_0. Strictly

speaking a nondimensionalization based on $\omega_{0,eq}(A)$ would be physically more consistent with (34), however, in the framework of the following analysis, the use of ω_0 was considered to be more effective for the presentation and use of the results. In the presentation of the calculated $\mu_{eq}(A)$ according to (3), the uncertainty in the data has been considered as a band of $\pm 1.96 RMSE$. As mentioned, this band is an approximation for the 95% confidence interval for any new experimental observation of $\mu_{eq}(A)$ according to the fitting (and shall not be confused with the 95% confidence intervals for the fitted coefficients of the assumed model). In using only $\pm 1.96 RMSE$ we have neglected the uncertainty in the fitted function, which is however small in comparison with $RMSE(\mu_{eq})$. The values of $RMSE(\mu_{eq})$ have already been reported in Figure 6 to Figure 9 for the tested conditions. Similarly to what has already been done, in the presentation of the results the uncertainty for ω_0 has been neglected, hence the following approximation has been used:

$$RMSE\left(\frac{\mu_{eq}(A)}{\omega_0}\right) \approx \frac{RMSE(\mu_{eq}(A))}{\omega_0} \tag{4}$$

According to (4) the 95% confidence intervals for $\mu_{eq}(A)/\omega_0$ can be approximated as $\pm 1.96 RMSE(\mu_{eq})/\omega_0$.

Results of this analysis are reported in Figure 33 to Figure 35 for conditions with $\overline{GM} = 2m$ and in Figure 36 to Figure 38 for conditions with $\overline{GM} = 4m$. In each figure *linear regression fits are reported only as qualitative indications of the trend, and there is absolutely no intention to provide any means for extrapolation*.

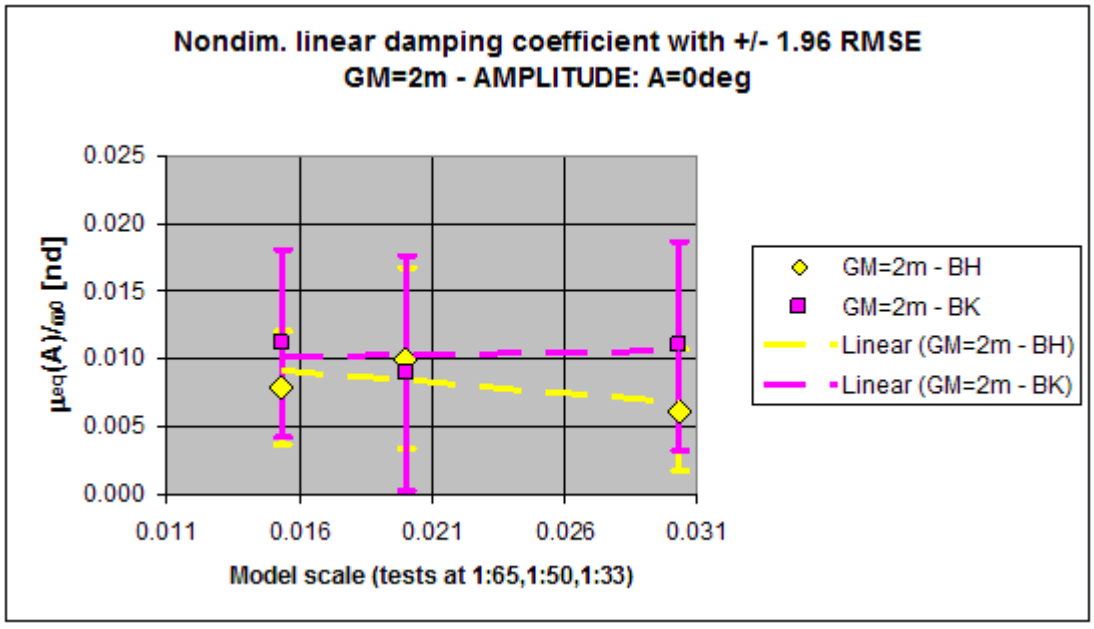

Figure 33: Dimensionless linear damping coefficient. $\overline{GM} = 2m$, rolling amplitude $A = 0\,\text{deg}$.

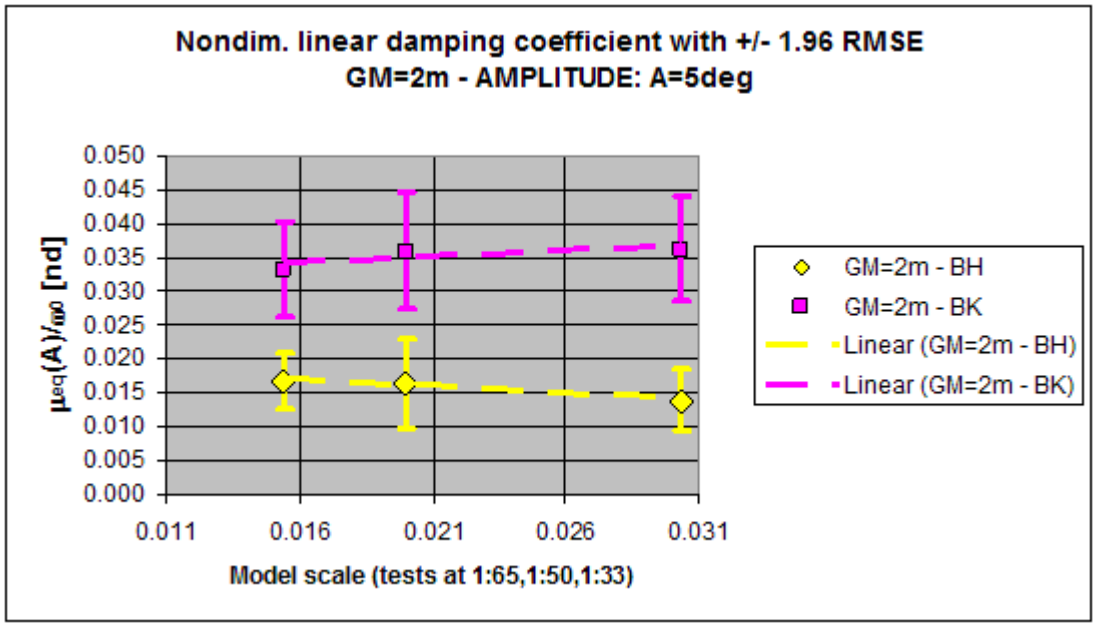

Figure 34: Dimensionless linear damping coefficient. $\overline{GM} = 2m$**, rolling amplitude** $A = 5\,\mathrm{deg}$**.**

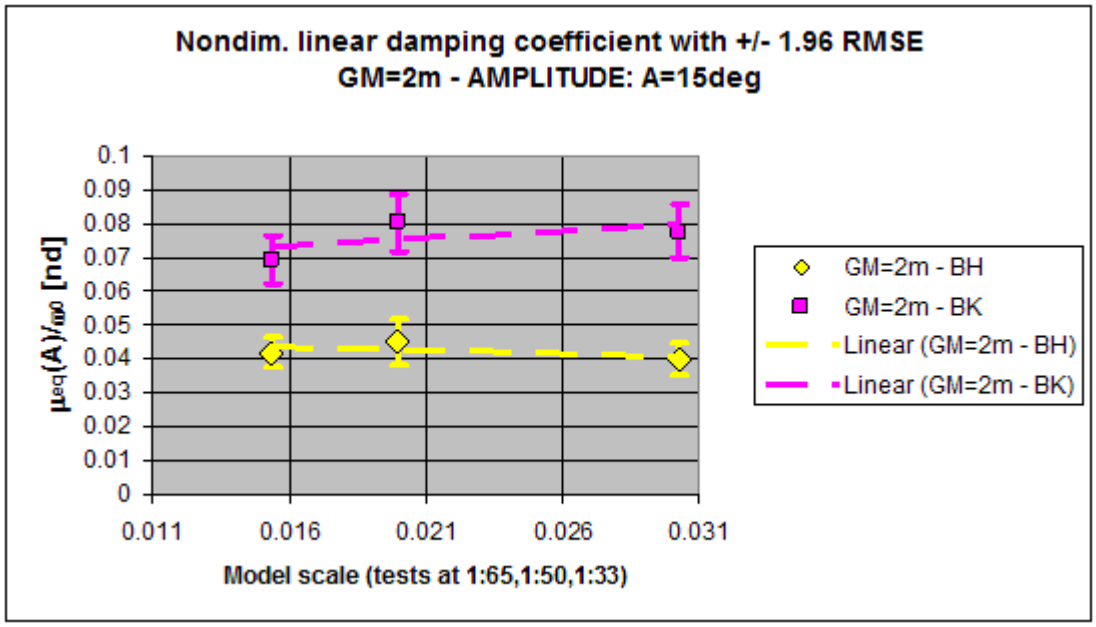

Figure 35: Dimensionless linear damping coefficient. $\overline{GM} = 2m$**, rolling amplitude** $A = 15\,\mathrm{deg}$**.**

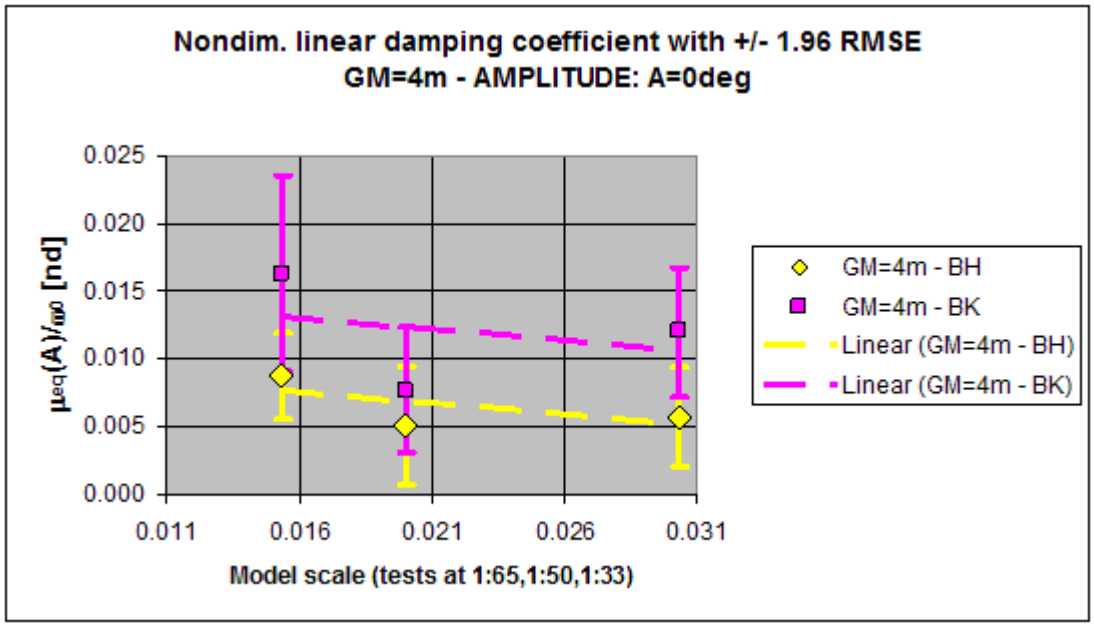

Figure 36: Dimensionless linear damping coefficient. $\overline{GM} = 4m$, rolling amplitude $A = 0\,\mathrm{deg}$.

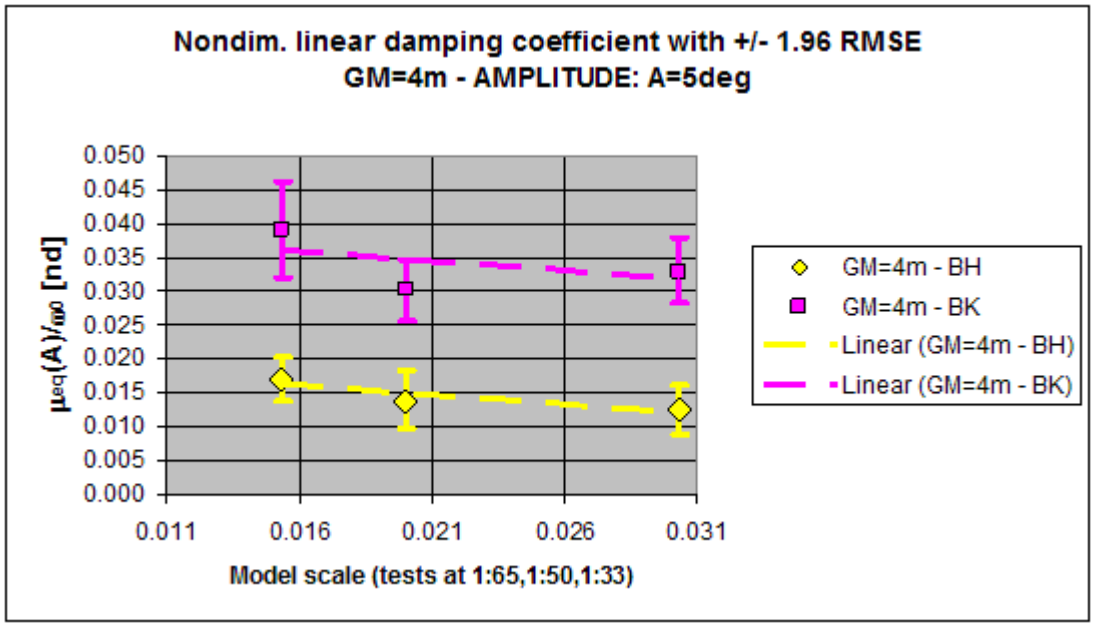

Figure 37: Dimensionless linear damping coefficient. $\overline{GM} = 4m$, rolling amplitude $A = 5\,\mathrm{deg}$.

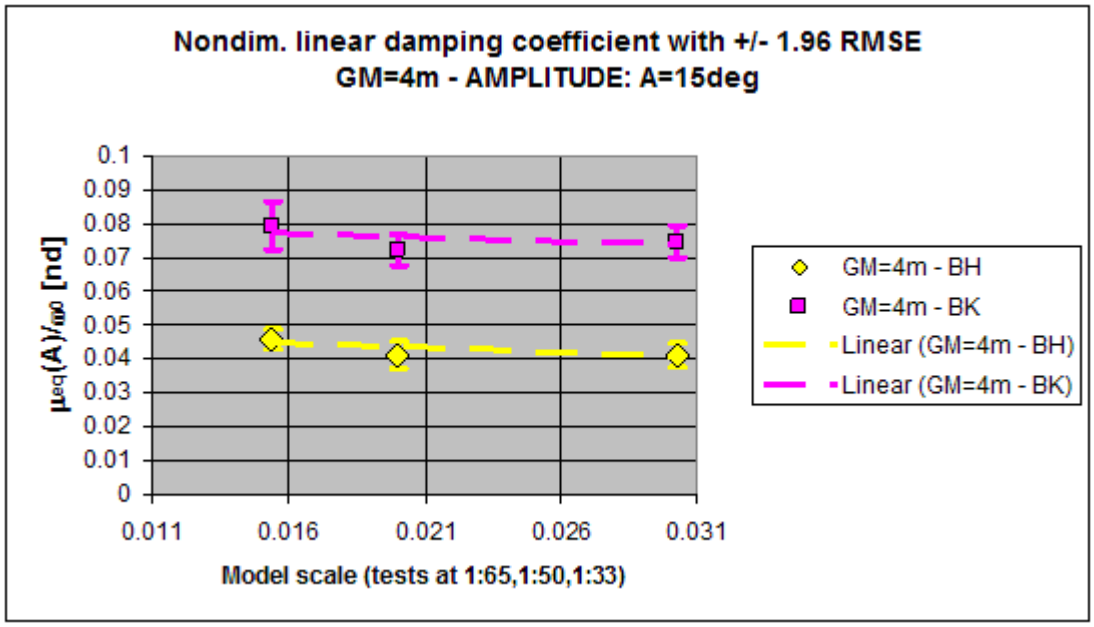

Figure 38: Dimensionless linear damping coefficient. $\overline{GM} = 4m$**, rolling amplitude** $A = 15\,\mathrm{deg}$**.**

According to the obtained results in Figure 33 to Figure 38 it is possible to provide some comments:

- In three cases ($\overline{GM} = 2m - BH$ and $\overline{GM} = 4m - BH / BK$) there is a tendency for the equivalent linear damping coefficient to decrease as the size of the model increases. The opposite tendency is seen for the case $\overline{GM} = 2m - BK$.
- Although a general trend is visible, it must be emphasized that the scattering of the data is quite significant and the differences of $\mu_{eq}(A)/\omega_0$ among different scales are of the order of magnitude of the uncertainty in the data.
- It is not possible to clearly quantify the scale effect on the obtained data due to the significant uncertainty involved in the process of elaboration and fitting of data. The relative level of uncertainty is especially significant in the case of small rolling amplitudes, with coefficients of variation reaching the order of 30%-40% in case of an equivalent linear damping calculation at a rolling amplitude of 0deg. On the other hand the 95% confidence interval significantly shrinks, in relative terms, as the calculation rolling amplitude increases thanks to the increase in damping. The significant dispersion of $\mu_{eq}(A)$ at small rolling amplitudes was also evident from the scatter plots of Figure 6 to Figure 15.
- It could be said that, *for the tested cases*, the uncertainty associated to data recording and analysis, although present in acceptable limits, and the uncertainty associated to the model and appendages' construction (which have not been quantified in this study, but are expected to be typical of GEOSIM series) seem to dominate over the scale effects and this also in view of the limited number of tested model scales (only three for each condition).

Damping correction according to MSC.1/Circ.1200

The "Interim guidelines for the alternative assessment of the Weather Criterion" [4] require that in the case of "small models" damping is to be corrected in order to take into account scale effects. In particular, the formulation of the damping correction

reported in [4] (the origin of which can be found in the work of Kato [25] as cited in [6] and then simplified in [7]) assumes that a laminar boundary layer is present at model scale [7] producing a frictional component for damping that, on the other hand, is assumed to be negligibly small (i.e. approximately zero) at full scale. According to this idea the frictional component of roll damping is estimated at model scale and it is *completely removed* from the measured roll damping. In principle the frictional component of roll damping should be removed at model scale and should be added back at full scale considering the difference in flow regime of the boundary layer (laminar / turbulent) in a way that is similar to what is usually done for the frictional component of the ship resistance in case of standard model tests for ship resistance. Again, in principle this could be accomplished using the complete formula of Kato [6] [25] taking into account both the laminar and the turbulent contribution to the frictional coefficient.
Here, however, we have applied the correction as required by [4] in order to assess the influence of such correction on the overall behaviour of (corrected) damping as the model scale is varied. First of all it is necessary to report that, according to [4], the correction of damping is to be performed when the model does not fulfil the scale requirements in §4.3.2 of [4], reported here for sake of clarity:

"*To avoid scale effect on roll damping, the model overall length should be at least 2m. However, the model should be scaled up, if necessary, to make the breadth of the bilge keels greater than 7 mm. For monohull ships having neither bilge keels nor sharp bilges, however, the model overall length should be at least 4 m unless frictional effect on roll damping is corrected with theoretical methods described later, but in any case not less than 2 m or a scale 1:75, whichever is greater.*"

The definition of "sharp bilges" is given in a footnote as follows:

"*'Sharp bilges' used here means that bilge radius is smaller than 1% of the ship's breadth and the angle between piece-wise lines representing the bilge is smaller than 120°.*"

Accordingly, for the tested ship, roll damping correction is required only for the model at scale 1:65 in bare hull condition. Indeed, the breadth of bilge keels is 0.8m at full scale (corresponding to 12mm at scale 1:65) and the overall length of the model is 220.1m at full scale (corresponding to 3.386m and 4.402m at scales 1:65 and 1:50 respectively). This meaning that in the case of the model fitted with bilge keels the damping correction is not required. On the other hand, in the case of the model in bare hull condition the overall length is sufficient (>4m) to avoid damping correction for scales 1:50 and 1:33, but the model is too small in case of scale 1:65. In addition, the model cannot be considered to have sharp bilges because the bilge radius is approximately 2.5m (full scale) corresponding to about 8% of the ship's breadth. It is probably worth questioning, at this stage, the use of overall geometrical quantities in matters that deal with the hydrodynamics of the hull: it would be probably more physically sound to consider, instead, quantities such as breadth and length associated to the underwater hull.
Damping correction in [4] is reported in terms of a correction for the Bertin's coefficient. However, according to [4] it is possible to transform any formula reported in terms of Bertin's coefficient (that is basically an amplitude dependent equivalent quadratic damping coefficient) into a formula given in terms of an equivalent

nondimensional linear damping coefficient μ/ω (thus avoiding the singularity of the Bertin's coefficient when the rolling amplitude tends to zero). The transformation of formula (4.6.1.2.1-1) in [4] leads to the following correction for the nondimensional linear damping coefficient μ/ω:

$$\delta\nu = \frac{2.11}{\pi}\cdot\frac{S\cdot r_s^2}{\Delta\cdot\overline{GM}\cdot T_\phi^{1.5}} = \delta\left(\mu/\omega\right)$$

$$S = L\cdot\left(1.7\cdot d + C_B\cdot B\right)$$

$$r_S = \frac{1}{\pi}\cdot\left[\left(0.877+0.145\cdot C_B\right)\cdot\left(1.7\cdot d + C_B\cdot B\right)+2\cdot\left(\overline{KG}-d\right)\right]$$

where (all data at model scale):

L: length of the ship at waterline (m)

B: moulded breadth of the ship (m)

d: mean moulded draught of the ship (m)

C_B: block coefficient

$\overline{GM}$: metacentric height corrected for free surface effect (m)

Δ: displacement (kg)

T_ϕ: roll period (s)

(5)

It is important to underline that [4] does not explicitly consider a variation of the rolling period in (5) with the amplitude, when actually, especially in case of low metacentric heights, this variation can be not negligible. In order to be consistent with the fact that, in this study, we have explicitly considered an amplitude dependence of the roll oscillation frequency, the correction (5) has been used as follows:

$$\delta\nu\left(A\right) = \delta\left(\frac{\mu_{eq}\left(A\right)}{\omega_{0,eq}\left(A\right)}\right) = \frac{2.11}{\pi}\cdot\frac{S\cdot r_s^2}{\Delta\cdot\overline{GM}\cdot\left(\frac{2\pi}{\widetilde{\omega}\left(A\right)}\right)^{1.5}} \approx$$

$$\approx \frac{2.11}{\pi}\cdot\frac{S\cdot r_s^2}{\Delta\cdot\overline{GM}\cdot\left(\frac{2\pi}{\omega_{0,eq}\left(A\right)}\right)^{1.5}} \Rightarrow$$

$$\Rightarrow \delta\mu_{eq}\left(A\right) \approx \frac{2.11}{\pi}\cdot\frac{S\cdot r_s^2\cdot\omega_{0,eq}^{2.5}\left(A\right)}{\Delta\cdot\overline{GM}\cdot\left(2\pi\right)^{1.5}}$$

(6)

Since in our case we have decided to report the amplitude dependent linear damping coefficient $\mu_{eq}\left(A\right)$ after dividing it by ω_0 it follows from (6) that:

$$\delta\mu_{eq}(A)=\frac{2.11}{\pi}\cdot\frac{S\cdot r_s^2\cdot\omega_{0,eq}^{2.5}(A)}{\Delta\cdot\overline{GM}\cdot(2\pi)^{1.5}}=\frac{2.11}{\pi}\cdot\frac{S\cdot r_s^2\cdot\omega_0^{2.5}}{\Delta\cdot\overline{GM}\cdot(2\pi)^{1.5}}\cdot\left(\frac{\omega_{0,eq}(A)}{\omega_0}\right)^{2.5}=$$

$$=\delta\mu_{eq}(A=0)\cdot\left(\frac{\omega_{0,eq}(A)}{\omega_0}\right)^{2.5} \tag{7}$$

$$\frac{\delta\mu_{eq}(A)}{\omega_0}=\delta\left(\frac{\mu_{eq}(A)}{\omega_0}\right)=\delta\left(\frac{\mu_{eq}(A=0)}{\omega_0}\right)\cdot\left(\frac{\omega_{0,eq}(A)}{\omega_0}\right)^{2.5}=$$

$$=\frac{2.11}{\pi}\cdot\frac{S\cdot r_s^2\cdot\omega_0^{1.5}}{\Delta\cdot\overline{GM}\cdot(2\pi)^{1.5}}\cdot\left(\frac{\omega_{0,eq}(A)}{\omega_0}\right)^{2.5}$$

For the model at scale 1:65 in bare hull condition the quantity $\delta\left(\mu_{eq}(A=0)/\omega_0\right)$ is $5.35\cdot10^{-3}$ in case of $\overline{GM}=2m$ and $3.76\cdot10^{-3}$ in case of $\overline{GM}=4m$. The overall effect on the amplitude dependent equivalent linear damping coefficient is reported in Figure 39 to Figure 44.

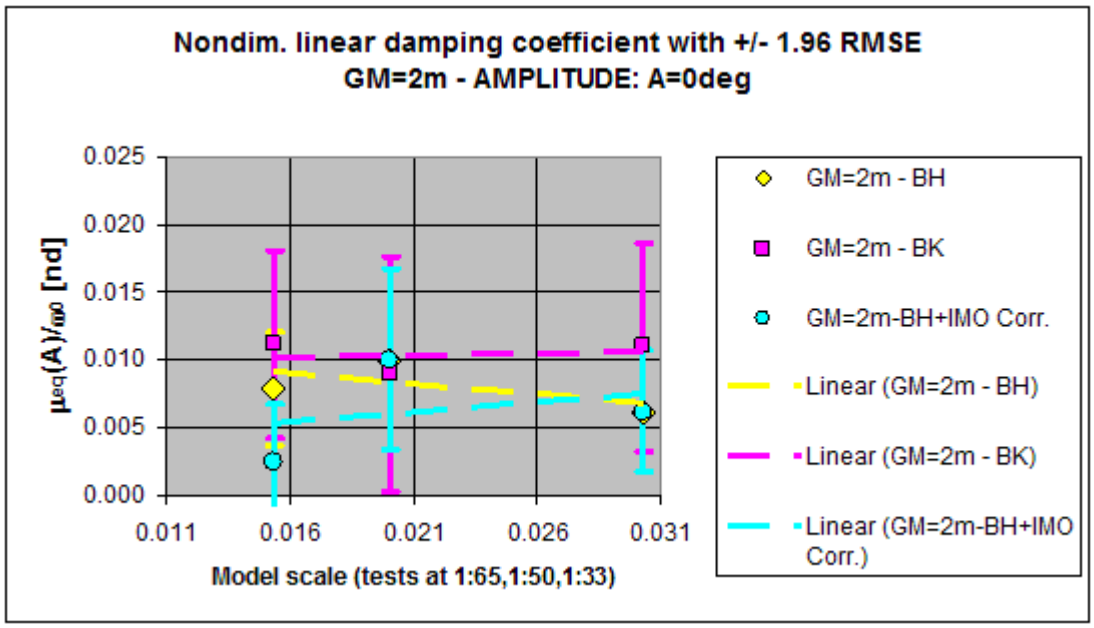

Figure 39: Dimensionless linear damping coefficient with and without IMO correction [4]. $\overline{GM}=2m$**, rolling amplitude** $A=0\,\text{deg}$**.**

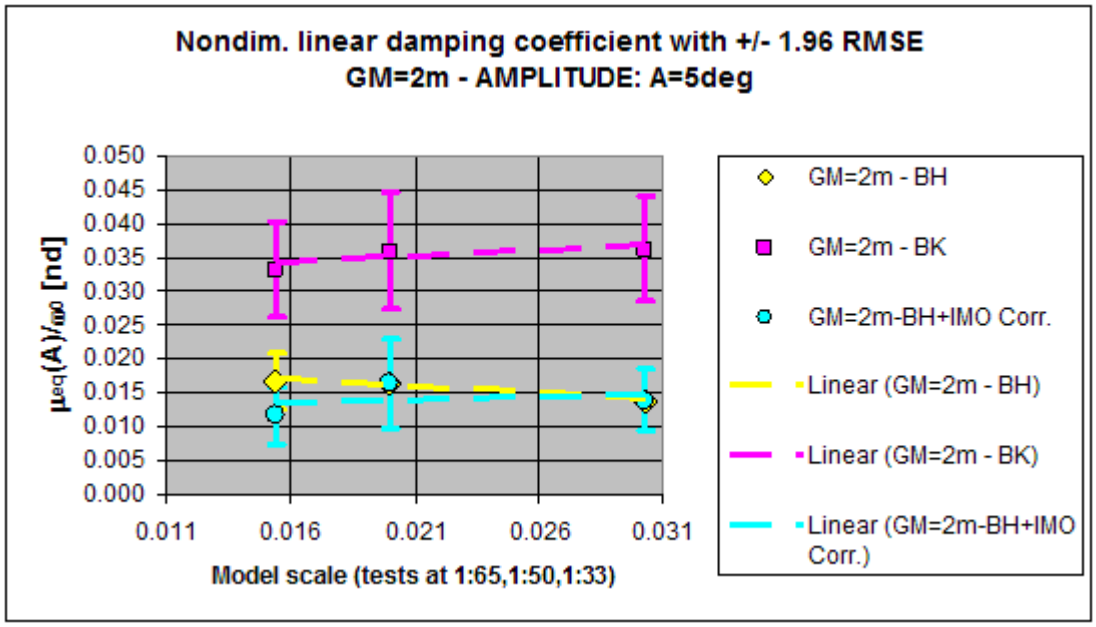

Figure 40: Dimensionless linear damping coefficient with and without IMO correction [4].
$\overline{GM} = 2m$**, rolling amplitude** $A = 5\,\mathrm{deg}$.

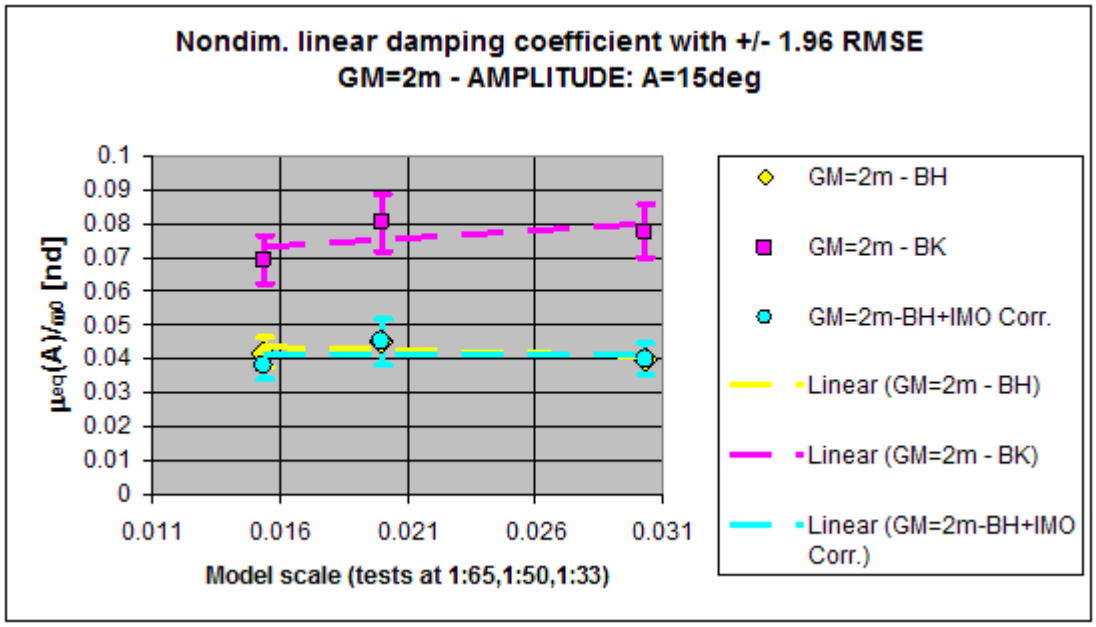

Figure 41: Dimensionless linear damping coefficient with and without IMO correction [4].
$\overline{GM} = 2m$**, rolling amplitude** $A = 15\,\mathrm{deg}$.

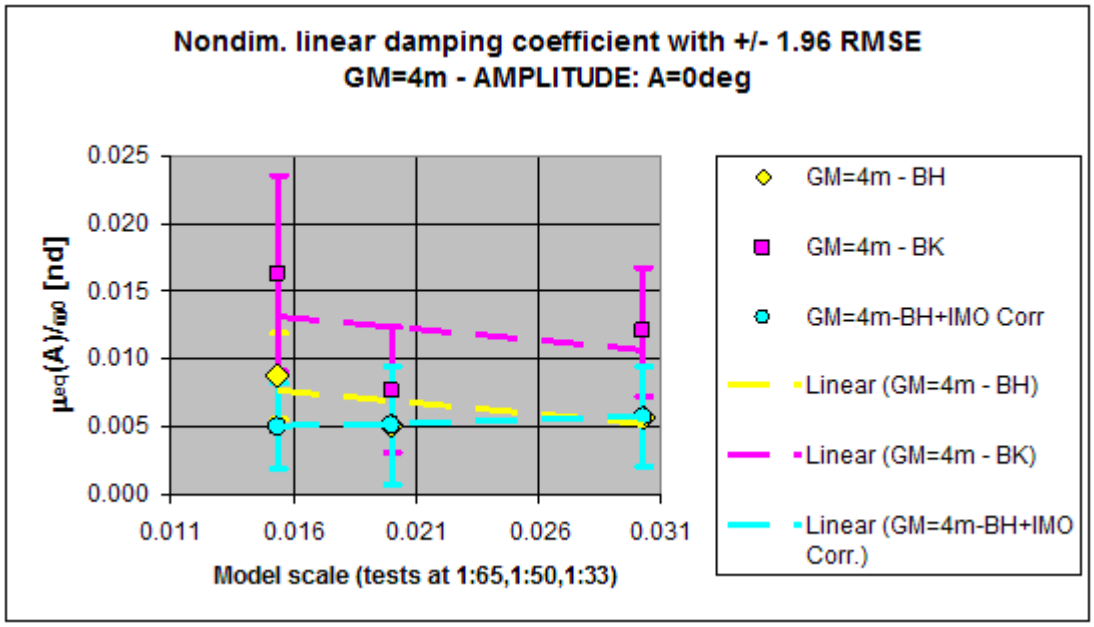

Figure 42: Dimensionless linear damping coefficient with and without IMO correction [4].
$\overline{GM} = 4m$**, rolling amplitude** $A = 0\,\mathrm{deg}$**.**

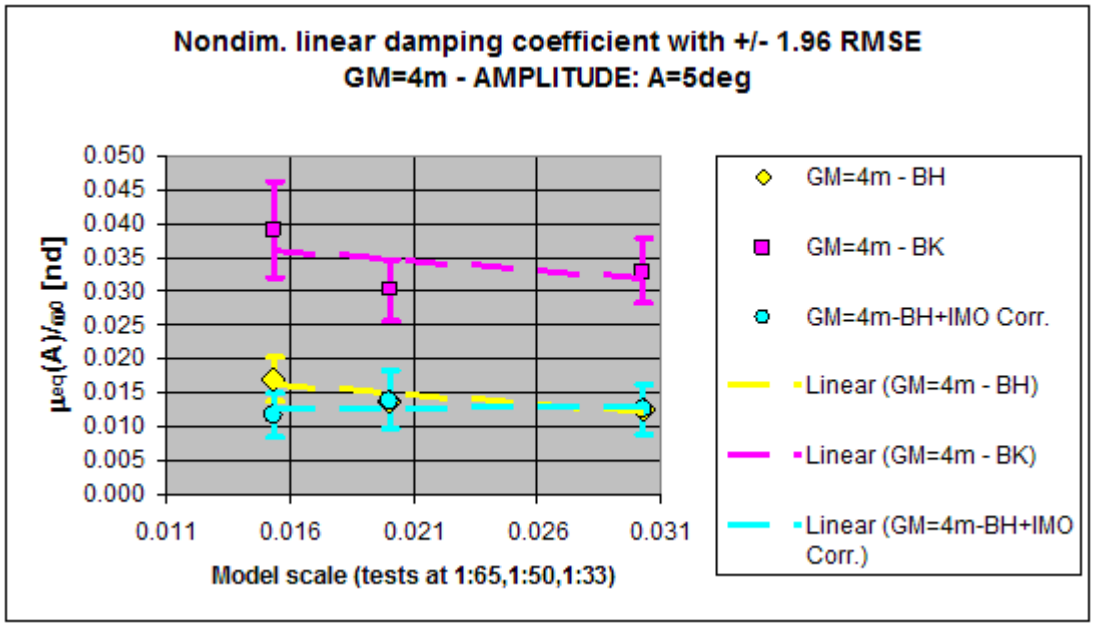

Figure 43: Dimensionless linear damping coefficient with and without IMO correction [4].
$\overline{GM} = 4m$**, rolling amplitude** $A = 5\,\mathrm{deg}$**.**

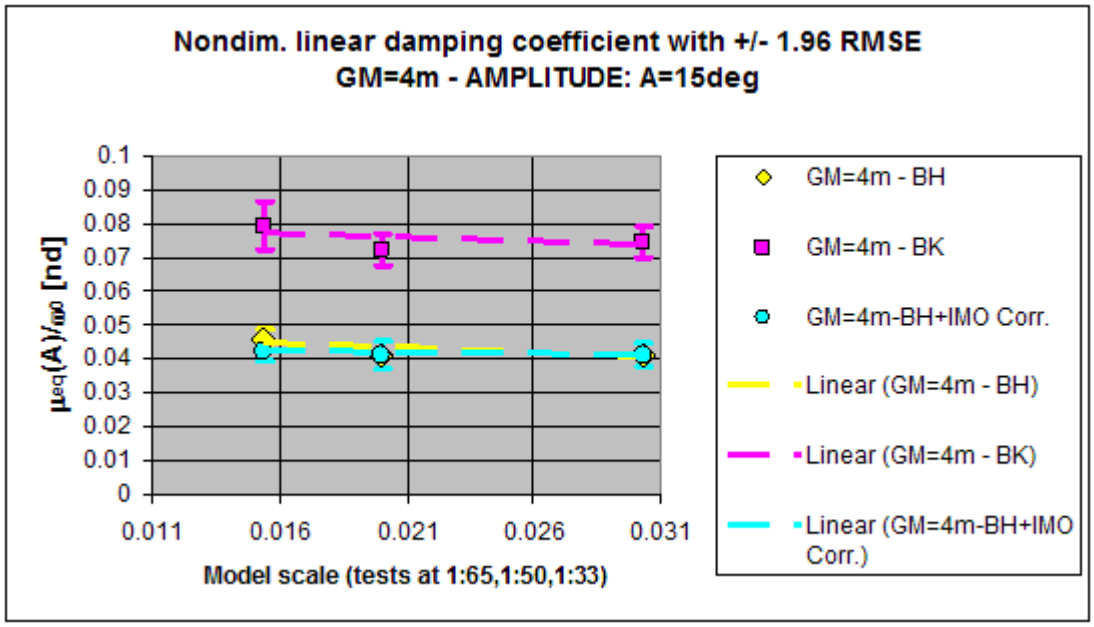

Figure 44: Dimensionless linear damping coefficient with and without IMO correction [4]. $\overline{GM} = 4m$**, rolling amplitude** $A = 15\,\mathrm{deg}$**.**

According to the obtained results it is possible to provide a series of comments:

- In case of $\overline{GM} = 4m$ the application of the IMO correction tends to remove the decreasing trend observed on damping as the model scale is changed. However in case of $\overline{GM} = 2m$ the correction seems to be too large and the original decreasing trend of damping is transformed in an opposite, increasing, trend.
- The effect of the damping correction is significant at small rolling amplitudes, where the IMO correction is about 68% of the originally measured (fitted) linear damping in case of $\overline{GM} = 2m$, and it is about 43% of the originally measured (fitted) linear damping in case of $\overline{GM} = 4m$. As the rolling amplitude increases the effect of the correction is less important thanks to the increase of the damping due to nonlinear effects.
- In case of prediction of large rolling amplitudes in beam waves, as it is the case for the experimental approach to the weather criterion [4], the influence of the IMO correction for scale effects is likely to be very limited.
- The simple removal of the estimated frictional component of roll damping for "small models" is questionable and a more systematic approach should be followed where frictional damping is estimated at model scale and removed, and then it is re-calculated at full scale and added back. Figure 45 shows the frictional damping component calculated according to [4] for the complete set of tested scales / conditions. Although the assumption of laminar flow for large models is questionable, and hence the approach in [4] is not completely applicable to "large models", the calculation has been performed only to show that the estimated magnitude of the frictional roll damping term is still quite large also for the model at scale 1:50 that is at the limit of the requirement for the application of the damping correction. The obtained "regularization" of the dependence of damping on model scale as could be claimed looking at Figure 42 to Figure 45 is probably a statistically fortunate case.

- It shall be also mentioned that, even if scale effects could in principle be corrected when damping is estimated from roll decays and the rolling amplitude is calculated according to any of the methodologies in [4] that are alternative to the direct measurement, it is more difficult to deal with scale effects when a model is actually tested in waves and the rolling amplitude is directly measured according to the standard procedure in [4]. In such case it would be necessary to: a) fit a dynamic model on the obtained results, b) correct the damping term of the fitted model for scale effects, and finally c) estimate, according to the corrected model, the rolling amplitude at full scale.

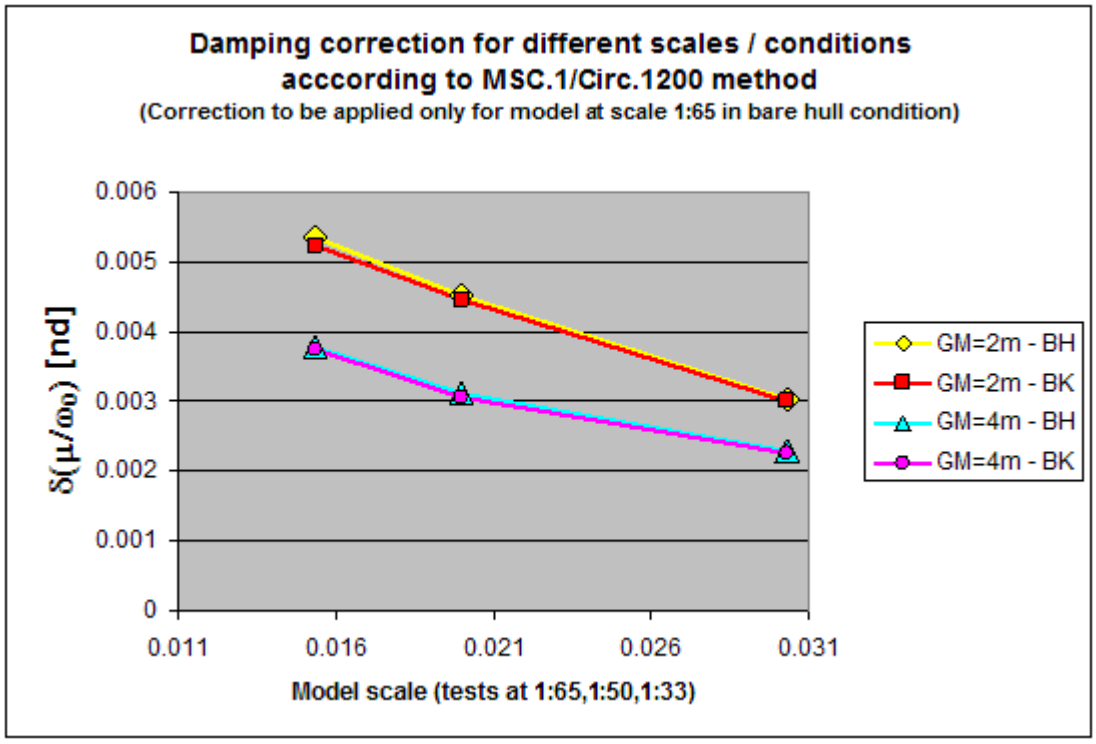

Figure 45: Calculation of the IMO damping correction [4] for the complete set of scales / conditions.

Concluding comments

According to the results of the analysis of roll decay tests it is possible to provide a series of summarising comments:

- The global level of uncertainty involved in the complete procedure for the determination of roll damping is mainly due to:
  - Uncertainty associated to the building of models. The differences among models, however, should be quite limited thanks to the numeric control of the milling machines.
  - Uncertainty associated to the construction and fitting of bilge keels. The associated uncertainty could be not negligible due to the manual work involved in the construction and fitting of bilge keels.
  - Uncertainty associated to the ballasting of the model, and setting up of the metacentric height and roll period. This is a completely manual work, hence the associated uncertainty is expected to be not negligible.
  - Uncertainty associated to the measuring of motions. In that respect errors mainly arise from misalignment of the reference frame (for

angular and rectilinear motions). Errors in setting the relative position of the reference frame with respect to the assumed centre of the ship-fixed reference system influence the measurement of rectilinear motions (not considered in this section). The precision of the measuring system is actually not a real problem, since the corresponding level of uncertainty is small in comparison to other effects.

  - Uncertainty associated to the methodology of analysis of the obtained data. This is probably one of the major sources of uncertainty. Here we should include also the fact that the analytical models used to represent the dissipation mechanism of roll damping have unavoidable limitations and cannot completely explain the behaviour of the experimental results. Additional limitations of the employed modelling and procedure of analysis, such as neglecting transient hydrodynamic effects by using a dynamic model with constant coefficients, also indirectly introduces parasitic effects in the determination of coefficients relevant to the application of the alternative assessment of the Weather Criterion.
  - Uncertainty associated to scale effects. In such case it would be better to say that the unavoidable scale effects are likely masked by the overall level of uncertainty and are extremely difficult to be singled out, finally adding to the remaining "noise".

- According to the fitting of experimental data it can be said that the average RMSE for μ_{eq}/ω_0 is of the order of $2.8\cdot10^{-3}$.
- Differences for μ_{eq}/ω_0 at 0deg, 5deg and 15deg for the (nominally) same loading condition among three different scales can be quantified by the standard deviation of $\mu_{eq}(A)/\omega_0$ for the same amplitude among different scales. According to the results it can be said that we have found an average standard deviation of $\mu_{eq}(A)/\omega_0$ among different scales of about $2.8\cdot10^{-3}$ (interestingly a value very close to the average RMSE from fittings).
- Combining the average RMSE associated to the fitting of $\mu_{eq}(A)/\omega_0$ and the average standard deviation of $\mu_{eq}(A)/\omega_0$ among different scales it is possible to consider a combined uncertainty of about $\sqrt{\left(2.8\cdot10^{-3}\right)^2+\left(2.8\cdot10^{-3}\right)^2}\approx4.0\cdot10^{-3}$, with a 95% confidence bound that can be approximated as $\pm1.96\cdot4.0\cdot10^{-3}\approx\pm7.8\cdot10^{-3}$. It can be seen that this confidence bound is significantly large when considering the nondimensional linear damping $\mu_{eq}(A)/\omega_0$ at small rolling amplitudes (in particular concerning $\mu_{eq}(A=0)/\omega_0$), while it is less significant when dealing with damping at large rolling amplitudes, especially in case of models fitted with bilge keels.
- The uncertainty in the modelling / measuring of the amplitude dependent damping shall be borne in mind when predicting rolling amplitudes, and such uncertainty should be propagated to the final results of the calculations (as far as practically possible).

- The problem of extrapolation of damping models to rolling amplitudes significantly larger than the maximum rolling amplitude used in roll decay experiments has been only briefly touched. However, this problem could become serious especially in bare hull condition where the use of a cubic damping coefficient, that leads to a significant growing of damping as the amplitude of roll increases, is necessary in order to fit the experimental data.
- Despite it has not been possible to clearly identify scale effects, the provided level of uncertainty for $\mu_{eq}(A)/\omega_0$ could be considered to include them to some extent. More controlled tests, with significantly less human intervention are necessary (and expectable) to clearly quantify differences associated to scale effects.
- The damping correction as proposed in [4] has been applied to the available experimental data. Results are quite fuzzy, and a definite conclusion on its suitability cannot be drawn. On the other hand some of the hypotheses on which such correction is based have been questioned, and it is probably worth trying to develop a more sound and robust methodology for scale effects correction on roll damping (that could follow the line of thinking of the widely used approach for the correction of the frictional component of ship resistance).

Roll tests in beam waves

Introduction

Beam wave tests represent one of the fundamental type of tests in the experimental assessment of Weather Criterion according to MSC.1/Circ.1200 [4]. The MSC.1/Circ.1200 [4] provides details concerning the way of executing tests and the wave characteristics to be used. Moreover, it provides indications concerning the minimum dimensions of models that are allowed to be tested, in order to avoid scale effects (this aspect has already been addressed when discussing roll decay experiments). In this section we report the results of a series of experiments in beam waves with an experimental arrangement consistent with [4]. The interest is in the comparison of, especially, the roll response curve obtained from the three available models in different loading conditions, with and without the fitting of bilge keels. It is anticipated that, due to limitations (that are common to a significant number of towing tanks) in the wave maker generation region, it was not possible to test the IMO required wave steepness according to [4] and, instead, smaller wave steepnesses have been tested in order to be able to directly compare the outcomes from different models.

This section is organized as follows:

- The used loading conditions are reported with a description of the experimental setup and technique (see also Appendix 2).
- An analysis of generated waves is shown in order to report how it was decided to neglect some tests.
- Two mathematical models used for the prediction of the rolling motion are briefly described.
- The experimentally measured roll response curves are reported for the various tested conditions.

- Motions other than roll are also discussed in a separate appendix (see Appendix 3).
- The obtained results are discussed in the light of the alternative experimental assessment methodology for the Weather Criterion.
- Some final summarising comments are given.

Loading conditions, testing setup and technique

Beam waves tests have been carried out for the three available model scales (1:33, 1:50 and 1:65) according to the following tests matrix:

- Model Scale: 1:33
  - GM=2m, Draught=6.6m, with and without bilge keels, wave steepness 1/80
  - GM=4m, Draught=6.6m, with and without bilge keels, wave steepness 1/80 and 1/40
- Model Scale: 1:50
  - GM=2m, Draught=6.6m, with and without bilge keels, wave steepness 1/80
  - GM=4m, Draught=6.6m, with and without bilge keels, wave steepness 1/80 and 1/40
- Model Scale: 1:65
  - GM=2m, Draught=6.6m, with and without bilge keels, wave steepness 1/80
  - GM=4m, Draught=6.6m, with and without bilge keels, wave steepness 1/80 and 1/40

For each condition not less than seven wave frequencies have been tested close to the natural roll frequency. The total number of executed tests in beam waves is 158.

The tested wave steepnesses used in beam waves tests have been selected on the basis of:

- The necessity of having directly comparable sets of tests for the same loading condition at the three tested scales. The intention was, indeed, to avoid any need for extrapolation / interpolation of roll response curves at wave steepnesses different from those generated.
- The available generation range of the wave maker, that limits the possibility of generating steep waves at low periods.

In order to be able to directly compare tests at different model scales it was necessary to abandon the idea of using the required IMO wave steepness as specified in [4]. Indeed, the IMO wave steepness required by the alternative assessment of the weather criterion is significantly large especially for ships with small rolling periods (see Table 4.5.1 in [4]). Using the average roll period from experiments with and without bilge keels from different scales, for the tested conditions the required IMO wave steepness would have been 0.060 (=1/16.6) in case of $\overline{GM} = 4m$ (experimental average roll period 12.8s), and 0.037 (=1/27.0) in case of $\overline{GM} = 2m$ (experimental average roll period 18.3s).

The model was almost completely free to drift, and a couple of ropes were connected at bow and stern to maintain a heading close to 90deg by human intervention. For each test a series of quantities have been measured, namely:

- Six degrees of freedom of the ship with respect to the carriage's turret, by means of a non-intrusive RODYM system [16].
- Wave elevation at a wave probe connected to the carriage's turret.

- Longitudinal and transversal (with respect to the tank) speed of the carriage's turret.

In addition, tests have also been video recorded. As can be noticed, all the measured data concerning the ship DOFs have been referred to the turret that, on the other hand, is not fixed, and moves longitudinally and transversally (with respect to the tank). The turret moves in order to keep the model in the visibility range of the cameras used for the measurement of ship motions.
Measured rectilinear ship motions have thus been transformed from a "turret fixed" reference system to a "tank fixed" reference system according to the procedure reported in Appendix 2. Concerning the measured wave amplitude, no transformations were applied, and the signal was kept in its original form.
Ship motions were subsequently analysed in order to obtain information on the ship behaviour at steady state under the action of waves. An example of the experimental data used for the analysis is reported in Figure 46.

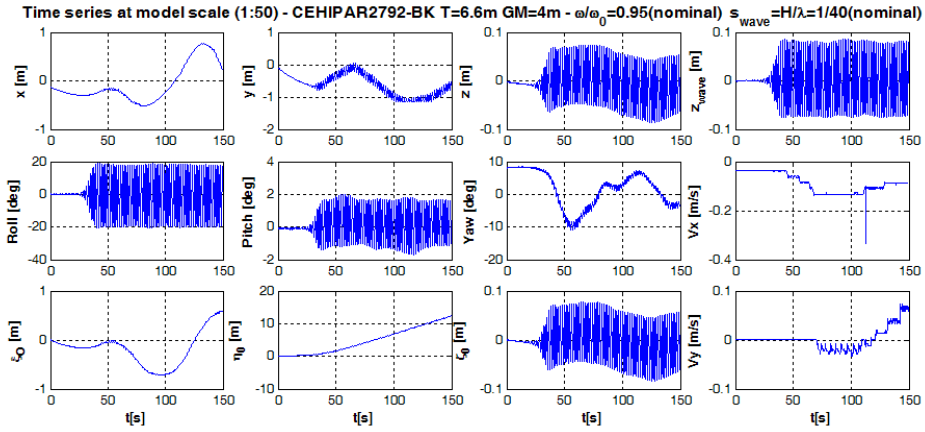

Figure 46: Example of experimental data.

Analysis of generated waves

The quality of generated waves for each test was assessed by comparing the required wave steepness with the estimated wave steepness obtained from measured data. It was decided to consider "acceptable" a test when the wave steepness doesn't differ more than 10% from the required one. Decreasing this margin would have led to a significant increase in the time needed for waves' pre-calibration, according to the towing tank procedure.
As reported in the previous section, the wave probe was fixed to the moving turret, and it was, hence, not convenient to use the measured wave elevation signal for the estimation of the period of the incoming wave (the turret was, indeed, not translating at a constant speed). Hence, in the stationary window used for the analysis of motions, we have used the measured wave elevation in order to obtain an estimation of the generated wave amplitude and then we have measured the average drift speed of the model by fitting a straight line on the signal $\eta_O(t)$ (ship's drift in the direction of wave's propagation, see Appendix 2). By using the linear dispersion relationship, taking into account the tank depth (5m), and the Doppler effect relationship, it has been possible to obtain an estimation of the incoming wave length. Then, from the estimation of the incoming wave length and the measured average wave height, the estimated steepness of the incoming wave was obtained and compared with the target value. Results are reported in Figure 47.

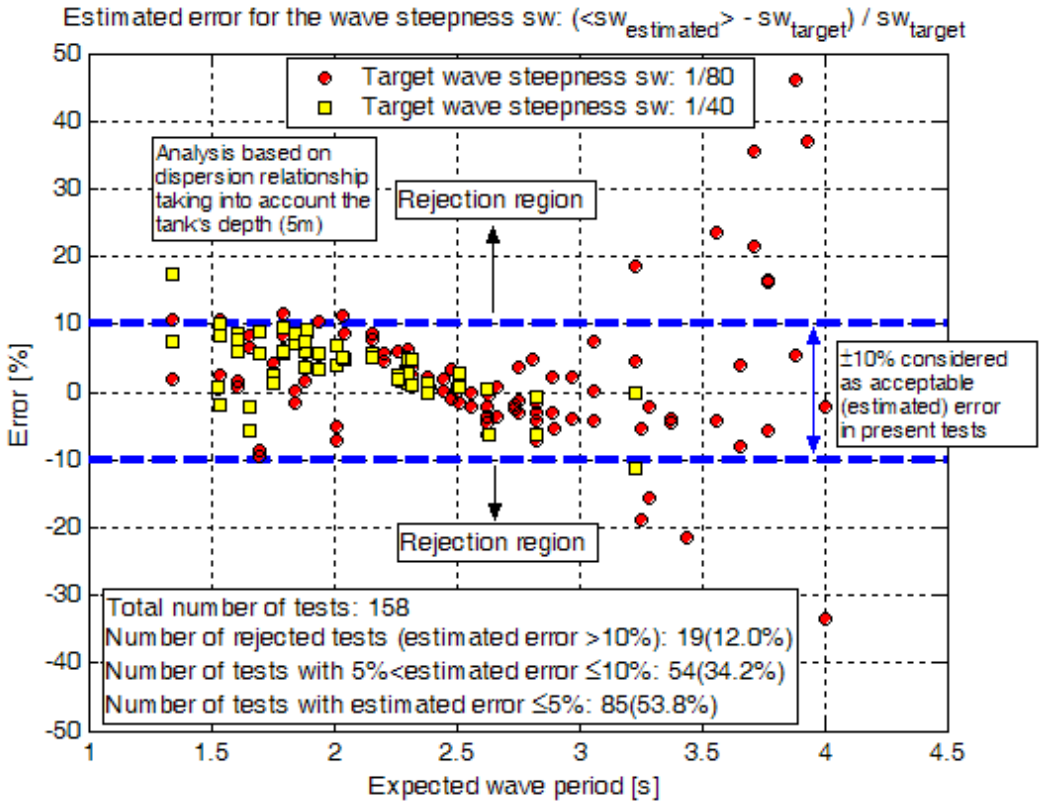

Figure 47: Analysis of generated wave steepness.

A trend is visible in Figure 47 towards generating too large steepnesses at small periods, and too small steepnesses at large periods. The best generation region is close to 2.5s. Among the total tests (158), 19 have been rejected and not used in the subsequent analyses. Table 5 shows a summary of the data coming from the analysis of wave quality.

Table 5: Data concerning wave quality for various cases.

Error [%] for steepness for NOT rejected tests

ID	Scale	GM[m]	Appendages	Natural roll frequency at FULL SCALE [rad/s]	Natural roll period at model scale [s]	MEAN	STD	CoV=STD/MEAN	Number of NOT rejected tests	Total number of tests	% of rejection	error<=5%	5%<error<=10%	error>10%
1	65	2	BH	0.346	2.250	-0.88	3.14	3.56	14	16	0.125	12	2	2
2	65	2	BK	0.341	2.285	-0.07	4.05	54.62	8	8	0.000	6	2	0
3	65	4	BH	0.491	1.588	2.80	5.79	2.07	15	16	0.063	3	12	1
4	65	4	BK	0.489	1.595	4.41	6.22	1.41	19	22	0.136	4	15	3
5	50	2	BH	0.353	2.521	1.67	3.30	1.97	6	8	0.250	5	1	2
6	50	2	BK	0.350	2.536	-1.81	3.80	2.10	8	9	0.111	7	1	1
7	50	4	BH	0.495	1.797	3.12	3.50	1.12	16	16	0.000	11	5	0
8	50	4	BK	0.486	1.829	2.91	4.12	1.41	14	16	0.125	9	5	2
9	33	2	BH	0.333	3.281	-1.66	3.79	2.28	4	7	0.429	4	0	3
10	33	2	BK	0.331	3.303	-3.03	5.15	1.70	5	8	0.375	2	3	3
11	33	4	BH	0.493	2.219	2.32	2.88	1.24	16	16	0.000	13	3	0
12	33	4	BK	0.488	2.239	2.20	4.11	1.87	14	16	0.125	9	5	2
											TOTAL:	85	54	19
											PERCENTAGES:	53.8	34.2	12.0

It is important to note that the estimation of the error on the wave steepness does not necessarily coincide with the error estimated for the wave height. The reason is to be sought in the influence of the limited depth of the towing tank. According to the headers of the experimental data files, the required wave height H_{req} was set according to the deep water linear dispersion, for a given target wave steepness $s_{w,\text{target}}$, namely, for a given wave period T_w:

$$H_{req} = s_{w,\text{target}} \cdot \lambda_{deep} = s_{w,\text{target}} \cdot \frac{g \cdot T_w^2}{2\pi}$$
$$\lambda_{deep} = \frac{g \cdot T_w^2}{2\pi} \tag{8}$$

where λ_{deep} is the wave length calculated using the deep water assumption. However, the actual wave length in limited depth shall be calculated, according to the linear dispersion relation, as solution of

$$\omega_w = \sqrt{g \cdot k_w \cdot \tanh\left(k_w \cdot d\right)}$$
$$k_w = \frac{2\pi}{\lambda_{actual}} \tag{9}$$

where λ_{actual} is the generated wave length, for a generation period T_w when the tank's depth is d. The error introduced on the actual generated wave steepness $s_{w,actual}$ when using (8) instead of (9) is given by:

$$s_{w,\text{actual}} = \frac{H_{actual}}{\lambda_{actual}} = \frac{H_{req}}{\lambda_{deep}} \cdot \frac{H_{actual}}{H_{req}} \cdot \frac{\lambda_{deep}}{\lambda_{actual}} = s_{w,\text{target}} \cdot \frac{H_{actual}}{H_{req}} \cdot \frac{\lambda_{deep}}{\lambda_{actual}} \Rightarrow$$
$$\Rightarrow \frac{s_{w,\text{actual}}}{s_{w,\text{target}}} = \frac{H_{actual}}{H_{req}} \cdot \frac{\lambda_{deep}}{\lambda_{actual}} \tag{10}$$

even assuming that the ratio H_{actual} / H_{req} is close to 1, the term $\lambda_{deep} / \lambda_{actual}$ introduces an error in the generated steepness according to the target one. Figure 48 shows that the ratio $\lambda_{deep} / \lambda_{actual}$ is significantly different from unity when the wave period is above, say 3s-3.5s for the tests carried out in this campaign.

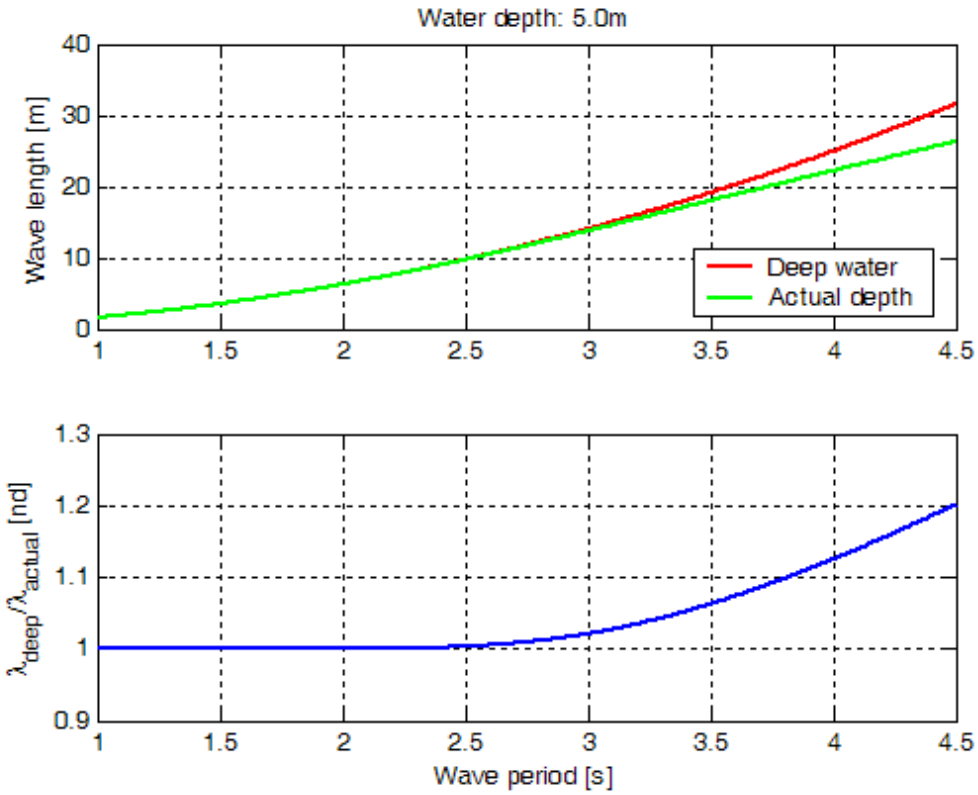

Figure 48: Effect of tank depth on generated wave length for a given period.

While the ratio $\lambda_{deep} / \lambda_{actual}$ influences the generated wave steepness as a consequence of the inaccurate assumption when using (8), the ratio H_{actual} / H_{req} represents a merit function to assess whether the wavemaker is able to generate the requested wave height for a given wave period. The error analysis limited to the ratio H_{actual} / H_{req} is shown in Figure 49: it can be seen that in the range of short wave periods, where the deep water assumption can be used, points in Figure 47 and Figure 49 basically coincide, while the effect of the term $\lambda_{deep} / \lambda_{actual}$ in (10) is visible for large wave periods.

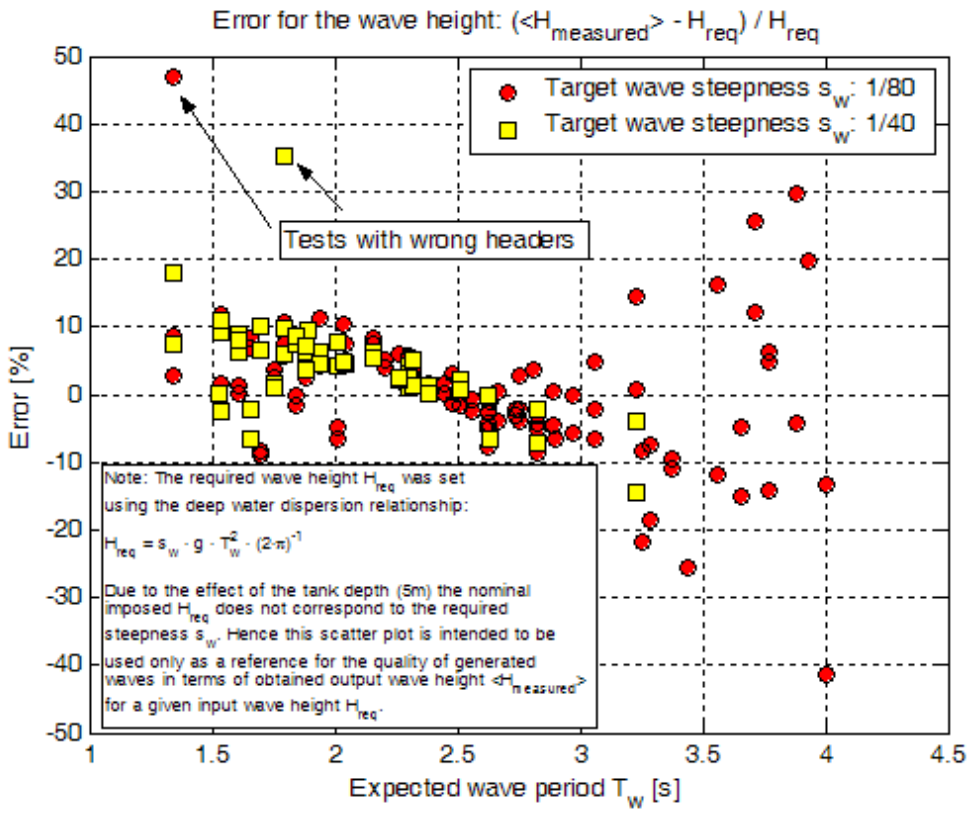

Figure 49: Error analysis for the generated wave height.

By separating data from error analysis for each different tested case it is possible to determine the average estimated error in the generated wave steepness (as well as the corresponding standard deviation) as a function of the tested model natural roll period (see Figure 50) and of the model scale (see Figure 51).

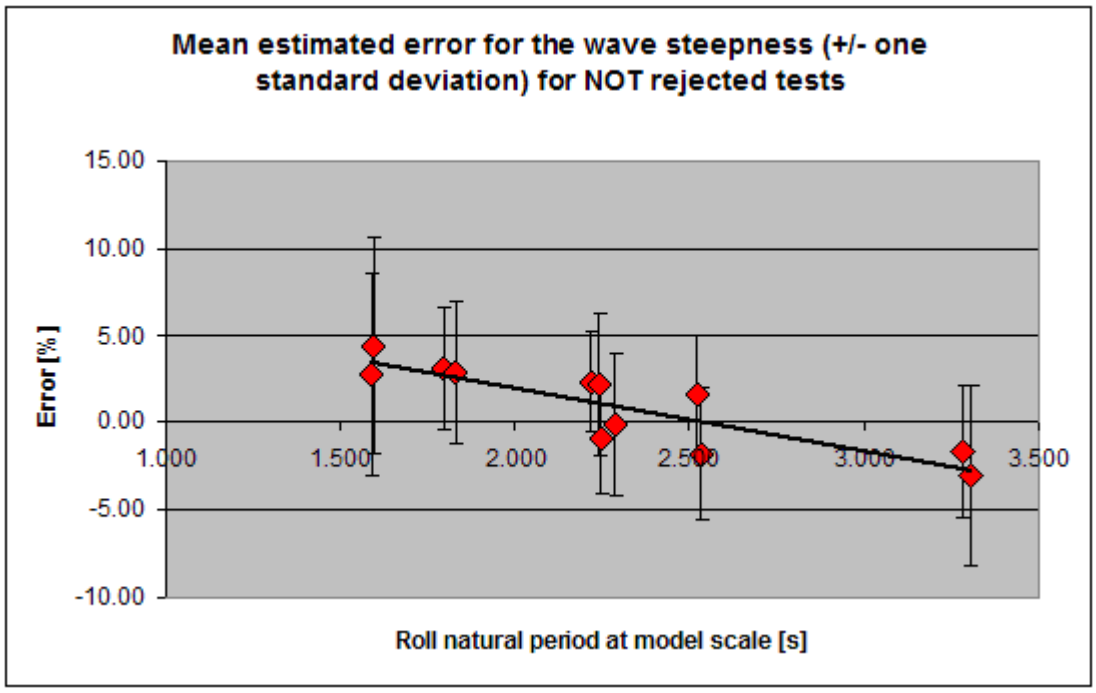

Figure 50: Mean estimated error for the wave steepness as a function of the model natural roll period.

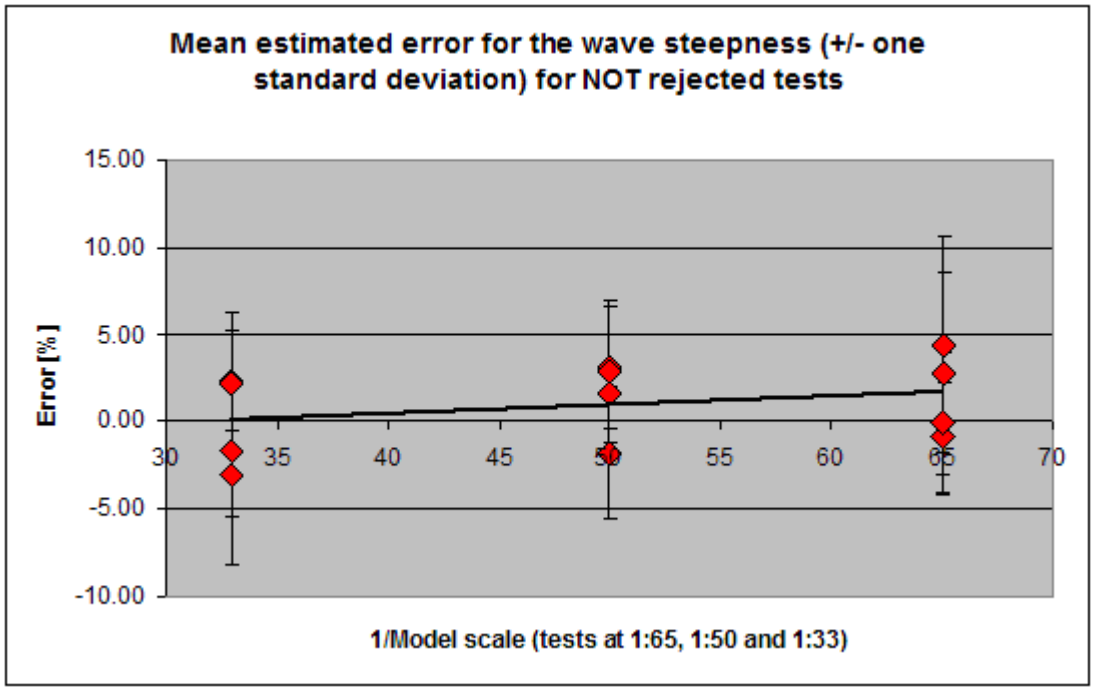

Figure 51: Mean estimated error for the wave steepness as a function of the model scale.

Results in Figure 50 and Figure 51 are of course consistent with those shown in Figure 47, and it can be seen that, the smaller the natural period of the model the more the actual estimated generated wave steepness is in excess of the required one. It can be seen that, on average, the smallest model (scale 1:65) has been tested with wave steepnesses slightly in excess (around 2%) of the target ones, while the largest model has been tested with average wave steepnesses in accordance with the required ones. When considering data based on model scale, however, it must be borne in mind that two loading conditions (GM=2m and GM=4m) have been considered for each model scale. In view of this it is noticeable that the cases with GM=2m have been tested with steepnesses smaller, on average, than the required one, while the opposite occurs in case of GM=4m loading condition. However, in general, the average errors are limited for all the tested cases, and part of these estimated errors could also be due to the estimation procedure for the wave length based on Doppler effect.

As a final note, it should be underlined that the deep water dispersion relationship is used, to a large extent as a default means in the majority of seakeeping tests and subsequent analysis (as this series of tests demonstrate). Although this is justified in the majority of cases where the wave length is sufficiently short (typically in seakeeping tests intended to address vertical motions, where the maximum wave length is of the order of 2 model's lengths), it seems that the same cannot be said in case of beam waves experiments, especially for large models with small metacentric heights (i.e. long periods in absolute sense). It is therefore recommendable, and advisable, to take into account the effect of the tank depth when planning and checking such tests. Moreover, it is not clear at this stage whether the limited depth could have influenced the results in terms of roll responses.

Mathematical models used in the simulation of ship motions

In the figures that will follow, results from numerical simulations are compared with experimental data. In particular two relatively simplified mathematical models have been employed in this work, namely:

- A 1-DOF nonlinear roll model based on a relative angle approach;
- A 2x3-DOF model using a nonlinear relative angle approach for sway-roll-yaw and a linear approach for surge, heave and pitch;

The background theory for the two methods can be found in [26], and here only brief descriptions are given. It is important to underline here, in connection with the discussion on the effect of the tank depth on the experimentally generated waves, that all the potential hydrodynamic calculations used in the numerical simulation of ship motions have been carried out under the deep water approximation. Hence, part of the discrepancies could also be due to the neglecting of the limited depth effects, but this aspect has not been investigated in this work.

1-DOF model

In this case the roll motion equation is written as:

$$\ddot{\phi} + 2\mu \cdot \dot{\phi} + \beta \cdot \dot{\phi}\left|\dot{\phi}\right| + \delta \cdot \dot{\phi}^3 = -\omega_0^2 \cdot \frac{\overline{GZ}\left(\phi - r(\omega) \cdot \pi \cdot s_w \cdot \sin(\omega t)\right)}{\overline{GM}} \tag{11}$$

where μ, β and δ are roll damping coefficients, ω_0 is the roll natural frequency, $\overline{GZ}$ is the calm water righting lever, $\overline{GM}$ is the calm water metacentric height, ω is the wave frequency, s_w is the wave steepness and $r(\omega)$ is the effective wave slope function determined from linear potential strip theory calculations according to the simplified decoupling procedure described in [26][27]. It is to be underlined that in model (11) the effect of drift speed is neglected. As a conclusion to the discussion on the determination of damping coefficients from different scales it was found that a clear trend was not evident from the obtained data, hence, in the simulations of model (11) the average damping coefficients from the three scales have been used. Similarly the roll natural frequency ω_0 has been taken as the average from the three tested models for each loading condition. Model's parameters for the various conditions are reported in Table 6, while Figure 52 shows the calculated effective wave slope function for the two loading conditions as a function of the wave frequency. In the potential hydrodynamic calculations bilge keels have been neglected, and the hydrodynamic coefficients have been calculated for the bare hull. In Figure 52, for each loading condition, the points corresponding to the effective wave slope calculated at the average natural frequency between configuration with and without bilge keels for the two values of $\overline{GM}$ are also marked. The effective wave slope at the roll natural frequency calculated using the direct hydrodynamic approach will be later compared with the effective wave slope coefficient as calculated according to the Weather Criterion.

Roll response curves in case of the 1-DOF model have been determined from the analysis of time histories coming from time domain numerical integration of equation (11).

Table 6: Coefficients used in 1-DOF numerical simulations.

Loading cond.	$\omega_0[rad/s]$	$\mu/\omega_0[nd]$	$\beta[rad^{-1}]$	$\delta\cdot\omega_0[nd]$
GM=2m - BH	0.344	0.81E-2	0.129	1.084
GM=2m - BK	0.341	1.03E-2	0.690	0
GM=4m - BH	0.493	0.65E-2	0.149	0.878
GM=4m - BK	0.488	1.20E-2	0.607	0

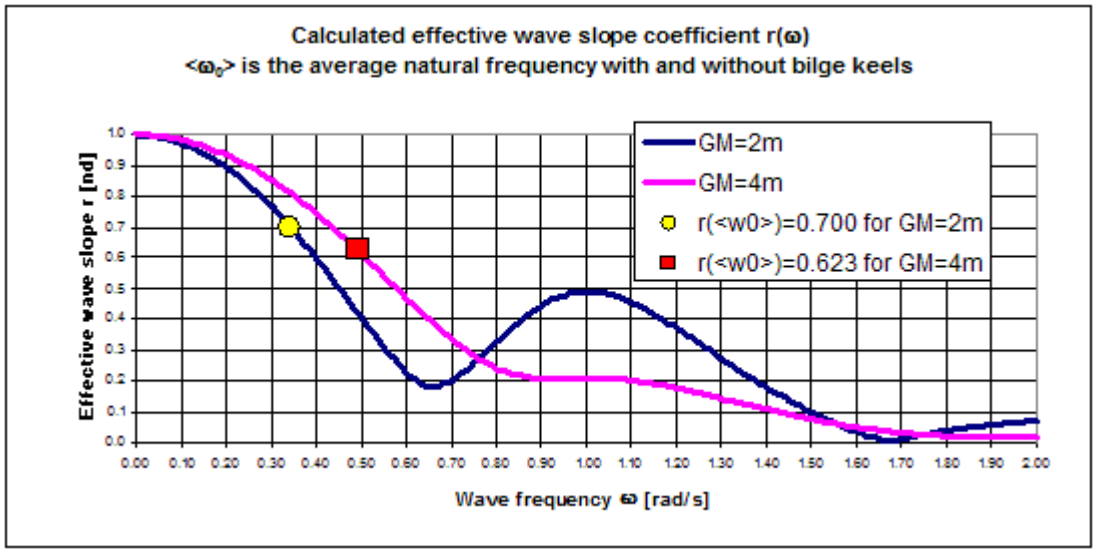

Figure 52: Calculated effective wave slope function.

3(x2)-DOF model

In this case the roll motion is considered coupled with sway and yaw. The 3-DOF model is obtained starting from standard zero speed linear seakeeping equations and transforming the linear roll restoring into a nonlinear roll restoring based on a "semi-empirical relative angle" γ_0. The model is intended to be used in frequency domain, and it is thus written in complex notation as follows:

$$\left(\underline{\underline{M}}+\underline{\underline{A}}(\omega)\right)\cdot\underline{\ddot{x}}+\underline{\underline{B}}(\omega,\underline{\dot{x}})\cdot\underline{\dot{x}}+\underline{\underline{C}}\left(\|\hat{\gamma}_0\|\right)\cdot\underline{x}=\underline{\hat{F}}_{FK}(\omega)+\delta\underline{\hat{F}}_{FK}\left(\omega,\|\hat{\gamma}_0\|\right)+\underline{\hat{F}}_{DIFF}(\omega)$$

$$\|\hat{\gamma}_0\|=\left\|\hat{x}_4-\frac{\hat{F}_{4,FK}}{\Delta\overline{OM}}\right\|$$

$$C_{44}\left(\|\hat{\gamma}_0\|\right)=\Delta\cdot\overline{GM}_{eq}\left(\|\hat{\gamma}_o\|\right) \qquad (12)$$

$$\text{with } \overline{GM}_{eq}\left(\|\hat{\gamma}_o\|\right)=\frac{1}{\|\hat{\gamma}_o\|}\cdot\frac{2}{\pi}\int_0^{\pi}\overline{GZ}\left(\phi=\|\hat{\gamma}_o\|\cdot\sin\alpha\right)\cdot\sin(\alpha)\,d\alpha$$

$$\delta\hat{F}_{4,FK}\left(\omega,\|\hat{\gamma}_0\|\right)=\frac{\overline{GM}_{eq}\left(\|\hat{\gamma}_o\|\right)-\overline{GM}}{\overline{OM}}\cdot\hat{F}_{4,FK}$$

In (12):

- $\underline{\underline{M}}$ is the generalised (6x6) mass matrix;
- $\underline{\underline{A}}(\omega)$ is the linear generalised added mass matrix;
- $\underline{\underline{B}}(\omega, \underline{\dot{x}})$ is the nonlinear generalised damping matrix;
- $\underline{\underline{C}}(\|\hat{\gamma}_0\|)$ is the restoring matrix where the coefficient $C_{44}(\|\hat{\gamma}_0\|)$ depends on the norm $\|\hat{\gamma}_0\|$ of the "semi-empirical relative angle" γ_0;
- $\underline{\hat{F}}_{FK}(\omega)$ is the complex vector (6x1) of generalised Froude-Krylov forces;
- $\delta\underline{\hat{F}}_{FK}(\omega, \|\hat{\gamma}_0\|)$ is a correction on $\underline{\hat{F}}_{FK}(\omega)$ to fulfil the low frequency limit for the model (12);
- $\underline{\hat{F}}_{DIFF}(\omega)$ is the complex vector (6x1) of generalised diffraction forces;
- $\overline{GM}$ is the metacentric height;
- $\overline{GZ}$ is the calm water righting lever;
- $\overline{OM}$ is the vertical distance between the centre of the seakeeping reference system and the transversal metacentre.

Nonlinearities of roll damping are introduced in the element B_{44} as follows:

$$\begin{aligned}
&\hat{\phi} = A_{roll} \cdot e^{-j\delta_{roll}} \\
&\left(B_{44} + B_{44,add}\right) \cdot \dot{\phi} + B_{quad} \cdot \dot{\phi}\left|\dot{\phi}\right| + B_{cub} \cdot \dot{\phi}^3 \rightarrow B_e \cdot \dot{\phi} \\
&B_e = B_{44} + B_{44,add} + B_{quad} \cdot \frac{8}{3\pi} \cdot \omega \cdot A_{roll} + B_{cub} \cdot \frac{3}{4} \cdot \left(\omega \cdot A_{roll}\right)^2
\end{aligned} \tag{13}$$

The additional linear damping coefficient $B_{44,add}$ is determined from an eigenvalues analysis of the basic linear seakeeping system of equations at a frequency ω_0 in order to match the experimental value of μ (see Table 6). Quadratic and cubic damping coefficients B_{quad} and B_{cub}, instead, are calculated from β and δ by using:

$$\begin{pmatrix} B_{quad} \\ B_{cub} \end{pmatrix} = \frac{\Delta\overline{GM}}{\omega_0^2} \cdot \begin{pmatrix} \beta \\ \delta \end{pmatrix} \tag{14}$$

Due to the limited difference in the roll natural frequency with and without bilge keels, it has been decided, in the 3-DOF approach, to use the average value of the natural frequency in order to reduce the number of pre-calculation needed for the application of the methodology. Coefficients $B_{44,add}$, B_{quad} and B_{cub} have been considered frequency independent.

The model (12) is solved in frequency domain by means of an appropriate zero search procedure. It is important to note that the frequency domain solution of (12) allows to disclose both (multiple) stable and unstable steady solutions when they exist for the same forcing frequency. On the other hand, the direct numerical integration of the 1-DOF model (equation (11)) does not allow to see unstable solutions, unless approximate analytical methods [28] or more complex numerical approaches (like continuation analysis [29]) are applied. Moreover, model (12) allows to address the

coupling of roll with sway and yaw, that is a feature completely missing in (11). On the other hand (12) is more complex to apply, requires numerical care in its solution, and it suffers of some consistency problems associated to changes in the centre of the seakeeping reference system [26]. In the present calculations the centre of the seakeeping reference system is assumed amidships, at the intersection between the waterline and the centreplane. Similarly to the case of the application of the 1-DOF model, also in the case of the 3-DOF the effect of drift has been neglected.

Roll response curves

Experimentally determined roll response curves are reported in Figure 53 to Figure 56. It is recalled that the used steepness does not correspond to the IMO requirements due to limitations in the available range of the wave maker. In the graphs ω_e is the measured encounter frequency (i.e. the measured roll frequency), while ω_0 is the measured roll natural frequency. Tests outside the acceptable $\pm 10\%$ estimated error on wave steepness (see Figure 47) have been neglected. Numerical simulations based on the two employed models are also superimposed to the experimental data. In the figures uncertainty bounds concerning the measured average roll amplitude have not been reported since they are in general very small with a coefficient of variation for the estimated average roll amplitude of the order of 2%-4% on average.

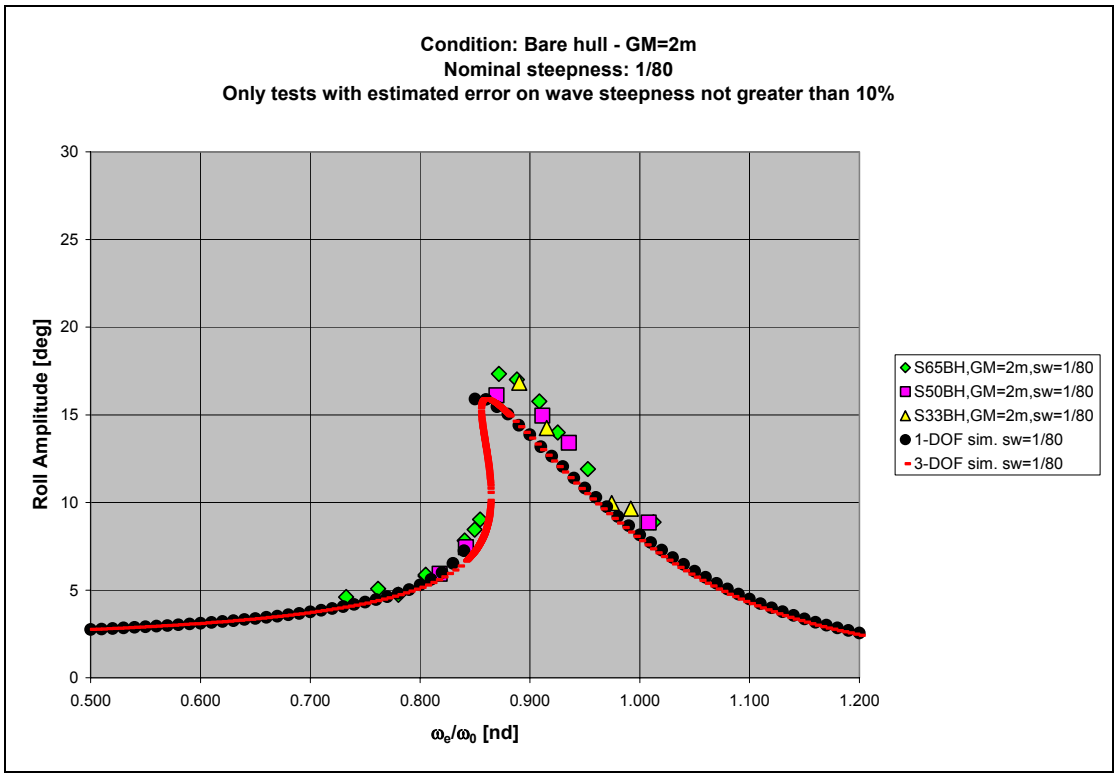

Figure 53: Roll response curves. $\overline{GM} = 2m$, bare hull.

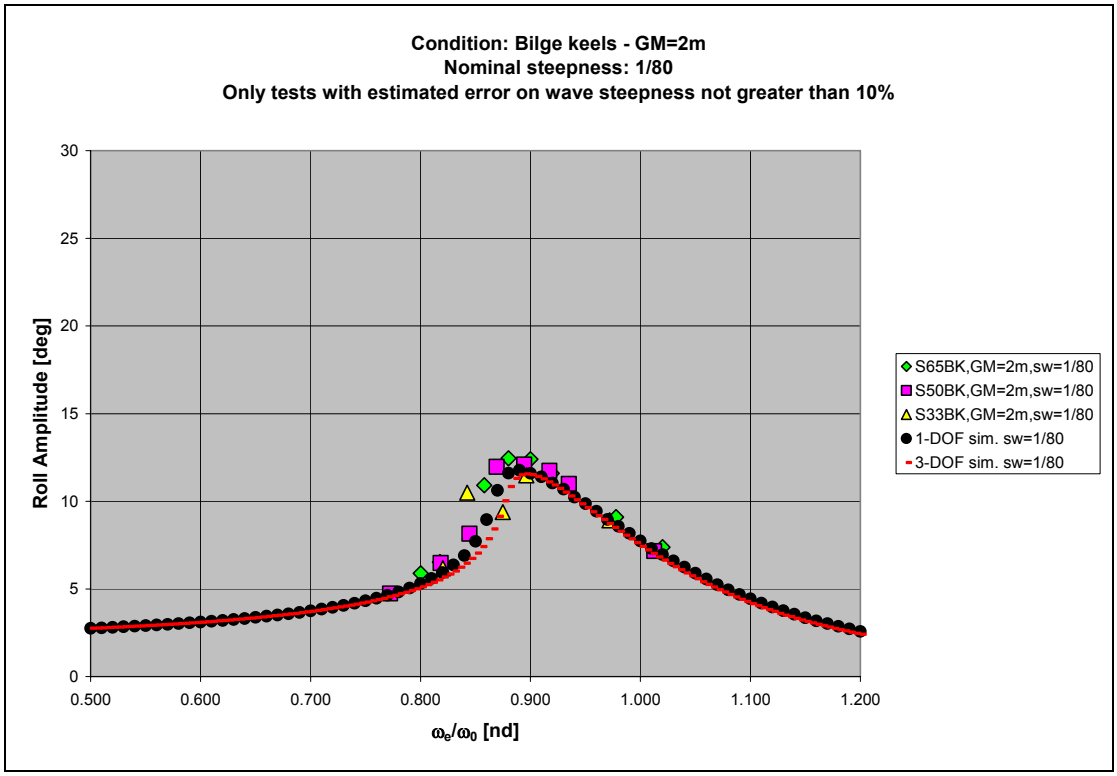

Figure 54: Roll response curves. $\overline{GM} = 2m$, bilge keels.

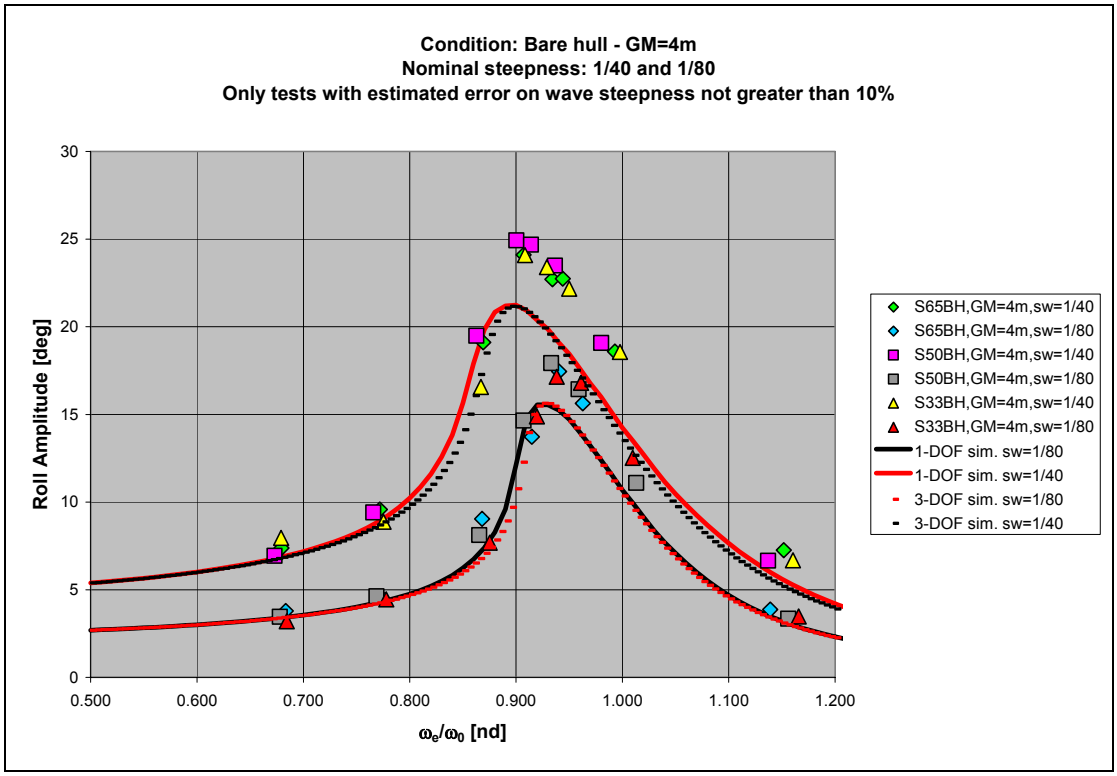

Figure 55: Roll response curves. $\overline{GM} = 4m$, bare hull.

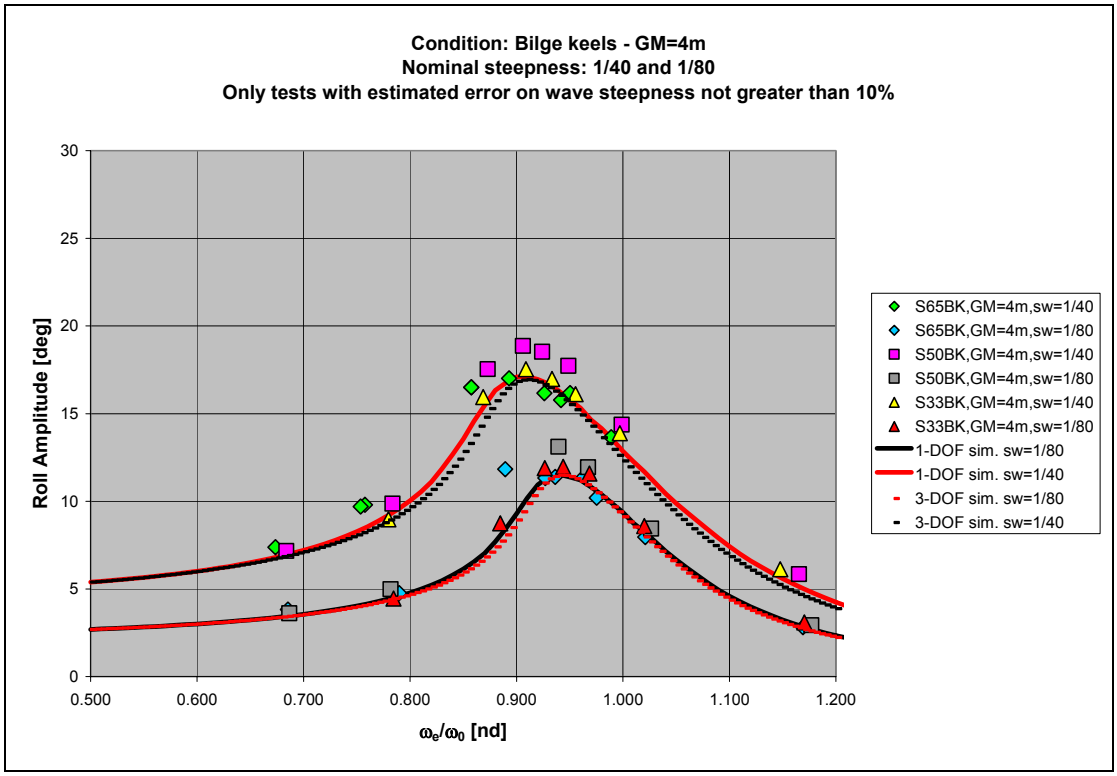

Figure 56: Roll response curves. $\overline{GM} = 4m$, bilge keels.

According to the evidence in Figure 53 to Figure 56, it is possible to provide a series of comments:

- There is a significant reduction of the maximum roll when fitting the ship with bilge keels.
- The difference of roll amplitude for the steepness $s_w = 1/80$ is not very large when comparing cases $\overline{GM} = 2m - BH$ and $\overline{GM} = 4m - BH$, and when comparing cases $\overline{GM} = 2m - BK$ and $\overline{GM} = 4m - BK$, and this result is consistent with the fact that the measured nondimensional amplitude dependent roll damping is not very dissimilar for the two values of metacentric height, as well as the calculated effective wave slope coefficient for the two loading conditions.
- Differences on roll peaks among different scales are limited and, in particular, not systematic. Similarly to what was found in case of roll decays, there seems not to be any evident strong scale effect, or, better, scale effects that are necessarily present, are in general masked by the global uncertainty. An exception is the case $\overline{GM} = 4m - BK$ at scale 1:50 (see Figure 56), that shows significantly larger peaks for the two tested wave steepnesses.
- There is an evident bending of the roll response curves towards the low frequency side due to the softening behaviour of the roll restoring. This bending is particularly important from a regulatory point of view because it proves that testing at a wave frequency equal to the roll natural frequency almost never leads to the determination of the actual peak or the roll response, and a sufficiently large range of frequency is to be tested to have a global picture of the nonlinear roll response curve. The bending is particularly evident in Figure 53 due to the large rolling (it is a bare hull series of tests) associated to a small metacentric height (2m).

- Numerical simulations carried out using the 1-DOF model and the 3-DOF model show in general similar results. In particular, when the peak of the response curve is of concern, the outcomes are almost identical.
- Numerical simulations are in very good agreement with experiments in case of tests carried out with bilge keels (see Figure 54 and Figure 56). Going to tests in bare hull conditions the agreement is good in case of relatively small maximum rolling amplitudes (see Figure 53), but worsens when the maximum rolling amplitude increases (see Figure 55, especially $s_w = 1/40$). One reason for the disagreement could be sought in the extrapolation of the bare-hull damping model (linear+quadratic+cubic in roll velocity) outside the tested range of rolling amplitudes available from roll decays. On the other hand, as expectable, the linear+quadratic damping model used for the bilge-keels cases proves to be more robust in case of extrapolations at large rolling amplitudes.
- The numerical simulation in Figure 53 shows a strong bending, confirmed by the experimental results, as well as a limited region of coexistent multiple steady state solutions. The possible existence of multiple steady states in beam regular waves is well known (see, e.g., [30][24]), and also recognised by [5]. Although in the experiments a direct check for multiple steady states has not been performed, the sharp jump in the roll response peak seems to confirm the possible presence of a fold bifurcation in the region of tested wave frequencies, as predicted by the numerical model.

Motions other than roll

As specified in the description of the experimental setup and technique the whole set of six degrees of freedom of the model has been measured by means of a non intrusive RODYM system [16] with a subsequent analysis procedure described in Appendix 2. In the context of the alternative assessment of Weather Criterion according to [4] motions different from roll are of limited importance (apart from yaw that is required to be kept sufficiently close to a beam sea condition). However data obtained from present tests represented also an interesting opportunity for an analysis of motions that are often dedicated less attention. In view of this, Appendix 3 describes the experimental results and the corresponding numerical simulations (when available) for the following quantities:

- Drift speed in the direction of wave propagation;
- Amplitude of sway oscillation at the reference point;
- Amplitude of yaw oscillation;
- Amplitude of heave oscillation at the reference point;
- Amplitude of pitch oscillation;

Link with the Weather Criterion

The obtained data from tests in beam regular waves, combined with the data from roll decay tests and from information gathered from the numerical simulations allow to critically discuss the application, or better, a slightly modified application, of the Weather Criterion [2][3] in the case of the tested ship, with particular emphasis on the coefficients [2][3] used for the determination of the "angle of roll to windward due to wave action" [4].
All the geometrical data necessary for the calculation of the coefficients involved in the application of the Weather Criterion (limited to the rolling angle) can be found in the section of this report describing the hull form.

We recall here that, according to the Weather Criterion, the "angle of roll to windward due to wave action" ϕ_1 is calculated as follows:

$$\phi_1 = 109 \cdot k \cdot X_1 \cdot X_2 \cdot \sqrt{r \cdot s} \tag{15}$$

In (15) the coefficient s is the wave steepness. Apart from the wave steepness, coefficients in (15) have been calculated for the CEHIPAR2792 and are reported in Table 7. In Table 7 two values of the coefficient k are reported, one is calculated taking into account the projected area of the skeg in the ratio $A_k / (L \cdot B)$, while the other one is calculated without considering the skeg area in A_k. As a reminder, A_k is defined as "total overall area of bilge keels, or area of the lateral projection of the bar keel, or sum of these areas" according to [2][3]. The reason for considering two options in the calculation of A_k is that it is not clear whether the skeg area shall be considered in A_k or not, and this aspect is subject to interpretation by the Administrations.

Table 7: Main parameters for the determination of the "angle of roll to windward due to wave action".

			$\overline{GM} = 2m$	$\overline{GM} = 4m$
		r	1.572	1.390
		X_1	0.800	
		X_2	0.934	
k	Bare hull	with skeg	0.814	
		without skeg	1.000	
	With bilge keels	with skeg	0.712	
		without skeg	0.960	

Looking at Table 7 it is immediate to notice the extremely large difference between the effective wave slope calculated according to the Weather Criterion and the effective wave slope coefficient calculated according to the proposed hydrodynamic procedure (see Figure 52). This point will be further elaborated later in this section.
As a further step we recall that the "angle of roll to windward due to wave action" ϕ_1 is not the actual prediction of the maximum rolling angle in beam regular waves with steepness s because it contains an "hidden" reduction factor taking into account the actual irregular nature of the sea (see [2][3][4]). Inverting the equation (4.1.1) in [4] it is possible to obtain an estimation of the so called "regular waves roll-back angle" ϕ_{1r} for a wave steepness s as:

$$\phi_{1r} = \frac{\phi_1}{0.7} = \frac{109 \cdot k \cdot X_1 \cdot X_2 \cdot \sqrt{r}}{0.7} \cdot \sqrt{s} \tag{16}$$

According to [4][31] the reduction factor 0.7 takes into account the actual irregular nature of the sea, indeed it reduces the actual measured peak of the roll response curve in regular waves (ϕ_{1r}) by 30% leading to the angle ϕ_1 finally used in the application of the Weather Criterion methodology [3]. As a general note, the functional relationship in (16) between the peak of the roll response curve, the effective wave

slope coefficient and the wave steepness can be rigorously obtained from an approximate solution of a 1-DOF roll model with pure linear restoring and pure quadratic damping by using the concept of amplitude dependent equivalent linear damping coefficient.

As said it was not possible to test the IMO required wave steepness due to limitations in the wave generation in particular for the largest and the medium size models. In order to discuss the application of the Weather Criterion methodology we could have followed two options:

1) The first option is to extrapolate the results of the experiments to larger wave steepnesses as requested by the Weather Criterion.
2) The second option is to use formula (16) considering the steepness s as a variable, and giving to this variable the value of the (nominal) steepnesses used in the tests.

The first procedure would be consistent with the methodology described in the "alternative procedures" in [4]. However, the extrapolation is often a dangerous process (as exemplified also in Figure 55 for the roll damping), hence we have decided to avoid it. We have thus followed the second way, and we have compared the rolling amplitudes predicted by (16), using coefficients in Table 7, with those obtained from experiments and those obtained by the 1-DOF and 3-DOF simulations.

Table 8 summarises the maximum rolling amplitudes obtained from experiments: the mean value among scales as well as the standard deviation of data are also reported, and will be used later for comparison. A note is necessary on the 11.5deg peak for the case $\overline{GM} = 2m - BK$ scale 1:33: the actual peak of the measured response curve is larger and about 12.3deg when considering all the tests and not only the not rejected ones, however the corresponding case has been neglected due to an estimated error on the wave steepness of 16%, that is outside the acceptable band used in this tests. Table 9 shows the predicted maximum rolling amplitudes according to (16) for the tested conditions, while Table 10 summarises experimental data and predictions according to the different methodologies with a calculation of the average involved error for each prediction method.

Table 8: Experimental maximum rolling amplitudes in the tested conditions

	Experimental maximum roll amplitudes (only not rejected tests)											
	s	Scale 65	Scale 50	Scale 33	Mean [deg]	STD [deg]	s	Scale 65	Scale 50	Scale 33	Mean [deg]	STD [deg]
GM=2m - BH:	0.0125	17.3	16.1	16.8	16.8	0.6						
GM=2m - BK:	0.0125	12.4	12.1	11.5	12.0	0.5						
GM=4m - BH:	0.0125	17.4	17.9	17.1	17.5	0.4	0.025	24.1	24.9	24.1	24.4	0.5
GM=4m - BK:	0.0125	11.8	13.1	12.0	12.3	0.7	0.025	17.0	18.9	17.5	17.8	1.0

Table 9: Prediction of maximum rolling amplitudes in the tested conditions according to the Weather Criterion methodology.

	Roll amplitude prediction according to WeC with modified steepness (/0.7 to remove the contribution for stochasticity)							
					s=1/80	Roll [deg]	s=1/40	Roll [deg]
With SKEG in Ak	GM=2m - BH:	109*k*X1*X2*r^0.5*/0.7=	118.7		0.0125	13.3		
	GM=2m - BK:	109*k*X1*X2*r^0.5*/0.7=	103.9		0.0125	11.6		
	GM=4m - BH:	109*k*X1*X2*r^0.5*/0.7=	111.7		0.0125	12.5	0.025	17.7
	GM=4m - BK:	109*k*X1*X2*r^0.5*/0.7=	97.7		0.0125	10.9	0.025	15.4
Without SKEG in Ak	GM=2m - BH:	109*k*X1*X2*r^0.5*/0.7=	145.9		0.0125	16.3		
	GM=2m - BK:	109*k*X1*X2*r^0.5*/0.7=	140.0		0.0125	15.7		
	GM=4m - BH:	109*k*X1*X2*r^0.5*/0.7=	137.2		0.0125	15.3	0.025	21.7
	GM=4m - BK:	109*k*X1*X2*r^0.5*/0.7=	131.7		0.0125	14.7	0.025	20.8

Table 10: Summary concerning maximum measured and predicted rolling amplitude for the tested conditions according to different methodologies.

		Definition of "Error": Err = ϕ_{calc} - ϕ_{exp} Definition of "%Error": %Err =100 * (ϕ_{calc} - ϕ_{exp})/ϕ_{calc}													
	Steepness	Ave. Max Roll Exp [deg]	2*STD exp [deg]	WeC with skeg in Ak	Err. [deg]	% Err	WeC without skeg in Ak	Err. [deg]	% Err	Sim. 1DOF	Err. [deg]	% Err	Sim. 3DOF	Err. [deg]	% Err
GM=2m - BH:	0.0125	16.8	1.2	13.3	-3.5	-26.3	16.3	-0.5	-2.8	15.9	-0.9	-5.4	15.9	-0.8	-5.3
GM=2m - BK:	0.0125	12.0	1.0	11.6	-0.4	-3.4	15.7	3.6	23.3	11.8	-0.2	-2.1	11.6	-0.5	-3.9
GM=4m - BH:	0.0125	17.5	0.8	12.5	-5.0	-40.2	15.3	-2.2	-14.2	15.6	-2.0	-12.5	15.6	-1.9	-12.0
GM=4m - BK:	0.0125	12.3	1.4	10.9	-1.4	-12.6	14.7	2.4	16.5	11.5	-0.8	-6.7	11.5	-0.8	-7.2
GM=4m - BH:	0.0250	24.4	1.0	17.7	-6.7	-38.1	21.7	-2.7	-12.4	21.2	-3.1	-14.8	21.2	-3.2	-15.2
GM=4m - BK:	0.0250	17.8	1.9	15.4	-2.4	-15.3	20.8	3.0	14.5	17.1	-0.7	-4.0	16.9	-0.9	-5.1
		Average error:			-3.2	-22.7		0.6	4.1		-1.3	-7.6		-1.3	-8.1
		Average absolute error:			3.2	22.7		2.4	13.9		1.3	7.6		1.3	8.1
		Average error BH:			-5.1	-34.9		-1.8	-9.8		-2.0	-10.9		-2.0	-10.8
		Average absolute error BH:			5.1	34.9		1.8	9.8		2.0	10.9		2.0	10.8
		Average error BK:			-1.4	-10.5		3.0	18.1		-0.6	-4.3		-0.7	-5.4
		Average absolute error BK:			1.4	10.5		3.0	18.1		0.6	4.3		0.7	5.4

Comparisons between experiments and predictions are also graphically summarised in Figure 57 and Figure 58.

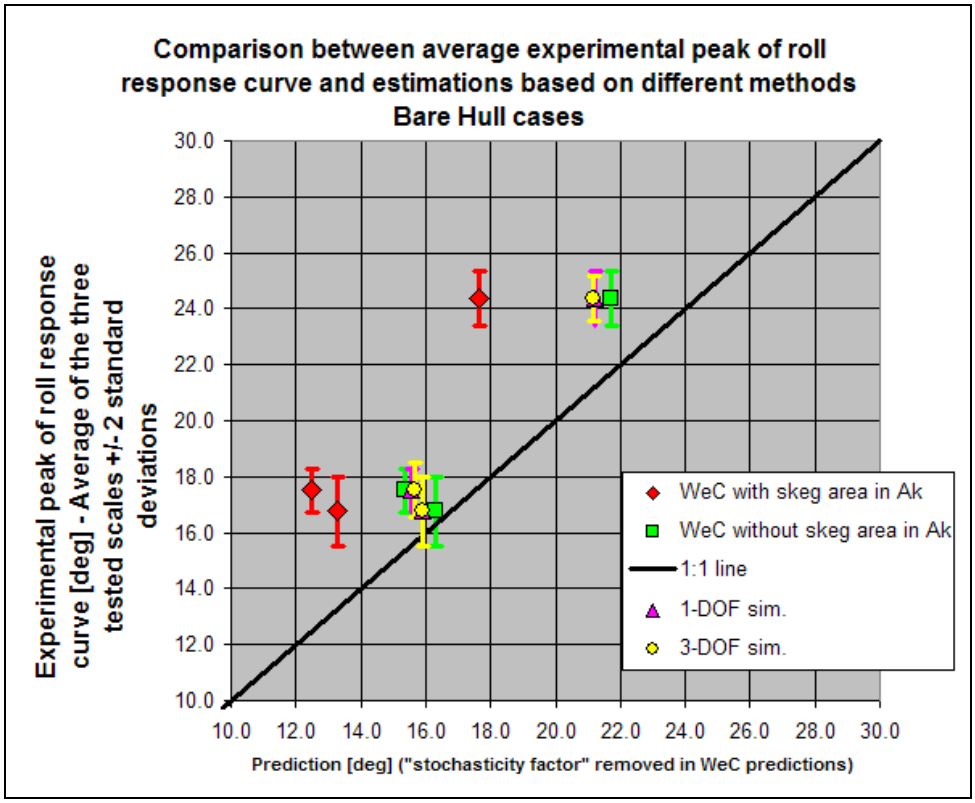

Figure 57: Comparison between experiments and predictions of maximum rolling amplitude in beam waves. Bare hull conditions.

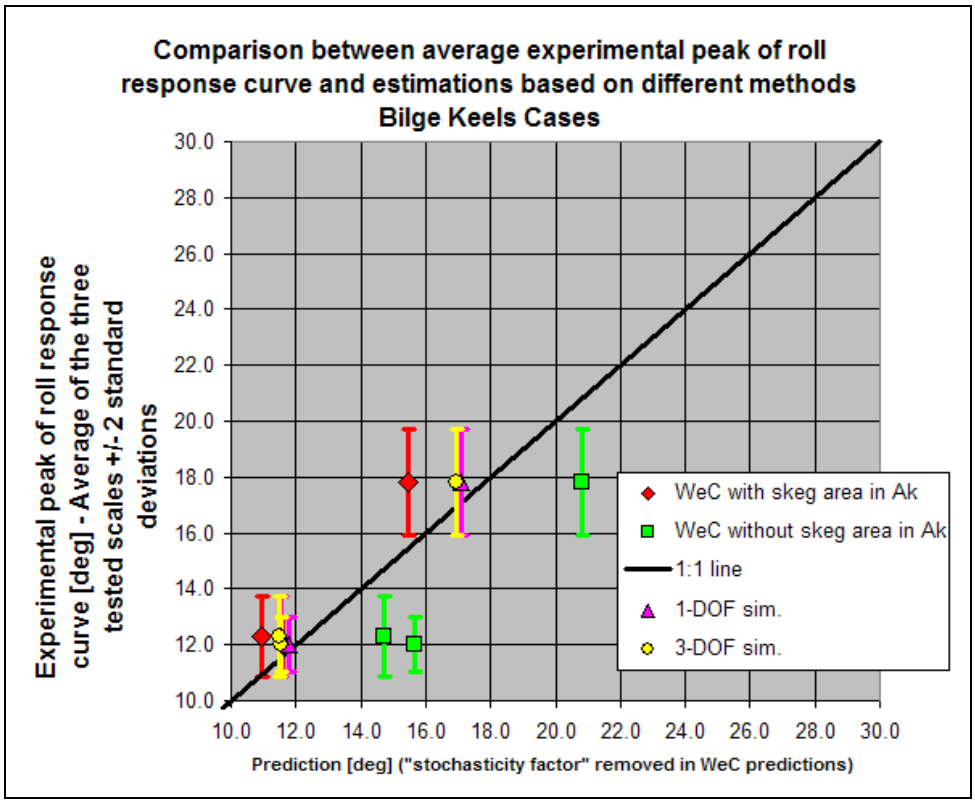

Figure 58: Comparison between experiments and predictions of maximum rolling amplitude in beam waves. Models fitted with bilge keels.

According to the obtained results it is possible to make a series of comments:

- Predictions obtained by the Weather Criterion method in general underestimate the measured rolling amplitude when the area of the skeg is included in A_k. On the other hand if the skeg area is not considered in A_k the WeC method underestimates the rolling amplitude in bare hull cases (see Figure 57), and overestimates the experimentally measured rolling amplitudes when models are fitted with bilge keels.
- Simulations based on the 1-DOF model and on the 3-DOF basically provides the same results. The actual roll peak is, on average, slightly underestimated. The underestimation is larger for bare hull models (see Figure 57) and the agreement is better, still with a slight underestimation, in cases where models were fitted with bilge keels (Figure 58).
- Looking at the error statistics in Table 10 it can be noticed that the worse predictions are given by the WeC method when the skeg area is considered in A_k. The WeC without skeg area in A_k shows improved error statistics, with a reduction on the average absolute percentage error from 22.7% to 13.9% using the whole sample. On the other hand, when bare hull and bilge keels cases are separated, it can be noticed that the improvement is given mainly by the strong reduction in the absolute percentage error for cases in bare hull condition, while the average absolute percentage error for cases with bilge keels is even significantly increased.
- Error statistics in case of 1-DOF and 3-DOF predictions are better than those of WeC without skeg in A_k in terms of average absolute percentage error. In case of bare hull cases WeC without skeg in A_k performs slightly better than 1-DOF and 3-DOF models, but in case of tests with bilge keels the numerical 1-DOF and 3-DOF predictions behave much better.
- The very similar outcomes from 1-DOF and 3-DOF models suggest the practical use of the much simpler 1-DOF instead of the more complex 3-DOF approach.
- Comparing Figure 52 and Table 7 it can be seen that the effective wave slope coefficient determined by the WeC method and the same coefficient based on hydrodynamic calculations are very different. Despite this difference the agreement between experimental results and prediction is comparable for the WeC (without skeg in A_k) and 1-DOF simulations. This means that the damping coefficient that is embedded in (16) is necessarily significantly larger than the actual experimental value, in order to compensate a too large effective wave slope. The quantity $0.7^{-1} \cdot 109 \cdot k \cdot X_1 \cdot X_2 \cdot \sqrt{r}$ is thus sufficiently correct as a whole, but the separation between damping and forcing seems to be not properly addressed.

There is another point that is worth to be addressed, namely the reduction effect of bilge keels on the maximum rolling amplitude. According to (15), or (16), the ratio of the roll peak amplitude with and without bilge keels is given by:

$$\frac{(\phi_{1r})_{BK}}{(\phi_{1r})_{BH}} = \frac{(\phi_1)_{BK}}{(\phi_1)_{BH}} = \frac{k_{BK}}{k_{BH}} \tag{17}$$

where the subscript "BH" indicates calculations performed in bare hull condition, while the subscript "BK" indicates calculations performed taking into account the presence of bilge keels. From the available experiments, the ratio $(\phi_{1r})_{BK}/(\phi_{1r})_{BH}$ can be directly obtained from experiments, while the ratio k_{BK}/k_{BH} can be directly calculated from Table 7. Table 11 shows an analysis of the experimentally determined ratio $(\phi_{1r})_{BK}/(\phi_{1r})_{BH}$ and the calculated ratio k_{BK}/k_{BH} with and without considering the skeg area in the computation of A_k.

Table 11: Roll amplitude reduction factor due to bilge keels.

	Estimation of "$\phi_{max,BK}/\phi_{max,BH}$" factor from experiments:				
	Scale 65	Scale 50	Scale 33	Mean	STD
GM=2m - sw=1/80:	0.718	0.751	0.682	0.717	0.034
GM=4m - sw=1/80:	0.678	0.731	0.698	0.702	0.027
GM=4m - sw=1/40:	0.706	0.756	0.728	0.730	0.025
			Joined sample:	0.716	0.028
			WeC with skeg in Ak:	0.875	
			WeC without skeg in Ak:	0.960	

From the results in Table 11 it can be seen that the effect on roll reduction due to the fitting of bilge keels as obtained in experiments is underestimated by the Weather Criterion. From experiments, a reduction of 28.4% (on average) of the roll peak amplitude with respect to the roll peak amplitude in bare hull condition has been achieved thanks to the fitting of the bilge keels. On the other hand, the reduction estimated by the WeC method is 12.5% when considering the skeg in A_k, and 4% when considering only the bilge keels in A_k. It seems, hence, that the relative effect of bilge keels is significantly underestimated by the present formulae in the standard WeC approach.

Concluding comments

Tests carried out in beam waves in this research and described in this section (as well as in the referred appendices) can be considered as a typical series of tests in the framework of the application of the alternative experimental assessment of the Weather Criterion [4][5]. Although the tested wave steepnesses were smaller than those required by [4][5] some experience has been gained through the execution of the tests.

It can be said, first of all, that the execution of completely free model tests poses a series of difficulties when the requirement, as in this case, is to keep the heading close to 90deg. The model is, indeed, quite sensitive to the initial transient and corrections are often necessary to yaw in order to keep the heading. When manual intervention is required, this poses some difficulties especially in case of large models.

The use of large models is often considered a means to avoid significant scale effects when propulsion / resistance tests are of concern. In the presented series of tests we have used three models ranging from 3.4m to 6.7m in length. The obtained results in terms of roll response curves did not show any significant difference that could be clearly ascribed to scale effects. Similarly to the outcome obtained from the analysis of roll decays, it seems that the scale effect (that must necessarily be present) is sufficiently small to be shadowed by the background scattering due to various sources

of experimental uncertainty. As a result, the obtained peaks of the roll response were very close each-other for the three tested models in the same conditions.
In none of the tested cases the peak of the response curve was found at an encounter frequency equal to the roll natural frequency. This is an expectable behaviour due to the nonlinear characteristics of the righting arm. A sufficient range of frequencies must be tested in order to have a good description of the peak of the roll response curve. Tests carried out exactly at the roll natural frequency are likely to provide a significant underestimation of the actual roll peak.
We have assessed the accuracy of the Weather Criterion formulation [2][3] in predicting the maximum rolling angle. The Weather Criterion basic formula for the prediction of the rolling angle has been applied using the nominal wave steepness set in the experiments. In applying the Weather Criterion formulation (removing the correction for the irregular nature of the sea) we have compared the outcomes of the predictions when the skeg area is either considered or omitted in the computation of the roll reduction factor. In addition, two mathematical models have been used, a 1-DOF (time domain) model based on a relative angle description for the restoring, and a similar, but 3-DOF and more complex (frequency domain) model. In case of the proposed mathematical models damping coefficients have been used as determined from roll decay experiments. From a comparison of the different methodologies it seems that the proposed 1-DOF with damping from experiments has the best overall performances in terms of average absolute value of the error with a tendency towards a slight underestimation of the experimental results. The measured rolling angle was usually underestimated by the Weather Criterion formula when the skeg is considered in the computation of the roll reduction factor, and better overall performances are obtained omitting the skeg area from the calculation. However, it was found that the reduction of roll amplitude given by the fitting of bilge keels is underestimated by the Weather Criterion.
The effective wave slope coefficient, that is a necessary piece in the 1-DOF calculations, has been determined from a direct hydrodynamic procedure based on linear potential theory. It was found that the effective wave slope coefficient at the roll natural frequency as calculated by the direct hydrodynamic procedure was significantly smaller than the effective wave slope coefficient as given by the formula in the Weather Criterion. It seems that, although the Weather Criterion formulation provides, on average, acceptable results in terms of roll angle, it is not able to correctly separate the wave forcing contribution (represented by the effective wave slope coefficient r) and the damping contribution (represented by the product $k \cdot X_1 \cdot X_2$): a (too) large effective wave slope coefficient is compensated by a (too) large damping, both likely far from actual real values.
The quality of generated waves has been assessed. The used procedure is an indirect one, since a wave probe was not available in a fixed tank position. The obtained results could, thus, be partially questionable in terms of achieved accuracy of the estimations. However, according to the used procedure, it was found that the average agreement between nominal and actually generated steepness was not bad, but that was quite difficult to obtain an error below 10%. From the whole set of experiments (globally 158), a total of 19, corresponding to about 12%, were considered as not acceptable and have been neglected in the analysis. Estimated errors below 5% have been obtained for 85 tests (53.8% of the total). In the analysis it was found that the commonly used deep water dispersion relationship between wave frequency and wave number can lead to not negligible error in case of long waves when the effect of the tank's depth is visible. This problem usually does not exist for seakeeping tests

associated to vertical motions, since in such case the tested waves are usually much shorter, but in case of beam sea resonance for large models, the considered waves could become sufficiently long for the depth effect to become clearly noticeable. Care should be taken of this aspect when planning and carrying out experiments.
Measured motions other than roll were also measured and analysed in a separate appendix. Some consistency problem has been found, that could have been introduced (this is only a conjecture) by an incorrect positioning/orientation/setting-up of the motion measuring system. Roll, however, seems to have not been (measurably) influenced. The analysis of transversal motions (yaw and sway) allowed to compare the simulations carried out using the 3-DOF model with the experimental results. The agreement for yaw was only qualitative, but in case of sway a good quantitative agreement was found. Vertical motions (heave and pitch) showed the less consistent results, and the reasons for such lack of consistency have not been fully understood, though some mistake in the reconstruction of vertical position of the reference point and pitch angle from the experimental setup seems to be, presently, the most reasonable justification.

Drift tests

Introduction

For this experimental campaign, drift tests were planned in order to investigate the possibility of having a heeling moment due to the hydrodynamic reaction to drift equivalent to a transversal drift reaction force "above water". In linear seakeeping calculations the hydrodynamic coefficients A_{42} and B_{42} are known to change their sign, in case of a rectangular two dimensional sections, as the beam-to-draught ratio is modified (see, e.g., Figure 6.9 to Figure 6.11 in [32]). A change of sign in A_{42} and/or B_{42} can lead to a change of sign of the hydrodynamic roll moment generated by an oscillatory sway $y(t)$, namely the moment $-A_{42}\cdot\ddot{y}-B_{42}\cdot\dot{y}$, as the beam-to-draught ratio is modified. More recently, Ishida & Fujiwara [33] investigated the same matter in case of oscillatory sway motion for small craft with large B/T ratios. They investigated the effect of the heeling angle in the obtained results and confirmed that the sway induced roll moment could be such to be "equivalent" to that given by a sway force "above water". In the development of the explanatory notes [5] to the MSC.1/Circ.1200 [4] the heeling moment induced by a steady lateral drift was investigated for a RoPax ferry with B/T=3.8 [5]. According to the results in [5] it was found that during a steady lateral drift, the roll moment created by the pressures acting on the underwater hull geometry can be considered as given by a force equal to the lateral drift force, but acting "above water". Although this result could seem, at first, surprising, it must be clarified that there isn't, of course, any real force above water: the system of pressures on the hull during the steady drift motion creates a rolling moment that is simply equivalent to the moment that would be generated by the total measured lateral force if it were considered to act along a line of action parallel to the waterplane and positioned above water.
This phenomenon, namely the sign and magnitude of the heeling moment created during a drift motion, is important in the framework of the experimental alternative assessment of the Weather Criterion [4] because it significantly influences the wind heeling moment to be used in the calculations. It was the intention of this project, therefore, to measure the heeling moment during drift tests at steady lateral drift speed

for different heeling angles. Although such tests have been actually carried out, the obtained results have been considered only partially reliable due to a series of observed inconsistencies in the data reconstructed from the experimental campaign. Since we have not been able to clarify, up to the moment of writing, a series of doubts concerning the obtained results, in this section we have reported only those data that have been judged sufficiently reliable and consistent. The remaining data are reported in Appendix 4 accompanied by a discussion on the reasons for considering such data as doubtful. To be more precise, the total drift force as measured by the dynamometer for the different tested models was found to provide a reasonable and consistent set of data. On the other hand, the scattering of data concerning the heeling moment due to drift was found to be very large and without clear underlying patterns when comparing different model scales. On the ground of a series of systematic investigations on the expected and measured ship sinkage and trim at zero speed, such large scattering was considered to be potentially associated to some systematic error / misunderstanding in the execution / setup of the experiments and/or in the data analysis. For such reasons it has deemed appropriate, at the stage of writing, to consider results for the heeling moment of too low standard quality.
This section is structured as follows:

- Firstly a description of the loading conditions, of the testing setup and technique is given, together with some information on the used methodology for the analysis of data.
- Results from the analysis of lateral drift force are given afterwards.
- Then a brief comment is given on results concerning the heeling moment, while a deeper discussion is reported in the separate Appendix 4.
- Some concluding remarks are finally reported.

Loading conditions, testing setup and technique

Drift tests have been carried out for the following cases:

- Model Scale 1:65, Draught=6.6m, with and without bilge keels.
- Model Scale 1:50, Draught=6.6m, with and without bilge keels.

During the tests the model was free to heave and pitch. Heeling angles ranged from 30deg windward to 40deg leeward and in all the tested cases the trim was nominally zero with the ship at zero heel. The heeling angle was imposed by means of an electric motor. The model was connected to a dynamometer attached to the carriage's turret by means of two vertical rods: while one rod was free to move only vertically, the second one was also free to rotate in order not to prevent a free pitch. Appropriate joints were placed at the connection of the rods to the model. According to the geometry of the system, the ship was free to heel around a longitudinal ship-fixed axis, while it was free to pitch around an earth-fixed axis parallel to the calm water plane and parallel to the ship-fixed transversal axis at zero heel and zero trim. According to this geometry heel and pitch are actually the naval Euler's roll and pitch angles. The ship's metacentric height was not carefully tested since, when it has reasonable values significantly smaller than the longitudinal metacentric radius, it only slightly influences trim during heel. Moreover, the actual vertical position of the centre of gravity of the ship is not relevant in this type of tests where only the hydrodynamic reaction moment is of concern with the model kept captive. The centre of gravity is only longitudinally adjusted in order to achieve a zero trim in upright position. According to the sign convention in the testing setup (see Figure 59), being the ship towed with a drifting direction to starboard, a portside heel corresponds to a "windward heeling", while a starboard heel corresponds to a "leeward heeling". The

largest model (scale 1:33) was not tested due to time constraints and difficulties in the setup of the experimental arrangement.

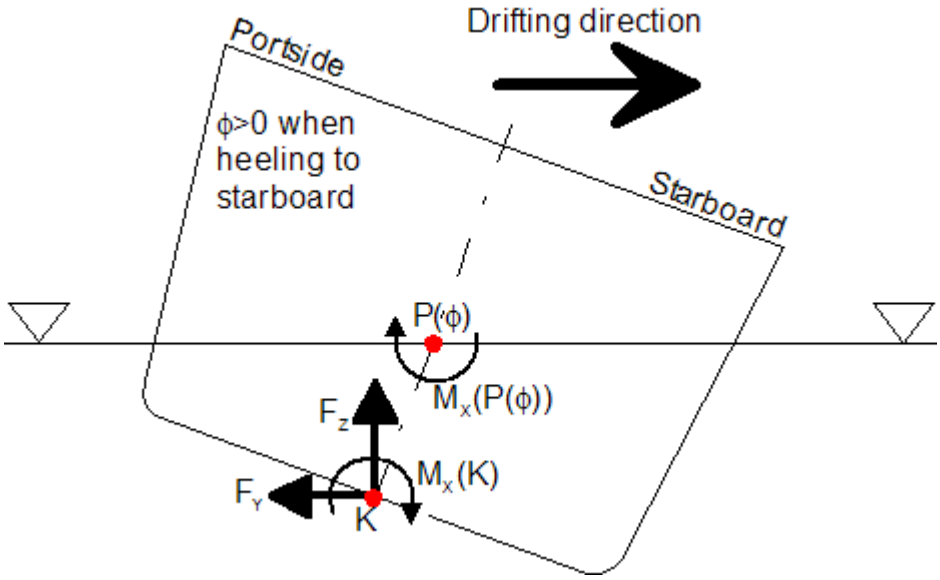

Figure 59: Signs convention for drift tests.

Six degrees of freedom were measured by means of a RODYM [16] non intrusive motion measuring system. The nominal reference point was positioned on the keel line at a longitudinal position corresponding to ship's centre of gravity. This longitudinal position also corresponds to the longitudinal position of the centre of buoyancy since the ship has zero trim at zero heel. According to hydrostatic calculations this point is about 2.66m aft of amidships. Although this is a misnomer, we will name in this section the reference point as the point "K" for sake of brevity (see Figure 59), bearing in mind that the actual keel point is on the keel line amidships, i.e. 2.66m forward of the used reference point.
Six forces where measured by a dynamometer connected to the carriage's turret. From the set of six forces the three components of the total force and of the total moment acting on the dynamometer could be determined with respect to the centre of the local reference system of the dynamometer. A transformation of this system of forces to the reference point allowed to obtain the system of three components force and three components moment with respect to the reference point "K" in Figure 59.
Original data concerning forces were significantly affected by noise induced, likely, by the turret's vibrations. In particular a strong noise was observed with characteristic frequencies in the range 7Hz-11Hz. Since it was not possible to mechanically remove such background noise, and because we are interested on average steady state quantities, all data were low-passed with a cut frequency of 3Hz before being processed. The transfer function of the used IIR filter is shown in Figure 60

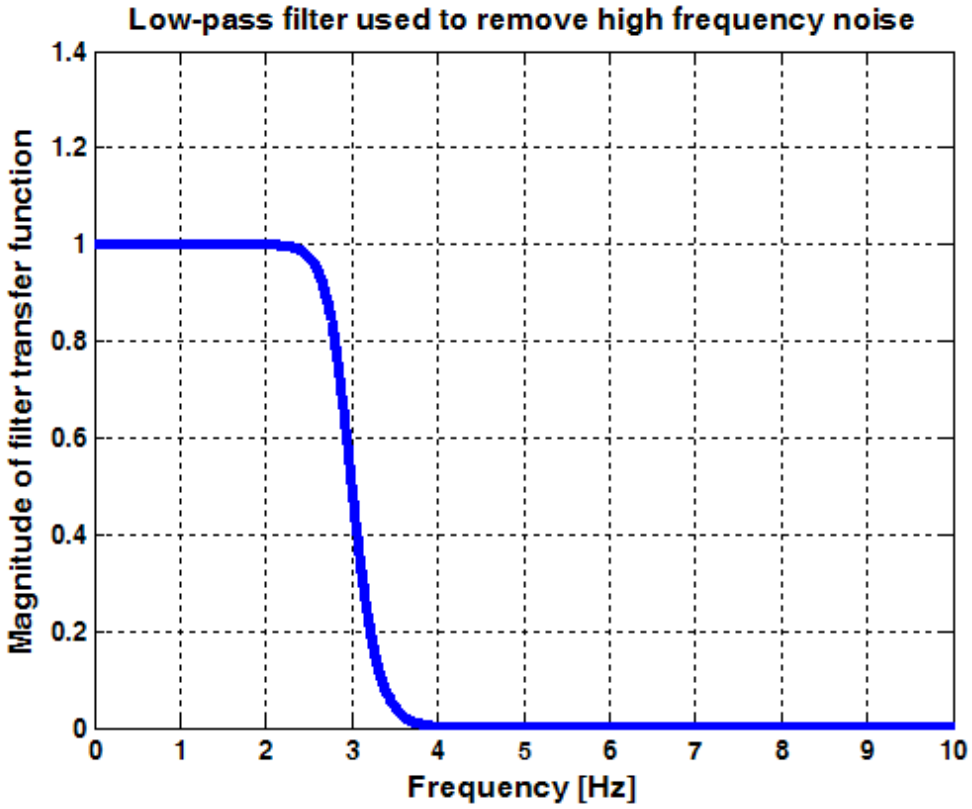

Figure 60: Transfer function of the filter used to remove high frequency noise.

It is important to underline that all the data analysis for drift tests refers to low-pass filtered data (with the exception of the measured drifting speed). Had the original raw data been used, the obtained standard deviations for each measured signal would have been extremely large, as it can be understood by the example reported in Figure 61 especially for the measured forces / moments. From the reported signals it can be noticed how large is the original noise. Just as a note reported to avoid confusions, although the drift motion is usually referred as "y", the drifting speed is reported as V_x because this is the conventional name given to the carriage speed in the longitudinal tank direction.

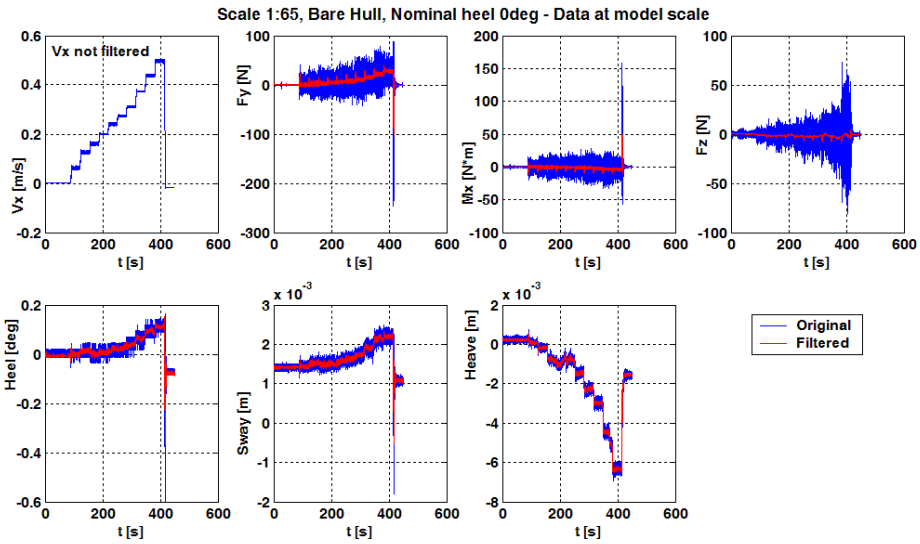

Figure 61: Example of measured signals before and after the low-pass filtering.

As can be seen from Figure 61 each test comprised a range of drift speeds, from 0m/s up to about 4m/s at full scale. Considering that the drift speed is roughly 10% of the incident mean wind speed for ships, like large passenger ships, having significant lateral windage area, it could be said that the tested drift speed range covers wind speed up to roughly 40m/s (78knots). The reference mean wind speed in the Weather Criterion is 26m/s [4] and this speed is likely covered by the tested range in case of a standard superstructures' arrangement.

In the analysis of the measured signals, time windows were chosen where the signals were sufficiently steady. Indeed, in the acceleration phase from a lower to a higher speed, transient effects occur that, although interesting, are not relevant in the present investigation and shall thus be omitted. For a given time history from a single test a series of time windows have been analysed, one for each target test speed (for instance, eleven speeds in case of Figure 61 including zero). In each window the average value of the measured signals and the standard deviation (root mean square value) were calculated (remember that we always refer to signals after the application of the low pass filter as discussed before). For a given generic signal $x_i(t)$ analysed in the time window $t \in [t_0, t_0 + T]$:

$$t \in [t_0, t_0 + T]$$

$$\text{Average: } \bar{x}_i = \frac{1}{T}\int_{t_0}^{t_0+T} x_i(t)\,dt \qquad (18)$$

$$\text{Standard deviation (RMS): } \sigma_{x,i} = \sqrt{\frac{1}{T}\int_{t_0}^{t_0+T} \left(x_i(t) - \bar{x}_i\right)^2 dt}$$

It is important to underline that the standard deviation $\sigma_{x,i}$ in (18) is the standard deviation associated to the signal x_i itself and shall not be confused with an estimation of the standard deviation of the estimated average $\bar{x}_i$. Indeed, the standard deviation associated to $\bar{x}_i$ is significantly smaller than $\sigma_{x,i}$ when the length T of the

time window is sufficiently larger than the typical correlation time of the noise. The standard deviation associated to $\bar{x}_i$ could be determined in principle, as a function of T, by using the autocorrelation function of the process $X_i(t)$ (see [34]). However, the autocorrelation function of an experimentally measured process is, in general, unknown a-priori, and it should be determined from the experimental data. Here it has been decided to report the uncertainty in terms of multiples of $\sigma_{x,i}$ as a measure of the dispersion of the measured (constructed) signal itself, and not as a measure of the dispersion of the calculated average $\bar{x}_i$. Accordingly, the uncertainty bands reported later in this section are larger than the uncertainty bands that should be associated to the average $\bar{x}_i$, and they basically represent a measure of noise (fluctuation with respect to the mean) in the analysed signal.
Expressions in (18) represent a direct processing stage based on the time histories, that maintain full information. Note that the generic analysed signal $x_i(t)$ could be a directly measured signal as, e.g., in the case of the speed V_x, or, in the majority of cases, it is a time domain variable obtained by combining time series from different sources. For example, in case of the total lateral drift force F_y the corresponding time series is obtained as the sum of the forces measured by two load cells.
However, in the post-processing phase it was necessary to combine the quantities obtained from the direct time domain analysis (18) in order to obtain new quantities. In such case we used the following approximation. Let a generic variable y be related to a vector of measured quantities $\underline{x} = (x_1, x_2, ..., x_N)^T$ by a generic function f, namely:

$$y = f(\underline{x}) \tag{19}$$

Assuming small deviations of the vector $\underline{x}$ from its average value, we can use the following first order Taylor expansion of (19):

$$\begin{aligned} y = f(\underline{x}) &\approx f(\underline{\bar{x}}) + \sum_{i=1}^{N} \left.\frac{\partial f}{\partial x_i}\right|_{\underline{\bar{x}}} \cdot (x_i - \bar{x}_i) = f(\underline{\bar{x}}) + \nabla f(\underline{\bar{x}}) \cdot (\underline{x} - \underline{\bar{x}}) \\ \underline{\bar{x}} &= (\bar{x}_1, \bar{x}_2, ..., \bar{x}_N)^T \\ \nabla f &= \left(\frac{\partial f}{\partial x_1}, \frac{\partial f}{\partial x_2}, ..., \frac{\partial f}{\partial x_N} \right) \end{aligned} \tag{20}$$

According to (20) the average value of y can be approximated as:

$$\bar{y} \approx f(\underline{\bar{x}}) \tag{21}$$

Moreover, assuming the fluctuations of the variables x_i to be uncorrelated it is possible to approximate the standard deviation of y as:

$$\sigma_y \approx \sqrt{\sum_{i=1}^{N} \left(\left. \frac{\partial f}{\partial x_i} \right|_{\underline{\bar{x}}} \right)^2 \cdot \sigma_{x,i}^2} \tag{22}$$

Of course (20), (21) and (22) represent a first approximation to the estimation of the average and standard deviation of the derived quantity y, but they can be considered as a reasonable fast and flexible tool able to provide information on average and dispersion of y in a post-processing stage, without the need to go back to the original time histories. Of course a better estimation would be obtained by constructing the time history $y(t) = f\left(\underline{x}(t)\right)$ and by analysing it according to (18): this would retain all the possible nonlinear features of the transformation function f as well as the possible statistical dependence of the fluctuations of the elements of the vector $\underline{x}(t)$. However, such a direct time domain approach would require to restart the analysis of the time series each time a new variable is constructed, making the approach time consuming when a large amount of data, as in this case, need to be analysed with a not negligible human intervention.

Analysis of lateral drift reaction force

As anticipated, here we are going to report the results concerning the lateral drift reaction force as measured in the tested conditions.
Results will be reported in dimensionless form in order to compare the two tested model scales. A drag coefficient C_D is thus defined as:

$$C_D = \frac{F_y}{\frac{1}{2} \cdot \rho_{water} \cdot A_{drift} \cdot V_{drift}^2} \tag{23}$$

where:

- F_y [N] is the total measured lateral force.
- A_{drift} [m^2] is the lateral underwater projected area at zero heel. This is a constant value of 1344m^2 at full scale for the tested draught of 6.6m.
- V_{drift} [m/s] is the lateral drift speed, and it corresponds to the measured speed V_x in Figure 61.
- ρ_{water} [kg/m^3] is the volumic mass of water, and it is assumed to be constant and equal to 1000kg/m^3.

While the time histories of F_y and V_{drift} were directly analysed, the drag coefficient has been calculated in a post processing phase. According to the procedure in (20)-(22) the average value of the drag coefficient and the corresponding standard deviation have been calculated as:

$$C_D = f\left(F_y, V_{drift}\right)$$

$$\overline{C}_D \approx \frac{\overline{F}_y}{\frac{1}{2}\cdot\rho_{water}\cdot A_{drift}\cdot\overline{V}_{drift}^2}$$

$$\sigma_{C_D} \approx \left[\frac{1}{\left(\frac{1}{2}\cdot\rho_{water}\cdot A_{drift}\cdot\overline{V}_{drift}^2\right)^2}\cdot\sigma_{F_y}^2 + \left(\frac{-2\cdot\overline{F}_y}{\frac{1}{2}\cdot\rho_{water}\cdot A_{drift}\cdot\overline{V}_{drift}^3}\right)^2\sigma_{V_{drift}}^2\right]^{\frac{1}{2}} \tag{24}$$

$$= \overline{C}_D\cdot\left[\left(\frac{\sigma_{F_y}}{\overline{F}_y}\right)^2 + \left(2\cdot\frac{\sigma_{V_{drift}}}{\overline{V}_{drift}}\right)^2\right]^{\frac{1}{2}}$$

According to (24) the coefficient of variation (CoV) of the drag coefficient can be expressed as a function of the coefficients of variation of the measured lateral drift force and the measured drift speed.

$$CoV\left(C_D\right) = \frac{\sigma_{C_D}}{\overline{C}_D} = \left[CoV^2\left(F_y\right) + 4\cdot CoV^2\left(V_{drift}\right)\right]^{\frac{1}{2}} \tag{25}$$

Note that (25) is the coefficient of variation of C_D and shall not be confused with the coefficient of variation of the estimated average $\overline{C}_D$, that, instead, should be based on the coefficients of variation of the estimated averages $\overline{F}_y$ and $\overline{V}_{drift}$. Results from the experiments are reported in Figure 62 to Figure 69. Each figure corresponds to a different nominal heeling angle. The calculated drag coefficient according to (23) is reported as a function of a dimensionless speed based on Froude scaling and defined as:

$$Fn_B = \frac{V_{drift}}{\sqrt{g\cdot B}} \tag{26}$$

where B is the ship breadth.

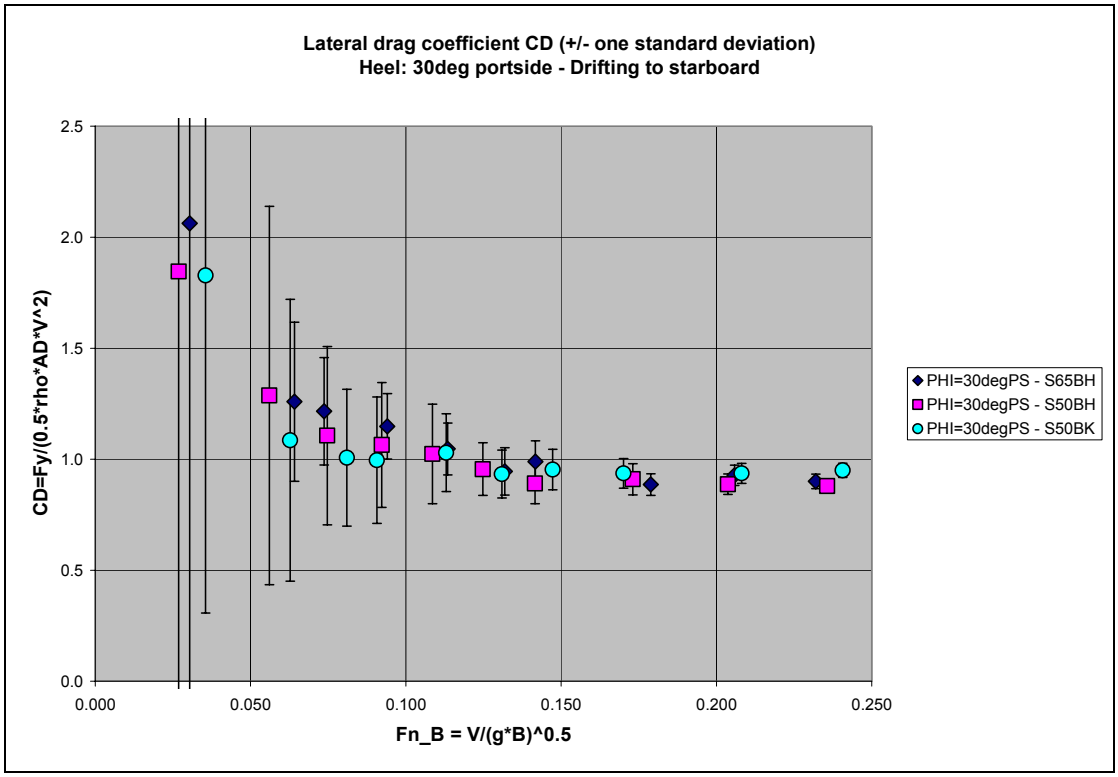

Figure 62: Lateral drag coefficient as measured from drift tests. Heel 30deg portside, drifting to starboard.

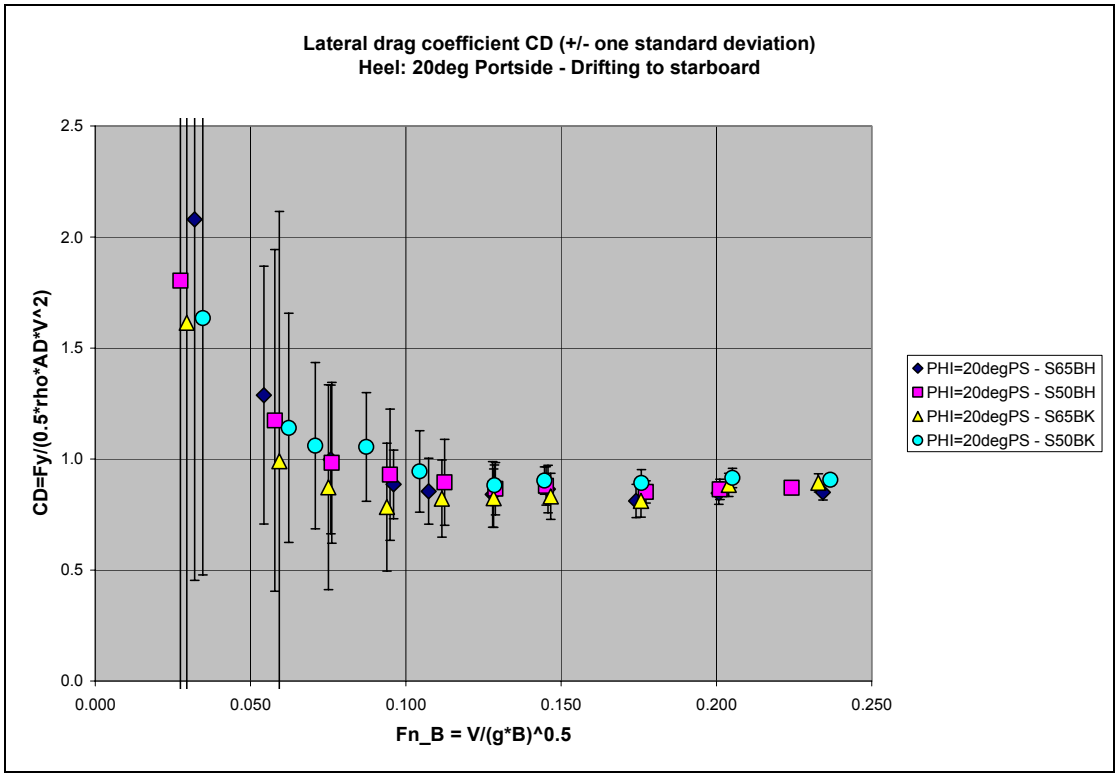

Figure 63: Lateral drag coefficient as measured from drift tests. Heel 20deg portside, drifting to starboard.

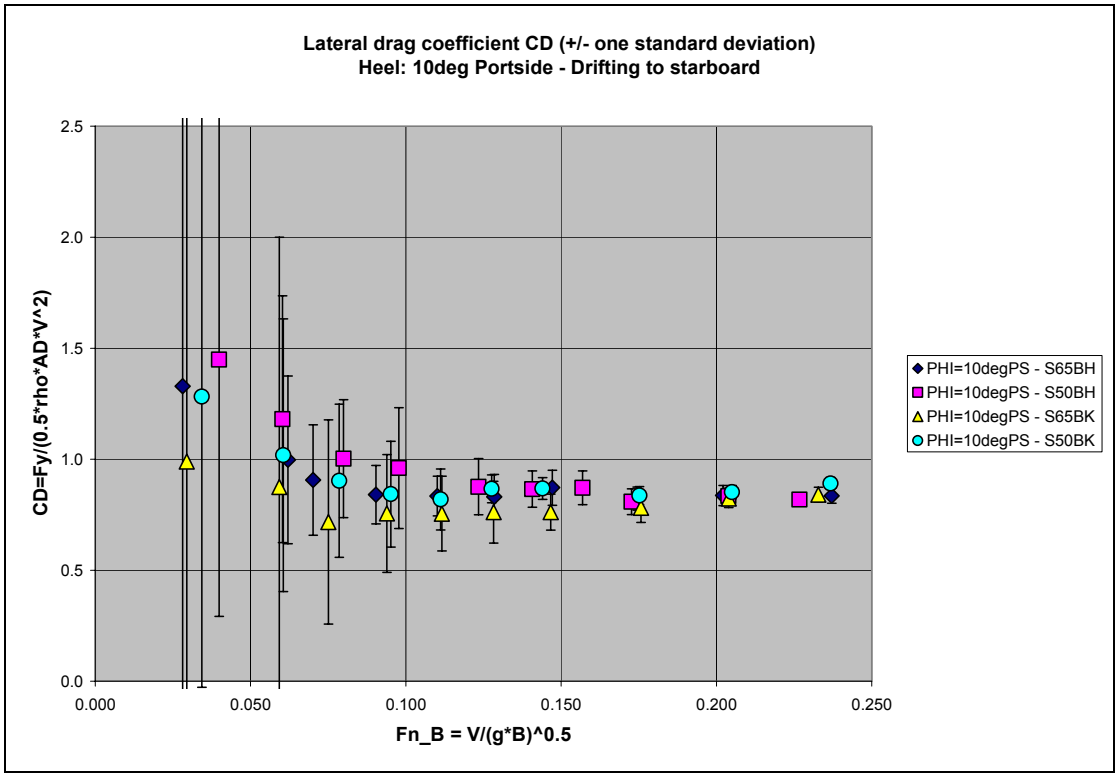

Figure 64: Lateral drag coefficient as measured from drift tests. Heel 10deg portside, drifting to starboard.

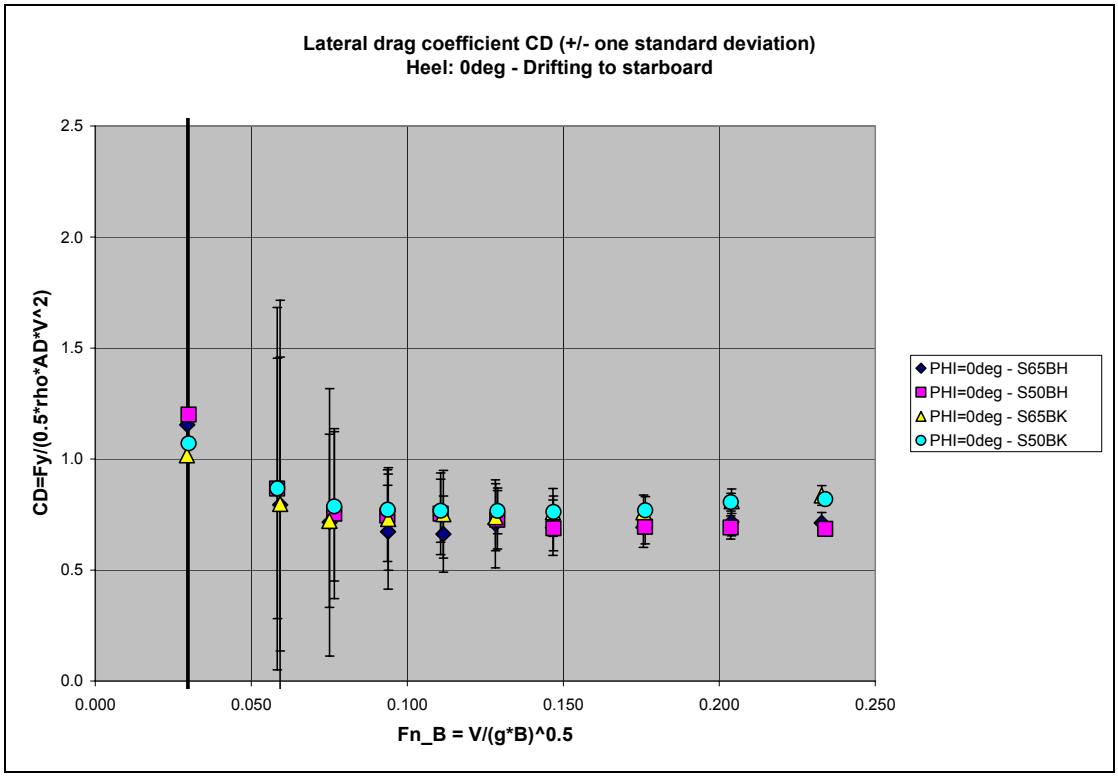

Figure 65: Lateral drag coefficient as measured from drift tests. Heel 0deg, drifting to starboard.

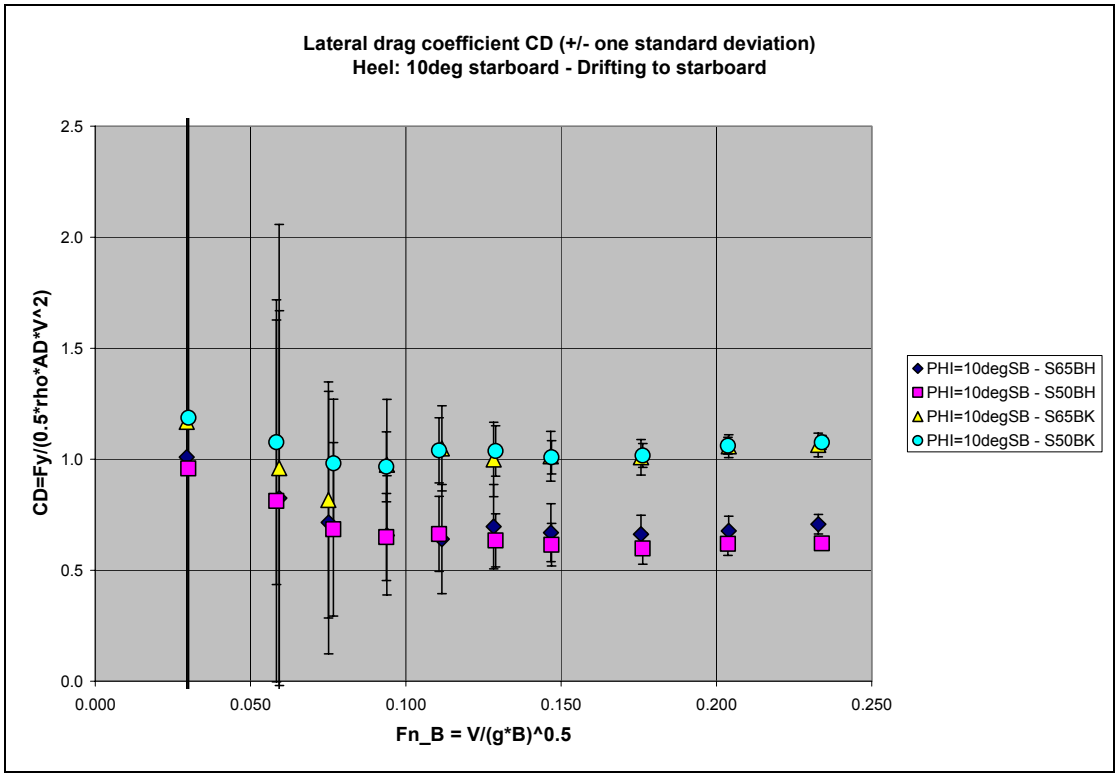

Figure 66: Lateral drag coefficient as measured from drift tests. Heel 10deg starboard, drifting to starboard.

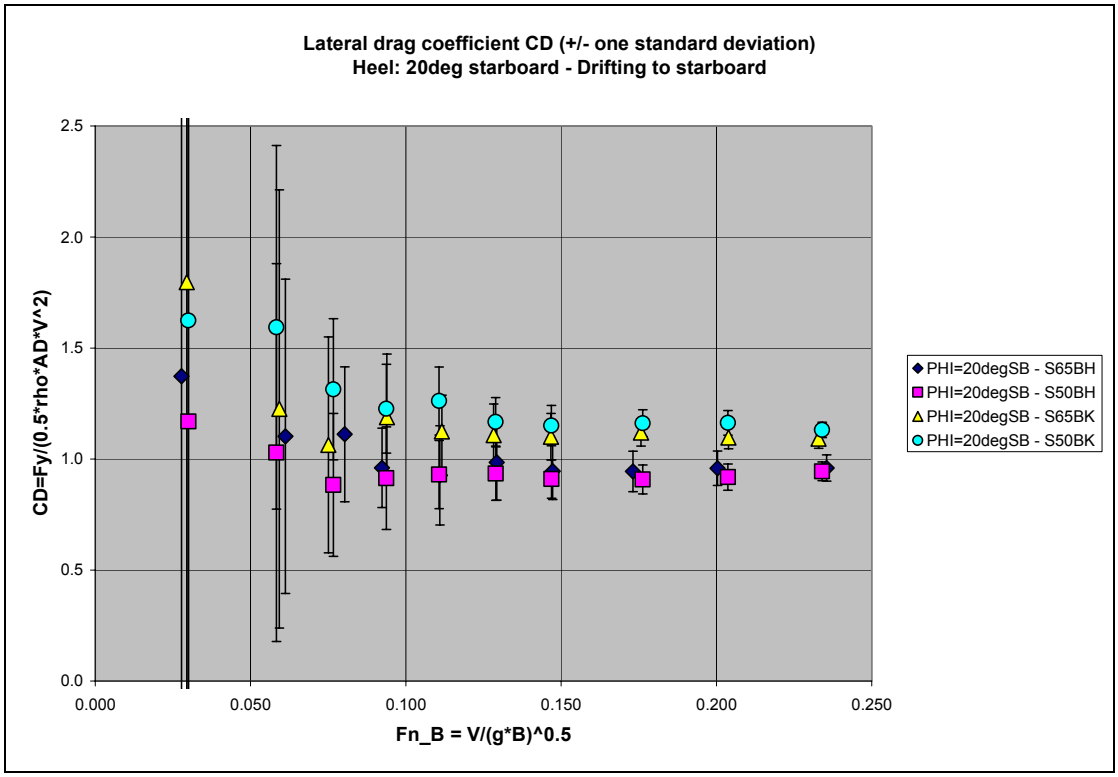

Figure 67: Lateral drag coefficient as measured from drift tests. Heel 20deg starboard, drifting to starboard.

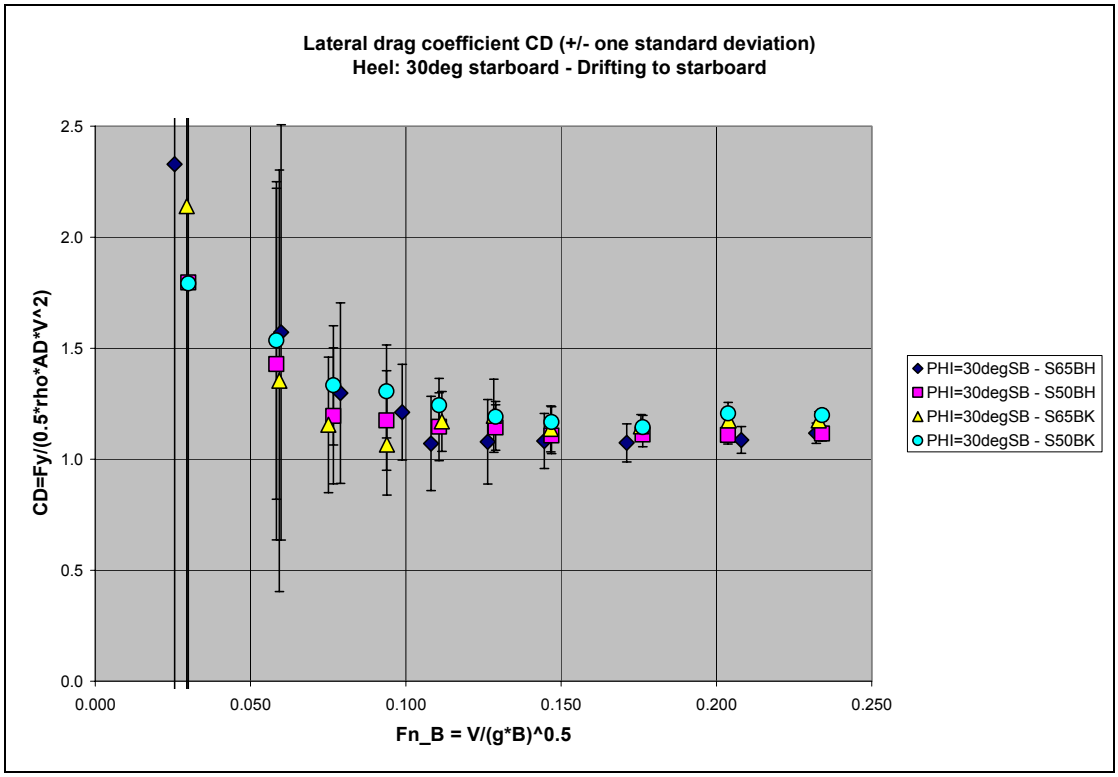

Figure 68: Lateral drag coefficient as measured from drift tests. Heel 30deg starboard, drifting to starboard.

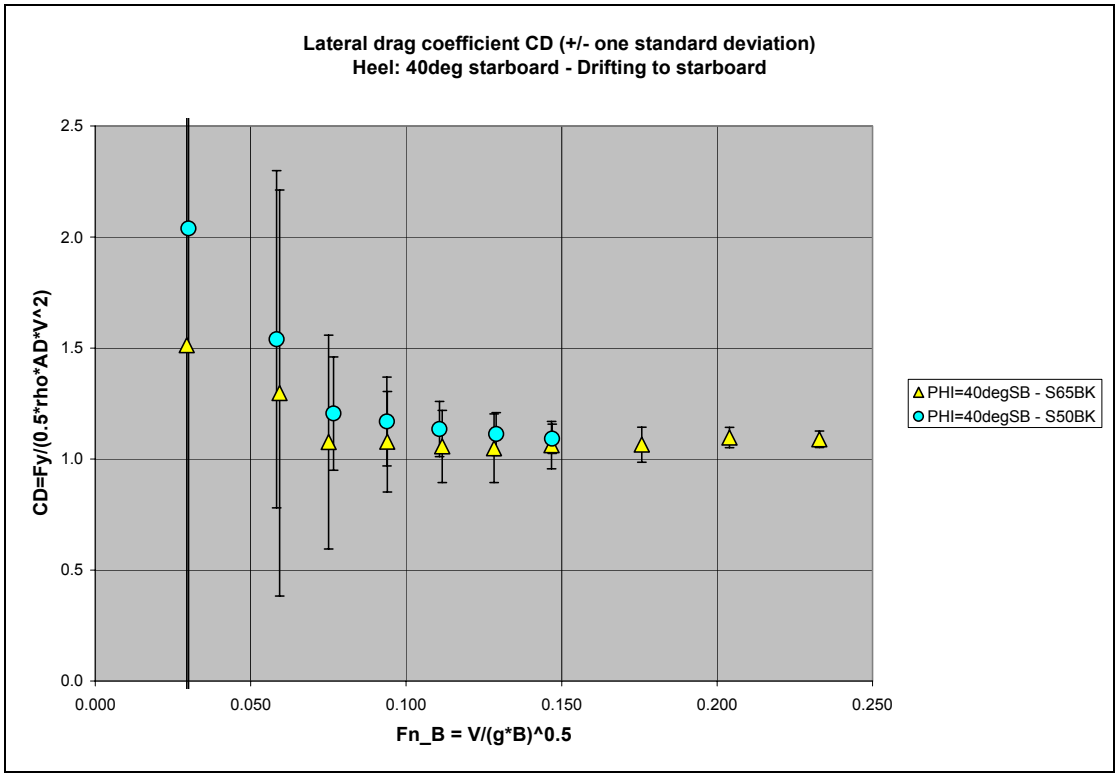

Figure 69: Lateral drag coefficient as measured from drift tests. Heel 40deg starboard, drifting to starboard.

Although the majority of figures contains data for both the scales and both the appendages' arrangement (bare hull and with bilge keels), in some figures some data are missing. In particular:

- In Figure 62 data for the model at scale 1:65 with bilge keels have not been recorded due to technical problems with the electric motor used to impose the heeling angle.
- In Figure 69 speeds higher than $Fn_B = 0.150$ were not tested for the model at scale 1:50 because, according to the towing tank, the model started to flood. It is not clear, at the moment of writing, why the same did not happen also for the model at scale 1:65, since the models are supposed to be identical and the wave pattern should be governed by Froude scaling.
- In Figure 69 tests with the models in bare hull condition were not carried out due to time limitation, and priority has been given to tests with models fitted with bilge keels.

According to the obtained results a series of comments can be made:

- The average drag coefficient has larger values for smaller speeds, and tends to firstly reduce and then stabilise as the drifting speed is increased.
- The uncertainty at low speed is much larger than the uncertainty at high speed. It could be worth reporting that the majority of the uncertainty in C_D is associated to the measurement of the lateral force, while the effect of the speed uncertainty is generally smaller. In particular, at low speeds the contribution from the speed uncertainty is usually small (of the order of 2-5%) due to a large coefficient variation of the measured drift force. On the other hand, at large speeds, the coefficient of variation of the measured force decreases faster than the coefficient of variation for the drift speed, and hence the contribution of the speed uncertainty increases (up to an order of 20-30%).
- Differences between average results at scale 1:50 and results at scale 1:65 are small in case of high speeds, but the spreading tends to increase at low speeds. This can be partially attributed to the larger global uncertainty in the measurements. However it is important to emphasise that a Froude scaling law as used in reporting data in Figure 62 to Figure 69 is not fully appropriate because it neglects effects due to the differences in Reynolds number. Hence, part of the spreading at low speed could also be attributed to the different Reynolds number at different scales for a given Froude number. However, a tentative to regularize data using plots based on Reynolds number did not help in seeing clear trends, hence, although the effect of differences in the Reynolds number must be present, it seems that the majority of the spreading could be attributed to measurement uncertainty.
- For sufficiently large values of Fn_B, above, say, 0.100-0.150, data are very consistent. The outcomes for the two tested scales do not show large differences. The magnitude of the differences between tests with and without bilge keels depends on the heeling angle.
- The "high speed" value of the drag coefficient depends on the heeling angle. However, it is important to bear in mind the fact that part of this variability shall be attributed also to the definition of C_D, which is based on the underwater projected area at zero heel. Since the underwater projected area is itself a function of the heeling angle, a definition of C_D based on the heeling dependent underwater projected area would have led to a different functional dependence of C_D on the heeling angle.

As it was noted, the measured drag coefficient tends to stabilise as the speed is increased. Hence we have calculated the average drag coefficient for the two highest

tested speeds for each heeling angle for each model, with the intention of having a single representative value for each heeling angle. The average value and the standard deviation attached to the data have been calculated as follows:

$$C_{D,ave} = \frac{1}{2}\cdot C_D\left(Fn_{B,N-1}\right) + \frac{1}{2}\cdot C_D\left(Fn_{B,N}\right)$$
$$\sigma_{C_{D,ave}} = \sqrt{\left(\frac{1}{2}\cdot\sigma_{C_D\left(Fn_{B,N-1}\right)}\right)^2 + \left(\frac{1}{2}\cdot\sigma_{C_D\left(Fn_{B,N}\right)}\right)^2} \quad (27)$$

where $Fn_{B,N}$ and $Fn_{B,N-1}$ are the two highest tested speeds among the set of N tested speeds for each condition. Results are reported in Figure 70.

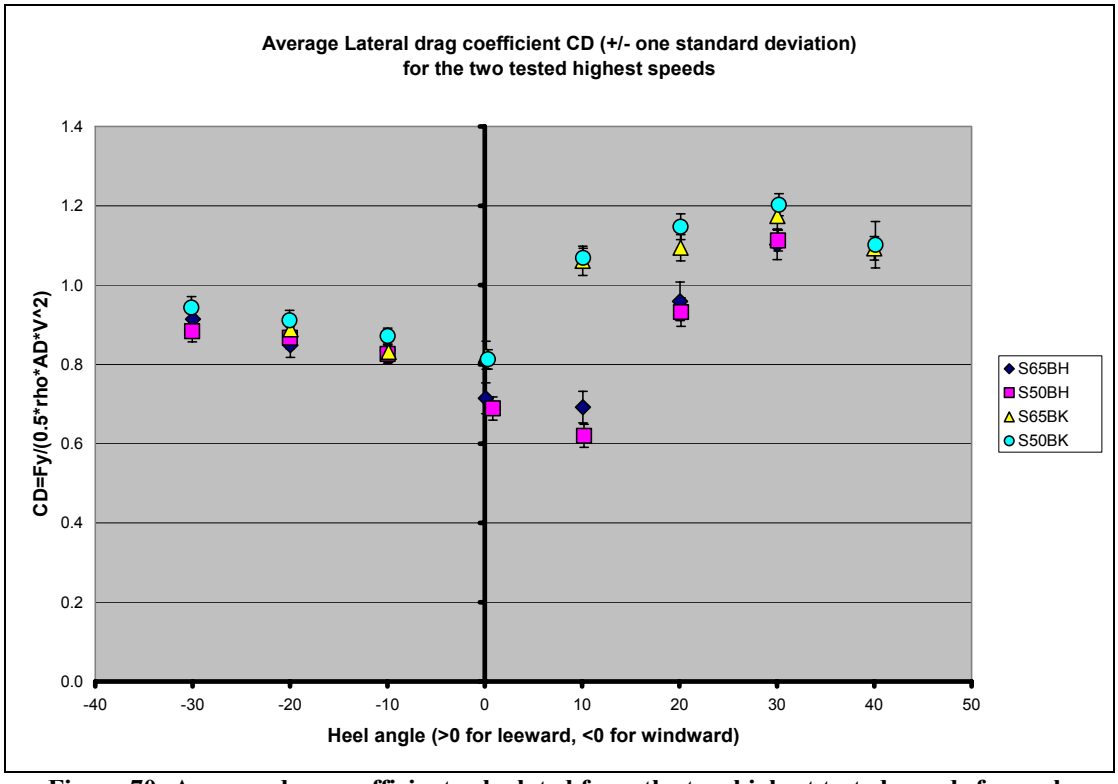

Figure 70: Average drag coefficient calculated from the two highest tested speeds for each condition.

According to Figure 70 we can see that data for the two different scales are consistent and differences are limited. In the representation in Figure 70 the effect of bilge keels is evident. The fitting of bilge keels leads to a general increase of the drag coefficient in the whole range of tested heeling angles (with a lack of data for comparison for 40deg to starboard). This increase is evident at zero heel and, in particular, at heeling angles to starboard (i.e. to windward: recall that the model is drifting to starboard). For heeling angles to portside the increase with respect to the bare hull condition is noticeable but less evident. There seems to be a sort of transition region for moderate heeling angles towards the drifting direction (around 10deg to starboard), where the drag coefficient with bilge keels is close to 1.1 while the drag coefficient in bare hull condition is close to 0.65. At 10deg of heel to starboard it is also visible the largest

discrepancy for the average drag coefficient in bare hull condition at scale 1:65 and at scale 1:50. The differences between drag coefficient with and without bilge keels at large heeling angles to starboard tend to decrease as the angle increases. One reason for the presence of such large difference around 10deg of heel to starboard could be sought in the flow separation at bilges. It could be guessed that an earlier stronger separation is induced by the presence of the bilge keels that, even at moderate heeling angles, represent clearly defined sharp separation points. On the other hand, in case of bare hull condition, since the ship bilges are not very sharp, a strong separation starts at bilges only when the heeling angle is sufficiently large.
In [5] a lateral drag coefficient was measured in case of wind tunnel tests on the superstructures of a RoPax for different heeling angles, according to the wind tests' procedure of [4]. Results from such tests are reported in Figure 71 for sake of reference.

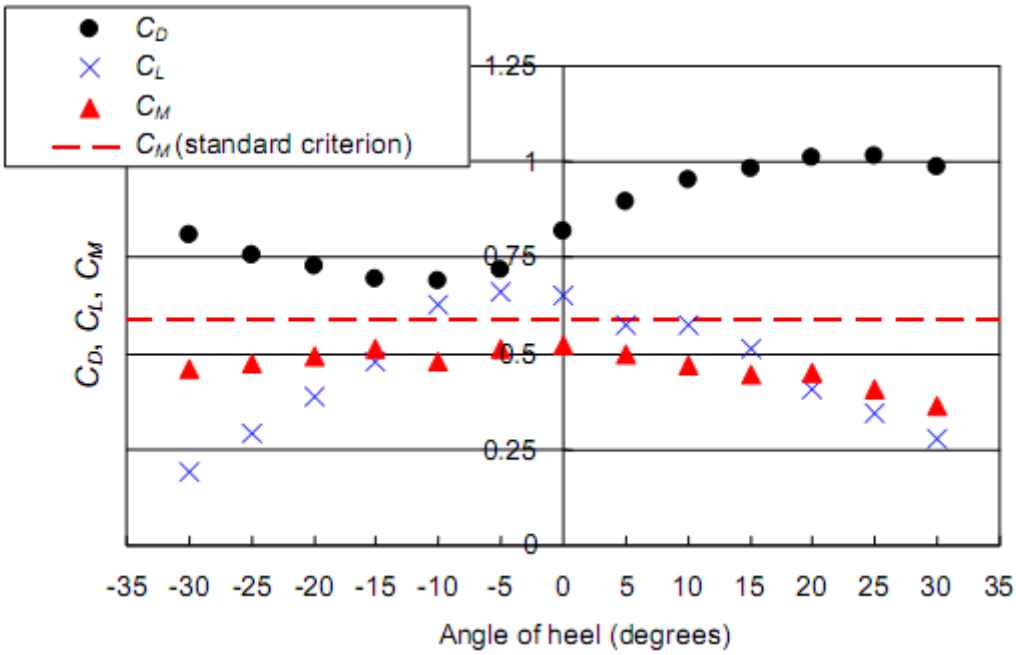

Figure 71: Measured drag coefficient (C_D), lift coefficient (C_L) and heeling moment coefficient (C_M) according to Figure 3.4 in [5] for wind tunnel tests on the superstructures of a RoPax ship. Positive heel when heeling to the leeward.

Although of course the tests whose results are reported in Figure 71 are very different from the drift tests carried out in this work, it is nevertheless possible to see a significant similarity in the angle dependence of the drag coefficient from wind tests in Figure 71 (referring to the above water portion of the ship tested in [5]) and the drag coefficient from drift tests with bilge keels in Figure 70 (referring the underwater portion of a ship). The order of magnitude of the drag coefficients is, as expectable, similar in both cases. Moreover the same increase on the drag coefficient is visible when the ship is heeled to the lee side (positive heel). This similarity could be also related to the fact that in both cases it could be assumed that sharp separation points exist where separation is forced.

Analysis of heeling moment due to drift

As reported at the beginning of this section the analysis of the heeling moment due to drift showed a series of inconsistencies that have not been resolved at the moment of

writing. Since there is a belief that such inconsistencies could have been mainly caused by some error / misunderstanding in the execution / analysis of tests or by some error in the data analysis, it has been decided to report the discussion in a separate appendix, namely Appendix 4.

Concluding comments

Drift tests with different angles of heel have been carried out and analysed.
Seemingly reliable data have been obtained for the lateral drag coefficient as the heeling angle is changed. The effect of bilge keels has been seen particularly in a range of heeling angles around 10deg to leeward, where the fitting of bilge keels significantly increased the drag coefficient. A significant scattering of the obtained data was found when testes are carried out at too low drifting speeds.
Concerning the roll moment induced by drift, a series of inconsistencies have been found in the measured / transformed data that prevented a robust interpretation of the results. Hence this aspect has been discussed separately in Appendix 4.

Final Remarks

The present experimental campaign has addressed roll decay tests, regular beam waves tests and drift tests for three GEOSIM models (scales 1:65, 1:50 and 1:33).
Each different type of test has been discussed in this report in a separate section, and summarising comments have been already provided at the end of each section in extended form.
One of the scopes of the analysis of roll decays was to clarify the matter of the possible presence of not negligible scale effects. From the analysis of results from roll decays it was not possible to disclose any clear trend that could clearly be associated to scale effects. In general the global uncertainty in roll decays' analysis seems to mask the unavoidable presence of scale effects. Since the models were of dimensions allowed by MSC.1/Circ.1200, it seems, hence, that the minimum required dimensions from MSC.1/Circ.1200 could be reasonable, but additional tests along the same line of those reported in this paper should be carried out to reach a definite conclusion.
The frictional damping correction reported in MSC.1/Circ.1200 has also been considered and tested and a critical discussion concerning its (proper) application has been given. The global level of uncertainty associated to the analysis of roll decay tests was found to be not negligible, hence due attention should be paid when planning, carrying out and analysing this type of tests in order to reduce sources of error. One problem that has been touched is the proper modelling of the damping function. In case of models fitted with bilge keels, a linear+quadratic model in roll velocity was usually suitable for fitting experimental data. In case of bare hull condition the same model was inappropriate, and an additional cubic term was required to obtain a good fitting of the data. However, this latter type of model seems to have limited extrapolation capabilities, therefore better types of modelling should be sought in bare hull condition in order to avoid unreasonable increases of damping at large rolling angles outside the range of tested rolling amplitudes with the consequent underestimation of roll amplitude at peak. According to the obtained results a damping model in bare hull condition showing a linear asymptotic behaviour at large rolling amplitudes for the equivalent linear damping coefficient could be advisable. Although such a model could be created without big troubles in case of regular harmonic excitation assuming an harmonic roll response (typically in case of beam regular waves at 1:1 resonance), the same cannot be said in case of a model to

be used also for irregular excitation. Therefore more attention seems to be needed on this point.
Regular beam waves tests have been carried out, underlining the difficulties introduced by the testing of large models, in particular the difficulty of generating sufficiently long and steep waves, as well as the difficulty in keeping the model with a heading close to 90deg. The quality of generated waves was assessed, pointing out possible problems introduced by the effect of the limited depth of the tank. The obtained results from these tests in terms of roll response curves did not show any significant difference that could be clearly ascribed to scale effects. Similarly to the outcome obtained from the analysis of roll decays, it seems that the scale effect (that must necessarily be present) is sufficiently small to be shadowed by the background scattering due to various sources of experimental uncertainty. As a result, the obtained peaks of the roll responses were very close for the three tested models in the same conditions. The shift of the peak of the roll response curve with respect to an encounter frequency equal to the roll natural frequency has been underlined, in order to recall that tests carried out at a wave encounter frequency equal to the roll natural frequency are almost never conservative, and the peak is usually at a different encounter frequency (typically an higher frequency for hardening restoring, or a lower one for softening restoring). The accuracy of the Weather Criterion prediction formula for the peak of the roll response curve has been assessed in comparison with the predictions obtained from two mathematical models. It was found that the prediction capabilities of the Weather Criterion formula are not bad as a whole, but the methodology seems to be not able to properly separate damping and forcing terms, and for this reason it would be worth an improvement. The influence of accounting or not the skeg in the computation of the roll reduction factor has also been assessed showing that, for this ship, better prediction are obtained if skeg is not considered in the calculation of the roll reduction factor for the presence of bar keel, bilge keels, etc.
Two mathematical models were proposed, respectively based on a single degree of freedom and on a three degrees of freedom approach. In both cases damping is taken from roll decay experiments, while forcing due to wave is introduced on the basis of direct hydrodynamic calculations. Prediction capabilities were found to be very similar among the two models, therefore the 1-DOF model, that is easier to apply, could be preferred for standard applications. The mathematical models performed usually better than the Weather Criterion prediction formula, however some prediction problems were found for the mathematical models in case of bare hull condition. From the obtained data, the reduction of roll due to the presence of bilge keels seems to be underestimated by the present Weather Criterion: even quite small bilge keels, as in this case, are able to significantly reduce the roll peak, and in particular this reduction is larger than what is predicted by the Weather Criterion.
Drift tests were carried out with the intention of addressing, mainly, the roll moment due to the hydrodynamic reaction to drift. Unfortunately, due to a series of inconsistencies in the obtained experimental data, this aspect was only briefly discussed, and more attention was given to the lateral drag coefficient. Models with scale 1:65 and 1:50 were tested, but the largest model was not tested due to time constraints and problems in the experimental arrangement. In case of large drifting speeds above, for this ship, about 3m/s full scale, a stable drag coefficient was found, with minor difference among the two tested scales. The tendency for the drag coefficient is to increase at lower speeds. On the other hand, for low speeds a significant scattering of data was found for the two scales, that could be due to effects associated to the differences in the Reynolds number. The majority of the uncertainty

in the low drift speeds range, however, is likely to be due to the experimental arrangement. The analysis of the lateral drag coefficient at high drifting speed revealed a not negligible effect of the fitting of bilge keels, in particular for moderate heeling angles to leeward.

Acknowledgements

The work described in this publication was supported by the European Community's Sixth Framework Programme through the grant to the budget of the Integrated Infrastructure Initiative HYDRALAB III, Contract no. 022441 (RII3).
The authors would like to acknowledge the help from the team of the CEHIPAR seakeeping basin for their support in the preparation of the experiments and for carrying out the test. In particular Dr. A. Maron, Mr. C. Gutierrez and Ms. M.E. Prieto.
Acknowledgments are also given to Prof. K.J. Spyrou and Mr. I. Karkaletsis for their participation to this project.

Disclaimer

References

[1] IMO Res. A.749(18) as amended by resolution MSC.75(69), "Code on Intact Stability for All Types of Ships Covered by IMO Instruments", London, 2002.

[2] IMO Document MSC85/28, "Report of the Maritime Safety Committee on Its Eighty-Third Session", To be published.

[3] IMO Document MSC85/3/2, "Adoption of the International Code on Intact Stability, 2008 (2008 IS CODE)", Note by the Secretariat, 23 June 2008.

[4] IMO MSC.1/Circ.1200, "Interim guidelines for alternative assessment of the Weather Criterion", London, 24 May 2006.

[5] IMO MSC.1/Circ.1227, "Explanatory notes to the interim guidelines for alternative assessment of the Weather Criterion", London, 11 January 2007.

[6] Himeno Y., Prediction of Ship Roll Damping – State of the Art, University of Osaka Prefecture, No. 239, September 1981.

[7] Ikeda, Y., Himeno, Y., Tanaka, N., "A Prediction Method for Ship Roll Damping", Report No. 00405 of Department of Naval Architecture – University of Osaka Prefecture, December 1978.

[8] Lloyd, A.R.J.M., “Seakeeping – Ship Behaviour in rough weather”, Ellis Horwood Series in Marine Technology, Ellis Horwood Limited, Chichester 1989.

[9] Dreossi, M., "Analisi critica di un metodo semi-empirico per la previsione dello smorzamento del moto di rollio (Critical analysis of a semi-empirical method for roll damping prediction)" (in Italian), University of Trieste, Academic Year 2004-2005.

[10] Ueno, K., "Influence of the Surface Tension of the Surrounding Water upon the Free Rolling of Model Ships", Memoirs of the Faculty of Engineering, Kyushu University, 12, 1950, pp. 21-58.

[11] Vossers, G., "Resistance, propulsion and steering of ships - Volume II C - Behaviour of ships in waves", The Technical Publishing Company H. Stam N.V., Haarlem, The Netherlands, 1962

[12] IMO, "International Convention for the Safety of Life at Sea, 1974", London, 2008

[13] Harvald, Sv.Aa., “Resistance and Propulsion of Ships”, Wiley-Interscience, John Wiley and Sons, 1983

[14] Valle, J., Perez-Rojas, L., Carrillo, E., "Influences of test parameters on roll damping coefficients", Proc. 7th International Conference on Stability of ships and Ocean Vehicles STAB2000, Vol. B., 7-11 February 2000, Lanceston, Tasmania, Australia, Martin Renilson Editor, pp. 751-766

[15] Bertaglia, G., Scarpa, G., Serra, A., Francescutto, A., Bulian, G., “Systematic Experimental Tests for the IMO Weather Criterion Requirements and Further Development Towards a Probabilistic Intact Stability Approach”, Proc. 7th International Ship Stability Workshop, 1-3 November 2004, Shanghai, China, pp. 63-74.

[16] METRIS, http://www.metris.com

[17] Journée, J.M.J., Adegeest, L.J.M.. "Theoretical Manual of Strip Theory Program SEAWAY for Windows", Report 1370, TU Delft & AMARCON, Septemebr 2003

[18] Cardo, A., Francescutto, A., Nabergoj R., "On Damping Models in Free and Forced Rolling Motion", Ocean Engineering, 1982, Vol. 9, No. 2, pp.171-179

[19] Bulian, G., “Estimation of nonlinear roll decay parameters using an analytical approximate solution of the decay time history”, International Shipbuilding Progress , Vol.51, No. 1, 2004, pp. 5-32.

[20] Nayfeh, A.H. “Problems in Perturbation”, John Wiley & Sons, 1979.

[21] Roberts, J.B., Spanos, P.D., "Random Vibration and Statistical Linearization", John Wiley & Sons, Chichester, 1990.

[22] Nayfeh, A.H., Mook, D.T., “Nonlinear Oscillations”, John Wiley & Sons, Inc., 1979.

[23] Penna, R., Contento, G., Francescutto, A., 1997. "Uncertainty analysis applied to the parameter estimation in nonlinear rolling", Proc. 6th International Conference on Stability of Ships and Ocean Vehicles STAB’97, Varna, Vol. 2, 1997, pp. 75–82.

[24] Tzamtzis, S., "Development and testing of a procedure for the alternative assessment of Weather Criterion on experimental basis" (In English), University of Trieste and National Technical University of Athens, Academic Year 2003-2004.

[25] Kato, H., On the Frictional Resistance to the Rolling of Ships, Journal of Society of Naval Architects of Japan, Vol. 102 (1958), p.115.

[26] Bulian, G., Francescutto, A., "Experimental results and numerical simulations on strongly nonlinear rolling of multihulls in moderate beam seas", Accepted for publication on Proceedings of the Institution of Mechanical Engineers - Part M - Journal of Engineering for the Maritime Environment

[27] Bulian, G., Francescutto, A., Maccari, A., "Possible simplified mathematical models for roll motion in the development of performance-based intact stability criteria – Extended and revised version", Quaderno di Dipartimento n° 46, Dept. DINMA, University of Trieste, January 2008.

[28] Francescutto, A., Contento, G., Biot, M., Schiffrer, L., "On the Effect of Excitation Modelling in the Parameter Estimation of Nonlinear Rolling", Proc. Eight International Offshore and Polar Engineering Conference (ISOPE98), Montreal, Canada, May 24-29, 1998, pp. 490-498.

[29] Spyrou, K.J., Tigkas, I., Scanferla, G., Gavriilidis, N., "Problems and Capabilities in the Assessment of Parametric Rolling", Proc. of the 10th International Ship Stability Workshop, 23-25 March 2008, Daejeon, Republic of Korea, pp. 47-55.

[30] Francescutto, A., Contento, G., “Bifurcations in Ship Rolling: Experimental Results and Parameter Identification Technique”, Ocean Engineering, Vol. 26, 1999, pp. 1095-1123.

[31] IMO Document MSC85/3/7, "Draft MSC circular to be approved in conjunction with the adoption of the International Code on Intact Stability, 2008 (2008 IS CODE)", Note by the Secretariat, 23 June 2008.

[32] Vugts, J.H., "The hydrodynamic coefficients for swaying, heaving and rolling cylinders in a free surface", Report No. 194, Technische Universiteit Delft, January 1968

[33] Ishida, S., Fujiwara, T.:, “On the Capsizing Mechanism of Small Craft in Beam Breaking Waves”, Proc. 7th International Conference on Stability of ships and Ocean Vehicles STAB2000, Vol. B., 7-11 February 2000, Lanceston, Tasmania, Australia, Martin Renilson Editor

[34] Bulian, G., Francescutto, A., Lugni, C., "Theoretical, numerical and experimental study on the problem of ergodicity and 'practical ergodicity' with an application to parametric roll in longitudinal long crested irregular sea", Ocean Engineering, Vol. 33 (2006), pp. 1007-1043. doi:10.1016/j.oceaneng.2005.09.004

Appendix 1: Theoretical background of the procedure used for the analysis of roll decays

In order to understand the theoretical background of the analysis of roll decays it is necessary to start with some fundamental considerations.
The first one concerns the dynamic modelling of free roll motion with a 1-DOF approach. Experimental roll decay data can indeed be described, quite often, by an uncoupled nonlinear differential equation having the following general form:

$$J_{xx}^{v} \cdot \ddot{\phi} + D\left(\dot{\phi}\right) + \Delta \cdot \overline{GZ}\left(\phi\right) = 0 \tag{28}$$

where ϕ [rad] is the roll angle, dots represent derivatives with respect to time, J_{xx}^{v} [kg*m^2] is the total roll moment of inertia including the effect of hydrodynamic added inertia, $D\left(\dot{\phi}\right)$ [N*m] is the damping moment function assumed to be dependent only on the instantaneous roll velocity $\dot{\phi}$, Δ [N] is the ship displacement and $\overline{GZ}\left(\phi\right)$ [m] is the ship righting lever. After dividing (28) by J_{xx}^{v} we get the more usual form

$$\begin{aligned} &\ddot{\phi} + d\left(\dot{\phi}\right) + \omega_0^2 \cdot r\left(\phi\right) = 0 \\ &d\left(\dot{\phi}\right) = \frac{D\left(\dot{\phi}\right)}{J_{xx}^{v}} \;\; ; \;\; \omega_0^2 = \frac{\Delta \cdot \overline{GM}}{J_{xx}^{v}} \;\; ; \\ &r\left(\phi\right) = \frac{\overline{GZ}\left(\phi\right)}{\overline{GM}} \;\; ; \;\; \overline{GM} = \left.\frac{d\overline{GZ}}{d\phi}\right|_{\phi=0} \end{aligned} \tag{29}$$

Equation (29) is, in general, nonlinear and for symmetric ships symmetrically loaded it is characterised by the following symmetry properties:

$$\begin{aligned} &d\left(-\dot{\phi}\right) = -d\left(\dot{\phi}\right) \\ &r\left(-\phi\right) = -r\left(\phi\right) \end{aligned} \tag{30}$$

Exact analytical closed form solutions for (29) do not exist in general, although they do exist for some special cases of (29). Analytical approximate techniques have been

widely used in the past to obtain approximate analytical closed form solutions of particular cases of (29) (see, e.g., [18][19][20]). In this work we will follow a different idea, which is based on the "classical" way of analysing roll decay curves by means of the so called decrement curve.
The fundamental assumption of the theoretical background that will follow is that, in a limited time window Δt centred at a time $\tilde{t}$, the nonlinear model (29) can be effectively replaced / approximated by a linear equivalent model as follows:

$$\ddot{\phi}+d\left(\dot{\phi}\right)+\omega_0^2\cdot r\left(\phi\right)=0 \quad \rightarrow \quad \ddot{\phi}+2\cdot\mu_{eq}\cdot\dot{\phi}+\omega_{0,eq}^2\cdot\phi=0$$
$$\text{in } \left[\tilde{t}-\frac{\Delta t}{2},\tilde{t}+\frac{\Delta t}{2}\right] \tag{31}$$

The idea is, therefore, to obtain a quantification of the coefficients μ_{eq} and $\omega_{0,eq}$ from the analysis of roll decays in order to finally obtain an estimation of a series of parameters that, as will be discussed later in detail, will characterise the damping and the restoring functions of the nonlinear model (29).
It is extremely important to underline that the simplification /substitution (31) is not uniquely defined and it is therefore necessary to better specify how the equivalent linear damping coefficient μ_{eq} and the equivalent natural frequency $\omega_{0,eq}$ shall be determined. In this work we start by introducing two error functions as follows:

$$\chi_d^2\left(\mu_{eq}\right)=\int_{\tilde{t}-\frac{\Delta t}{2}}^{\tilde{t}+\frac{\Delta t}{2}}\left[2\cdot\mu_{eq}\cdot\dot{\phi}(t)-d\left(\dot{\phi}(t)\right)\right]^2 dt$$
$$\chi_r^2\left(\omega_{0,eq}^2\right)=\int_{\tilde{t}-\frac{\Delta t}{2}}^{\tilde{t}+\frac{\Delta t}{2}}\left[\omega_{0,eq}^2\cdot\phi(t)-\omega_0^2\cdot r\left(\phi(t)\right)\right]^2 dt \tag{32}$$

Then we define μ_{eq} and $\omega_{0,eq}^2$ as those quantities that minimise the error functions in (32), thus, by imposing a zero gradient, we get:

$$\frac{\partial\chi_d^2}{\partial\mu_{eq}}=0\Rightarrow\mu_{eq}=\frac{1}{2}\cdot\frac{\int_{\tilde{t}-\frac{\Delta t}{2}}^{\tilde{t}+\frac{\Delta t}{2}} d\left(\dot{\phi}(t)\right)\cdot\dot{\phi}(t)\,dt}{\int_{\tilde{t}-\frac{\Delta t}{2}}^{\tilde{t}+\frac{\Delta t}{2}}\dot{\phi}^2(t)\,dt}$$
$$\frac{\partial\chi_r^2}{\partial\omega_{0,eq}^2}=0\Rightarrow\omega_{0,eq}^2=\omega_0^2\cdot\frac{\int_{\tilde{t}-\frac{\Delta t}{2}}^{\tilde{t}+\frac{\Delta t}{2}} r\left(\phi(t)\right)\cdot\phi(t)\,dt}{\int_{\tilde{t}-\frac{\Delta t}{2}}^{\tilde{t}+\frac{\Delta t}{2}}\phi^2(t)\,dt} \tag{33}$$

Definitions in (33) are quite general and it is probably worth mentioning that this way of thinking has significant similarities with the statistical linearization technique [21]. Moreover, the introduced definition for the equivalent linear damping is substantially

equivalent to what is done when the equivalent linear damping coefficient is defined on the basis of an equivalent energy dissipation per cycle from the nonlinear damping and the equivalent linear damping terms [6]. Last but not least, definitions in (33) reduce to a first harmonic Fourier expansion of $d(\dot{\phi})$ and $r(\phi)$ under the assumption of harmonic behaviour for $\phi(t)$ (and consequently for $\dot{\phi}(t)$) and in such case similarities are evident with the more general harmonic balance method [22].
Let us now consider a general roll decay curve, such as that reported in Figure 72: time instants t_i and t_{i+1} are assumed to correspond to consecutive local extremes C_i and C_{i+1} of the roll time history.

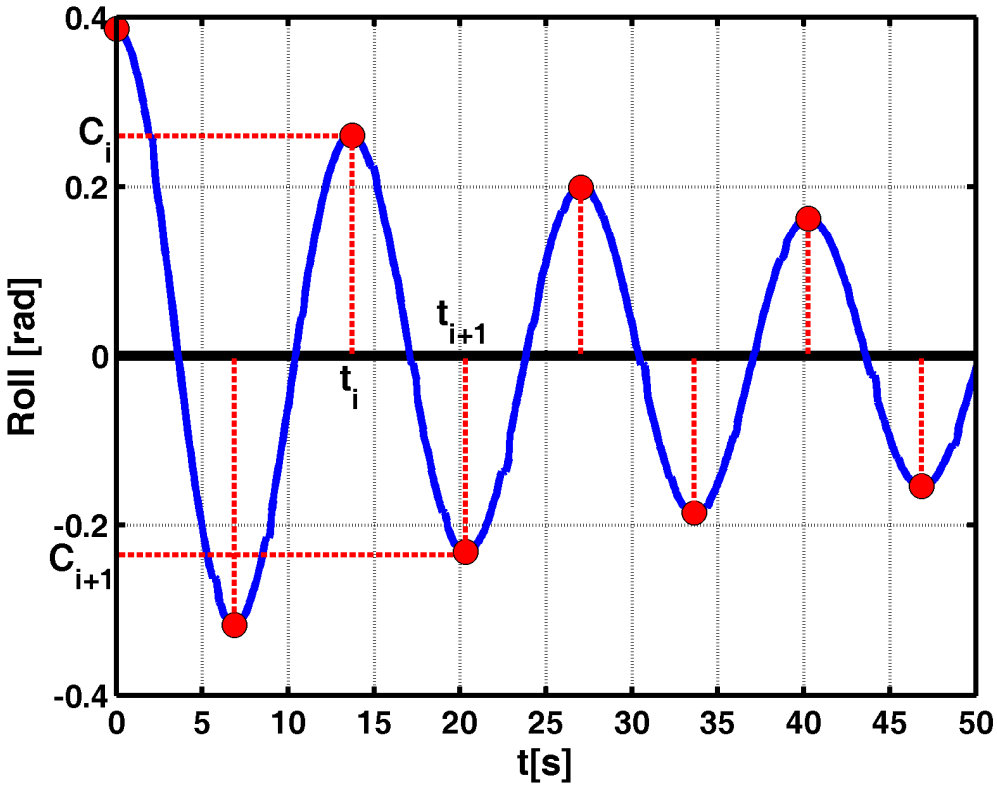

Figure 72: Example of roll decay curve.

With reference to Figure 72, the idea is to assume that, in each half roll cycle, the roll behaviour can be approximate by the following linear differential equation:

$$\ddot{\phi} + 2 \cdot \mu_{eq,i} \cdot \dot{\phi} + \omega_{0,eq,i}^2 \cdot \phi = 0 \quad \text{in } [t_i, t_{i+1}] \tag{34}$$

where the coefficients $\mu_{eq,i}$ and $\omega_{0,eq,i}$ are assumed to change from half cycle to half cycle. According to (34), and remembering that

$$\forall i \quad \phi(t_i) = C_i \quad \wedge \quad \dot{\phi}(t_i) = 0 \tag{35}$$

the roll decay for the i-th half cycle can be approximated, in principle, by the following analytical solution:

$$\phi(\tau) \approx \exp\left(-\mu_{eq,i} \cdot \tau\right) \cdot \left(A \cdot \cos\left(\tilde{\omega}_i \cdot \tau\right) + B \cdot \sin\left(\tilde{\omega}_i \cdot \tau\right)\right)$$

with

$$\tau = t - t_i \quad ; \quad A = C_i \quad ; \quad B = \frac{\mu_{eq,i}}{\tilde{\omega}_i} \cdot C_i \quad ; \quad \tilde{\omega}_i = \sqrt{\omega_{0,eq,i}^2 - \mu_{eq,i}^2} \tag{36}$$

Assuming that the system is lightly damped, as it is usually the case, then $\frac{\mu_{eq,i}}{\tilde{\omega}_i} << 1$ and (36) can be approximated by

$$\begin{aligned} \phi(\tau) &\approx \exp\left(-\mu_{eq,i} \cdot \tau\right) \cdot C_i \cdot \cos\left(\tilde{\omega}_i \cdot \tau\right) \\ \dot{\phi}(\tau) &\approx -\exp\left(-\mu_{eq,i} \cdot \tau\right) \cdot C_i \cdot \tilde{\omega}_i \cdot \sin\left(\tilde{\omega}_i \cdot \tau\right) \end{aligned} \tag{37}$$

According to the assumption that (37) is a good representation of the roll decay in the time interval $\left[t_i, t_{i+1}\right]$ it follows that the characteristic parameters $\mu_{eq,i}$ and $\omega_{0,eq,i}$ can be determined as:

$$\begin{aligned} \mu_{eq,i} &\approx \frac{1}{t_{i+1} - t_i} \ln\left(\frac{|C_i|}{|C_{i+1}|}\right) \\ \tilde{\omega}_i &\approx \frac{\pi}{t_{i+1} - t_i} \\ \omega_{0,eq,i} &\approx \sqrt{\tilde{\omega}_i^2 + \mu_{eq,i}^2} \end{aligned} \tag{38}$$

Note also that, under the assumption of lightly damped system

$$\ln\left(\frac{|C_i|}{|C_{i+1}|}\right) \approx \frac{|C_i| - |C_{i+1}|}{|C_i|} << 1 \tag{39}$$

Moreover, if we consider that the reduction $|C_i| - |C_{i+1}|$ of the roll envelope in half roll cycle is sufficiently small, it is possible to associate the characteristic parameters $\mu_{eq,i}$ and $\omega_{0,eq,i}$ to the average roll envelope A_i for the i-th half roll cycle, calculated as:

$$A_i = \frac{|C_i|}{t_{i+1}-t_i}\int_0^{t_{i+1}-t_i} \exp\left(-\mu_{eq,i}\cdot\tau\right)d\tau = \\ = |C_i|\cdot\frac{1-\exp\left(-\mu_{eq,i}\cdot\left(t_{i+1}-t_i\right)\right)}{\mu_{eq,i}\cdot\left(t_{i+1}-t_i\right)} = \\ = \frac{|C_i|-|C_{i+1}|}{\ln|C_i|-\ln|C_{i+1}|} \underset{\frac{|C_i|-|C_{i+1}|}{|C_i|}<<1}{\approx} \frac{|C_i|+|C_{i+1}|}{2} \tag{40}$$

As a result of this analysis, it is possible to obtain, for each experimental decay a scatter plot of the quantities $\mu_{eq,i}\left(A_i\right)$ and $\omega_{0,eq,i}\left(A_i\right)$. Moreover it is possible to aggregate $\mu_{eq,i}\left(A_i\right)$ and $\omega_{0,eq,i}\left(A_i\right)$ coming from different roll decays performed on the same model in the same conditions. The aggregation of data from different decays was one of the important aspects that led to the selection of the roll decrement approach for the determination of the nonlinear damping / restoring parameters in this work, due to the not perfect repeatability of initial conditions for different decays.
The last step to be performed is to link the experimentally determined estimations of $\mu_{eq}\left(A\right)$ and $\omega_{0,eq}\left(A\right)$ with the original nonlinear model (29) using definitions (33). To accomplish this task it is firstly necessary to provide an explicit analytical form for $d\left(\dot{\phi}\right)$ and $r\left(\phi\right)$. Concerning damping, a typical expression that has shown by experience to be able to handle both the bare hull condition and the case of models fitted with bilge keels is the linear+quadratic+cubic in velocity model, namely:

$$d\left(\dot{\phi}\right) = 2\cdot\mu\cdot\dot{\phi} + \beta\cdot\dot{\phi}\left|\dot{\phi}\right| + \delta\cdot\dot{\phi}^3 \tag{41}$$

Model (41) has three free parameters, i.e. μ, β and δ. However, in case of ships fitted with bilge keels, the reduced linear+quadratic model, i.e. (41) with $\delta = 0$, is often sufficient. In general, the form of the damping model is selected after a visual observation of the behaviour of the experimentally determined curve of $\mu_{eq}\left(A\right)$.
Concerning restoring, taking into account the property (30), it is common to consider an odd polynomial representation of $r\left(\phi\right)$ as follows:

$$r\left(\phi\right) = \sum_{n=1,3,5,7,\ldots} \gamma_n\cdot\phi^n \\ \text{with } \gamma_1 = 1 \tag{42}$$

The next step is to calculate μ_{eq} and $\omega_{0,eq}^2$ using (33) but approximating the roll behaviour in each half cycle with an harmonic motion with constant amplitude equal to the average roll amplitude A in each half roll cycle (see (40)), and frequency equal to the amplitude dependent damped roll frequency. According to this approximation, and considering (41) and (42), we obtain the following results:

$$\phi(\tau) \approx A \cdot \cos\left(\widetilde{\omega}(A) \cdot \tau\right)$$
$$\dot{\phi}(\tau) \approx -A \cdot \widetilde{\omega} \cdot \sin\left(\widetilde{\omega}(A) \cdot \tau\right)$$
$$\widetilde{\omega}(A) = \sqrt{\omega_{0,eq}^2(A) - \mu_{eq}^2(A)}$$

$$\mu_{eq}(A) = \frac{1}{2} \cdot \frac{\int_0^{2\pi/\widetilde{\omega}(A)} d\left(\dot{\phi}(\tau)\right) \cdot \dot{\phi}(\tau) d\tau}{\int_0^{2\pi/\widetilde{\omega}(A)} \dot{\phi}^2(\tau) d\tau} =$$
$$= -\frac{\int_0^{2\pi} d\left(\dot{\phi} = -A \cdot \widetilde{\omega} \cdot \sin(\alpha)\right) \cdot \sin(\alpha) d\alpha}{2\pi A \cdot \widetilde{\omega}} =$$
$$= \mu + \frac{4}{3\pi} \cdot \beta \cdot \left(\widetilde{\omega}(A) \cdot A\right) + \frac{3}{8} \cdot \delta \cdot \left(\widetilde{\omega}(A) \cdot A\right)^2 \tag{43}$$

$$\omega_{0,eq}^2(A) = \omega_0^2 \cdot \frac{\int_0^{2\pi/\widetilde{\omega}(A)} r\left(\phi(\tau)\right) \cdot \phi(\tau) d\tau}{\int_0^{2\pi/\widetilde{\omega}(A)} \phi^2(\tau) d\tau} =$$
$$= \omega_0^2 \cdot \frac{\int_0^{2\pi} r\left(\phi = A \cdot \cos(\alpha)\right) \cdot \cos(\alpha) d\alpha}{\pi A} =$$
$$= \omega_0^2 \cdot \sum_{n=1,3,5,7,\ldots} \gamma_n \cdot 2 \cdot \frac{n!!}{(n+1)!!} \cdot A^{n-1}$$

where the double factorial is defined as:

$$k!! = \begin{cases} k \cdot (k-2) \cdot (k-4) \cdot \ldots \cdot 1 & \text{if } k \text{ is odd} \\ k \cdot (k-2) \cdot (k-4) \cdot \ldots \cdot 2 & \text{if } k \text{ is even} \\ 1 \text{ if } k = 0, -1 \end{cases} \tag{44}$$

Alternatively, the double factorial can be calculated using the gamma function as:

$$k!! = \begin{cases} \Gamma\left(1+\frac{k}{2}\right)\cdot\sqrt{\frac{2^{k+1}}{\pi}} & \text{if } k \text{ is odd} \\ \Gamma\left(1+\frac{k}{2}\right)\cdot\sqrt{2^{k}} & \text{if } k \text{ is even} \\ 1 \text{ if } k = 0,-1 \end{cases} \tag{45}$$

with

$$\Gamma(x) = (x-1)! = \int_0^\infty t^{x-1}\cdot \mathrm{e}^{-t}\, dt$$

In case of standard monohull ships, if the initial heeling angle is not too large, a 5th degree polynomial is sufficient to reproduce the restoring behaviour with sufficient accuracy and in such case:

$$\begin{aligned} &\frac{\overline{GZ}(\phi)}{\overline{GM}} = r(\phi) \approx 1+\gamma_3\cdot\phi^3+\gamma_5\cdot\phi^5 \Rightarrow \\ &\Rightarrow \omega_{0,eq}^2(A) = \omega_0^2\cdot\left(1+\frac{3}{4}\cdot\gamma_3\cdot A^2+\frac{5}{8}\cdot\gamma_5\cdot A^4\right) \end{aligned} \tag{46}$$

Finally, expressions (43) (with the simplification (46), when appropriate) represent parametric models for the equivalent linear damping $\mu_{eq}(A)$ and the equivalent natural frequency $\omega_{0,eq}(A)$ estimated from experiments.

The whole procedure for the estimation of the parameters of the nonlinear model (29) considering (41) and (42) (or (46)) can be summarised as follows:

1) Determine extremes C_i and corresponding time instants t_i from an experimental roll decay time series (after appropriate filtering of the raw measured signal);
2) For each half cycle determine:
   - The average amplitude A_i (see (40));
   - The equivalent linear damping coefficient $\mu_{eq,i}$ to be associated to A_i (see (38));
   - The equivalent linear frequency $\omega_{0,eq,i}$ to be associated to A_i (see (38));
3) Aggregate data obtained for different roll decays according to 1) and 2);
4) Fit the analytical model (43) (or (46)) to the experimental scatter plot of $\left[\omega_{0,eq}^2(A)\right]_{\text{exp.}}$ through a least square fitting in order to obtain the restoring coefficients ω_0^2 and γ_n $n = 3,5,\ldots$. For this fitting it is actually convenient to perform a fitting of $\omega_{0,eq}^2$ as a function of the variable $z = A^2$ (see (43)).
5) Fit the analytical model (43) to the experimental scatter plot of $\left[\mu_{eq}(A)\right]_{\text{exp.}}$ through a least square fitting in order to obtain the damping model coefficients

μ, β and δ (if necessary). For this fitting it is actually convenient to consider μ_{eq} as a function of the variable $z = \widetilde{\omega}(A) \cdot A$ (see (43) or (46))

From the least square fitting of the analytical models for damping and restoring to the experimental data it is possible to have confidence intervals associated to the fitted parameters and it is also possible to have an estimation of the prediction bounds for the fitting, i.e. a quantification of the residual dispersion of experimental data with respect to the assumed model.

Appendix 2: Obtaining ship position and attitude in tank-fixed reference system starting from experimental data

Introduction

During experimental tests 6-DOF ship motions have been measured by means of a Krypton system *fixed to the carriage turret*. The Krypton system measures three translations and three Euler angles (according to the Naval Architecture conventions 1)yaw-2)pitch-3)roll). Moreover the instantaneous longitudinal and transversal velocities of the carriage have also been measured, together with the wave amplitude measured by a wave gauge also fixed to the turret. The raw measured quantities at model scale are (see Figure 73 and Figure 74):

- Time t [s];
- Wave amplitude z_{wave} [m];
- Surge motion x [m];
- Sway motion y [m];
- Heave motion z [m];
- Roll motion ϕ [deg];
- Pitch motion ϑ [deg];
- Yaw motion ψ [deg];
- Velocity V_X [m/s] of the turret in the longitudinal tank's direction;
- Velocity V_Y [m/s] of the turret in the transversal tank's direction;

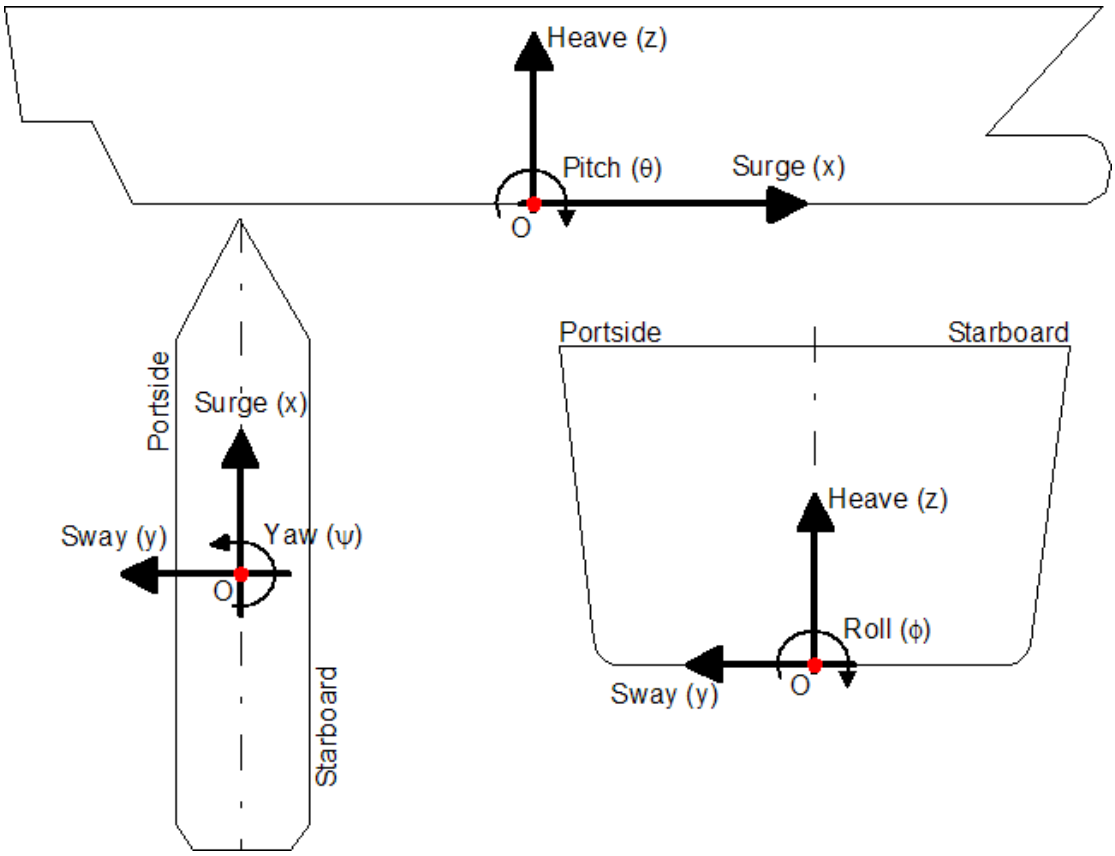

Figure 73: Convention for ship motions measurement.

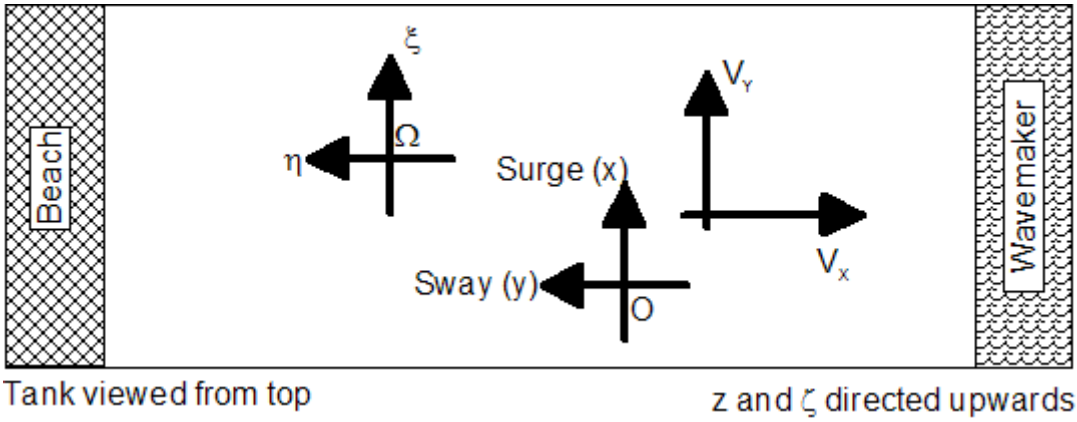

Figure 74: Reference systems.

Calculation of motions w.r.t. a tank fixed reference system

Since translations are given with respect to a moving reference system (the turret), it is necessary to transform all the data in order to obtain the position and attitude of the model with respect to a tank fixed reference system. Let now $\Omega\xi\eta\zeta$ be a right-handed tank fixed reference system defined as follows (see Figure 15):

- ζ pointing upwards (the gravity is therefore $(0,0,-g)^T$);

- η parallel to the longitudinal tank's direction and oriented from the wavemaker to the beach (in such a way that generated waves propagates along the positive η direction)
- ξ along the transversal tank direction and $\hat{\xi} = \hat{\eta} \wedge \hat{\zeta}$ (ξ oriented from left to right when looking from the wavemaker to the beach)

Note that the tank-fixed system $\Omega\xi\eta\zeta$ is parallel to the Krypton reference system $Oxyz$.

The carriage position, i.e. the position of the Krypton measuring device, in the reference system $\Omega\xi\eta\zeta$ can be obtained from the measured speeds V_X and V_Y as follows:

$$\begin{cases} \xi_K(t) = \xi_K(t=0) + \int_0^t V_Y(t)\,dt \\ \eta_K(t) = \eta_K(t=0) - \int_0^t V_X(t)\,dt \\ \zeta_K(t) = \zeta_K(t=0) \end{cases} \tag{47}$$

where $\left(\xi_K(t=0), \eta_K(t=0), \zeta_K(t=0)\right)^T$ is the *unknown* initial position of the carriage. Since the system $Oxyz$ is parallel to the system $\Omega\xi\eta\zeta$, and since the Krypton reference system measures the *relative* position $\left(x_O(t), y_O(t), z_O(t)\right)$ of the reference point with respect to the position of the Krypton measuring device, we can determine the coordinates of the reference point "O" w.r.t. the system $\Omega\xi\eta\zeta$ as follows:

$$\begin{cases} \xi_O(t) = x_O(t) + \xi_K(t) = x_O(t) + \xi_K(t=0) + \int_0^t V_Y(t)\,dt \\ \eta_O(t) = y_O(t) + \eta_K(t) = y_O(t) + \eta_K(t=0) - \int_0^t V_X(t)\,dt \\ \zeta_O(t) = z_O(t) + \zeta_K(t) = z_O(t) + \zeta_K(t=0) \end{cases} \tag{48}$$

Since the initial position $\left(\xi_K(t=0), \eta_K(t=0), \zeta_K(t=0)\right)^T$ is unknown, we fix *by convention*, that

$$\left(\xi_O(t=0), \eta_O(t=0), \zeta_O(t=0)\right)^T = (0,0,0)^T \tag{49}$$

and finally:

$$\begin{cases} \xi_O(t) := \left[x_O(t) - x_O(t=0) \right] + \int_0^t V_Y(t)\,dt \\ \eta_O(t) := \left[y_O(t) - y_O(t=0) \right] - \int_0^t V_X(t)\,dt \\ \zeta_O(t) := \left[z_O(t) - z_O(t=0) \right] \end{cases} \tag{50}$$

Position of the reference point "O" w.r.t. the ship fixed reference system

The position of the reference point "O" for beam sea tests and roll decay tests and in case of drift tests is slightly different according to the information provided by the towing tank.
In case of beam sea tests and roll decay tests the reference point "O" is on the keel line, amidships, on the centreplane. In case of drift tests the reference point "O" is on the keel line, below the ship's centre of gravity, on the centreplane. The centre of gravity is positioned longitudinally in such a way to have zero trim. This leads to a centre of gravity positioned 2.66m aft of midship at the test draught of 6.6m.

Appendix 3: Analysis of motions other than roll

This Appendix describes the experimental results and the corresponding numerical simulations (when available) for the following quantities:

- Drift speed in the direction of wave propagation;
- Amplitude of sway oscillation at the reference point;
- Amplitude of yaw oscillation;
- Amplitude of heave oscillation at the reference point;
- Amplitude of pitch oscillation;

A final series of summarising comments is also given.

Drift speed in the direction of wave propagation

Drift speed has been calculated by fitting a straight line to the signal of the ship position along the main tank direction in the time window of the recorded time history considered as stationary. Results from this analysis are reported in Figure 75 to Figure 78.

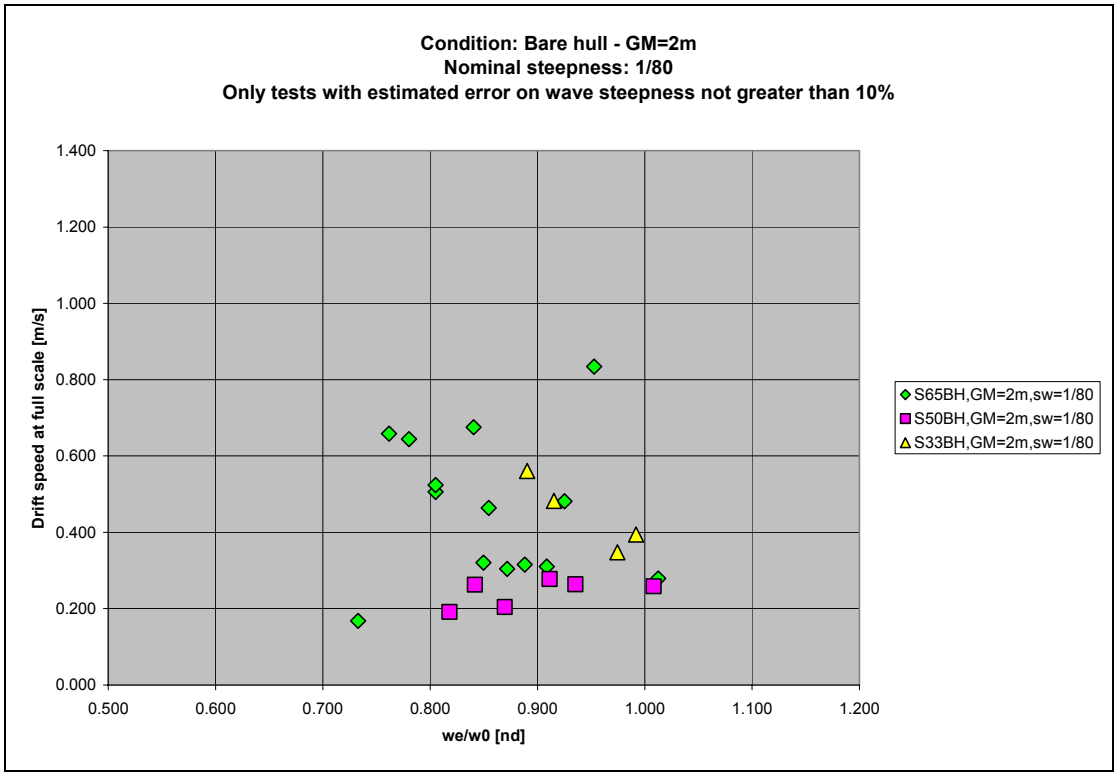

Figure 75: Stationary drift speed. $\overline{GM} = 2m$, bare hull.

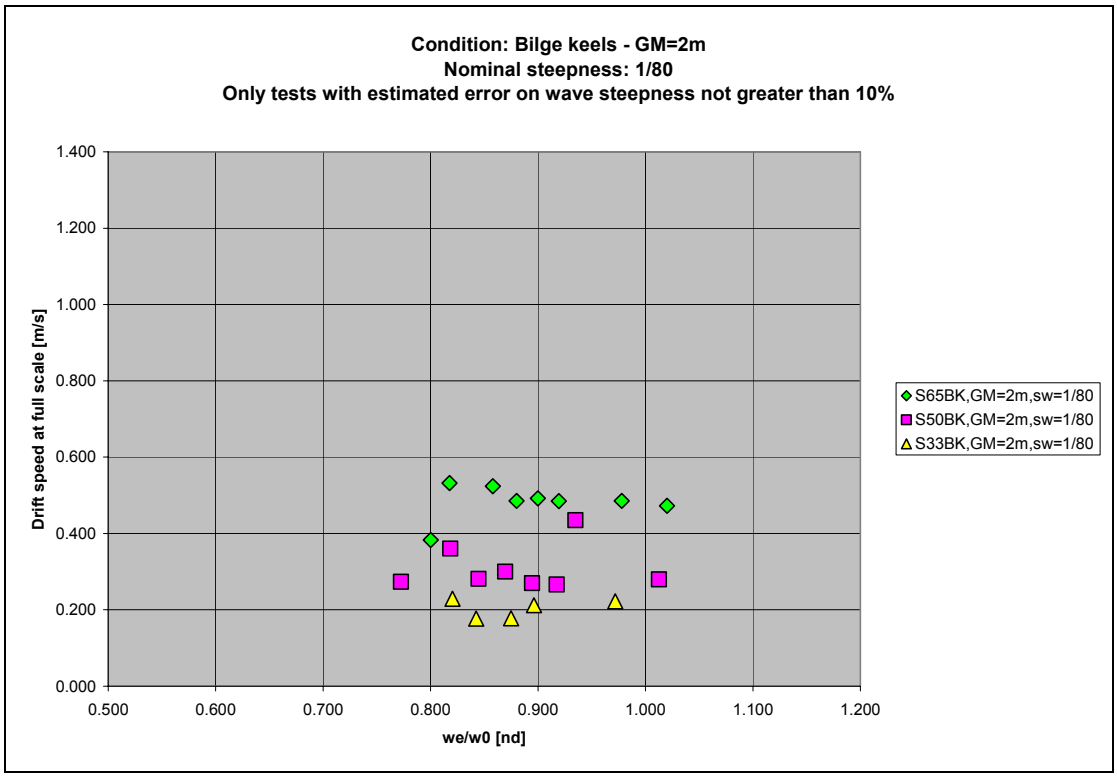

Figure 76: Stationary drift speed. $\overline{GM} = 2m$, bilge keels.

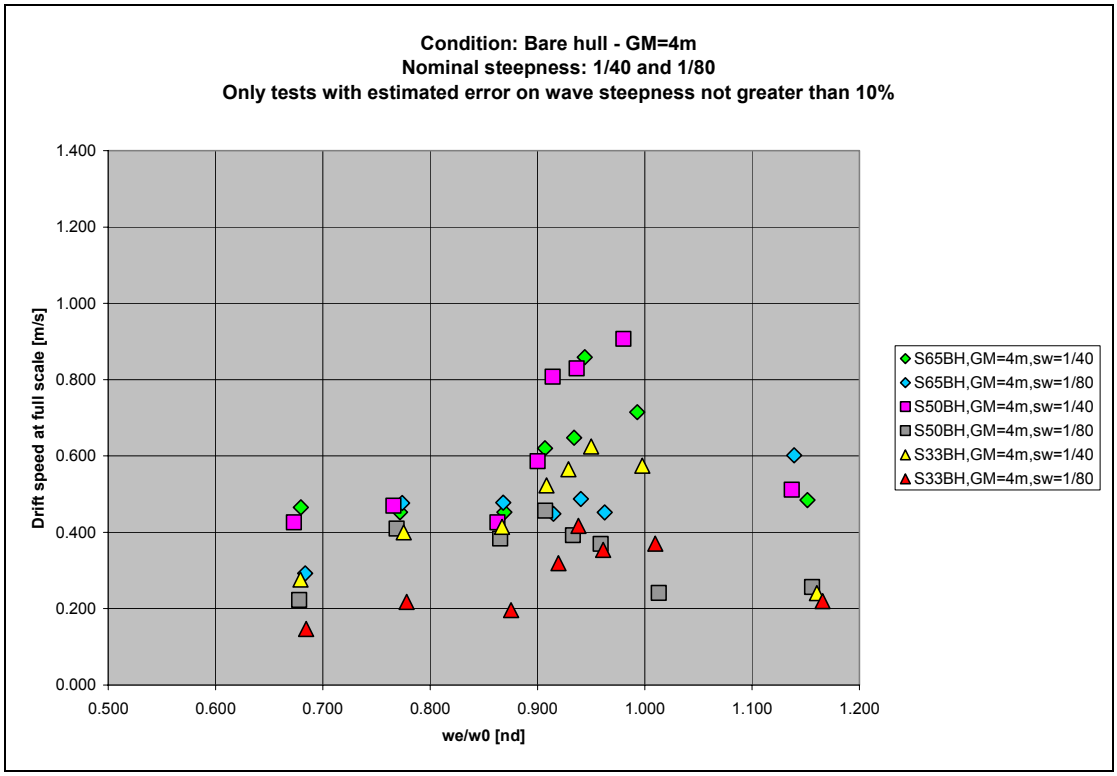

Figure 77: Stationary drift speed. $\overline{GM} = 4m$, bare hull.

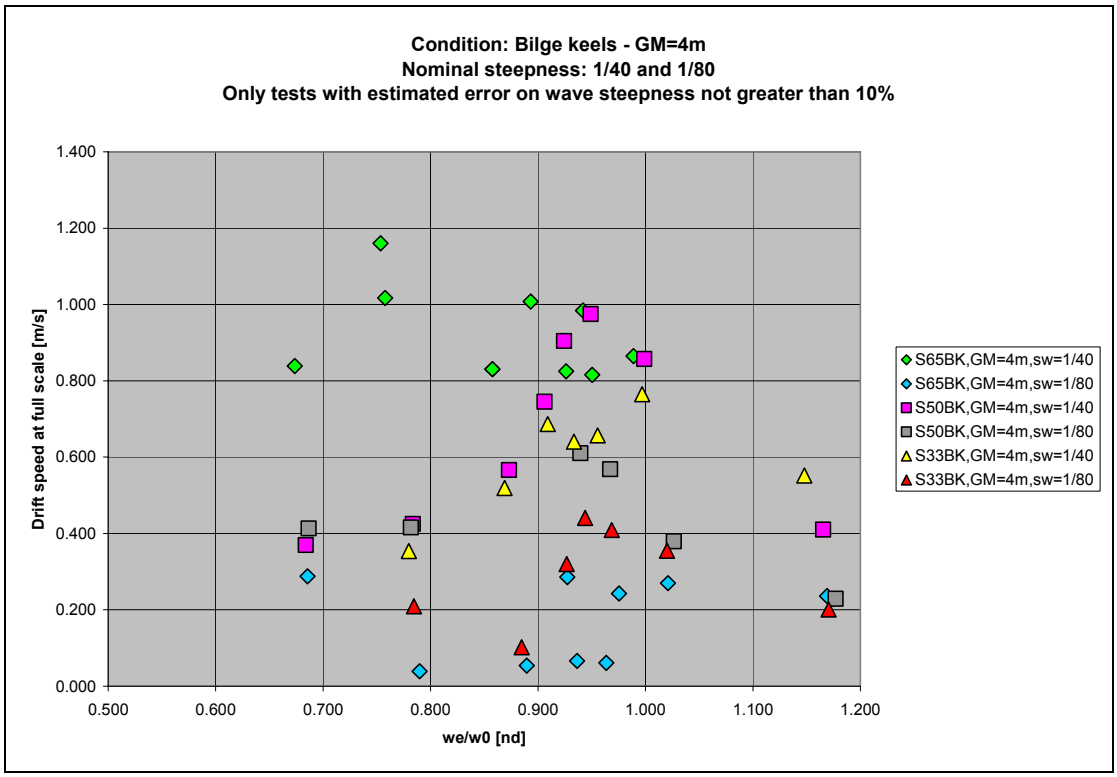

Figure 78: Stationary drift speed. $\overline{GM} = 4m$, bilge keels.

The scattering of the data is significant, especially in case of $\overline{GM} = 4m$, and it is not possible to see any clear trend. The standard deviation for the estimated drift speed is in general much smaller than the observed scattering, hence the differences among different scales should come from some different source. For sure part of the

difference is associated to the arbitrary selection of the time window, and part could come from the effect of yaw corrections to keep the beam sea condition. However, a more refined analysis should be carried out to clearly understand the source of the observed differences.

Sway oscillation at the reference point

The amplitude of sway oscillations has been analysed. The sway motion nominally refers to a reference point taken, in this series of experiments, amidships on the keel line. After removing the fitted linear drift trend due to the steady drift motion (to be precise a quadratic polynomial is removed as trend in order to reduce possible oscillations on the envelope of the oscillatory signal), the remaining oscillatory signal has been analysed. Results from this analysis are reported in Figure 79 to Figure 82. Figures also show the results from the numerical simulation using the 3-DOF model, where sway, roll and yaw are (hydrodynamically) coupled.

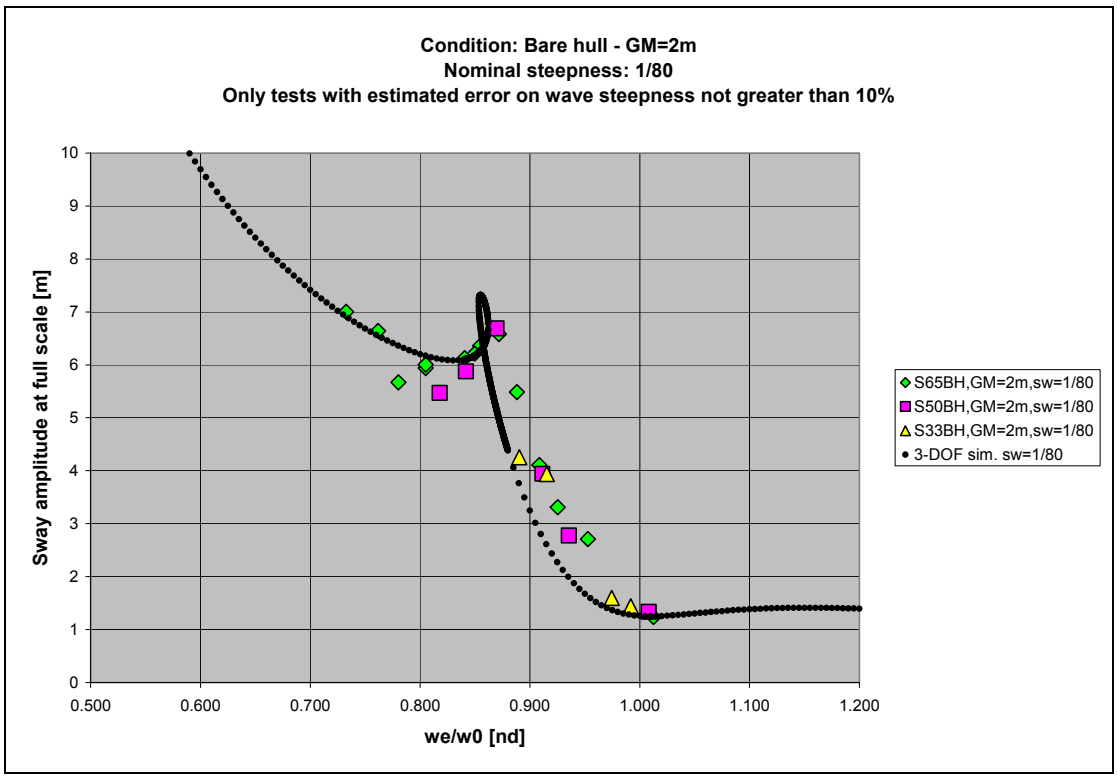

Figure 79: Amplitude of sway oscillation. $\overline{GM} = 2m$, bare hull.

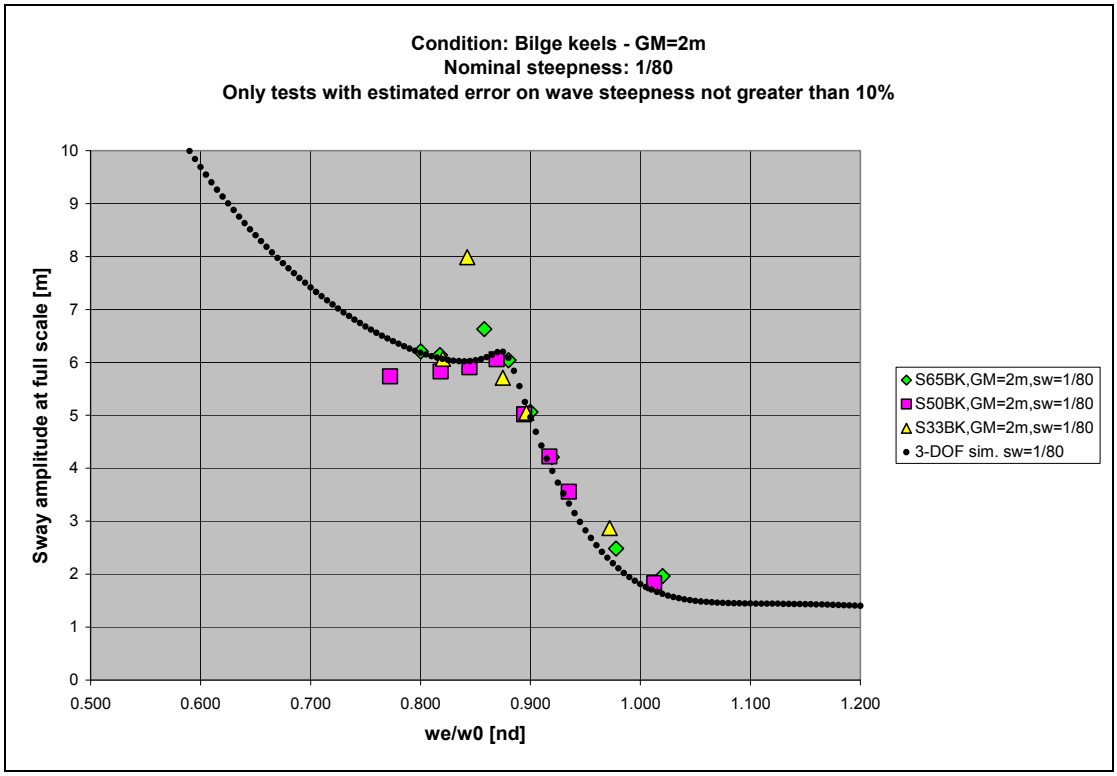

Figure 80: Amplitude of sway oscillation. $\overline{GM} = 2m$, bilge keels.

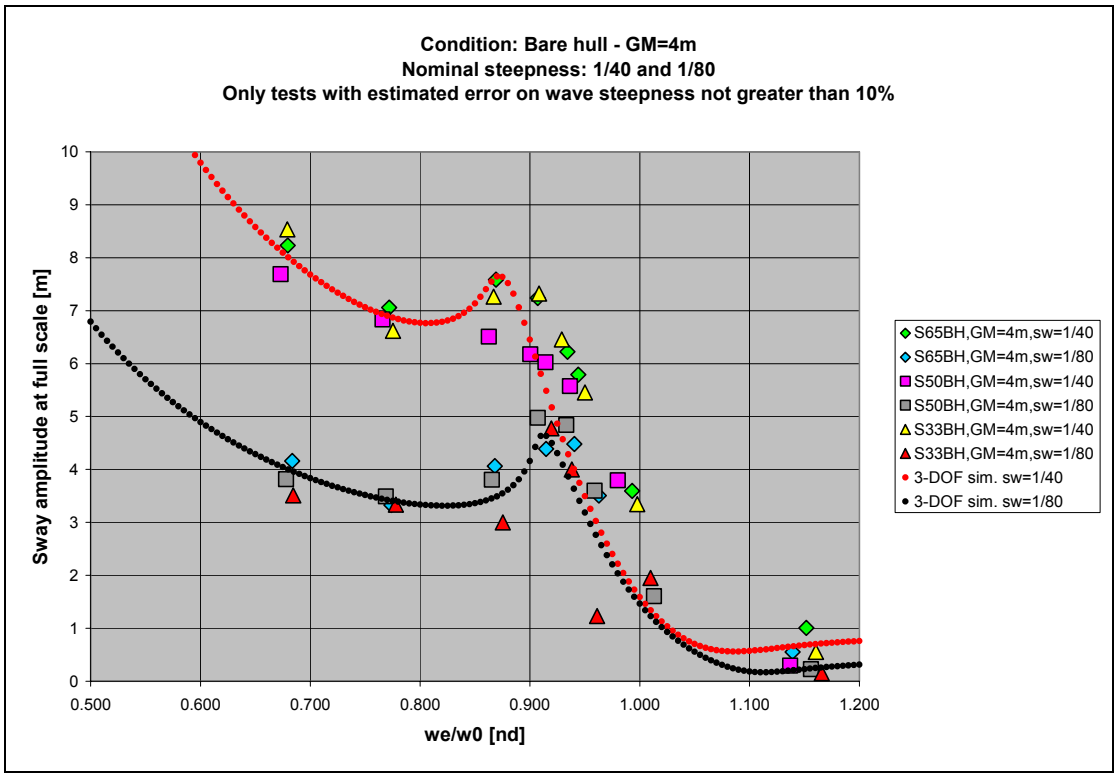

Figure 81: Amplitude of sway oscillation. $\overline{GM} = 4m$, bare hull.

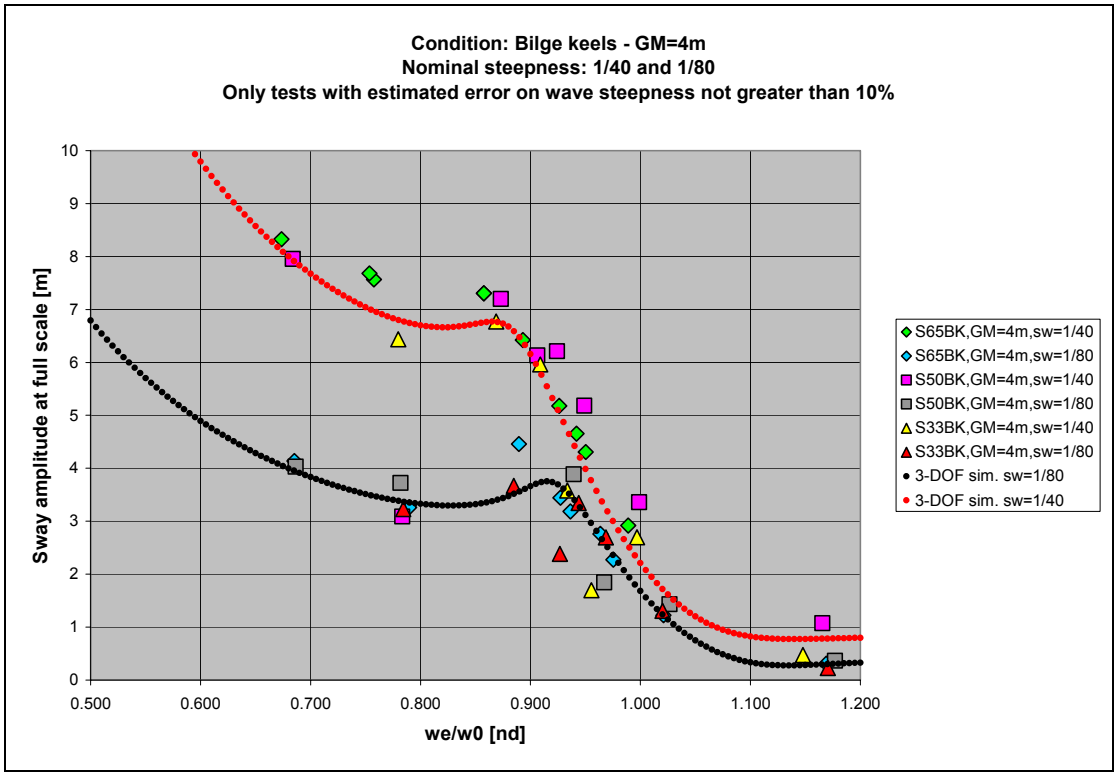

Figure 82: Amplitude of sway oscillation. $\overline{GM} = 4m$, bilge keels.

Also in case of amplitude of sway oscillations the scattering is not negligible. However a certain consistency is visible among different scales. The superposition of results from simulations helps in catching the trend of points. Some of the discrepancies among different scales could be due to a wrong setting of the RODYM measuring system (this possibility will be discussed in more details when dealing with heave amplitude), and in particular to errors associated to the setting of the position of the reference point. Looking at Figure 79 to Figure 82, a series of observations can be made:

- First of all it is extremely interesting to discuss Figure 79, with the guidance of Figure 53. As can be seen a closed loop is visible in the sway response in a range of frequencies close to the peak of the roll response curve. We have already discussed the fact that, in that range of frequencies, the roll response is multivalued. Accordingly, also the computed sway response using the 3-DOF modelling is multivalued, due to the coupling with roll. It can also be noticed the seemingly sharp local peak of the experimental response curve that seems to agree with the numerical simulations.
- When bilge keels are fitted in case of $\overline{GM} = 2m$ (see Figure 80) the roll response becomes single valued for the tested steepness, and the sway response curve modifies accordingly. Apart from some scattering of the experimental data, the agreement between simulations and experiments is good.
- Going now to the case $\overline{GM} = 4m$, in bare hull condition (Figure 81) and with bilge keels (Figure 82), we can see that again the experimental results are quite well explained by the numerical modelling. However the scattering of experimental data is quite large. The introduction of bilge keels reduces roll motion and, in turns, tends to reduce the local sway peak due to the roll

coupling. This feature is more evident in case of numerical simulations, but seems to be visible (at least on average) also from experimental data, especially in case of the smallest tested steepness.

The sway-roll coupling can be appreciated also when different types of plots are used. In Figure 79 to Figure 82 the amplitude of sway oscillation has been reported as a function of the ratio between the encounter (roll) frequency and the natural roll frequency. This representation allows to easily point out the roll resonance region. An alternative representation, shown in Figure 83 to Figure 86, reports the amplitude of the sway oscillation as a function of the amplitude of roll oscillation.

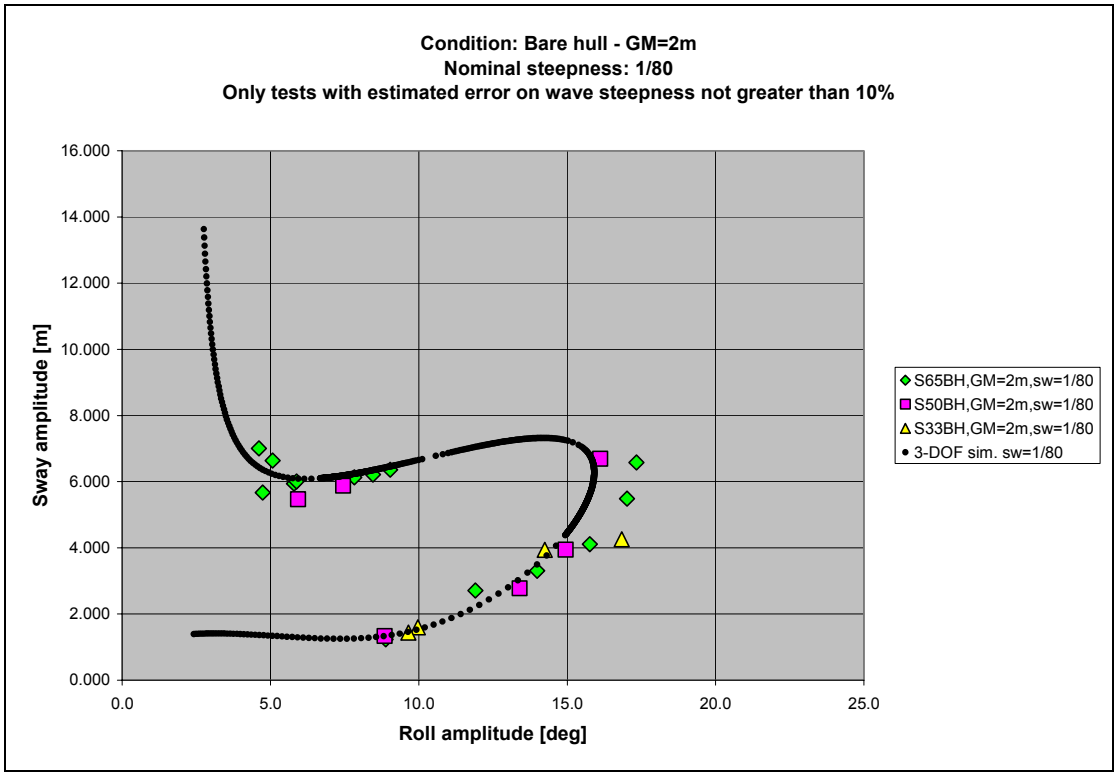

Figure 83: Amplitude of sway oscillation as a function of roll amplitude. $\overline{GM} = 2m$, bare hull.

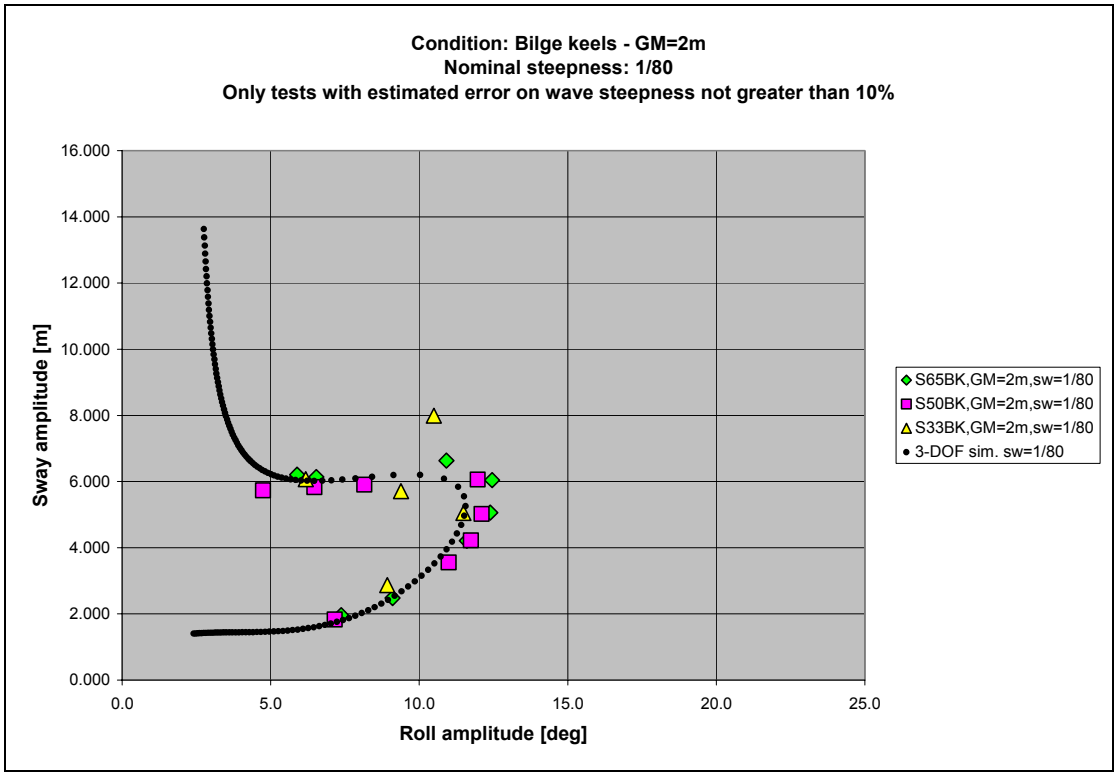

Figure 84: Amplitude of sway oscillation as a function of roll amplitude. $\overline{GM} = 2m$, bilge keels.

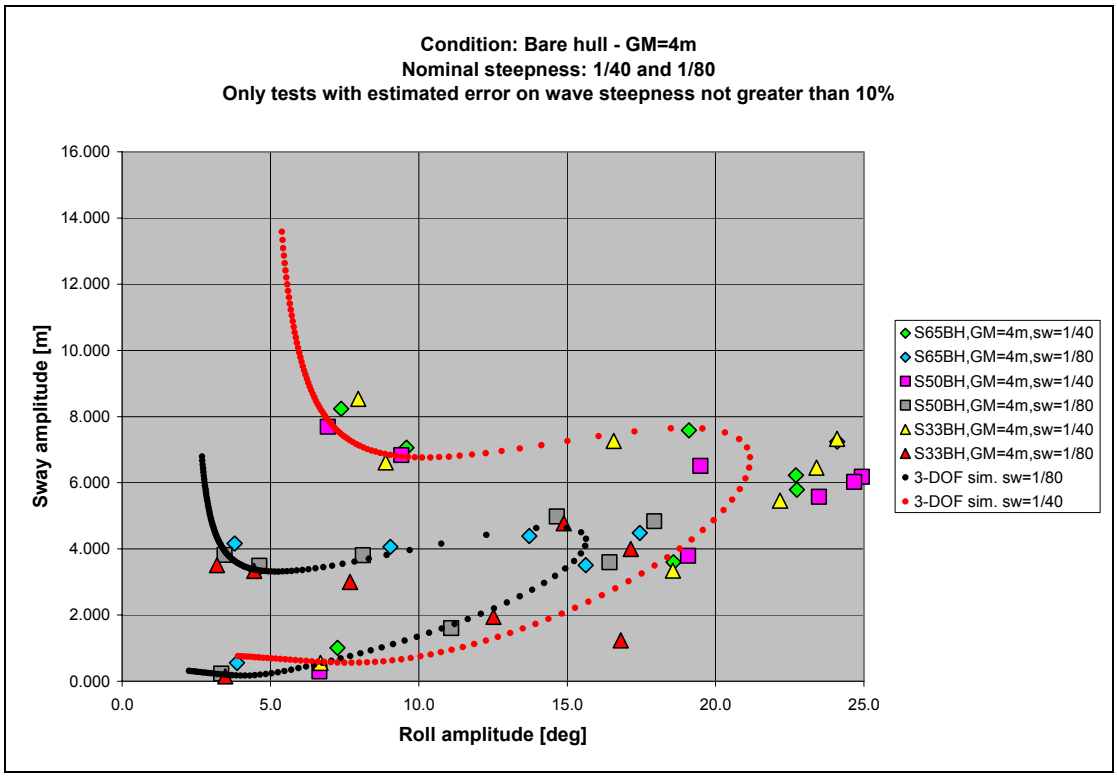

Figure 85: Amplitude of sway oscillation as a function of roll amplitude. $\overline{GM} = 4m$, bare hull.

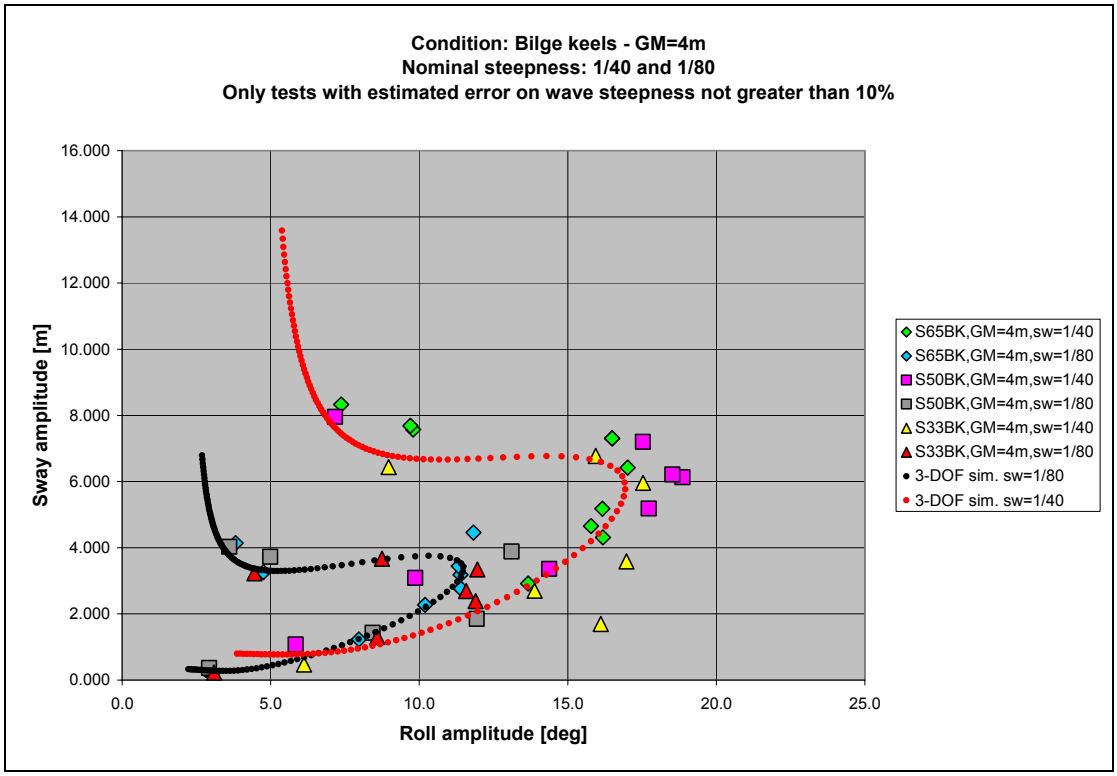

Figure 86: Amplitude of sway oscillation as a function of roll amplitude. $\overline{GM} = 4m$, bilge keels.

The observed agreement between experiments and simulations is good in case of tests with bilge keels. In case of tests in bare hull condition, the problems already observed in Figure 55 reflect in a not exciting agreement for the case $\overline{GM} = 4m$. On the other hand, in case of $\overline{GM} = 2m$, the agreement between simulations and experiments is good, especially close to the (likely present) fold bifurcation around 7deg.

Yaw oscillation

The amplitude of yaw oscillations has been analysed. The recorded yaw signal is, among all the DOFs, the most complex to analyse, since it contains strong trends with superimposed oscillations, and a not negligible quantity of noise. It is also quite influenced by manual corrections to keep the heading. In the analysis time window, the yaw motion has been filtered using a band-pass filter centred on the mean roll oscillation frequency. The scope of the band pass filter is to remove both the low frequency and the high frequency components, leaving an oscillatory signal that is expected to be mostly governed by the wave action and by the yaw-sway-roll coupling. Similarly to the case of sway, results concerning the measured amplitude of yaw oscillations are presented: a) as a function of the ratio between the encounter frequency and the natural roll frequency (Figure 87 to Figure 90), and b) as a function of the roll amplitude (Figure 91 to Figure 94).

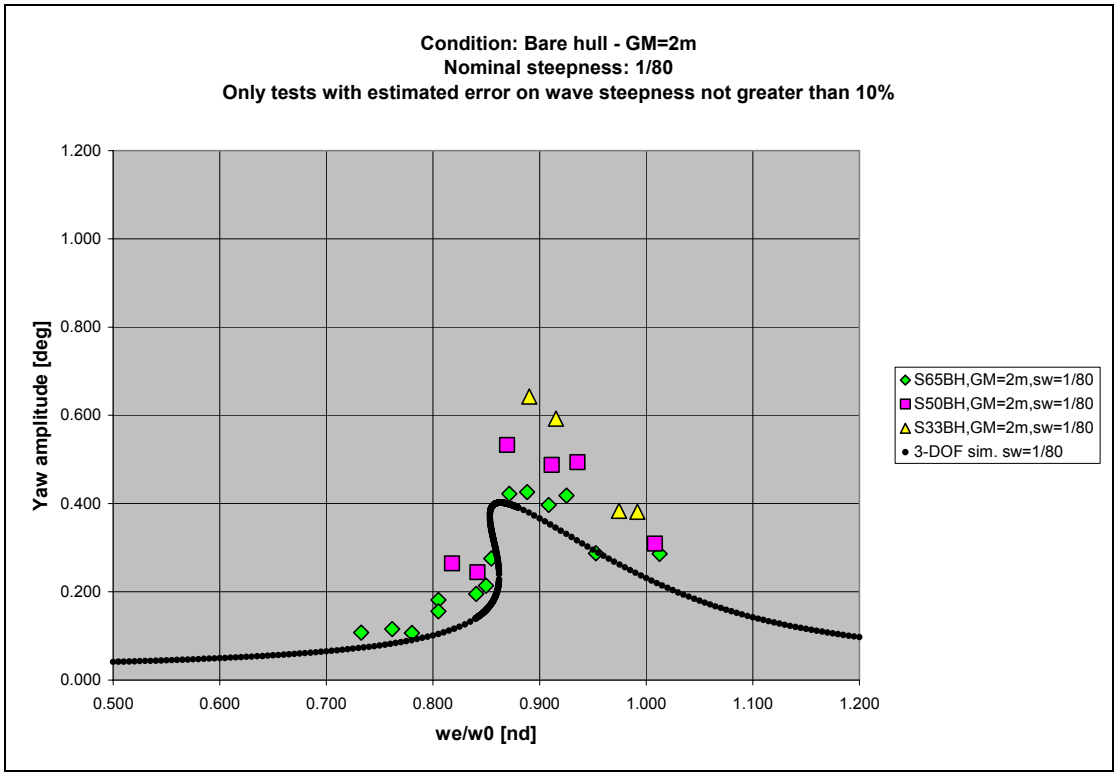

Figure 87: Amplitude of yaw oscillation. $\overline{GM} = 2m$, bare hull.

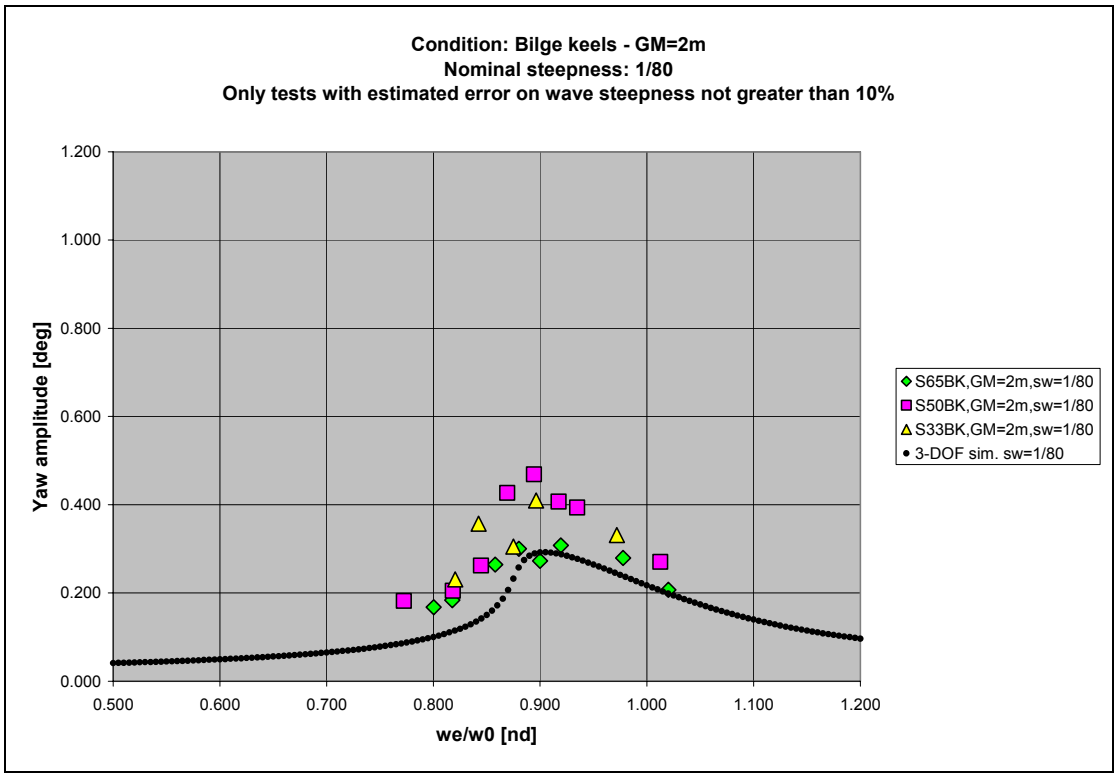

Figure 88: Amplitude of yaw oscillation. $\overline{GM} = 2m$, bilge keels.

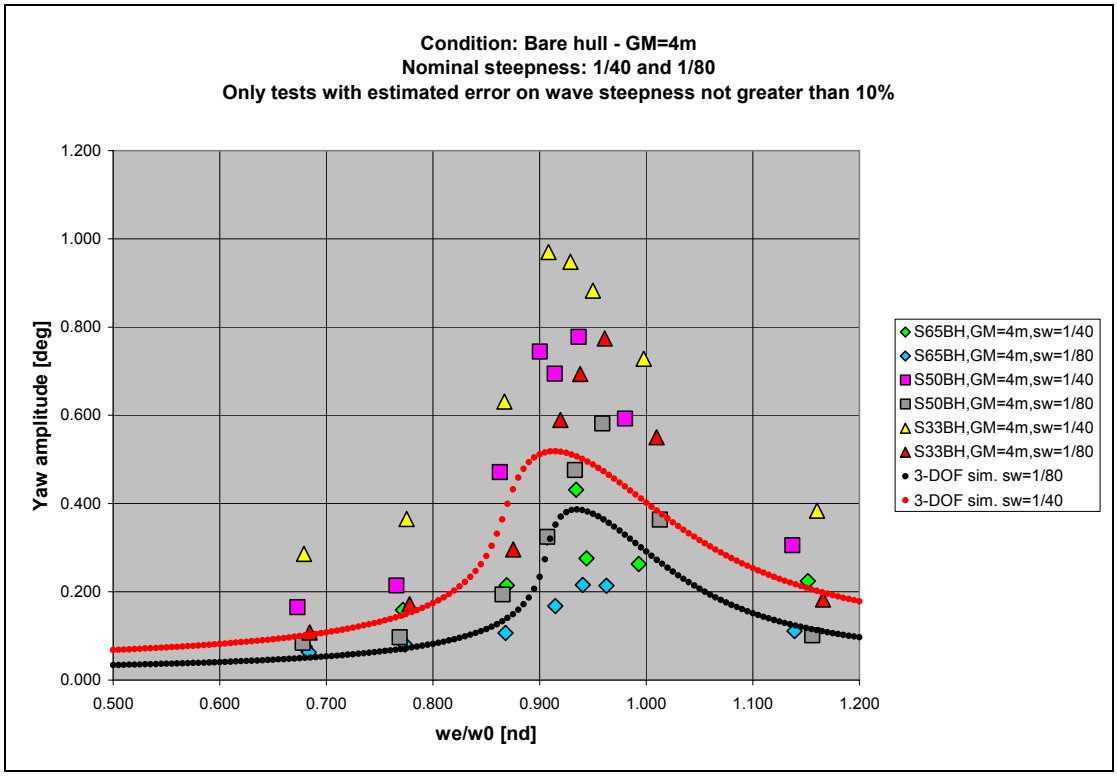

Figure 89: Amplitude of yaw oscillation. $\overline{GM} = 4m$, bare hull.

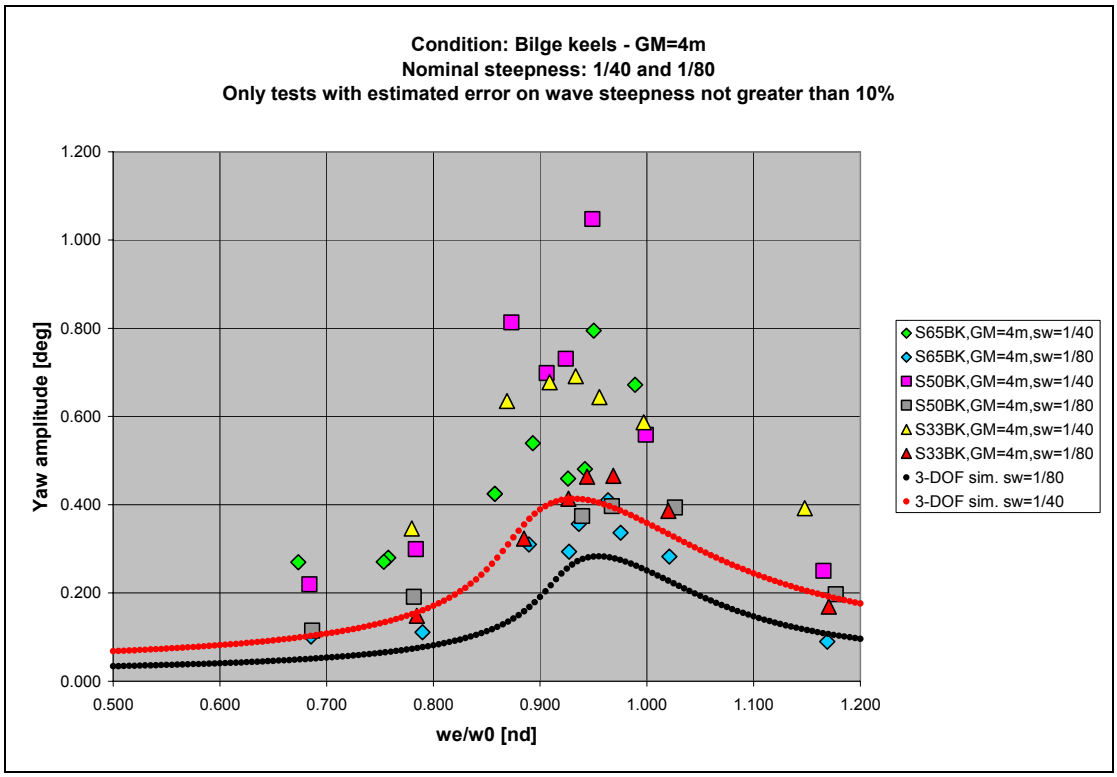

Figure 90: Amplitude of yaw oscillation. $\overline{GM} = 4m$, bilge keels.

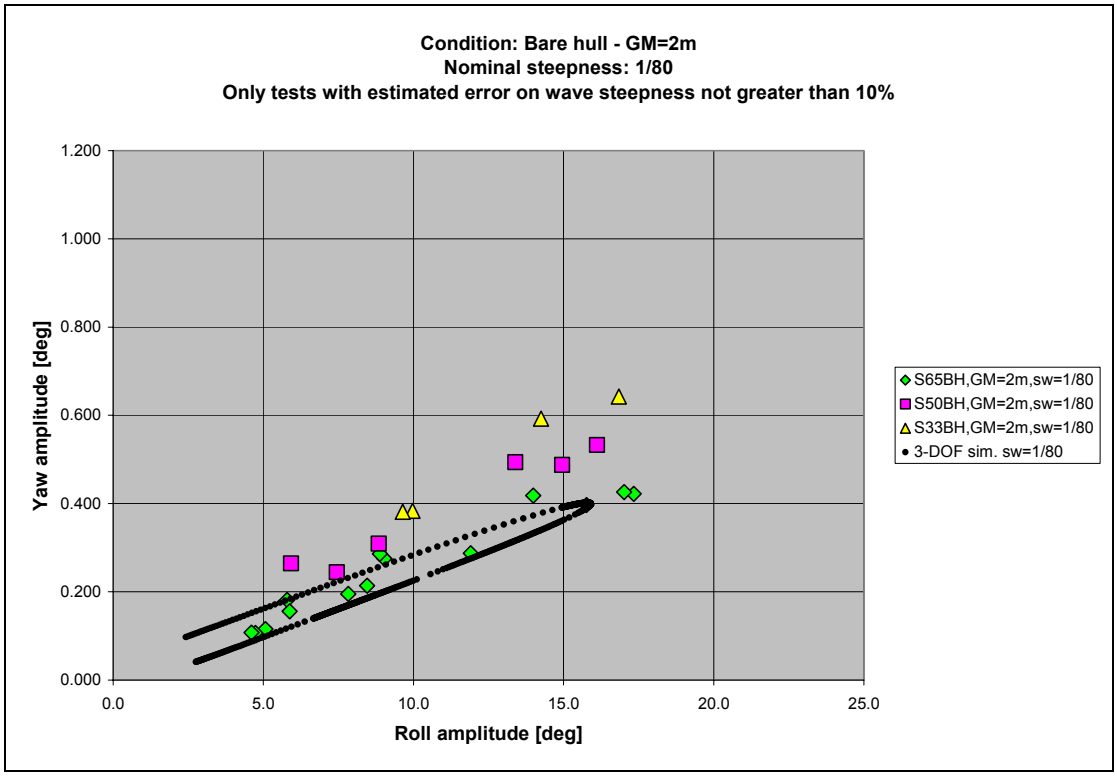

Figure 91: Amplitude of yaw oscillation as a function of roll amplitude. $\overline{GM} = 2m$, bare hull.

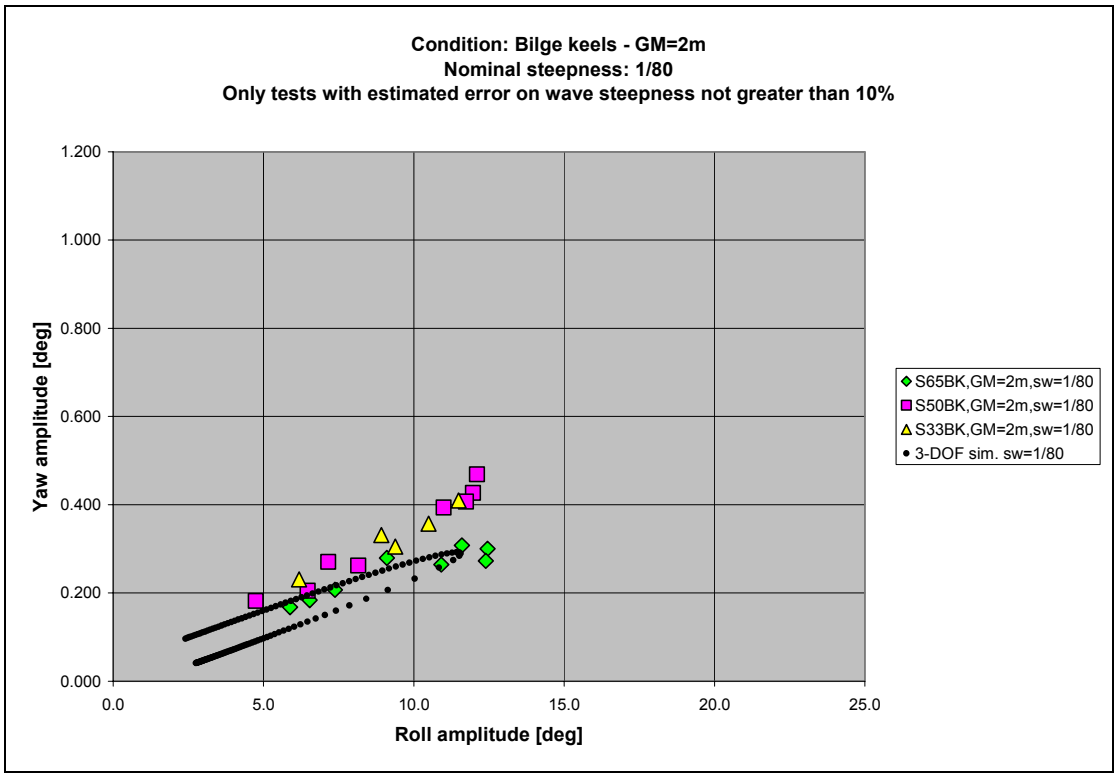

Figure 92: Amplitude of yaw oscillation as a function of roll amplitude. $\overline{GM} = 2m$, bilge keels.

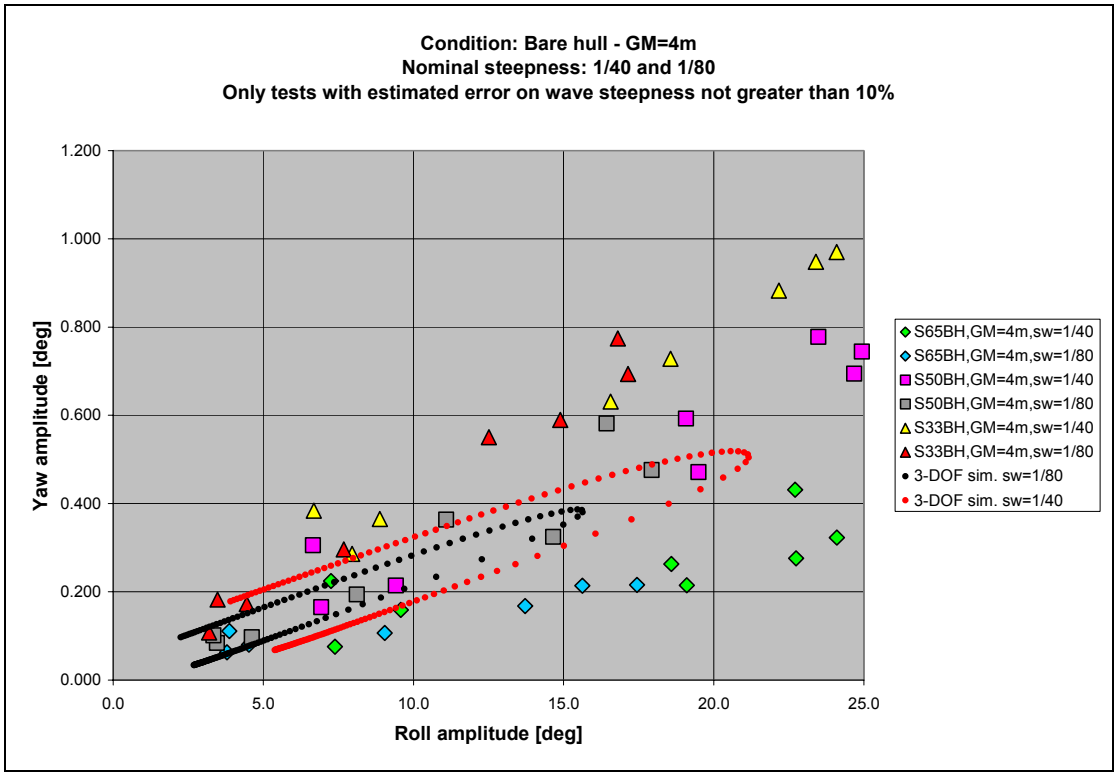

Figure 93: Amplitude of yaw oscillation as a function of roll amplitude. $\overline{GM} = 4m$, bare hull.

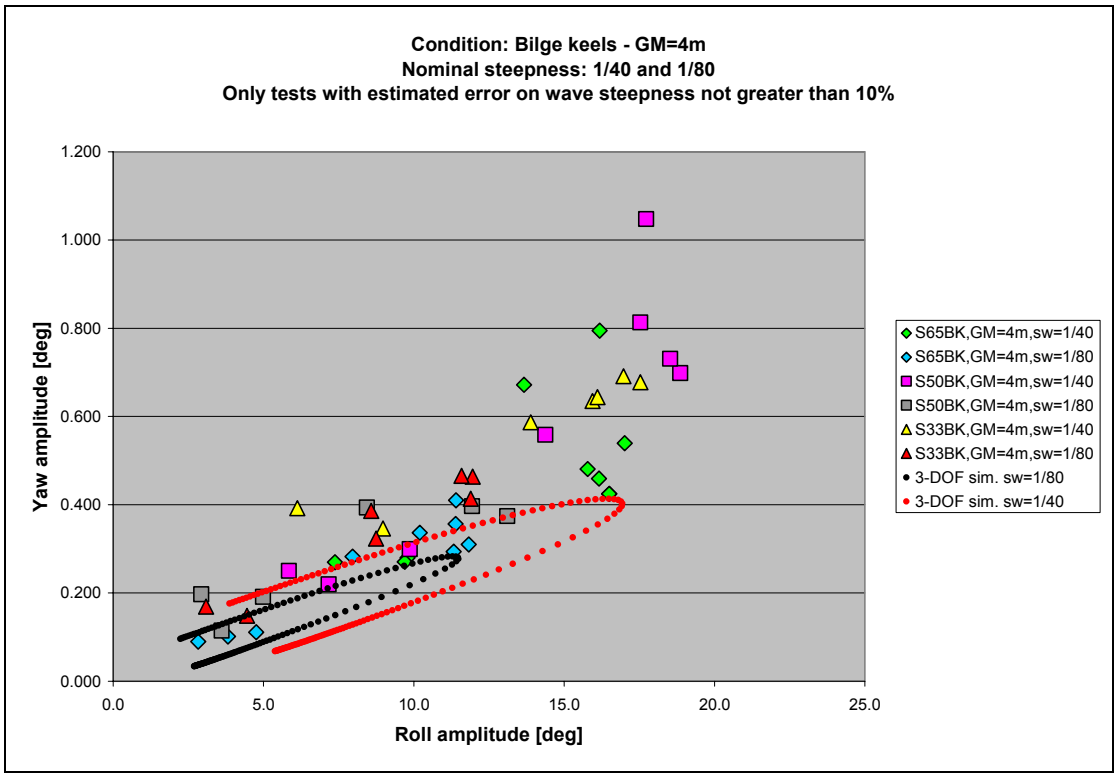

Figure 94: Amplitude of yaw oscillation as a function of roll amplitude. $\overline{GM} = 4m$, bilge keels.

According to the obtained results it is possible to comment as follows:

- The scattering of data is quite significant, in particular for conditions with $\overline{GM} = 4m$. This could be due to the effect of manual corrections to the heading or to the methodology of filtering / analysis of the signals. Data for

$\overline{GM} = 2m$ seem to be more consistent, and a general reduction of yaw for the smaller model seems to be present. A smaller yaw motion for the smaller model (scale 1:65) seems to be, however, a common feature, at least on average.

- The agreement between simulations and experiments is usually not very good quantitatively, although the qualitative behaviour is caught by simulations. However, it must be emphasized that the used 3-DOF modelling introduces viscous effects only on roll damping, and coefficients for the DOFs of yaw and sway are only based on potential theory. It is expectable that viscous effects play a not negligible role in the determination of yaw amplitude, and hence the used 3-DOF model cannot be considered fully appropriate for the purpose of dealing with yaw unless additional terms, reflecting viscous effects, are introduced in the model.
- The experimental yaw amplitude response curve in Figure 87 shows a significant bending towards the low frequency side, that is reflected by the numerical simulations, and that is associated to the low frequency bending of the roll response curve. A region of multiple steady states for yaw is also predicted as a consequence of the coupling with roll.

Heave oscillation at the reference point

The amplitude of heave oscillations has been analysed. The heave motion nominally refers to a reference point taken, in this series of experiments, amidships on the keel line. According to linear calculations using the nominal 90deg heading, the heave transfer function (i.e. the ratio between heave amplitude and wave amplitude) is basically unitary in the majority of tested cases, with a departure from unity reaching 1.02 in case of tests carried out with $\overline{GM} = 4m$ in the high frequency tail of the roll response curve. However, linear calculations do not account for the influence of roll into heave and for nonlinearities in the heave response as a function of the wave amplitude. In the 3-DOF model used for simulations surge, heave and pitch are treated linearly coupled, and uncoupled from roll, sway and yaw (that, on the other hand, comprise part of nonlinear effect through the implementation of a nonlinear roll restoring). As a first approximation, the effect of roll into heave of a point in the centreplane should be seen as a second harmonic component in the heave signal (roughly proportional to something close to the square of the rolling amplitude). Here we are analysing the envelope of the heave oscillation, hence, to some extent, the first and the second harmonic of the motion are both mixed in the estimation of the average heave oscillation amplitude, since this type of analysis is basically intended for harmonic motions. It must be said that this considerations are correct when the ship is symmetric and the reference point is placed amidships. On the other hand, if the reference point at which heave is measured, is placed off the centreplane, there is a direct (linear) influence of roll into heave. Neglecting the effect of other motions, the heave of a point placed transversally off the centreplane by a quantity δy can be computed, at a first approximation for small rolling angles, as:

$$z(t, \delta y) \approx z(t, \delta y = 0) + \delta y \cdot \phi(t) \tag{51}$$

The quantity we are expected to measure is $z(t, \delta y = 0)$, namely the heave at the centreplane (in particular amidships on the keel line), but, if an offset δy is present, a

direct effect of the rolling amplitude could become strongly visible in the heave signal. These preliminary considerations are important for a proper interpretation of the obtained results.
Figure 95 to Figure 98 show the heave amplitude made nondimensional through the wave amplitude, as a function of the measured rolling amplitude.

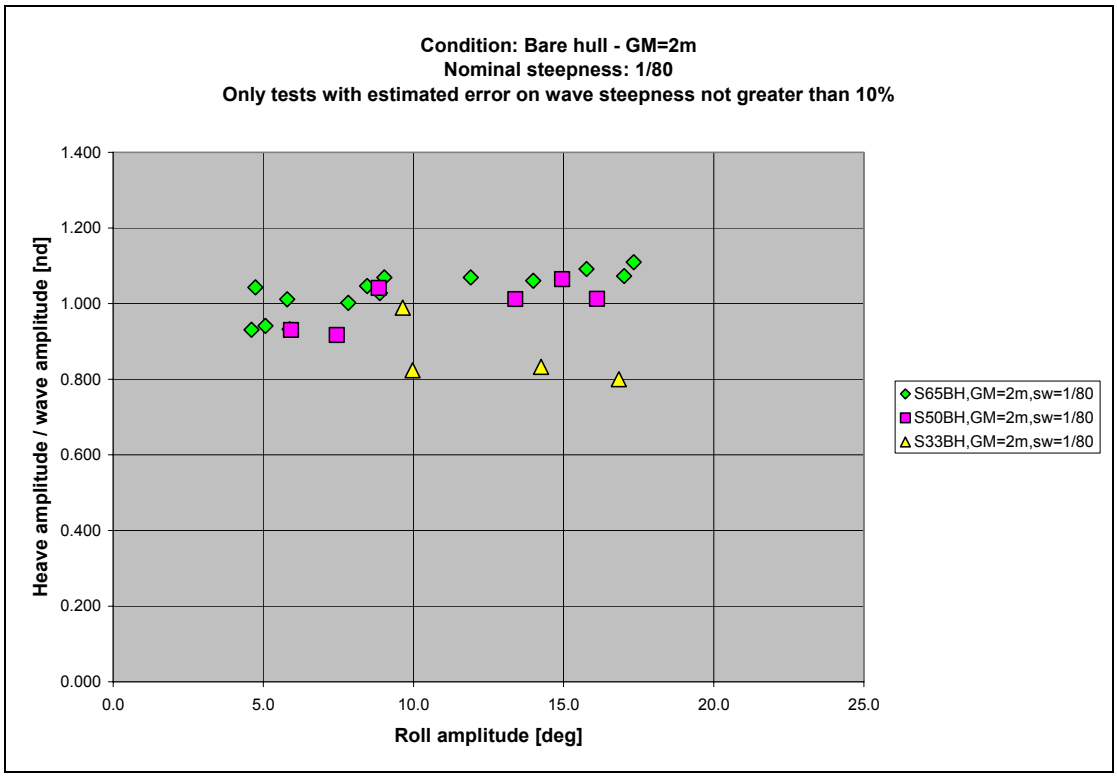

Figure 95: Nondimensional amplitude of heave oscillation as a function of roll amplitude. $\overline{GM} = 2m$**, bare hull.**

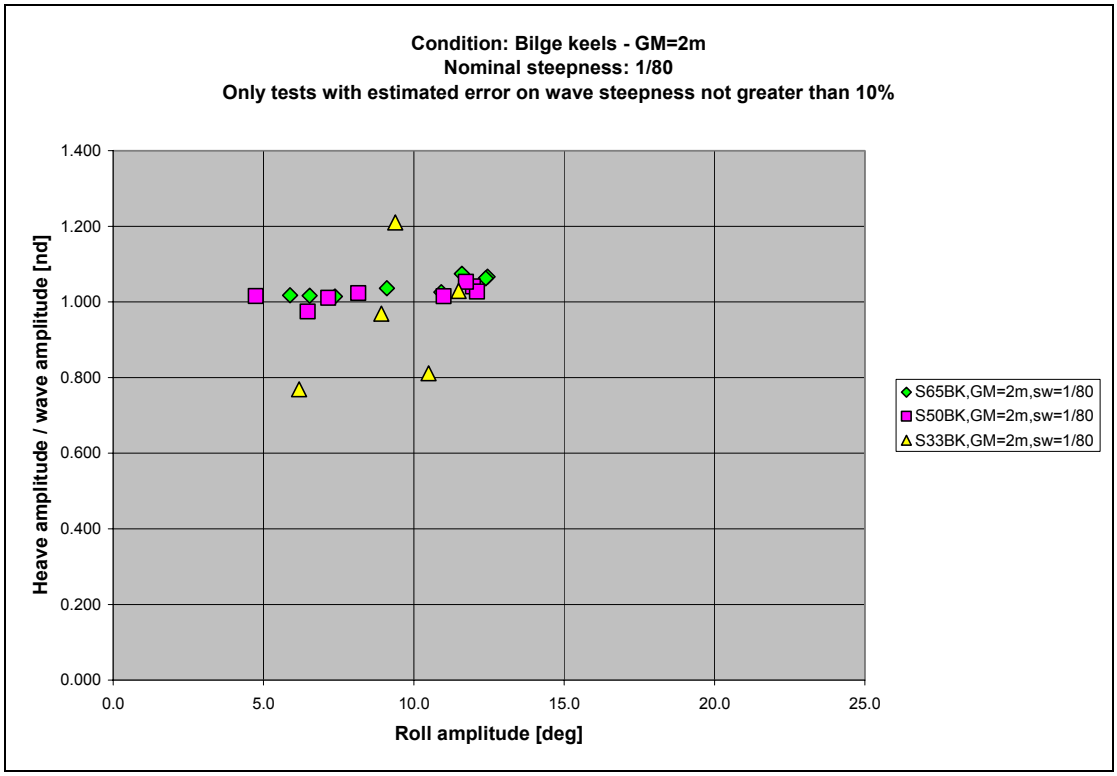

Figure 96: Nondimensional amplitude of heave oscillation as a function of roll amplitude. $\overline{GM} = 2m$, bilge keels.

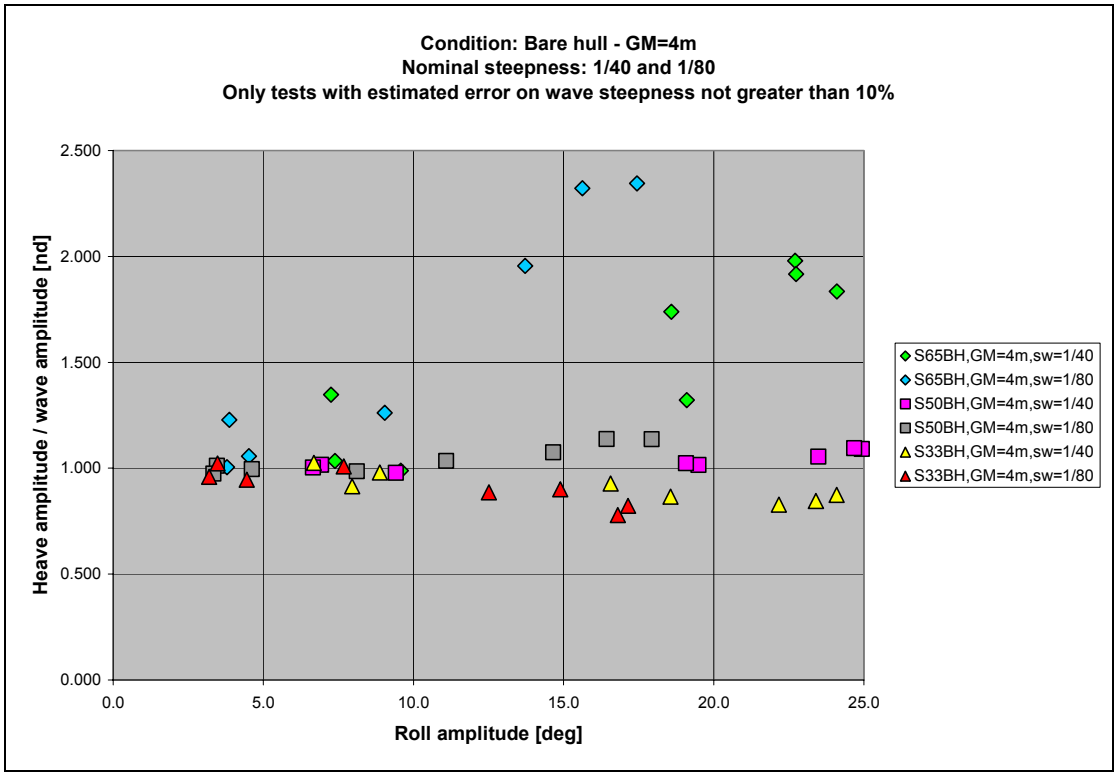

Figure 97: Nondimensional amplitude of heave oscillation as a function of roll amplitude. $\overline{GM} = 4m$, bare hull.

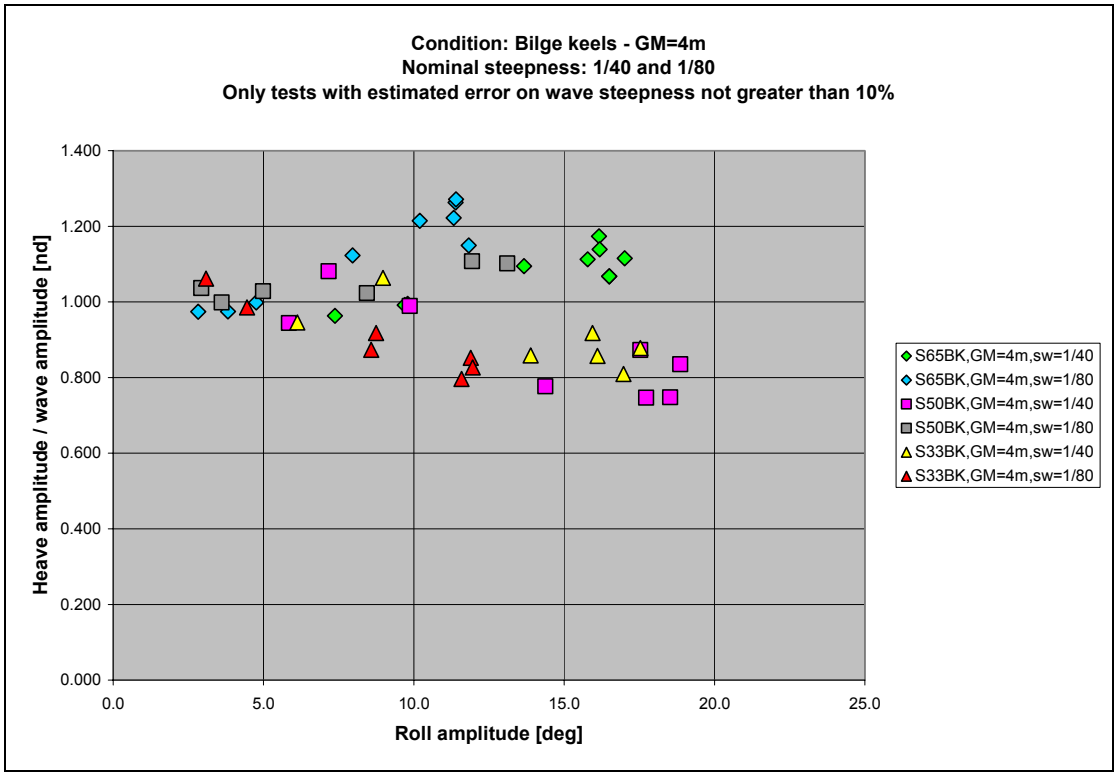

Figure 98: Nondimensional amplitude of heave oscillation as a function of roll amplitude. $\overline{GM} = 4m$, bilge keels.

Looking at the obtained results it is possible to provide a series of comments:

- The scattering of the data is significant. In case of $\overline{GM} = 2m$ the scattering is particularly evident for the largest model (scale 1:33), while data for models at scale 1:65 and 1:50 are quite consistent. In case of $\overline{GM} = 4m$ the scattering is significant in all cases.
- Results are, in general, consistent for the same model, but differences are evident when comparing results for models having different scales, in the same loading condition.
- The influence of roll on the amplitude of heave oscillation is in general evident, and in particular extremely strong in case $\overline{GM} = 4m - BH$, scale 1:65, as visible in Figure 97. Also in Figure 98 there is a quite strong influence of the roll amplitude on the nondimensional heave. At this stage it seems difficult that the observed dependence of heave on roll could be due to the nonlinear coupling of roll into heave. The guess is that, in the setting of the motion measuring system, some offset δy has been introduced (see (51)) finally creating spurious effects on the measured heave signal that roughly linearly depend on the roll amplitude. Although it has not been possible to have a confirmation of this conjecture, it seems a reasonable possibility consistent with the data. It must be noted that, of course, a possible transversal shift δy in the setting of the reference centre also influences the measured sway motion when nonlinear effects are taken into account. However the introduced error in case of sway is of less importance than in the case of heave. A much larger influence on sway would be introduced by a vertical shift of the reference centre.

- Part of the scattering could be associated to analysis time windows where motions are not yet sufficiently stationary. However, it seems that some of the differences among different models could be associated to some error in the setting of the RODYM measuring device.

According to the analysis of the measured heave motion, taken into account the scattering of data (that could be only partially associated to analysis time windows where motions are not yet sufficiently stationary) and the seemingly inconsistencies between different experiments, it seems that, at the present stage, heave motion measurements cannot be considered fully reliable.

Pitch oscillation

The amplitude of pitch oscillations has been analysed. The original intention was to try to assess the effect of roll into pitch in terms of oscillation amplitude. Although a relation has been found, as will be clear from the results, it is not, on the other hand, clear, the real source of this relation. Results are shown in Figure 99 to Figure 102.

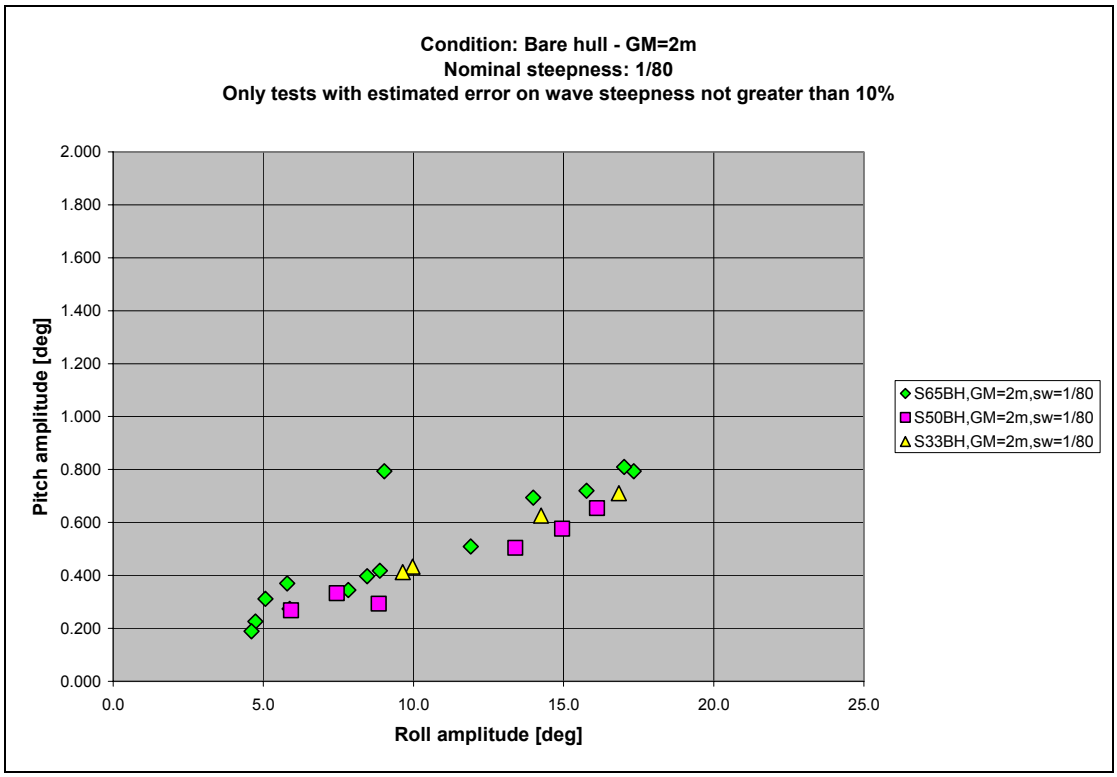

Figure 99: Amplitude of pitch oscillation as a function of roll amplitude. $\overline{GM} = 2m$, bare hull.

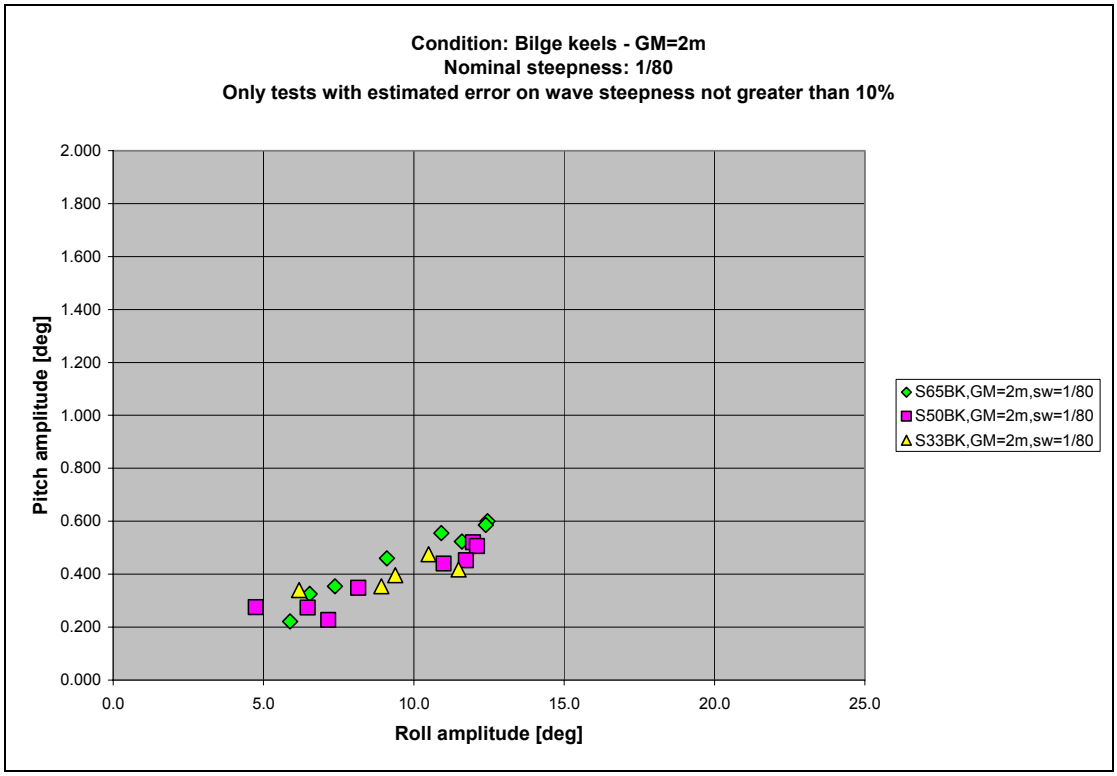

Figure 100: Amplitude of pitch oscillation as a function of roll amplitude. $\overline{GM} = 2m$, bilge keels.

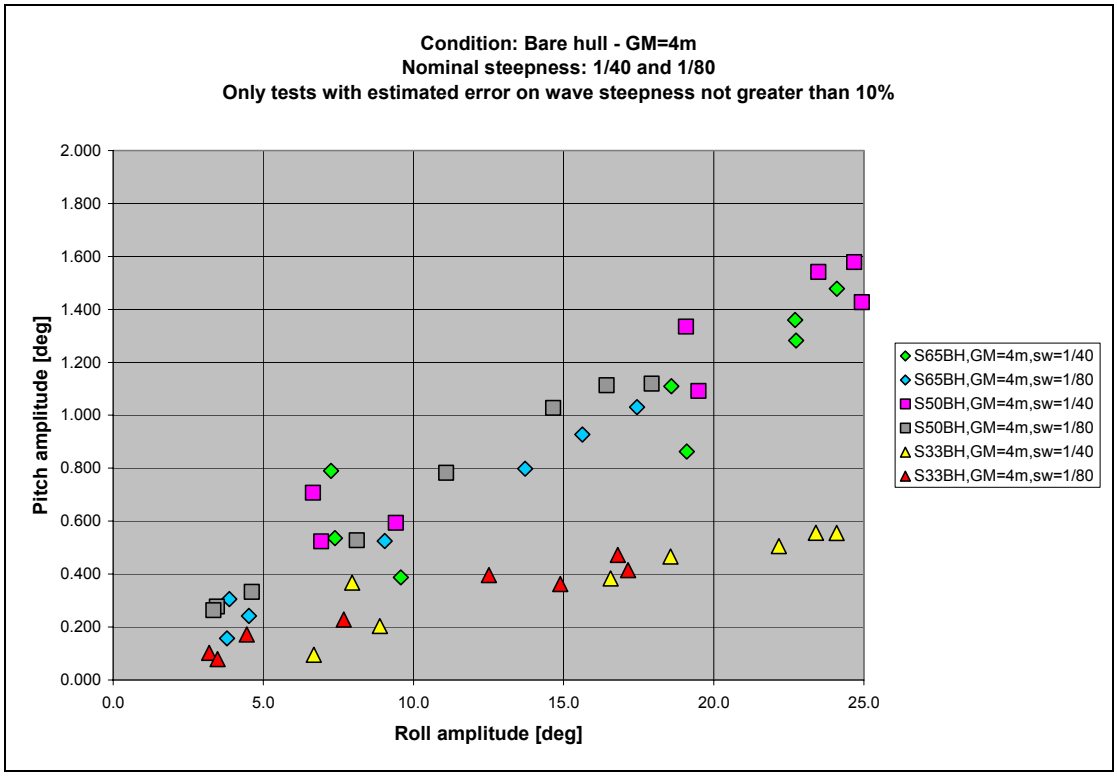

Figure 101: Amplitude of pitch oscillation as a function of roll amplitude. $\overline{GM} = 4m$, bare hull.

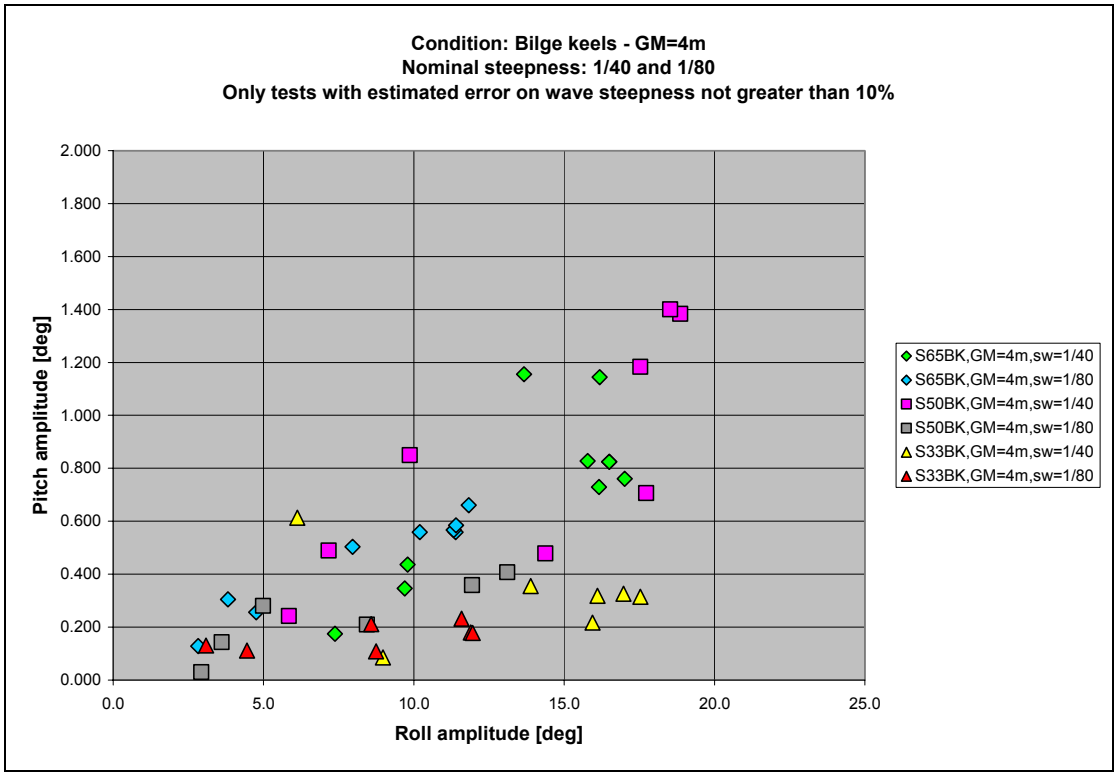

Figure 102: Amplitude of pitch oscillation as a function of roll amplitude. $\overline{GM} = 4m$, bilge keels.

According to the obtained results, it is possible to make a series of comments:

- There is a strong relation between roll amplitude and pitch amplitude.
- The consistency of data among different scales is good for $\overline{GM} = 2m$. In case of $\overline{GM} = 4m - BH$ data at scale 1:33 are significantly different from those obtained for scales 1:65 and 1:50. In case $\overline{GM} = 4m - BK$ the scattering is significant.

Although the observed relations could support the idea of an actual strong influence of roll into pitch, there are a series of doubts concerning the interpretation of the obtained data.

First of all, the roll effect into pitch should appear, mainly, as a second harmonic forcing. This means that, if we assume the roll effect to be dominant(as it seems to appear from the obtained results), a second harmonic should be dominant in pitch time series in comparison with the first harmonic term due to the direct effect of waves: unfortunately it is not so, and the Fourier analysis shows, in the large majority of cases, a dominant first harmonic. It is not clear, then, how the roll could affect pitch as a dominant first harmonic forcing. A dominant first harmonic should be associated to a dominant response due to waves. However, in the region of tested waves, the 90deg-heading linear pitch response is extremely small. In order to obtain pitch responses comparable to the measured ones, it would be necessary to conjecture a possible not negligible deviation from the condition of 90deg heading, that, on the other hand, is not supported from the available time records of yaw. One explanation for the obtained results could come from a possible misalignment of the RODYM reference frame: a misalignment of the reference frame with respect to the ship axes could lead to a measurement of pitch that is influenced by spurious (geometrical) effects of roll. This explanation is reasonable, however, what is much less reasonable

is that a misalignment has occurred of a very similar magnitude in case of different models. Indeed we have found a quite remarkable consistency of obtained data among different scales. The possibility of misalignments of the RODYM reference frame, although not remote, seems not to fully explain the obtained results.
Finally we are not in the position to guarantee the reliability of pitch motion measurement, hence pitch data should be considered with caution.

Summarising comments

According to the obtained data for motions other than roll it seems that data concerning heave motion could have been influenced by some error in the setting of the centre of the reference frame. This error, if confirmed, could have also caused problems, though of a much more limited magnitude, concerning sway. In general, sway data are quite consistent and are in agreement with simulations. Consistency of yaw data is worse, and this could be due to the technique used for the analysis, but the agreement with simulations is qualitatively good. Heave data in some cases should be regarded as not reliable. In case of pitch a strong correlation between pitch amplitude and roll amplitude has been found, but the frequency domain analysis did not show an expected strong second harmonic, as would be expectable in case of a roll forcing into pitch. Hence pitch data requires further consideration. The encountered problems confirm the difficulty in carrying out high quality experiments in waves with completely free models.

Appendix 4: Measured roll moment during drift tests - Outcomes and doubts

The roll moment induced by steady drift was also addressed during the tests. Actually this quantity was the quantity of major importance at the time of planning the experiments. However, in the analysis of the data obtained from the towing tank, a series of inconsistencies have been found that were hardly explainable as scale effects. The obtained scattering of data seems, indeed, to have been caused by some error / misunderstanding in the process of the execution of tests / analysis of data.
Here we start from describing some of the observed inconsistencies concerning the ship attitude at zero speed when heeled. Afterwards results from the analysis of the roll moment are reported and discussed. Of course such results are reported only for sake of completeness, and they are by no means considered to be reliable.

Ship attitude at zero speed - Calculations and experimental results

Measured pitch and vertical shift of the keel point have been compared with hydrostatic calculations. Since the ship was free to heave and pitch, it was expected to obtain a good correlation between experiments and calculations. Unfortunately it was not so, as it will be clear soon.
Figure 103 reports a comparison between the hydrostatically calculated and the actually measured vertical shift of the reference point. It can be noticed that experimental data for the two tested scales are very consistent, but the disagreement with calculations is very large.

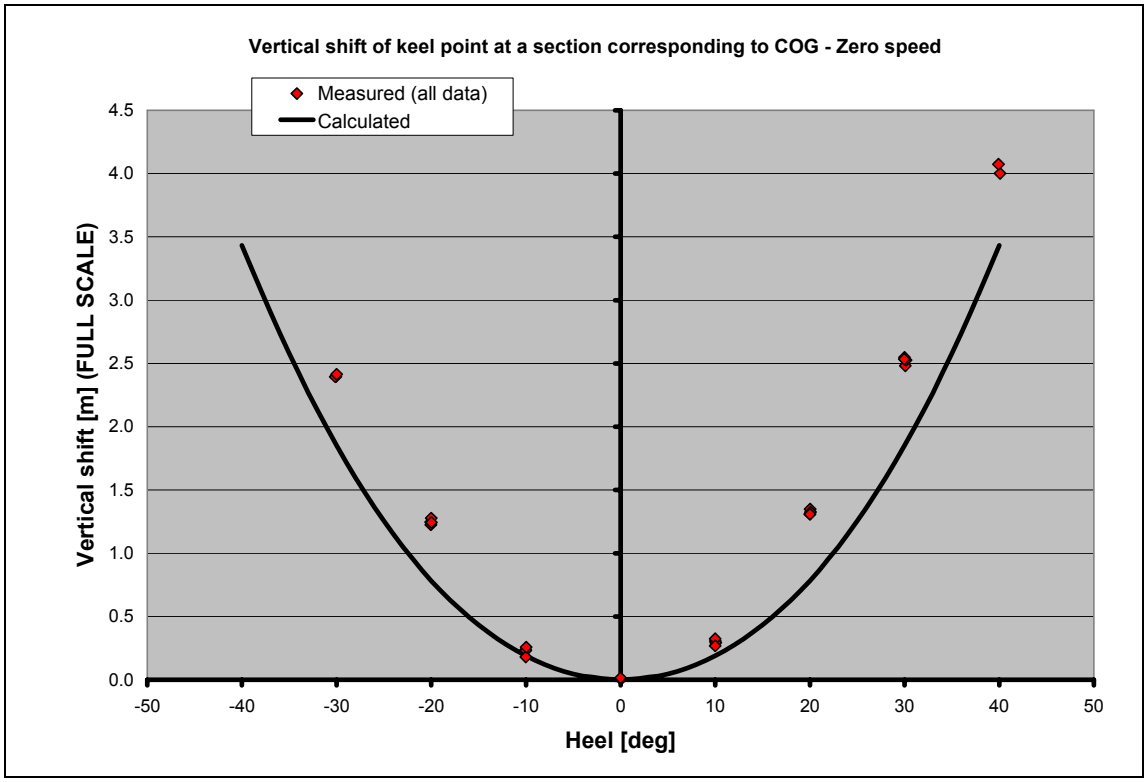

Figure 103: Comparison between measured and calculated vertical shift of the reference point due to heel.

A similar situation is found when considering the pitch induced by heel (see Figure 104). Measured data are very consistent among different scales, but the measured pitch is much larger than the hydrostatically calculated pitch.

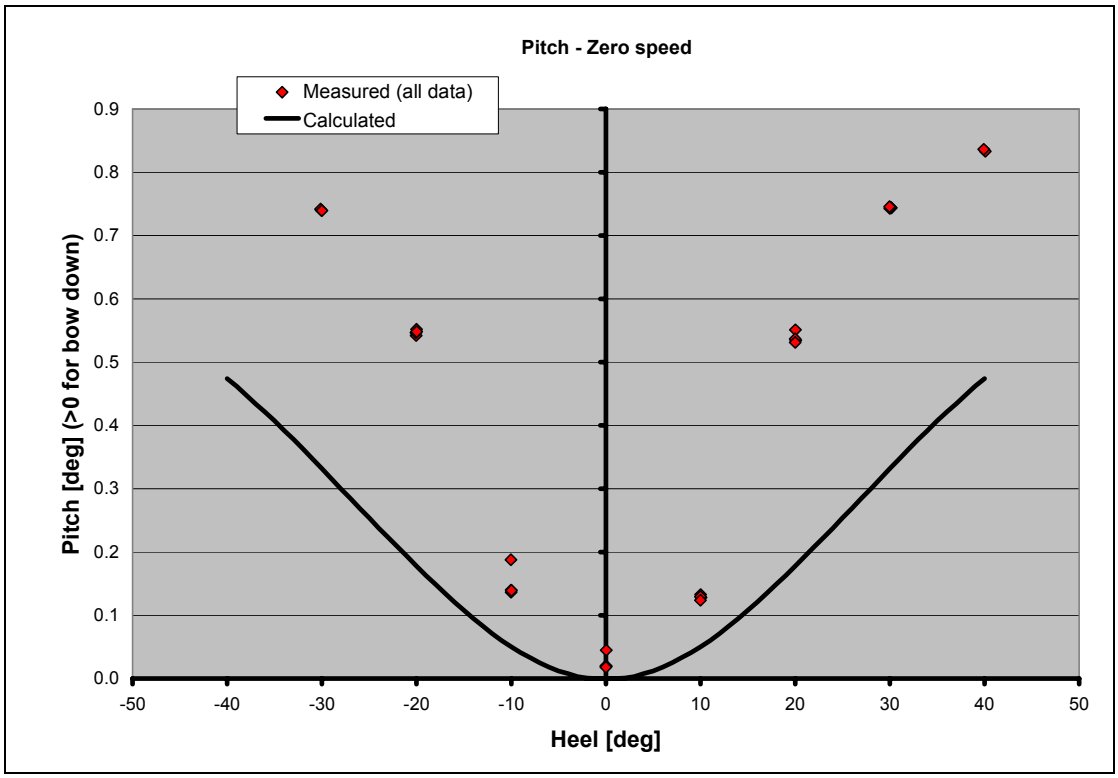

Figure 104: Comparison between measured and calculated pitch due to heel.

The consistency of the data for different scales can also be seen when checking the dependence on speed of the difference between the hydrostatic calculations and the actual measurements for the vertical shift of the reference point (see Figure 105 to Figure 112). The dynamic sinkage effect (increase of draught) as the speed is increased is clearly visible in all cases. The $\pm\sigma$ range is reported, but it is too small to be visible since it is masked by the points' markers.

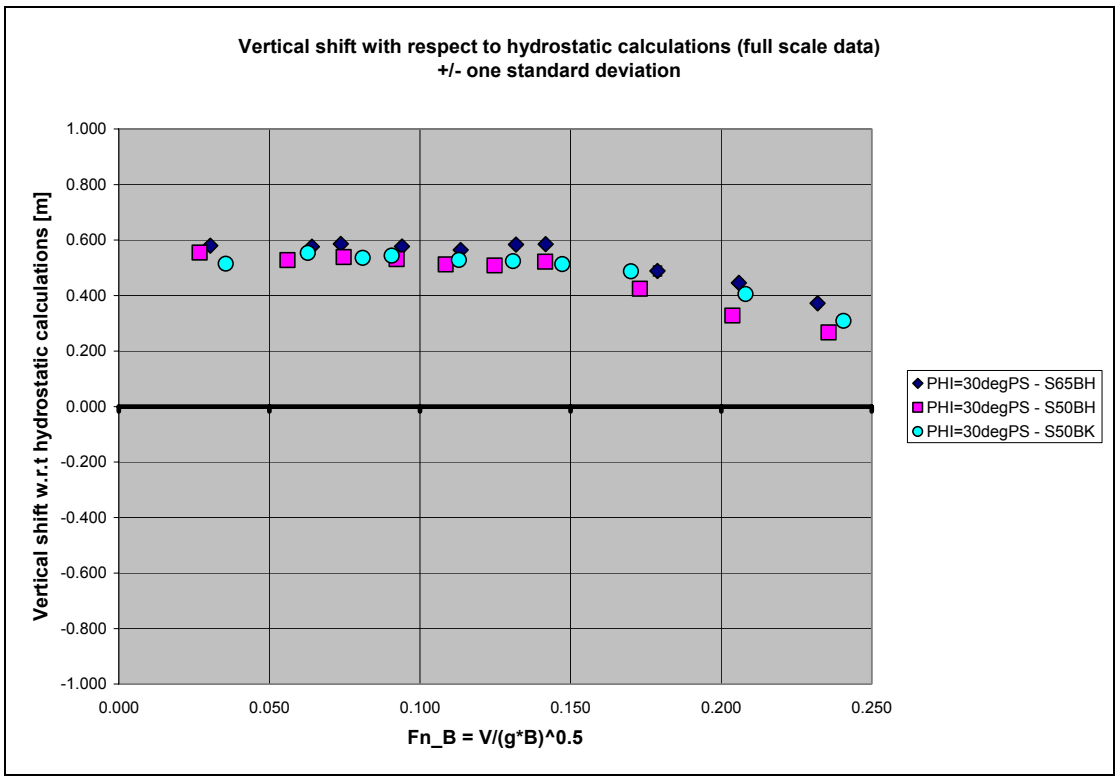

Figure 105: Difference between measured and calculated vertical shift of the reference point. Heel 30deg portside, drifting to starboard.

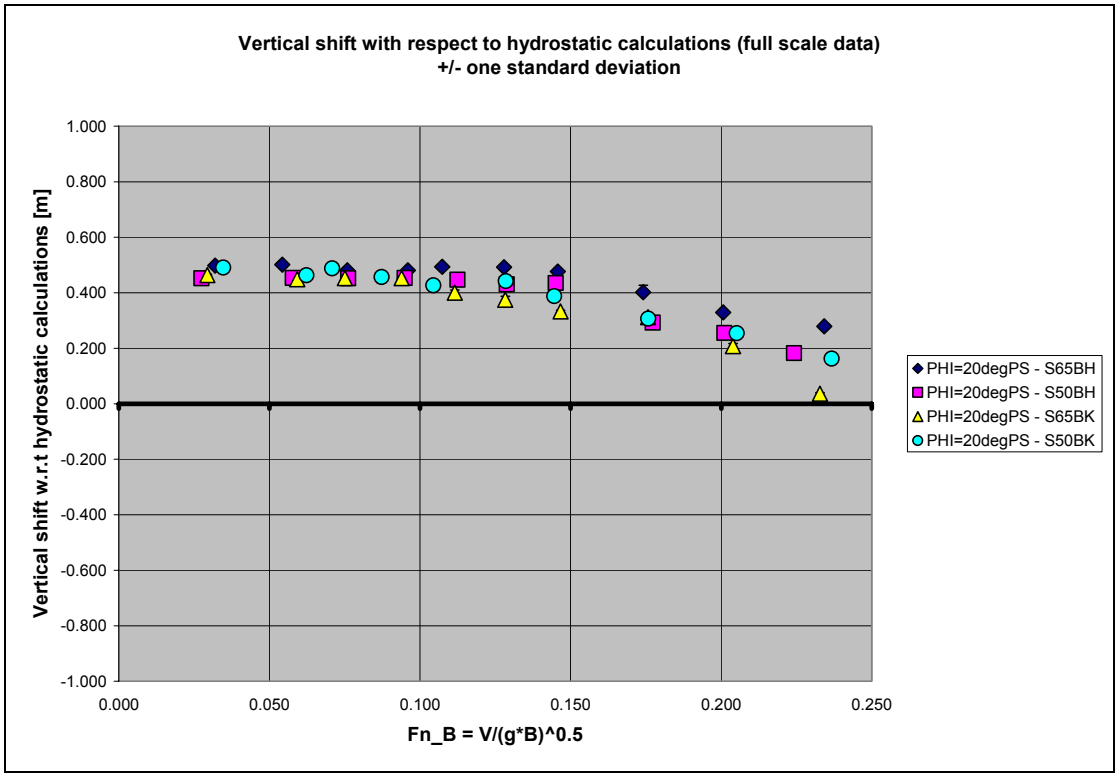

Figure 106: Difference between measured and calculated vertical shift of the reference point. Heel 20deg portside, drifting to starboard.

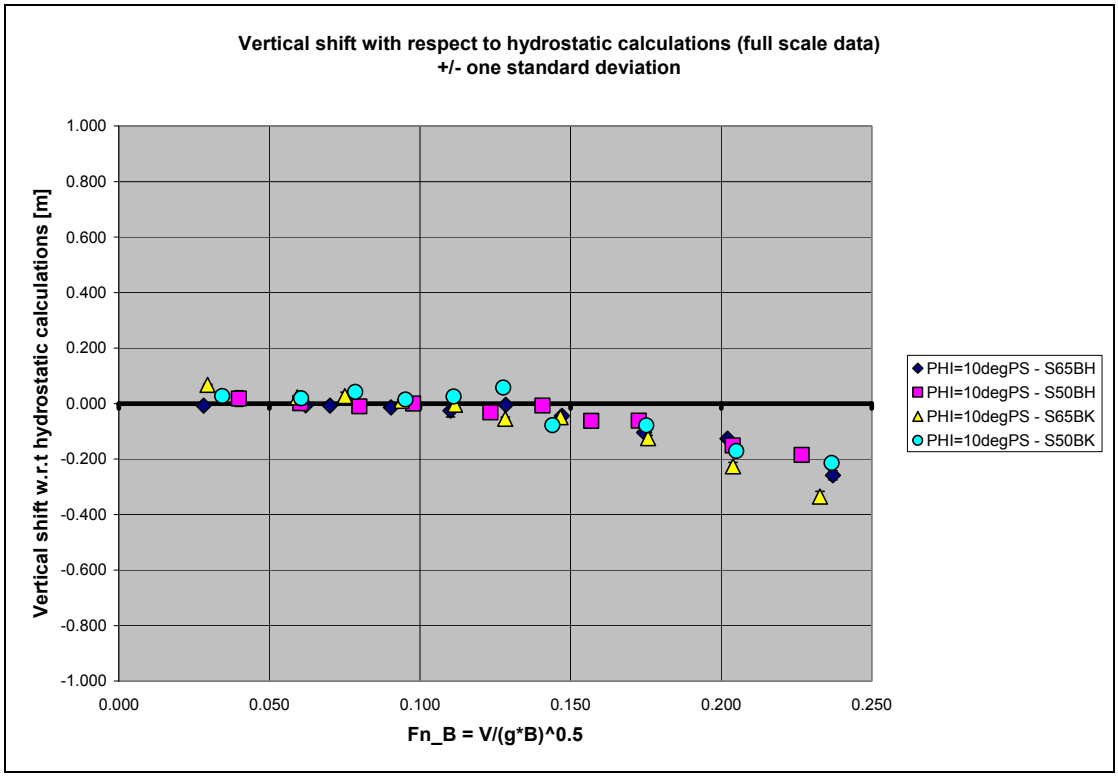

Figure 107: Difference between measured and calculated vertical shift of the reference point. Heel 10deg portside, drifting to starboard.

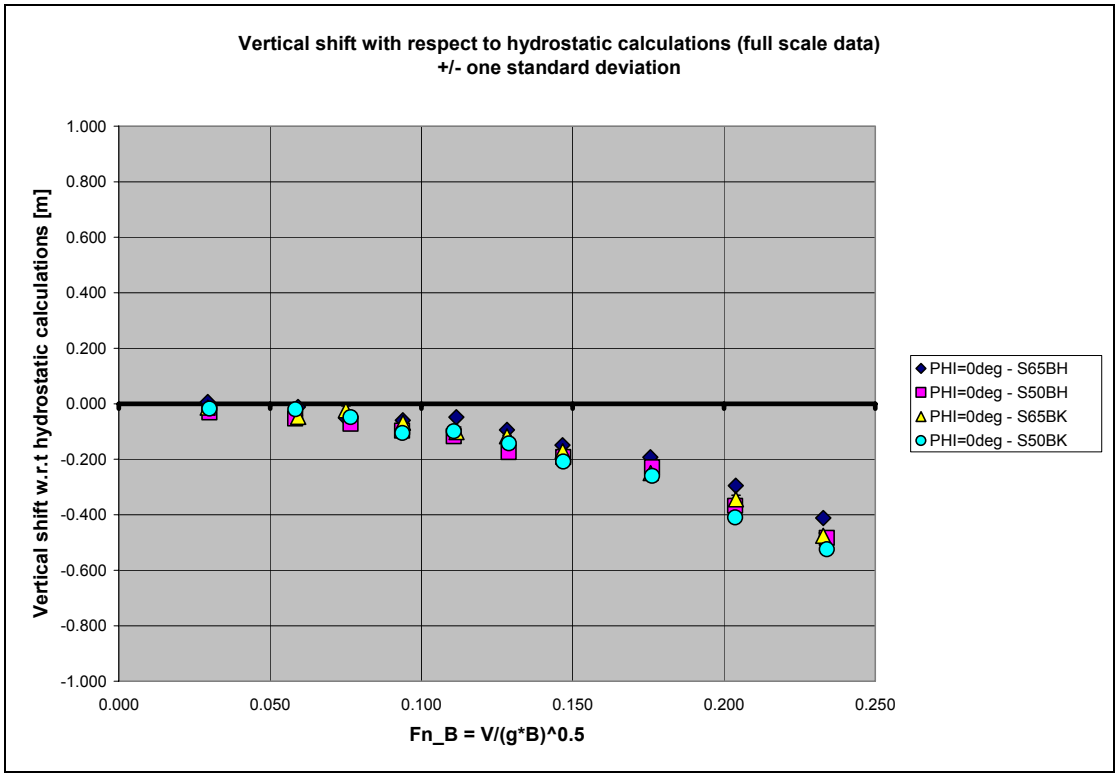

Figure 108: Difference between measured and calculated vertical shift of the reference point. Heel 0deg, drifting to starboard.

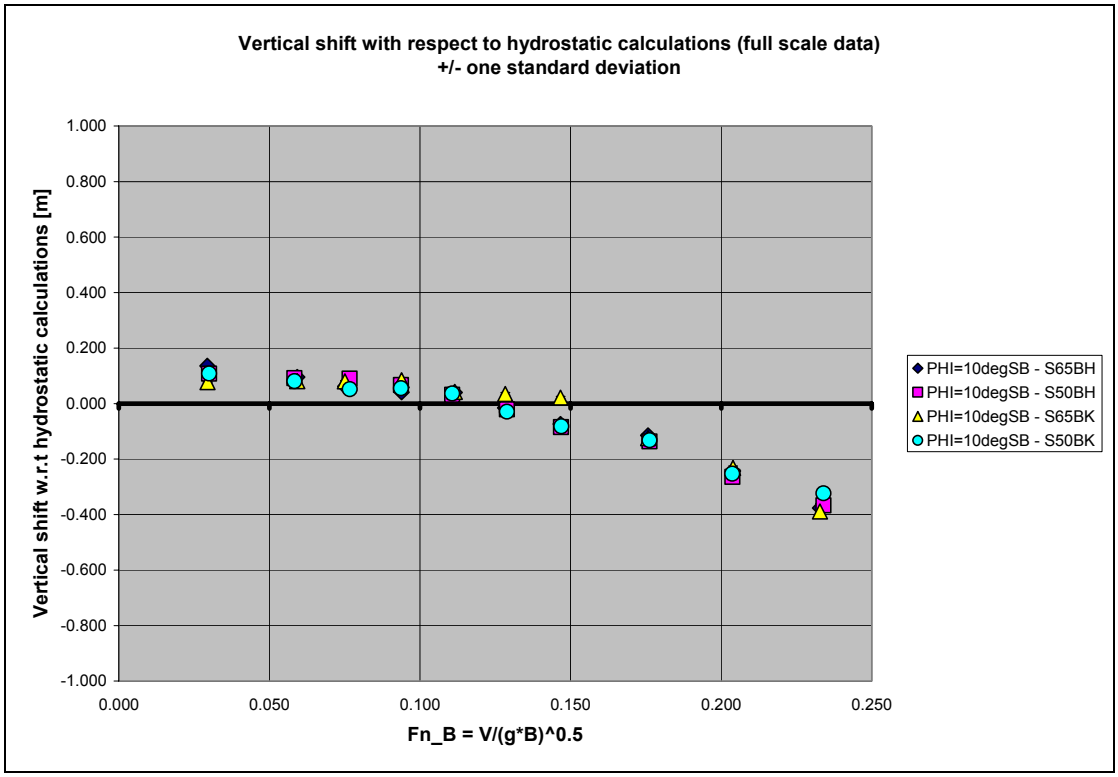

Figure 109: Difference between measured and calculated vertical shift of the reference point. Heel 10deg starboard, drifting to starboard.

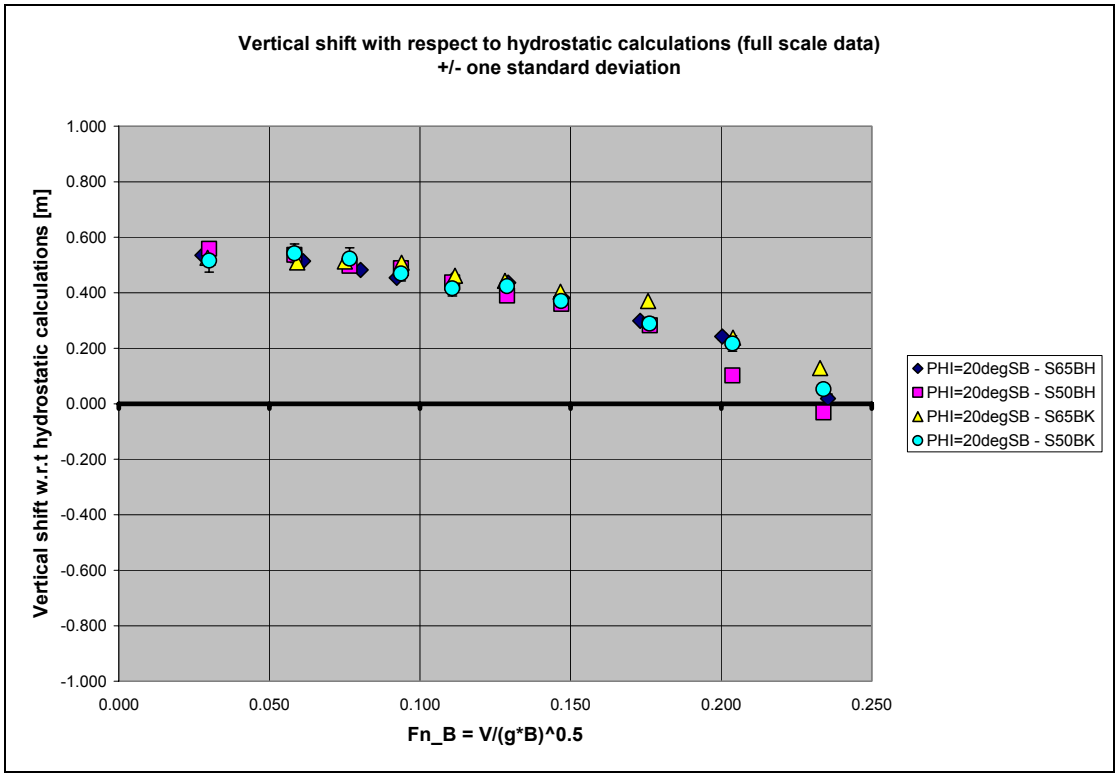

Figure 110: Difference between measured and calculated vertical shift of the reference point. Heel 20deg starboard, drifting to starboard.

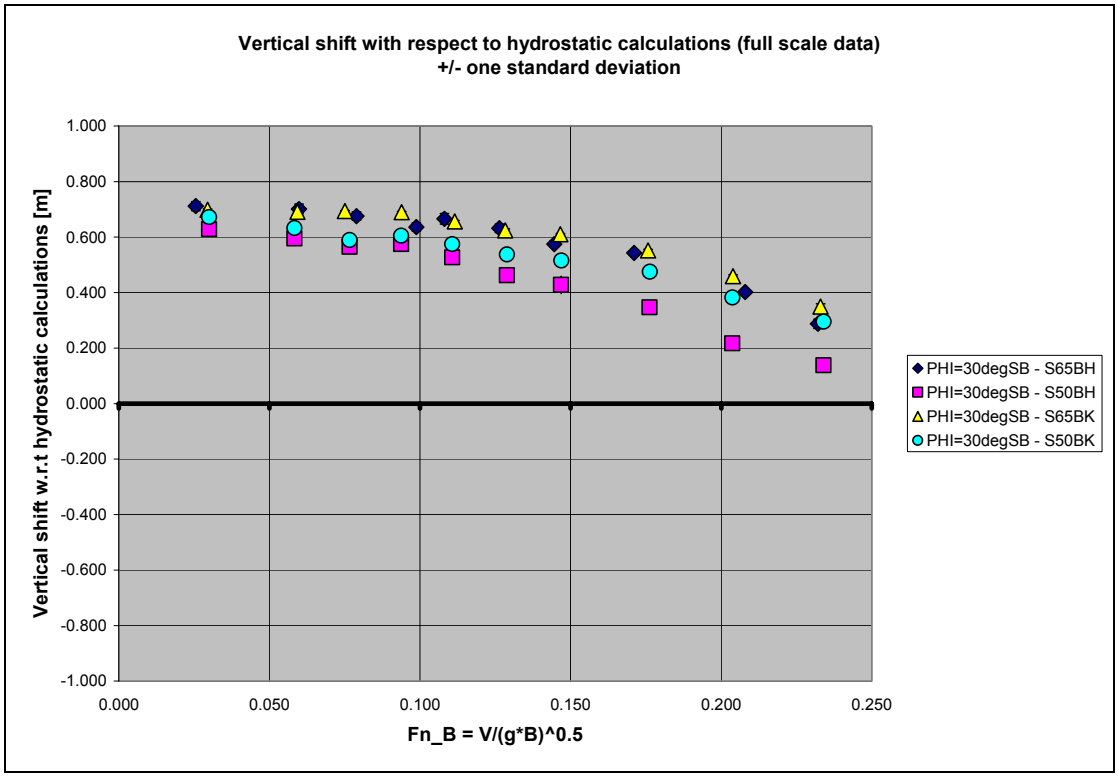

Figure 111: Difference between measured and calculated vertical shift of the reference point. Heel 30deg starboard, drifting to starboard.

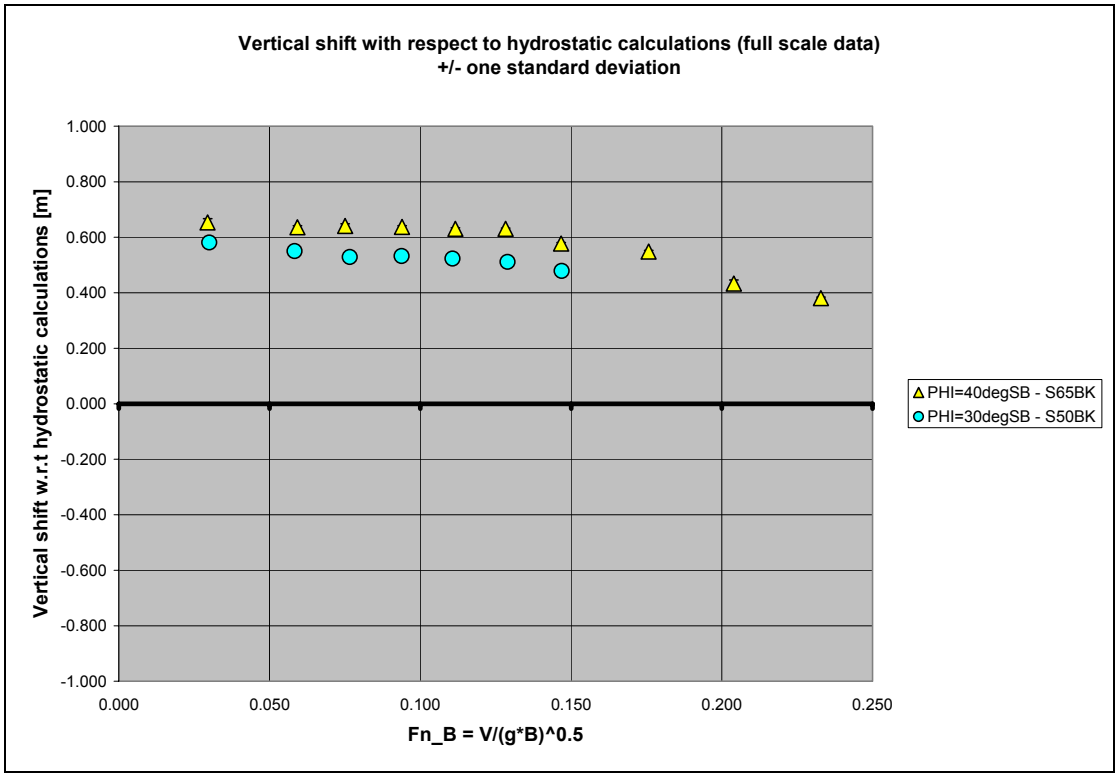

Figure 112: Difference between measured and calculated vertical shift of the reference point. Heel 40deg starboard, drifting to starboard.

At the moment of writing it is not clear the reason behind the differences between calculations and measurements. Hydrostatic calculations have been double checked, confirming the outcomes with very minor differences due to different numerical implementations of the hydrostatic codes. Considering heave, it could be guessed that the reference point was systematically set in a position different from the nominal one. However, in case of pitch, there should be no influence from the actual setting of the reference point. A misalignment of the reference frame could be considered as the cause for such large differences in the pitch, however it is very unlikely that the same misalignment was present in both the models (scale 1:50 and 1:65) to obtain so consistent results. Finally, a possible reason could be related to some constraints geometrically induced by the restraining system.
Since the calculation of roll moment induced by drift is carried out by a transport of moments to the reference point, and since the position of the reference point is actually measured, any error in the determination of the position of such point strongly influences the results for the roll moment, as it is discussed below.

Roll moment due to drift

Roll moment was calculated with respect to the reference point starting from the six forces measured by the dynamometer at experimental stage. In order to carry out this calculation, the relative position of the ship reference point with respect to the centre of the dynamometer's local reference system was determined from measured ship motions. Accordingly, the moment $M_x(K)$ was determined (see Figure 59) and provided by the towing tank. The "measured" moment $M_x(K)$ was analysed in order to determine average value and standard deviation from time series. Afterwards, in a post-processing stage, the moment $M_x(P(\phi))$ was determined with respect to the

point $P(\phi)$ given by the intersection of the waterplane and the centreline. In carrying out this calculation the nominal ship attitude was used as given by hydrostatic calculations. The average and standard deviation for $M_x\left(P(\phi)\right)$ were determined in the post-processing phase using the simplified method in (20)-(22). The basic formulae are as follows:

$$\text{Average: } \overline{M}_x\left(P(\phi)\right) = \overline{M}_x(K) + \overline{F}_y \cdot \overline{KP}\left(\overline{\phi}\right)\cdot\cos\left(\overline{\phi}\right) + \overline{F}_z \cdot \overline{KP}(\phi)\cdot\sin(\phi)$$

$$\text{Standard deviation: } \sigma_{MX(P)} = \sqrt{\begin{matrix}\sigma^2_{MX(K)} + \left(\overline{KP}\left(\overline{\phi}\right)\cdot\cos\left(\overline{\phi}\right)\right)^2\sigma^2_{Fy} + \\ +\left(\overline{KP}\left(\overline{\phi}\right)\cdot\sin\left(\overline{\phi}\right)\right)^2\sigma^2_{Fz} + \\ +\left(\begin{matrix}\overline{F}_z\cdot\overline{KP}\left(\overline{\phi}\right)\cdot\cos\left(\overline{\phi}\right)+ \\ -\overline{F}_y\cdot\overline{KP}\left(\overline{\phi}\right)\cdot\sin\left(\overline{\phi}\right)\end{matrix}\right)\cdot\sigma^2_{\phi}\end{matrix}} \tag{52}$$

Again, it is important to bear in mind that $\sigma_{MX(P)}$ is a measure of dispersion for $M_x\left(P(\phi)\right)$ and shall not be confused with the standard deviation to be associated to the estimated average $\overline{M}_x\left(P(\phi)\right)$, that, instead, is significantly smaller and depends on the length of the time window of analysis and on the autocorrelation function of $M_x\left(P(\phi)\right)$.

However the formula for the standard deviation of $M_x\left(P(\phi)\right)$ has been simplified. First of all the contribution of the uncertainty on the heeling angle, according to the measured data, is extremely small, and has thus been neglected. Moreover the quantity $\overline{KP}\left(\overline{\phi}\right)$ was calculated at the nominal heeling angle instead of being calculated at the actual heeling angle, in order to avoid the repetition of hydrostatic calculation for angles with very small differences. The differences between the nominal and the actual average heeling angles are, however, very small, hence this approximation can be considered appropriate. Accordingly, the simplified formula for the standard deviation of $M_x\left(P(\phi)\right)$ becomes:

$$\sigma_{MX(P)} \approx \sqrt{\sigma^2_{MX(K)} + \left(\overline{KP}\left(\phi_{\text{nominal}}\right)\cdot\cos\left(\overline{\phi}\right)\right)^2\sigma^2_{Fy} + \left(\overline{KP}\left(\phi_{\text{nominal}}\right)\cdot\sin\left(\overline{\phi}\right)\right)^2\sigma^2_{Fz}} \tag{53}$$

It shall be noted that, in principle, the total vertical force F_z should be zero since the model is free to heave in the tested configuration. From the measured data, the total vertical force is extremely small in comparison with the product $\rho g A_{WP}$ (ρ: [kg/m^3] volumic mass of water, g: [m/s^2] gravitational acceleration, A_{WP}: [m^2] waterplane area at zero heel), this meaning that it should not have caused any significant variation of draught. However the average value of F_z is not negligible in comparison with the lateral force. The reason behind a not zero total vertical force is not clear, but it is probably due to the mechanical friction of the system.

From the knowledge of the average value of $M_x\left(P(\phi)\right)$ and of the lateral force F_y the conventional equivalent vertical position of the reaction force, H_{Fy} is defined as:

$$H_{Fy} = \frac{M_x\left(P(\phi)\right)}{F_y} \tag{54}$$

A positive value of H_{Fy} means that the reaction is to be considered "below water", while a negative value of H_{Fy} means that the reaction is to be considered "above water". Note, however, that when the net vertical force, as in our case, is not zero, the definition (54) is questionable, since it contains, in a hidden way, the contribution from F_z. According to (54) we can calculate the linearised average value of H_{Fy} as well as the linearised standard deviation of H_{Fy} as:

$$\begin{aligned} \overline{H}_{Fy} &= \frac{\overline{M}_x\left(P(\phi)\right)}{\overline{F}_y} \\ \sigma_{H_{Fy}} &= \left|\overline{H}_{Fy}\right| \cdot \sqrt{\left(\frac{\sigma_{MX(P)}}{\overline{M}_x\left(P(\phi)\right)}\right)^2 + \left(\frac{\sigma_{Fy}}{\overline{F}_y}\right)^2} \end{aligned} \tag{55}$$

Results for each inclination angle are shown in Figure 113 to Figure 120. Note that in the figures H_{Fy}, as well as the corresponding standard deviation, are made dimensionless by using a reference draught T_{ref} equal to the upright draught at zero speed (6.6m full scale). Moreover note that the vertical axis in the figures is directed downwards.

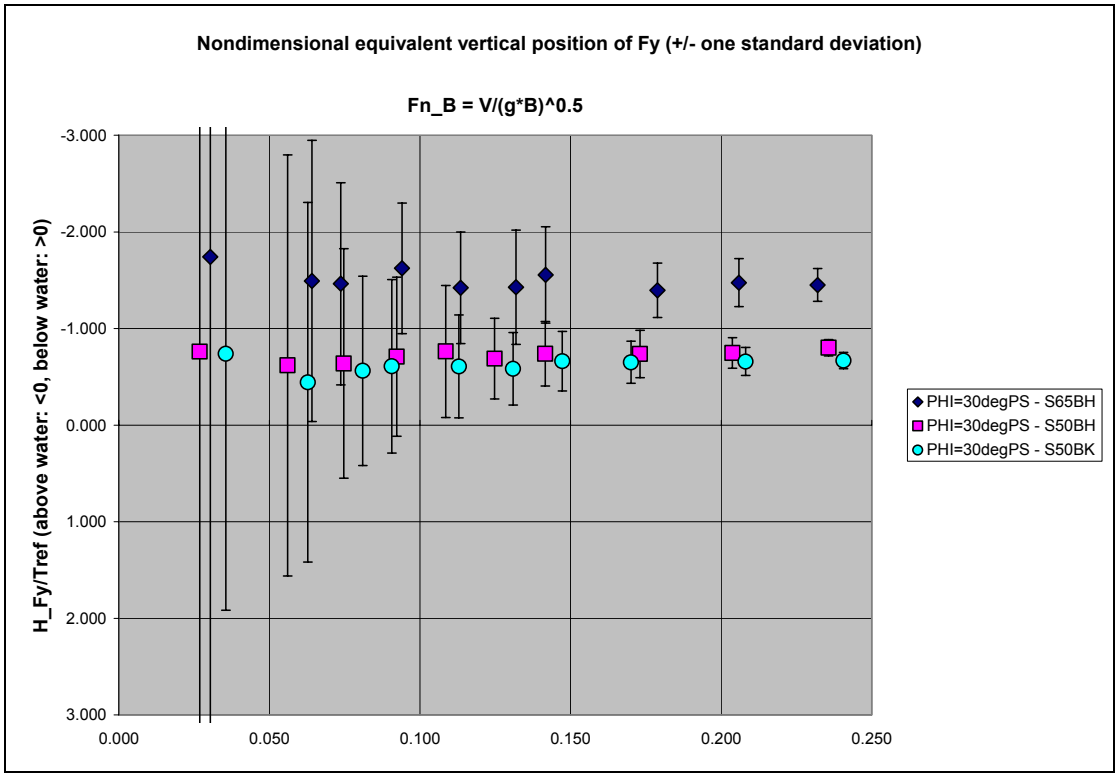

Figure 113: "Equivalent vertical position" H_{Fy} / T_{ref} of the lateral hydrodynamic reaction. Heel 30deg portside, drifting to starboard.

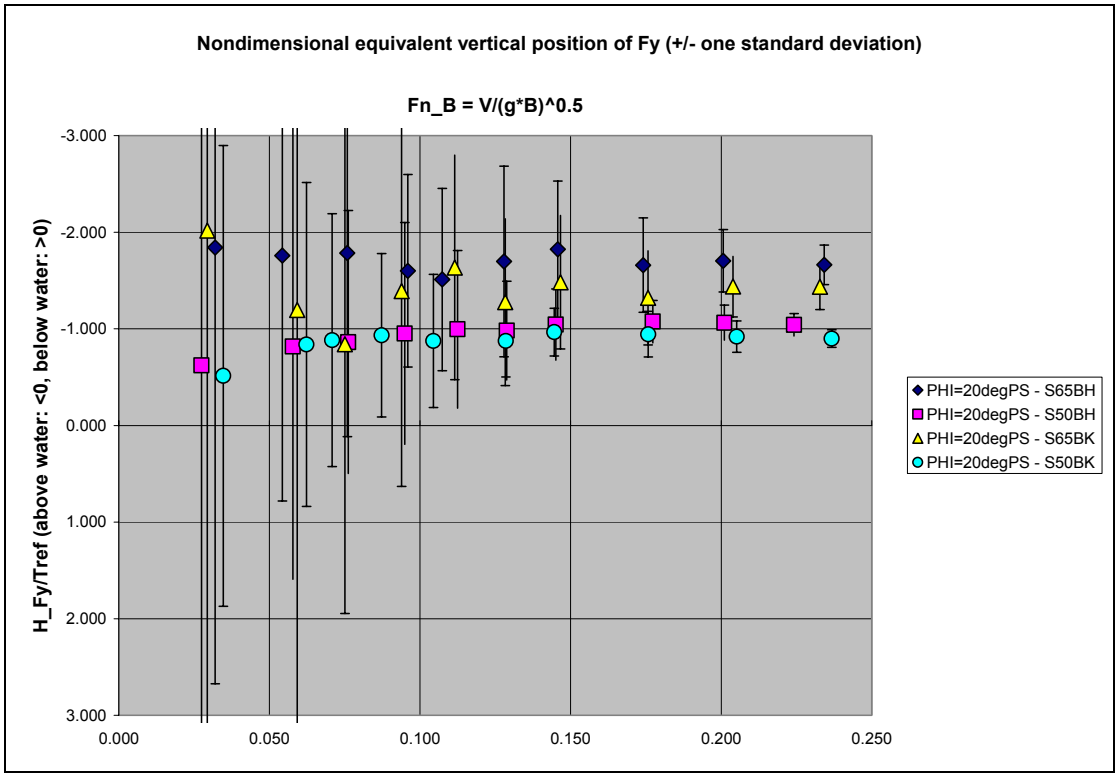

Figure 114: "Equivalent vertical position" H_{Fy} / T_{ref} of the lateral hydrodynamic reaction. Heel 20deg portside, drifting to starboard.

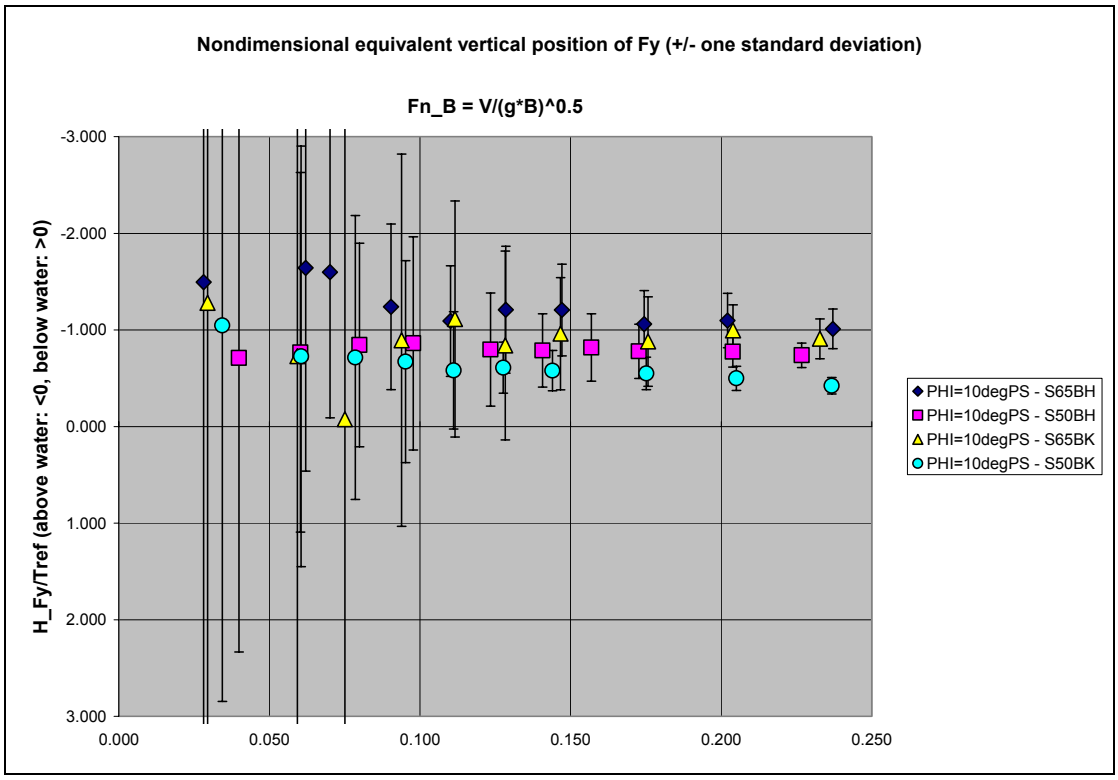

Figure 115: "Equivalent vertical position" H_{Fy} / T_{ref} of the lateral hydrodynamic reaction. Heel 10deg portside, drifting to starboard.

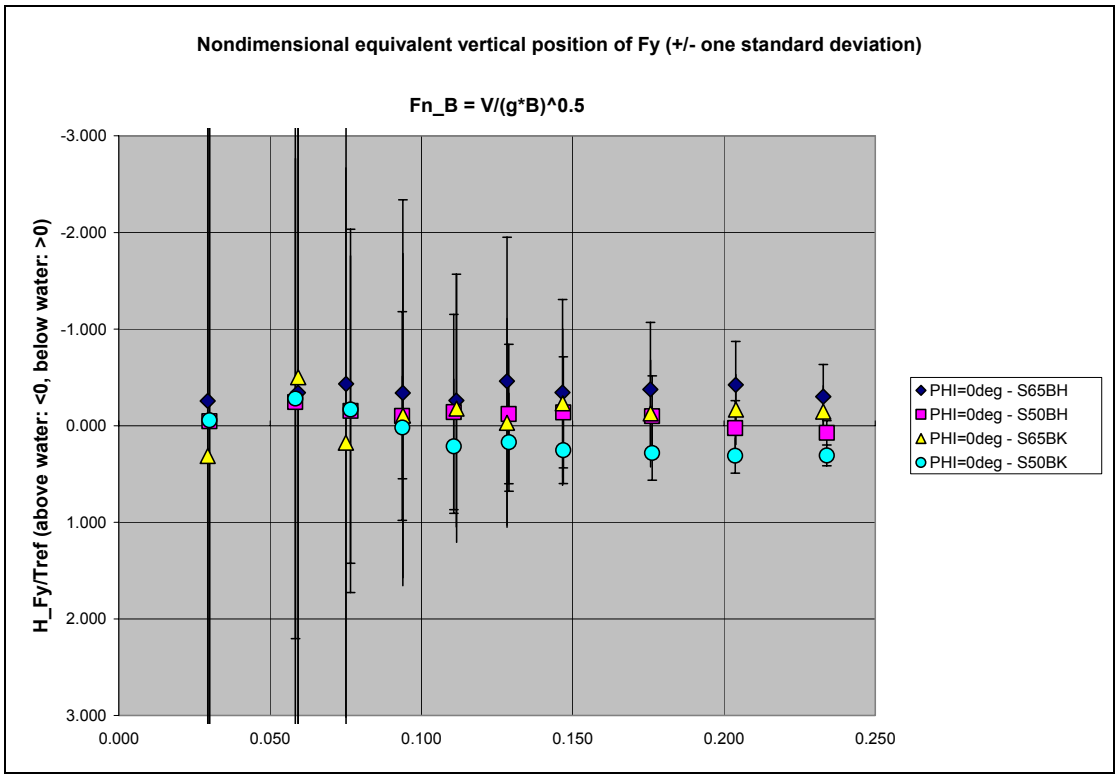

Figure 116: "Equivalent vertical position" H_{Fy} / T_{ref} of the lateral hydrodynamic reaction. Heel 0deg, drifting to starboard.

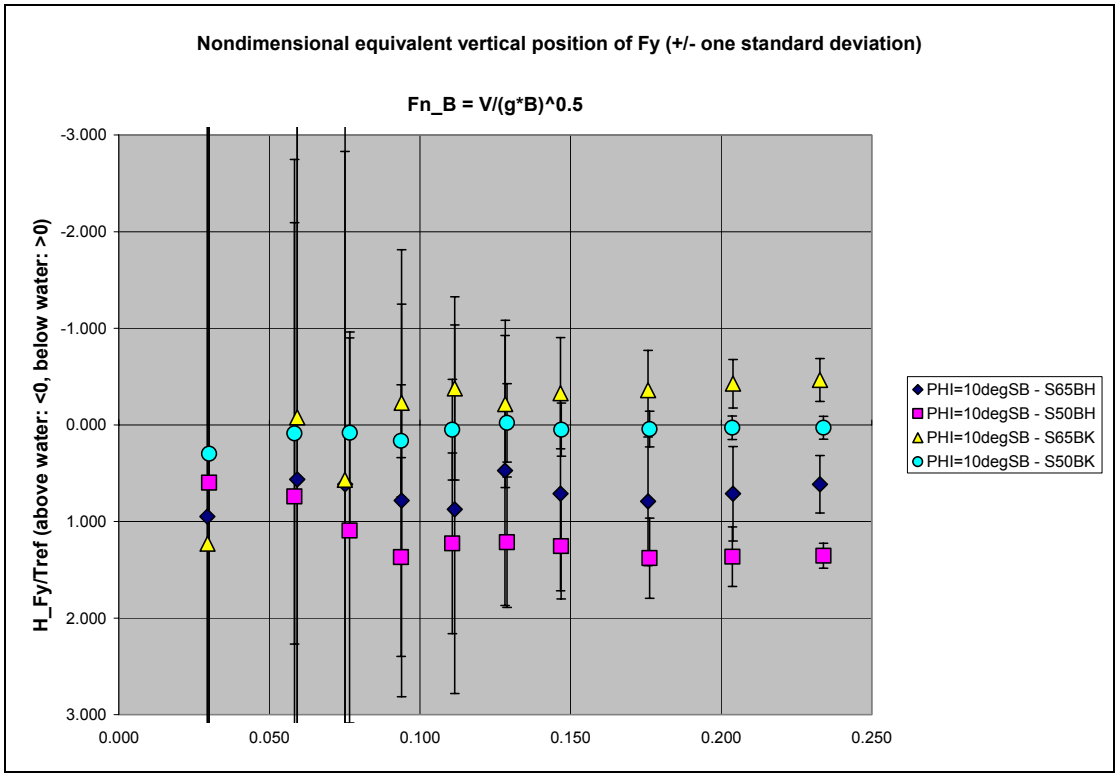

Figure 117: "Equivalent vertical position" H_{Fy} / T_{ref} of the lateral hydrodynamic reaction. Heel 10deg starboard, drifting to starboard.

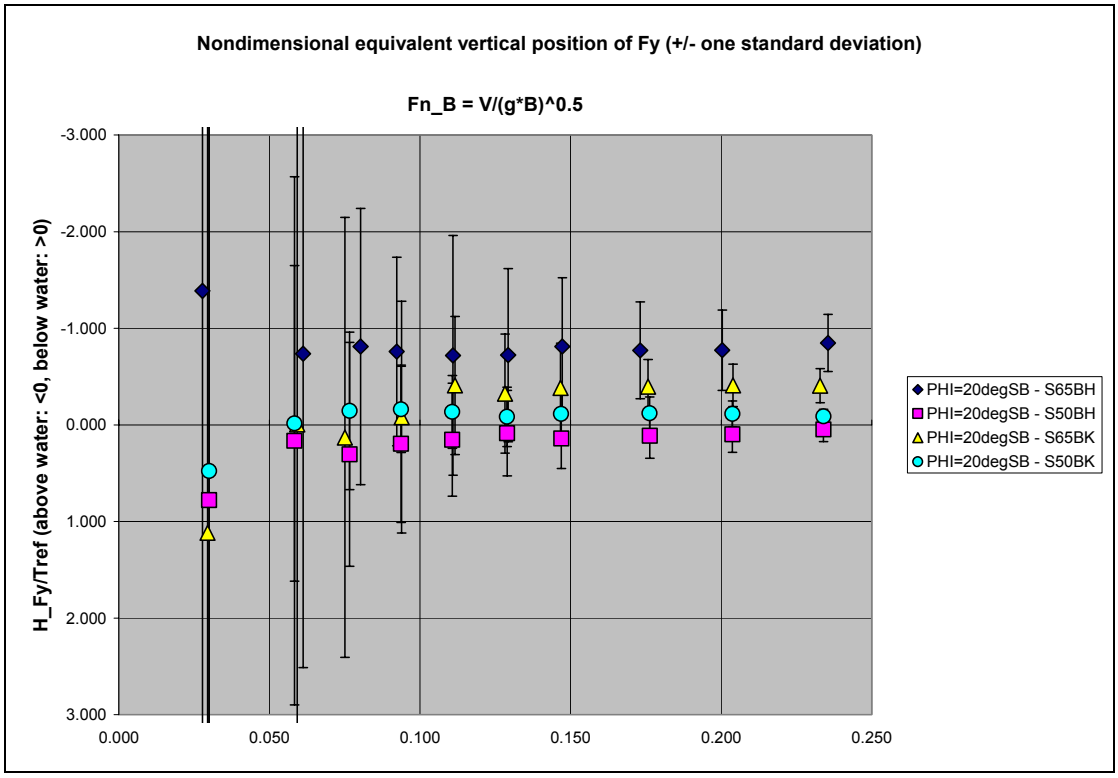

Figure 118: "Equivalent vertical position" H_{Fy} / T_{ref} of the lateral hydrodynamic reaction. Heel 20deg starboard, drifting to starboard.

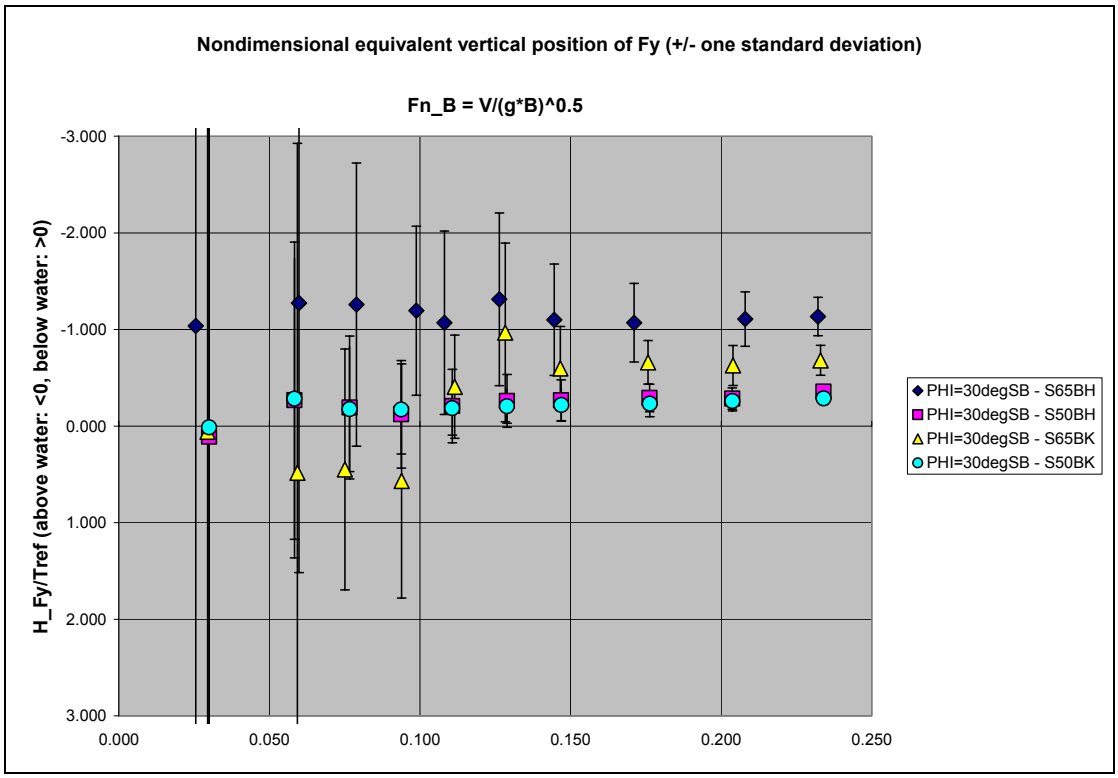

Figure 119: "Equivalent vertical position" H_{Fy} / T_{ref} of the lateral hydrodynamic reaction. Heel 30deg starboard, drifting to starboard.

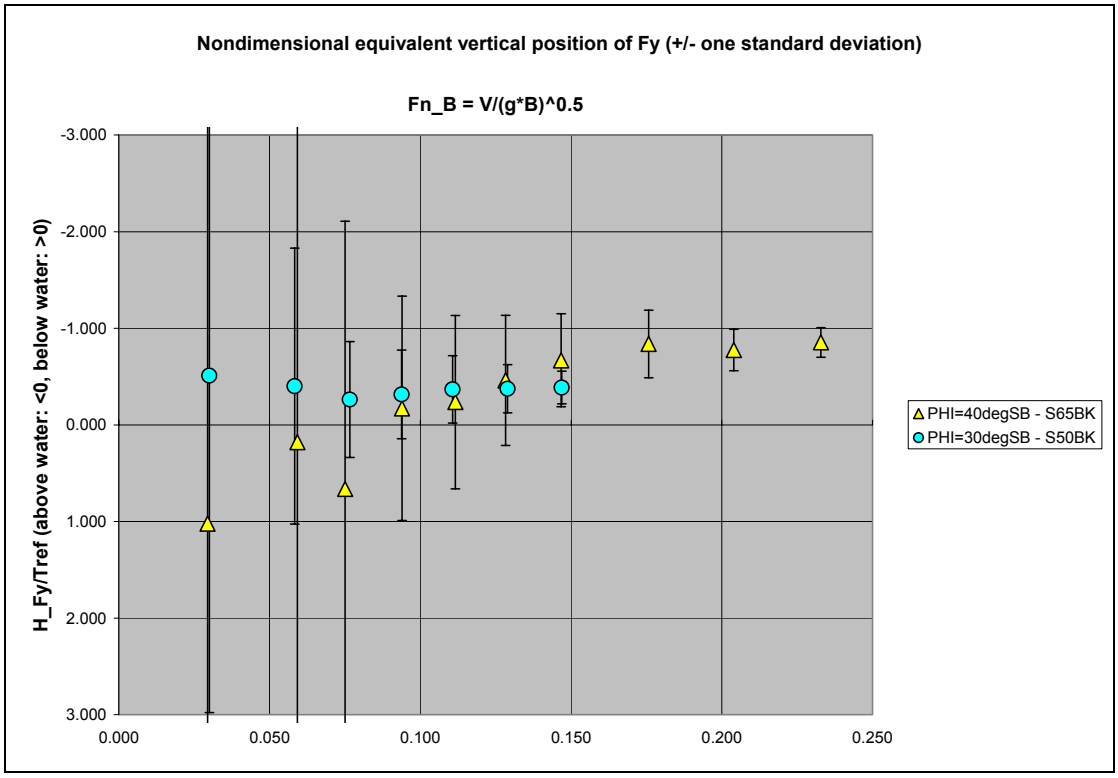

Figure 120: "Equivalent vertical position" H_{Fy} / T_{ref} of the lateral hydrodynamic reaction. Heel 40deg starboard, drifting to starboard.

From the reported figures it can be seen that the scattering is significant with also a significant uncertainty. While data are consistent for a given scale and condition (with or without bilge keels), there is a lack of consistency among the two scales. In a way similar to that followed for the analysis of the lateral hydrodynamic reaction (see (27)), the average of the obtained results for the two highest speeds has been calculated together with a measure of dispersion. The outcomes are plot as a function of the heeling angle in Figure 121.

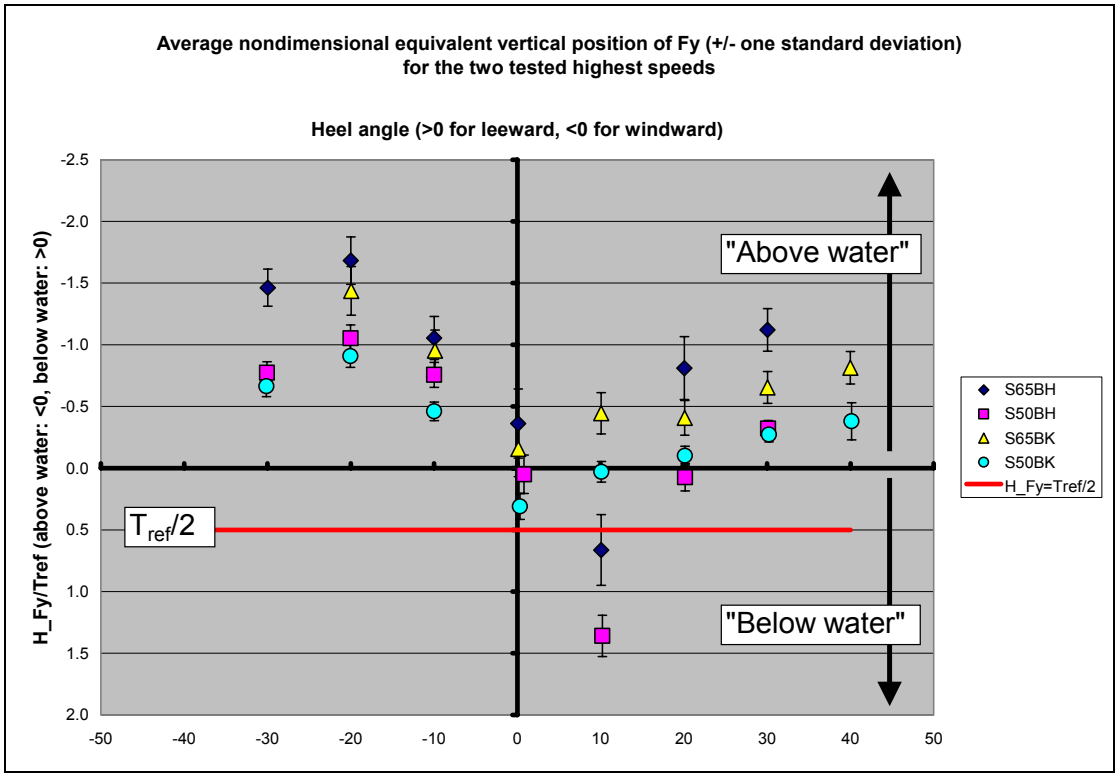

Figure 121: Average "Equivalent vertical position" H_{Fy}/T_{ref} of the lateral hydrodynamic reaction calculated from the two highest tested speeds for each condition.

Although each single set of data in Figure 121 is quite consistent, it is not clear whether the observed differences among different data sets are due to a real hydrodynamic phenomenon or whether they are simply due to errors in the experimentation / data analysis. In general there seems to be a tendency for H_{Fy} to be negative, i.e. "above water". This would be consistent with the findings in [5]. The shape (but not the actual values) of $H_{Fy}(\phi)$ is also quite similar to the results in [5], but it is not possible to guarantee, at the moment of writing, on the reliability of data concerning the moment due to the hydrodynamic reaction to drift. The presence of a not zero net vertical force with magnitude that is not negligible with respect to the lateral drift force complicates the interpretation of data. It is however interesting to note the increased dispersion of the data for the heeling angle 10deg starboard, the same angle for which the analysis of the drag coefficient C_D showed the largest differences between bare hull models and models fitted with bilge keels (see Figure 70).